Advanced Engineering of Contact Lens Coatings using Electrohydrodynamic Atomization

Prina Mehta

2018

A thesis submitted in partial fulfilment of the requirements for

PhD in Pharmaceutical Engineering

Awarded by

De Montfort University

Abstract

While the eye presents numerous opportunities for drug delivery (DD); there are many challenges met by conventional methods. Despite the exponential growth in research to overcome these downfalls and achieve sustained and controlled DD, the anatomical characteristics of the eye still pose formulation challenges.

The research presented in this thesis utilises Electrohydrodynamic Atomization (EHDA) to engineer novel coatings for ocular contact lenses. EDHA was selected to develop coatings for the delivery of timolol maleate (TM); with the intention of achieving sustained drug release for treatment of glaucoma. The work presented here is a proof-of-concept; showing the versatility of a promising technique by applying it to a DD remit within which EHDA has not yet been fully exploited: Ocular Drug Delivery (ODD).

The first step was to identify a suitable polymeric matrix to act as the vehicle/carrier and see the effects of different polymers on the *in vitro* release of TM and *ex vivo* TM permeation. Hereafter, based on the results of this work, 4 different PEs were incorporated to attempt to enhance TM release and permeation through the cornea. Further modification of the formulations saw the effect of integrating chitosan on the release of TM from the electrically atomised coatings.

Characterisation of the atomised coatings at each stage demonstrated highly stable matrices, which possessed extremely advantageous morphologies and sizes (within the nanometre range). All coatings also demonstrated adequate to high encapsulation efficiencies (EEs) (>64%) with the highest EE being 99.7%. *In vitro* release (i.e. cumulative percentage release) steadily increased upon introduction of additives to the base polymeric formulations yielding different release profiles; ranging from biphasic profiles to triphasic profiles. *Ex vivo* analysis and biological compatibility testing also presented promising results.

The use of EHDA has not yet been explored in depth within the ocular research remit. It has shown great potential in the work presented here; engineering on demand lens coatings capable of sustaining both TM release and TM permeation.

Declaration

I declare all the work presented in this thesis has been undertaken by myself. The work has not been submitted for any other professional qualification.

The work presented here is entirely original and to the best of my knowledge does not impinge on any rules or copyright laws. Any collaborative work or work from external sources have been stated explicitly, cited and referenced accordingly within the main essay.

Signed:

Date:

Acknowledgments

First, I would like to thank my supervisor, Professor Zeeshan Ahmad. Without your support, motivation and outrageous sense of humour I would never have progressed this far. I would also like to thank my EHDA family who all thrived to motivate me, even when morale was down.

Acknowledgment also goes to the technical support I received at DMU. Many thanks and appreciation goes to Dr Rachel Armitage, Liz O'Brien and Leonie Hughes for all the essential help they provided all throughout the 3 years.

I would also like to acknowledge DMU for financially supporting me throughout my PhD.

A special thanks goes to the amazing friends I have made on this journey. Without all the banter, coffee and most importantly cake, I would not be where I am today. A big shout out to Mayur, Allison, Mina, Claire, Amrat and Angela for listening to all my rants, keeping me sane and unknowingly spurring me through my journey.

The biggest thanks goes to my parents, my family and friends for wholeheartedly supporting me through my academic career and pushing me to reach my full potential. There are no words to describe their unparalleled support and guidance; for which I am extremely grateful.

Publications and Conferences

Publications

KHAN, H. et al. (2014) Smart Microneedle coatings for controlled delivery and biomedical analysis. *Journal of Drug Targetting*, 22, pp. 790-795.

MEHTA, P. et al. (2015) New platforms for multi-functional ocular lenses: engineering double-sided functionalized nano-coatings. *Journal of Drug Targeting*, 23 (4), pp. 305-310.

MEHTA, P. et al. (2017) Pharmaceutical and biomaterial engineering via electrohydrodynamic atomization technologies. *Drug Discovery Today*, 22, pp. 157-165.

MEHTA, P. et al. (2017) Approaches in topical ocular drug delivery and developments in the use of contact lenses as drug-delivery devices. *Therapeutic Delivery*, 8, pp. 521-541.

MEHTA, P. et al. (2017) Electrically atomised formulations of timolol maleate for direct and on-demand ocular lens coatings. *European Journal of Pharmaceutics and Biopharmaceutics*, 119, pp. 170-184.

MEHTA, P. et al. (2017) Development and characterisation of electrospun timolol maleate-loaded polymeric contact lens coatings containing various permeation enhancers. *International Journal of Pharmaceutics*, 532, pp. 408-420.

MEHTA, P. et al (2018) Broad Scale & Fabrication of Healthcare Materials for Drug and Emerging Therapies Via Electrohydrodynamic Techniques. *Advanced Therapeutics.* doi: 10.1002/adtp.201800024

MEHTA, P. et al (2018) Engineering and Development of Chitosan-based Nanocoatings for Ocular Contact Lenses. (Submitted, Minor Revisions)

MEHTA, P. et al (2018) Assessing the ex vivo permeation behaviour of functionalised contact lens coatings engineered using electrohydrodynamic techniques. (In Preparation)

Conferences

MEHTA, P., AHMAD, Z.; *Electrically atomised active-polymer coatings for drug eluting ocular lenses*. 7th International PharmSci Conference, 5-7th September 2016, University of Strathclyde, Glasgow, UK.

MEHTA, P., AHMAD, Z.; *Electrically atomised active-polymer coatings for drug eluting ocular lenses*. EPSRC EHDA Network International PharmTech Conference, 4th November 2016. De Montfort University, Leicester, UK.

MEHTA, P., AL-KINANI, A., ALANY, R., AHMAD, Z.; *Development and Characterisation of electrospun timolol maleate-loaded fibrous coatings for ocular lenses.* 5th Quality by Design Symposium, 29th March 2017. De Montfort University, Leicester, UK.

MEHTA, P., AL-KINANI, A., ALANY, R., AHMAD, Z.; *Development and Characterisation of electrospun timolol maleate-loaded fibrous coatings for ocular lenses.* 8th International PharmSci Conference, 5-7th September 2017, University of Hertfordshire, Hatfield, UK.

MEHTA, P., AL-KINANI, A., ALANY, R., AHMAD, Z.; *Assessing the permeation enhancing properties of chitosan on the permeation of anti-glaucoma drug timolol maleate.* 6th Quality by Design Symposium, 21st March 2018. De Montfort University, Leicester, UK.

MEHTA, P., AL-KINANI, A., ALANY, R., AHMAD, Z.; *Developing electrospun timolol maleate-loaded fibrous nanocoatings for ocular lenses.* 19th World Congress on Materials Science and Engineering, 11th – 13th June 2018. Barcelona, Spain.

Table of Contents

List of Figures

List of Tables

Abbreviations

5FU	5 Fluorouracil
ACG	Angle Closure Glaucoma
AH	Aqueous Humour
ANOVA	Analysis of Variance
API	Active Pharmaceutical Ingredient
ATR	Attenuated Total Reflection
AV	Applied Voltage
BA	Bioavailability
BAB	Blood Aqueous Barrier
BAC	Benzalkonium Chloride
BCOP	Bovine Corneal Opacity and Permeability
BRB	Blood Retinal Barrier
BSA	Bovine Serum Albumin
CA	Contact Angle
CDs	Cyclodextrins
CLs	Contact Lenses
CoEHDA	Coaxial Electrohydrodynamic Atomization
COES	Coaxial Electrospinning
DD	Drug Delivery
DHCL	Doxorubicin hydrochloride
DL	Drug Loading
DI	Dye Intensity
DOX	Doxorubicin
DSC	Differentia Scanning Calorimetry
EC	Electro-Conductivity
EDTA	Ethylenediaminetetraacetic acid
EE	Encapsulation Efficiency
EHDA	Electrohydrodynamic Atomisation

ES	Electrospinning
Esy	Electrospraying
FR	Flow Rate
FTIR	Fourier Transform Infrared
HA	Hydroxyapatite
HG	Hydrogel
HPLC	High Pressure Liquid Chromatography
HPMC	Hydroxypropyl Methacrylate
IOP	Intraocular Pressure
IR	Infrared Radiation
MAA	Methacrylic Acid
MBs	Microbubbles
MI	Molecular Imprinting
MIC	Minimum Inhibition Concentration
MPs	Microparticles
NF	Nanofibers
NP	Nanoparticle
NSAID	Non-Steroidal Anti-Inflammatory Drug
o/w	oil-in-water
ODD	Ocular Drug Delivery
PAA	Polyacrylic acid
PAN	Poly(acrylonitrile)
PBS	Phospate Buffer Saline
PCL	Polycaprolactone
PE	Permeation Enhancer
PEG	Polyethylene glycol
PEO	Poly (ethylene oxide)
pHEMA	poly (hydroxyethyl methacrylate)
PLA	Polylactic acid
PLAGA	Poly (lactic-co-glycolate)
PLGA	Poly (lactic-glycolic acid)
PLLA	Poly (L-lactic acid)

PLLAC	Poly(l-lactide-co-ε-caprolactone)
PMMA	Poly (methyl methacrylate)
PNIPAM	Poly (N-isopropylacrylamide)
POAG	Primary Open Angle Glaucoma
PVA	Polyvinyl acid
PVP	Poly (vinyl pyrrolidone)
SEM	Scanning Electron Microscopy
siRNA	small interfering RNA
SN	Single Needle
ST	Surface Tension
TGA	Thermogravimetric Analysis
TM	Timolol Maleate
VE	Vitamin E
w/o	water-in-oil
WD	Working Distance
WHO	World Health Organisation
XRD	X-Ray Diffraction

Chapter 1 Introduction

1.1 Fundamentals

The generation of complex nanostructures with multifaceted release kinetics and multifunctional characteristics has resulted from critical developments within the pharmaceutical and drug delivery (DD) remit. Advances in conventional DD methods, although met with reservation and hesitancy, have the ability to overcome flaws in simpler concepts, hence allowing relevant research to have high impact on key areas of research and development.

There are currently several methods which have been developed to yield such structures but each have drawbacks. Solvent evaporation, precipitation, emulsification and spray drying are a few paradigmatic methodologies used to produce NPs with explicit morphologies (Huanbutta et al, 2016; Khajavi and Abbaspour, 2012; Rasekh et al, 2008; Liao, Chew and Leong, 2006). Whilst these methods can successfully produce structurally stable particles of various morphologies there is the drawback of potentially inducing product degradation as a consequence of some of the processing conditions required/necessary for successful particle production (e.g. elevated temperatures and shear stresses). For example, the nature and functionality of biomaterials (e.g. proteins) or active pharmaceutical ingredients (APIs) can be compromised due to high temperatures required for spray drying, inducing protein denaturation. Other drawbacks include non-uniformity in particle size and size distribution, particularly in emulsification where large particles are often yielded.

Electrohydrodynamic atomization (EHDA) is a promising technique and of great interest in the field of pharmaceutics and nanotechnology. It is a versatile method that atomises liquids to produce uniform (with respect to size and morphology) micro- and nano-structures. The process of EHDA is based on an electrically imposed liquid jet exiting a nozzle in the form of particles or fibers. Process parameters and physical liquid properties can be altered, resulting in various EHD modes, (e.g. cone-jetting, spindle, dripping).

EHDA is a cost effective, simple, one step process and easily amendable to achieve optimum conditions for the production of nanostructures at ambient temperatures. The resulting products can subsequently be utilised for numerous pharmaceutical applications with the advantage of producing structures with controlled size and shape, as the following literature review will criticize in **Section 2.4**.

Glaucoma is the term used to refer to a group of optic conditions which result in progressive loss of retinal ganglion cells and their corresponding axons ultimately leading to loss of vision. There is currently no cure for glaucoma and being the second leading cause of blindness in the world, it is clear why addressing such a global issue is important (Tham et al, 2014). The main dosage form used in the treatment of glaucoma is eye drops; however, poor compliance with medication alongside anatomical and physiological barriers present demanding challenges for topical/local eye DD.

The focus on ODD has expedited in recent years in a bid to address limitations associated with conventional dosage forms. The exponential growth in related publications along with material development has led to research being directed at the potential of various ocular DD devices, the most common being contact lenses (CLs). The concept was first introduced in the 1960's; however initial research demonstrated complications with both drug loading and drug release (lack of sustained, controlled release). Research to improve drug release from CLs with various coating methods and drug loading techniques has been presented, many with promising results.

1.2 Aims and Objectives

The ultimate aim of this research was to show the capabilities of EHDA as a potential method for the coating of CLs. It was vital to show how EHDA works, current applications of this promising technique (with respect to drug loading and delivery) as well as how this can be utilised or applied to my field of research.

The research to be presented here aims to acknowledge the fundamental principles of EHDA and its utilisation to achieve TM encapsulation within a polymeric carrier. The work also intends to modify formulations to optimise the EHDA process and help increase TM permeation, both *in vitro* and *ex vivo*.

In order to accomplish this, a series of studies were conducted:

- Establishing and optimisation of the important parameters of single needle EHDA
- Synthesis of TM-loaded polymeric nanostructures using single needle EHDA
- Establishing the most suitable polymeric matrix
- Modification of formulation to increase TM permeation
- Further formulation optimisation to sustain TM release

1.3 Structure of thesis

Chapter 1 is an introduction to the thesis; providing a brief insight into the ocular condition glaucoma, as well as contact lenses and the EHDA process. This chapter briefly touches upon the disadvantages of current ocular drug delivery methods and devices along with a succinct outline of EHDA principles, criteria and application. Chapter 2 will delve deeper into the matters touched upon in chapter 1. An extensive literature review will show conventional and current approaches in glaucoma treatment, the fundamental principles and application of EHDA and utilisation of ocular lenses as DD devices. Chapter 3 outlines the materials and methods used in this study and chapters 4 to 6 comprise the experimental studies carried out for the chosen thesis subject. Chapter 4 consist of characterising and optimising the fabrication of atomised TM-loaded samples containing PVP, PNIPAM or a composite of both. The *in vitro* drug release studies as well as *ex vivo* corneal permeation studies showed the structures that had the greatest potential to release TM were TM-loaded composite beaded fibers. This formulation was taken through to Chapter 5, which looks at improving the corneal permeation of TM. Here 4 different permeation enhancers (PEs) were incorporated into the initial solutions with 2 different drug loadings (5% and 15%w/w of the polymer) to assess the ability of the PEs to increase TM penetration through the cornea. Biological evaluation of all the formulations also aided the efforts to distinguish the most promising formulation for further modification for sustained release of TM. Chapter 6 demonstrates the effect of incorporating chitosan at different concentrations (1%, 2%, and 5%) with PE borneol on TM release from the electrospun structures. Chapter 7 concludes the thesis with a summary of findings and touching upon future work in this innovative arena of pharmaceutics. Appendix A presents supplementary data to compliment some of the work presented in this thesis.

Chapter 2 Literature Review

2.1 The Eye

2.1.1 Introduction

The eye is one of the most easily accessible organs of the human body. Despite this, the physiology and anatomy of the eye poses challenges with respect to ODD (Rathod, Kapadia and Sawant, 2017; Forrester et al., 2015; Mitra, Anand and Duvvuri, 2005). As a result of these hurdles, effective ocular formulations and devices must be developed in order to target specific ophthalmic tissue and to help control ophthalmic disease progression. To be able to overcome these barriers in ODD and to develop efficient devices for DD, it is important to fully understand and appreciate the eye; especially the relevant anatomical and physiological characteristics that may alter drug pharmacokinetics.

2.1.2 Anatomy of the Eye

The eye can be seen as a spherical entity made up of 2 spheres: the anterior chamber (front 1/3 of the eye) and the posterior chamber (back 2/3 of the eye). It is made up of several structures, all of which have specific functions with regards to the physiology of the eye (**Figure 2.1**).

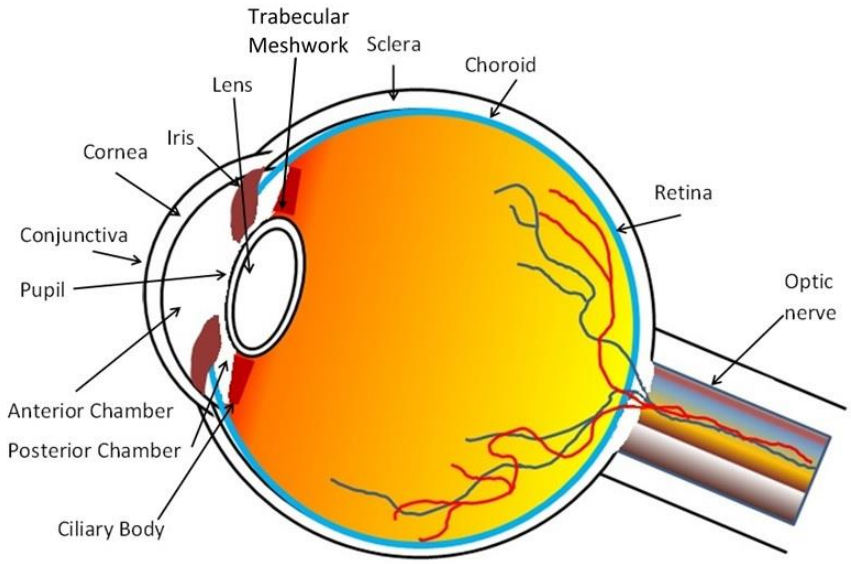

Figure 2.1 Structure of the Eye

2.1.2.1 The Cornea

The cornea is a transparent structure which makes up 7-10% of the eye. Its role is predominantly to protect the front of the eye and provide a majority of the optical focusing power, focusing the light that enters the eye (Forrester et al., 2015). The cornea is approximately 500 µm thick and 11 mm in diameter with no blood vessels. Due to this avascular nature and lack of blood supply, the cornea receives its nutrition from tears and the aqueous humour (AH), the gel-like substance that occupies the space behind the cornea.

The cornea is a multi-layered tissue, consisting of 5 layers. The outer most layer is made up of non-keratinised cells which are flattened and nucleated and connected via desmosomes. This layer, known as the corneal epithelium, is six cells (50-60 µm) thick. It is impenetrable to hydrophilic or polar molecules with molecular weight greater than 60 Da (for example glucose and ions), while lipophilic molecules such as oxygen or steroids can pass through via solubilisation in the lipid cell membrane. Below this comes the Bowman's Layer (also known as the Anterior Limiting Laminar); a posterior boundary that is separated from the epithelium by a thin basal lamina. It is 8-12 µm thick and made up of collagen fibrils (type I, III, IV, VI) 20-30 nm in diameter. The Bowman's layer merges with the corneal stroma, dense connective tissue (85% of the cornea) consisting of 200 to 250 layers of keratinocyte-containing collagenous lamellae of predominately type I collagen, each layer 1-2.5 µm thick.

Following the stroma is Descemet's membrane. A unique characteristic of this layer is its ability to repair itself following injury, which justifies its primary function to protect against infections and injuries. This layer consists of 2 sections; an anterior banded section which makes up 1/3 of the layer and the homogenous posterior section which makes up the final 2/3. Rich in basement membrane glycoproteins and type IV collagen, this is a layer approximately 5-20 µm thick which is connected to the final inner layer of the cornea, the endothelium, a very porous monolayer membrane. This one-cell thick layer contributes to the transparency of the cornea and also maintains corneal hydration through the presence of a water pump (maintaining corneal hydration in turn controls corneal thickness).

2.1.2.2 Additional Structures that make up the Eye.

The iris is the pigmented structure of the eye, located between the cornea and lens. Whilst the cornea focuses the light coming into the eye, the iris controls the amount of light entering the eye. The process by which it achieves this is similar to that of a diaphragm. The iris can dilate or contract the pupil, hence allowing more or less light in, respectively. The lens is a transparent structure which changes in shape to increase or decrease the amount of refracting power applied to the light coming into the eye. It is located behind the iris and focuses the light allowed through the iris onto the retina.

The ciliary body is an important part of the eye between the iris and choroid as it holds the lens in place and produces the AH. The AH is a transparent liquid gel which occupies the space between the lens and the cornea. It provides nutrients such as amino acids and glucose to the cornea and the lens. Its production exerts pressure in the space between the cornea and the lens, this pressure is known as the intraocular pressure (IOP) (Acott and Kelley, 2008). A complex structure called trabecular meshwork maintains the IOP at adequate levels (12-22mmHg) by controlling production and drainage (Martin, 1992). If this pressure is compromised, then the consequence can be severe, as with glaucoma where an increase of IOP causes blindness. The trabecular meshwork is located where the cornea meets the iris and allows the AH to drain into a set of tubes called the Canal of Schlemm to systemic blood flow. The AH is also believed to have an immunological function in that it defends against pathogens due to the presence of immunoglobulins in the gelatinous fluid.

The sclera is the white of the eye; it is an opaque white tissue 5-30 µm thick predominately made up of Type I collagen. It serves as anchor tissue for extraocular muscles. The retina can be seen as an extension of the brain as it is a layer of nerve tissue which is stimulated by light. This induces an electrochemical reaction in which electrical impulses are transmitted to the brain, resulting in vision. The conjunctiva is a vascularised membrane that lines the inside of the eyelid and covers the sclera. It facilitates lubrication of the eye via the production of mucus and tears. There is also a microbiological aspect to the conjunctiva; it prevents microbes entering the eye. The choroid consists of layers of blood vessels between the sclera and the retina and provides nourishment to the back of the eye. The optic nerve carries the electrical impulses from the

photoreceptor cells (rods and cones) in the retina to the visual cortex in the brain. In glaucoma, this can become damaged due to increase in IOP.

2.1.3 Drug Transport through the Cornea

The main route for drug transport to the anterior chamber is via the cornea. There are two recognised pathways for drug transport: paracellular movement and transcellular movement. Paracellular movement involves the transport of molecules between cells whilst transcellular movement involves the molecules travelling through the cells, in this case passing through all 5 layers of the cornea (**Figure 2.2**).

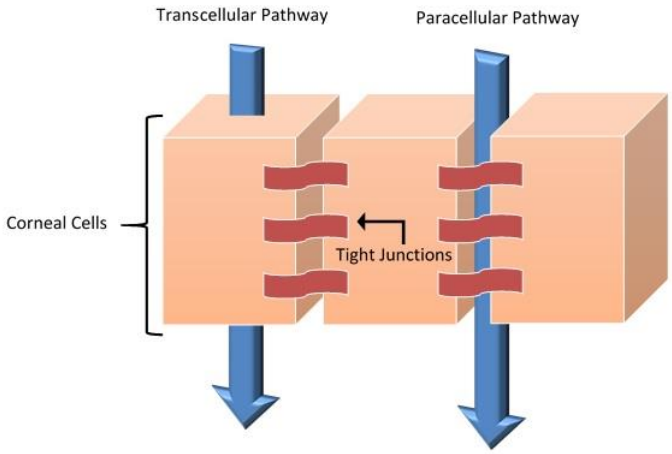

Figure 2.2 Schematic diagram illustrating the transcellular and paracellular movement of drug molecules through corneal tissue

2.1.3.1 Paracellular Transport

This mechanism of drug transport comprises the drug molecules moving through the spaces between cells (Forrester, 2008). This mode of transport is often unlikely in corneal drug delivery due to the cellular arrangement of the outer corneal epithelium. A majority of ocular drugs are too large (<100Da) to pass through and across the Bowman's Layer. Paracellular movement is possible through the stroma but as a result of its hydrophilic nature, transport is limited to only polar molecules. Hydrophilic molecules can also pass through pores in the epithelial layer but larger molecules are often limited by tight junctions.

2.1.3.2 Transcellular Transport

Transcellular movement through a membrane is based on diffusive methods or partitioning into and within cell membranes (Forrester, 2008). There are two main pathways for drug molecules to reach the anterior chamber behind the cornea. The first pathway, known as the lateral route, involves the drug molecule partitioning from the hydrophilic stroma into the lipophilic endothelium followed by diffusion within the lipid rich endothelium and partitioning into the AH. The alternate route, the transverse route, entails partitioning of drug molecules out of the anterior cell membrane into the posterior cell membrane and diffusing out.

2.1.4 Barriers in Ocular Drug Delivery

It is clear to see why the structure of the cornea poses such a challenge to achieve high drug bioavailability (BA) in the eye. As a result of years of research, the factors that affect drug permeation have been established and categorised into 3 groups: physiochemical factors, physiological factors and formulation factors. Physiochemical aspects are associated with the drug properties that affect drug diffusion whilst physiological barriers refer to precorneal factors. A summary can be found in **Table 2.1** (Forrester, 2008; Forrester et al, 2015; Agrahari et al., 2016; Djebli et al, 2017).

Table 2.1 Summary of the factors that affect ocular drug permeation

Physiochemical	
Partition Coefficient	To successfully permeate through the multiple layers of the cornea, ocular drugs must possess amphiphilic traits; be both lipophilic and hydrophilic. Drugs with low partition coefficients are unable to permeate the corneal epithelium and those with high partition coefficients reside in the epithelium. The partition rate in the anterior segment is very low resulting in insufficient drug amount or drug concentration in the AH.
Molecular Weight	Small molecules (<500Da) are able to diffuse through corneal membranes as passive diffusion is the prevalent mechanism of transport
Solubility	Drug solubility will dictate the permeation rate of the drug through the cornea. A poorly soluble drug will prevent therapeutic concentrations of drug reaching the target tissue (anterior chamber). A highly soluble drug can however also result in drug saturation ad even overdose, resulting in unwanted side effects.
Ionisation Constant	A majority of ocular drugs are weak acids or bases at physiological conditions. At eye pH (7.2), there will be partial ionisation of these drugs, resulting in higher corneal permeation due to a larger percentage of drug being in its unionised form. The ionised form of the drug will pass through the cornea via transcellular transport; hence not achieving an effective dose in the AH.
Physiological	
Dilution via tears	Upon blinking, the drug is constantly diluted by tear fluid production, reducing the concentration of the drug permeating the eye.
Nasolacrimal Drainage	Typical precorneal volume on the eye surface is approximately 7µl but it can hold up to 20µl-30µl. The production of tears is approximately 1.2µl/min, meaning a turnover rate of 16% per minute. A typical eye drop is around 50µl; meaning the excess product that cannot be held in the precorneal area drains into the nasolacrimal duct and taken away into the systemic blood flow. The larger the volume instilled on the eye, the more drug that will be drained away via the nasolacrimal duct.
Properties of the membrane	Factors such as thickness, porosity and amphiphilic balance of the tissue will also dictate drug permeation through the cornea. The complexity of the cornea composition proves to be a great barrier to drug permeation. Due to its lipophilic nature, the epithelium is the rate limiting barrier for hydrophilic compounds while the hydrophilic nature of the stroma (a result of type I collagen) is the biggest barrier for lipophilic molecules.
Formulation	
Concentration	Increasing drug concentration can increase drug permeation however it is vital not to exceed the maximum safety concentration and toxicity levels which could result in hypertonicity; increasing nasolacrimal drainage.
Particle Size	Due to poor solubility of ocular drugs, suspensions are often the port of call or a back in ODD. As the drug is present as physical particles, the retention time in the eye is increased, increasing drug bioavailability. However, particles that are larger than 10µm are detected as foreign bodies and are readily removed from the eye via tear drainage.

2.1.5 Routes of Administration in Ocular Delivery

There are three main administration routes for the treatment of ocular conditions: topical, local ocular and the systemic approach. The selected approach is often determined by the targeted tissue and ocular condition. The topical line of therapy is preferred predominantly due to cost and patient compliance. Ease of administration for a patient is also a major advantage with topical delivery of ocular drugs (Wilson, 2004). However, despite being a non-invasive method, only 5% of the drug reaches the targeted tissue. High tear turnover rate (16% per minute) and dilution (as a result of tear production) can also have a significant effect on drug delivery causing the drug to be pumped into the drainage canals and taken away in systemic circulation (Wilson et al., 2011).

For treatment of posterior segment conditions, systemic approaches are taken through the use of tablets. Like topical delivery, only 1-5% of the drug reaches the targeted region due to the nature of the eye tissue. Systemic administration of drugs for ocular conditions are often rejected due to the very small ratio of eye to the body (Agrahari et al., 2016). Many ocular drugs also have multiple effects on different systems of the body. For example, anti-glaucoma drug timolol also acts as a non-selective β-adrenergic blocking agent acting on the sympathetic nervous system, which can cause a decrease in blood pressure and can slow cardiac activity and lung function (Pratt et al., 2015).

Anatomical barriers (due to the various structures that make up the eye) make precise drug delivery challenging. For example, the blood aqueous barrier (BAB) and the blood retinal barrier (BRB) limit the BA of the drug and are the major barrier for drug delivery to the anterior segment and posterior segment, respectively. The BAB is a bilayer membrane consisting of an endothelium of ciliary blood vessels and the non-pigmented ciliary epithelium. The nature of the two distinct layers and the presence of the tight junctions limit the entry and/or permeation of drugs into the intraocular region. The BRB is a physiological barrier made up of two segments. The inner BRB consists of tight junctions between retinal capillary endothelial cells whilst the outer BRB is made up of retinal pigment epithelial cells held together by tight junctions. While systemic administration is favourable for drug delivery to the retina, the BRB mediates the penetration of drugs. Due to the selective permeability of this membrane, frequent dosing is

essential to ensure therapeutic effect (Thrimawithana et al., 2011). However, frequent administration can result in systemic toxicity and adverse side effects.

As a result of low BA and potential side effects, more novel approaches have been developed to improved ODD to the posterior segment. One such approach is intravitreal injections. Despite low patient compliance, these injections are capable of delivering therapeutic agents directly to the target tissue, bypassing the anatomical barriers of the eye. Using a very fine needle (30-G diameter), the drug solution is injected directly to the vitreous and retina. Regardless of the delivery of the drug at high concentrations directly to the targeted region, drug distribution is not homogenous. Another challenge with intravitreal injections concerns the clearance of the drug. Direct delivery to the vitreous means drug clearance occurs either via the anterior pathway or posterior pathway. The aqueous clearance pathway consists of the drug diffusing through the AH and is subsequently drained whilst the posterior pathway involves drug management across the BRB, requiring active transport (Mitra et al., 2005). Due to this, hydrophilic solutes with high molecular weight remain in the vitreous humour for extended period of time. This, alongside repetitive perforation of the eye tissue can lead to the development of conditions such as endophthalmitis and cataracts.

Research in this field is constantly evolving, resulting in developments of more innovative methods to overcome limitations of conventional methods of ODD. Periocular administration can effectively deliver drugs to the posterior chamber. DD using this method can advance to the posterior segment in one of three ways: transceral, systemic circulation (through the choroid) and the anterior pathway through the tear film and cornea, the AH and the vitreous humour (Moisseiev and Loewenstein, 2017). Whilst boasting high drug levels, the risks of subconjunctival and retrobulbar haemorrhage is high alongside increased probability of fast drug elimination via systemic circulation.

2.2 Conventional Topical Ocular Drug Delivery Dosage Forms

The choice of dosage form or device for ocular drug delivery is dependent on an array of aspects, predominately the ocular condition in question and the severity of the condition. The following section will discuss conventional topical approaches for therapeutic ODD.

2.2.1 Eye Drops

Eye drops make up approximately 90% of all topical ocular formulations, in the form of solutions, suspensions and emulsions (Conway, 2008). As a result of the nature of the targeting tissue and the mode of application, extreme care is needed for such formulations to be isotonic, non-invasive and sterile. Despite ease of formulation and patient compliance, making eye drops favourable to both manufacturers and patients alike, there are some drawbacks. Less than 5% of the drug from a typical eye drop (50 µL) actually permeates the cornea (Schopf et al., 2015). Precorneal volume is around 7 µL; hence most of the administered eye drop overflows and leaks from the eye. In addition to this, anatomical, physiological, metabolic and biochemical properties and barriers of the eye can result in drug loss via nasolacrimal drainage (Schopf et al., 2015). Here, the diluted formulation (due to instigation of tear production upon introduction of eye drop) can be carried away to the blood stream or nasal cavity reducing the amount of drug/active reaching targeted site. Consequently, frequent administration of drug is needed in order to achieve the therapeutic drug levels in the eye.

In a bid to improve the residence time of the drug in the eye, additives such as viscosity enhancers, permeability enhancers and cyclodextrins have been incorporated into formulations.

Aceclofenac, a non-steroidal anti-inflammatory drug (NSAID), is commonly used to treat anterior chamber inflammation alongside pain and inflammation associated with post-operative treatment. Dave and Paliwal used preservatives such as methyl paraben, propyl paraben, benzalkonium chloride (BAC) and viscosity enhancer hydropropyl methylcellulose (HPMC) to decrease the permeability coefficient of the NSAID (Dave and Paliwal, 2014). Moreover, the apparent permeability coefficient was also reduced by increasing the solution pH value from 6.0 to 8.0. The combination of MP, PP and BAC enabled an increase in the transcorneal permeation of this active drug whilst pharmacodynamics *in vivo* studies showed this novel formulation was

more effective than commercially available Voltaren® ophthalmic drops 0.1% (diclofenac sodium).

Some ocular drugs (e.g. dexamethasone (Shulman et al., 2015)) and metabolites (e.g. prednisolone (Couto et al., 2014)) are poorly-soluble or insoluble in aqueous media. These materials can be complexed with cyclodextrins (CDs) to form water soluble inclusion complexes, increasing their solubility. CDs are amphiphilic (they have both hydrophobic and hydrophilic regions) cyclic oligosaccharides which have been extensively used to improve the solubility and stability of some ocular drugs such as dexamethasone (Shulman et al., 2015), dorzolamide (Gudmundsdottir et al., 2014; Johannesson et al., 2014), ciprofloxacin (Nijhawan and Agarwal, 2003) and cyclosporine A (Kapoor and Chauhan, 2008). Nijhawan and Agarwal developed a ciprofloxacin-loaded ophthalmic preparation by inclusion complexes of ciprofloxacin hydrochloride with hydroxypropyl-β-CDs. The complexes (produced using freeze drying) exhibited increased water solubility of the drug, stability, biological activity and ocular tolerance when compared to a commercially available ocular formulation (Nijhawan and Agarwal, 2003). Couto et al exploited the amphiphilic nature of dimethyl-β-CDs to form complex with prednisolone and HPMC. Prednisolone (a water insoluble corticosteroid) manipulates the body's immune system response conditions such as arthritis, cancers and eye conditions (e.g. keratitis). Dimethyl-β-CDs increased drug water solubility and maintained pseudoplastic behaviour in the suspension that presented a d90 lower than 90 µm (particle size) (Couto et al., 2014).

2.2.2 Emulsions

Incorporating additives is one approach to improve liquid formulations for topical drug delivery to the eye. Modifying the physical properties of the ocular cells (e.g. membrane permeability, cellular uptake), attempts to increase drug penetration and drug presence at the site of action is another common approach.

Emulsions are often used to improve the solubility of poorly soluble drugs. They are heterogeneous dispersions of oil in water (o/w) or water in oil (w/o), usually with the addition of surfactants or co-surfactants (Khadka et al., 2014). Emulsions are considered to be advantageous to topical ODD due to their ability to increase membrane permeability and cellular uptake (due to the presence of surfactants) (Gasco et al., 1989). The underlying theory for this

revolves around the fact that surfactants interact with the lipid bilayer around ocular cells modifying their physiochemical properties. Surfactant saturation in the lipid bilayer consequently leads to the formation of micelles which act to remove lipids from the cell membrane by solubilisation, in turn increasing the membrane permeability. This fundamental principle has led to numerous studies finding increased drug concentration in vital structures of the eye (Bar-Ilan et al., 1994; Acheampong et al., 1996). There are various ways of categorising emulsions, the most common is via droplet size. Nano-(submicron) emulsions usually contain droplets 100-1000nm in diameter whilst droplets in micro-emulsions range from 10nm to 100nm and in macroemulsions 0.5 μm to 100 μm.

The use of emulsions in topical ODD was first investigated in 1989, for the treatment of glaucoma. Incorporation of surfactant lecithin to an o/w microemulsion increased the BA of timolol in the AH when administered to the conjunctival sac of rabbits. When compared to a lecithin-free formulation there was 3.5 times as much drug present in the AH (Gasco et al., 1989). Lidocaine, (a hydrophobic drug), has been entrapped in various oil-in-water microemulsions (~10-20 nm particle size) before dispersion through poly (hydroxyethyl methacrylate) (pHEMA) lenses (Gulsen and Chauhan, 2005). Gulsen et al found that these particles gave a burst release at first (35% of drug) followed by 80% and 95% of the drug being released within 4 days and 9 days, respectively.

More recently, topical ODD with respect to emulsions have turned to nanoemulsions; o/w or w/o. The dispersed phase is in the form of nanodroplets 50-200 nm in diameter heterogeneously dispersed within the external immiscible phase. These formulations are useful for the delivery of both hydrophilic and lipophilic drugs (Tamilvanan and Benita, 2004), however they are still subject to emulsion instabilities: coalescence (droplets coming together to make larger droplets), flocculation (aggregation of droplets to give 3D clusters without coalescence) and Otswald ripening (growth of emulsion droplet due to changes in chemical potential). Nanoemulsions have been investigated for the delivery of a wide range of bioactive molecules like antibacterial agents (e.g. cetalkonium chloride (Daull, Lallemand and Garrigue, 2014)) and anti-glaucoma drugs (e.g. dorzolamide hydrochloride (Ammar et al., 2010)). The anti-glaucoma drug delta-8-tetrahydrocannabinol was one of first drugs to be encapsulated successfully into a nanoemulsion for topical ODD. The lipophilic drug was incorporated into the oil phase of a

submicron emulsion (mean droplet size: 130±41 nm) and showed an intense and long lasting reduction effect for the IOP. This formulation remained stable after steam autoclaving and after storage for 9 months (Muchtar et al., 1992). These promising results sparked a search for more biocompatible actives for extended action in the eye.

Incorporation of surfactants ultimately affects the charge of formulation and due to this cationic surfactants have been found to increase BA of drugs due to electrostatic interactions between the cornea and membrane protein (mucin); hence, increasing drug residence time in the cornea (Daull et al., 2012; Wei et al., 2011). However, their toxicity is a disadvantage that needs to be overcome and because of this very few have been approved for ocular use.

Novagali, a French pharmaceutical company, developed a cationic nanoemulsion that improved drug delivery by exploiting the negative charge of ophthalmic cells at physiological pH. The use of positively charged formulations can increase the electrostatic interactions between the formulation and biological tissue, consequently increasing the residence time. This innovative technology has already been used to deliver cyclosporin A (Cyclokat® and Vekacia®) (Lallemand et al., 2012) with several more applications in the pipeline including latanoprost delivery for glaucoma treatment (Ismail et al., 2011).

More recently, emulsion cross-linking and formulation optimisation via factorial design was utilised to improve precorneal residence time and drug penetration of the hydrophilic antibiotic doxycycline hydrochloride. The particles (331-850 nm size range) encapsulated around 45-80% of the drug. This formulation showed sustained drug release with significant antibacterial effect on strains of *Staphylococcus aureus* and *Escherichia coli* ($p<0.011$) as compared to doxycycline hydrochloride aqueous solution (Pokharkar, Patil and Mandpe, 2015).

2.2.3 Hydrogels

Hydrogels (HGs) are hydrophilic polymeric matrices capable of swelling after water uptake, allowing drug diffusion in and out of the system. Once swollen, the HG matrix is approximately 60-90% water (Kang-Mieler and Mieler, 2016). These gels can form before administration or *in situ*; however, more emphasis has been placed on the latter due to ease of administration and precision of solution compared to gels (Anumolu et al., 2009). Phase transition on the ocular

surface increases formulation residence time and hence increases drug exposure. Both natural polymers (e.g. gelatin (Prabhu et al., 2015), dextran (Chau-Minh Phan et al., 2014), alginate (Liu, Griffith and Li, 2008), chitosan (Cheng et al., 2014; Prabhu et al., 2015), polysaccharides (Xu et al., 2013)) and synthetic polymers (e.g. HEMA) (Hu and Li, 2013; Rapado and Peniche, 2015), glycolic acid (Gasmi et al., 2015; Do et al., 2015) have been used as swellable matrices. It is important to note that the selection of polymer is crucial due to the effect on the final HG properties. Due to different polymers having different advantageous characteristics, it is common to blend two or more polymers to obtain optimised HG systems. For example, chitosan has been blended with gelatin and glycerol phosphate to develop a thermoresponsive HG which enhanced *in vitro* and *in vivo* compatibility for the delivery of latanoprost (Cheng et al., 2014). *In vivo* release studies in rabbit models demonstrated steady drug concentration in the aqueous humour without burst release. This sustained release system continued for 8 days with IOP being restored within this time period and maintained for a further 31 days (Cheng et al., 2014).

Chitosan has also been combined with PNIPAM to exploit the thermosensitive nature of PNIPAM to develop an *in situ* thermoresponsive HG for the delivery of antiglaucoma drug TM (Cao et al., 2007). *In vivo* studies showed increased drug permeation in rabbit cornea in the absence of any cytotoxicity. Compared to conventional TM eye drops, despite the onset of action being observed at t=0.5 hours, the HG demonstrated stronger IOP reduction, highlighting the potential of chitosan-PNIPAM blend for improving efficacy of TM (Cao et al., 2007).

Temperature is not the only stimulus that has been employed to trigger the swelling of HG matrices; pH triggered systems (e.g. Poly acrylic acid (PAA) (Dubey and Prabhu, 2014; Patel et al., 2012)), ionic strength (e.g. sodium alginate (Khan et al., 2015; Nanjwade et al., 2012; Shastri, Patel and Parikh, 2010)) and enzyme substrate systems have also been evaluated. PAA is a polymer which has a large array of applications, including as a thickening agent, a suspending agent and emulsifying agent. In physiological conditions and aqueous environment, PAA is an anionic polymer and is commonly combined with HPMC to increase the viscosity of the formulation, ultimately increasing drug residence time (Dubey and Prabhu, 2014).

Dubey et al studied the *in vivo* IOP lowering activity of PAA (carbopol C 934p)-HPMC stimuli sensitive HG (Dubey and Prabhu, 2014). Once administered to the eye, the pH changed

accordingly causing the HG to increase in viscosity, providing sustained release of the drug. *In vitro* release studies demonstrated zero order release with 90% of the drug (TM, brimonidine tartrate) being released within 8 hours; exhibiting sustained release. The ability of the novel stimuli-sensitive TM and brimonidine tartrate loaded HG to lower IOP was compared to a marketed formulation. Whilst the marketed formulation was able to lower the IOP, it failed to maintain this reduction. The newly formulated HG with a combination of both drugs achieved greater IOP reduction, which was maintained for a longer time than the marketed formulation (Dubey and Prabhu, 2014).

Sodium alginate is a viscosity enhancer often used in drug delivery due to its ability to undergo gelation as a result of changes in ionic strength (Mandal et al., 2012). Sodium alginate is susceptible to phase change when exposed to divalent ions such as magnesium and calcium; an ion which is abundant in tear fluid (Mandal et al., 2012; Liu et al., 2010). This property of sodium alginate has been exploited to increase drug residence time. For instance, along with methyl cellulose it was successfully used to formulate a novel *in situ* gelling matrix for therapeutically efficacious sustained release and stable ophthalmic drug delivery of moxifloxacin hydrochloride (Nanjwade et al., 2012). There are also some marketed formulations already available for topical ocular delivery of TM. Timoptic-XE® is based on anionic heteropolysaccharide derived from gellan gum. In this product, an aqueous solution of gellan gum, in the presence of a cation (in precorneal tear fluid), has the ability to gel, allowing prolonged exposure to the product, increasing drug release.

2.2.4 Contact Lenses

Whilst there have been attempts to improve conventional methods to accomplish extended drug exposure time to ophthalmic tissue, these methods are no longer adequate for treating ocular conditions. Despite good patient compliance and simple administration, there are some fundamental drawbacks with respect to the formulation itself (e.g. eye-drops, hydrogels). The extended residence time, blurred vision (as a result of increased formulation viscosity) (Gupta et al., 2007) and poor availability (due to nasolacrimal drainage) can limit the application/administration of such formulations to specific times (e.g. night) (McGhee, Dean and Danesh-Meyer, 2002).

As a result the need to overcome these challenges, research has shifted focus onto developing various ocular devices for successful, controllable drug delivery. The most common device to emerge from this research are contact lenses (CLs). CLs are polymeric discs which are inserted into the eye and come into contact with the cornea; held to the corneal tear film by surface tension (Lin and Svitova, 2010; Vidal-Rohr., 2018). The primary function of contact lenses is to correct vision imperfections (e.g. conditions such as astigmatism and myopia) (ElShaer et al., 2014), but their uses have also been exploited in cosmetics/aesthetics as well as therapeutics and theranostics (Peng, Kim and Chauhan, 2010; Thomas, Lähdesmäki and Parviz, 2012; Kaczmarek et al., 2014; Tashakori-Sabzevar and Mohajeri, 2015a).

The idea of CLs was first conceptualised by Sir John Herschel in 1832; with the first glass CL being developed in 1887. In the 1960's, there was a major breakthrough for CLs where Wichterle and Lim experimented with soft, water-absorbent materials for biological use (Wheeler et al., 1996) whilst advances in material development led to a breakthrough in the topical ocular drug delivery arena. The crosslinking of monomer 2-hydroxyethyl methacrylate with ethylene glycol dimethylacrylate yielded pHEMA. This polymer is capable of forming flexible hydrophilic hydrogels (ElShaer et al., 2014). The characteristic capacity for pHEMA to retain up to 38% water forming flexible systems was able to overcome the disadvantages met with earlier proposed rigid materials (e.g. glass).

Due to advances in material development, monomers (e.g. tris(trimethylsiloxy) silane) were the choice to fabricate silicone hydrogels (Vanderlaan et al., 1999). These lenses possessed increased oxygen permeability, unlike conventional pHEMA lenses and therefore could be worn for prolonged periods of time. Silicone lenses have a more rigid structure, accordingly development and manufacture was much easier. It is only in the last two decades that CLs have been considered as useful devices suitable for drug delivery for such drugs as antibiotics, NSAIDs and anti-glaucoma drugs. As a result, many concepts (conventional and novel) to alter HG lenses have been introduced to achieve sustained/extended ocular drug delivery. For example, timolol has been incorporated into contact lenses which exhibited 12 hours of sustained release (Alvarez-Lorenzo et al., 2002) while lidocaine-loaded contact lenses demonstrated a sustained release over 8 days (Gulsen, Li and Chauhan, 2005).

2.2.4.1 Mechanisms of Drug Loading

It has only been in the last two decades that ocular lenses have been considered as an advantageous device suitable for drug delivery. Various methods have since been developed to produce drug eluting contact lenses.

2.2.4.1.1 Soak and Release

One of the first attempts to develop drug loaded CLs involved soaking pre-prepared or commercial lenses in a saturated aqueous drug solution, allowing the drug to be taken into the hydrophilic matrix of the lens (via diffusion). This conventional method was first proposed over 40 years ago (Waltman and Kaufman, 1970) and is now commonly used for the delivery of anti-glaucoma drugs (Hillman, 1974; Kim, Conway and Chauhan, 2008; Peng, Burke et al., 2012; Peng, Ben-Shlomo et al., 2012), antihistamines (Soluri, Hui and Jones, 2012; Karlgard et al., 2003) and antibiotics (Peng et al., 2010). Upon insertion in the eye, initial burst release of drug is achieved followed by sustained release via diffusion. The drug solution can alternatively be topically applied to the eye with the lens *in situ*.

Hillman et al were one of the first to utilise this method using the cholinergic anti-glaucoma drug pilocarpine hydrochloride. A blend of vinyl pyrrolidone/acrylic monomers were used as CL material. The resulting hydrophilic lenses was soaked in a 1% drug solution and inserted into the eyes of patients with acute closed angle glaucoma. An average of 54.8% IOP reduction was observed within 2 hours, notably comparable to the 49.7% IOP reduction seen with intensive pilocarpine treatment (1-2 drops every minute for 5 min, every 5 min for 30 min) (Hillman, 1974).

More recently, the potential delivery of hyaluronic acid from CLs was assessed for the treatment of dry eye syndrome. The HG CLs loaded with hyaluronic acid exhibited release for up to 48 hours; whilst maintaining the physical properties of the lens. *In vivo* release pharmacokinetics in rabbit tear fluid demonstrated an effective increase in residence time in comparison to eye drops (Maulvi, Soni and Shah, 2015).

In an attempt to retard the diffusion of hydrophilic drugs from CLs for sustained release, vitamin E (VE) has been incorporated into lens matrices to provide a hydrophobic barrier (Peng et al., 2010; Peng et al., 2012; Peng, Burke and Chauhan, 2012; Hsu, Fentzke and Chauhan, 2013; Hsu

et al., 2015; Kim, Peng and Chauhan, 2010). Soaking of lens in VE:ethanol solution prior to drug loading poses a barrier to the drug molecules when diffusing out of the matrix, presenting the potential for sustained drug delivery which is advantageous for conditions where frequent doses are essential.

Cytinosis is a rare genetic condition which mostly affects children in which the amino acid 'cysteine' accumulates in vital organs (eye, kidney, pancreas and brain). Hsu et al developed lenses loaded with cysteamine with incorporation of VE to achieve sustained drug release (K. Hsu et al., 2013). Addition of VE increased drug duration from 10 minutes to 3 hours in solution. The lenses exhibited therapeutic concentration of the drug within 2 hours of the lenses being worn, mimicking the action of hourly eye drops. Hsu et al also demonstrated that 20-30% of VE increased the release of moisturising agent dexpanthenol and osmoprotectant betaine (compatible solutes that restore cell volume, stabilise proteins and protect cells from hyperosmolarity stress (Giannaccare, Fresina and Versura, 2016) from silicone lenses to 10 hours; 60 times longer than unmodified lenses (Hsu et al., 2015). Topical anaesthetics such as lidocaine, bupivacaine and tetracaine (all hydrophilic at physiological pH) were loaded into VE soaked lenses (Peng et al., 2012). These lenses continually released drug for 1-7 days, beneficial for post-operative pain of corneal surgery.

Along with impeding drug diffusion, VE aggregates can provide UV protection to the cornea without altering lens transparency. Operating at a wavelength smaller than that of visible light ensures there is no obstruction with respect to vision (Gonzalez-Chomon, Conchiero and Alvarez-Lorenzo, 2013). Although the method of soak and release has been met with various successes, the main challenge is to achieve and maintain controlled release kinetics.

2.2.4.1.2 Molecular Imprinting

Molecular Imprinting (MI) is a more recent technique in which nano-cavities are created within the lens matrix, which are subsequently used in molecular recognition. Incorporation of functional monomers (e.g. methacrylic acid (MAA)) on polymer backbone advances drug affinity to the lens by providing sufficient binding sites for drugs (Hiratani and Alvarez-Lorenzo, 2004). Selection of the functional monomer is crucial; they must be compatible with the lens material and also have high affinity to the active. The process of MI is based on arranging the functional

monomer around the drug molecules during polymerisation, creating a fixed, rigid structure due to the cross-linking stage in polymerisation (Hiratani and Alvarez-Lorenzo, 2004). The drug and any unreacted monomers are extracted leaving behind nano-cavities that only have molecular recognition for that particular drug. The lens can then be loaded by soaking in drug solution. MI is also a sought out technique as it enhances the spatial arrangement of the lens matrices, ensuring maximum drug loading.

Timolol has been used with MAA acting as the functional monomer and ethylene glycol dimethacrylate as the cross-linker due to its ionic interaction with timolol (Korogiannaki et al., 2015; Tashakori-Sabzevar and Mohajeri, 2015b; Alvarez-Lorenzo et al., 2002; Guidi, Korogiannaki and Sheardown, 2014). Hiratani et al were among the first to evaluate the *in vivo* potential of MI N-N-diethylacrylamide lenses (Alvarez-Lorenzo et al., 2002; Hiratani and Alvarez-Lorenzo, 2002). Using different concentrations of the cross linker ethylene glycol dimethacrylate, Hiratani et al utilised the MI method to increase timolol loading capacity. Imprinted contact lenses increased the hydrogels affinity for timolol, demonstrating prolonged drug release in the tear fluid of rabbits. Timolol from MI lenses was detected for 180 minutes; two fold longer than that found by non-imprinted lenses and three times longer than the 60 minutes observed with 0.25% aqueous eye drops (Alvarez-Lorenzo et al., 2002). The same team also prepared imprinted HGs that increased the uptake of broad-spectrum antibiotic norfloxacin (300 fold) using acrylic acid as the monomer (Alvarez-Lorenzo et al., 2006).

Other therapeutic agents have also benefitted from MI including NSAIDs (where a tenfold increase ibuprofen and diclofenac loading capacity with sustained release for up to a week was observed (Andrade-Vivero et al., 2007)) and antibiotics (e.g. polymyxin B and vancomycin (Malakooti, Alexander and Alvarez-Lorenzo, 2015), ciprofloxacin (Hui, Sheardown and Jones, 2012; Hui, Willcox and Jones, 2014)).

Hui et al developed imprinted lenses with acetic acid and acrylic acid (the functional monomer) that extended the release duration of ciprofloxacin to 3-14 days (Hui et al., 2012). Using various ratios of acetic acid to ciprofloxacin solution, Hui et al also developed MI silicone lenses (Hui et al., 2014). Compared to non-imprinted lenses, the modified lens matrices released ciproflaxcin for a considerably longer time (p<0.05). The MI lenses were evaluated for the ability to inhibit

gram negative bacterium *Pseudomonas aeruginosa.* Lenses loaded with 0.3% ciprofloxacin demonstrated complete bacteria inhibition for initial two days, showing inhibitory concentrations of drug were being reached/released from the lenses. However, after day three, an increase in the bacterial concentration was observed; this was thought to be due to the reduction of ciprofloxacin concentration after being released from the lenses. Although differences in bacteria population was observed when comparing both non-imprinted lenses and MI lenses; they were not statistically significant (p>0.05) (Hui et al., 2014).

2.2.4.1.3 Modifying Lens Composition

The permeability of ocular therapeutic agents can be affected by their charge in physiological conditions. Modifying the lens composition and exploiting the ionic interactions of functional monomers can potentially aid in achieving sustained and/or controlled drug release (Hsu, Gause and Chauhan, 2014). Variations in these side groups ultimately affect the final properties of the HG lenses; subsequently, the monomer used and its ratios can be altered to achieve specific criteria. Incorporating cationic or anionic functional monomers (also known as ligands), can increase the weak interactions (e.g. hydrogen bonding, electrostatic forces), allowing the HG matrices to store charged drugs on the basis of ion exchange reactions. Ergo, the percentage of HG matrix that is made up of ligands will be directly proportional to the drug loading efficiency (Hsu et al., 2014).

MAA is the most common ligand used to increase the ionic interactions in lenses, predominantly in pHEMA lenses and is highly anionic and hydrophilic. Release kinetics of various ophthalmic drugs from MAA-loaded lenses has been studied numerous times, all yielding promising results (Uchida et al., 2003; Sato et al., 2005; Garcia-Millan, Koprivnik and Javier Otero-Espinar, 2015). Uchida et al have developed contact lenses using hydrogels with cationic functional groups on the side chain (using methacrylamidopropyltrimethylammonium chloride and 2-hydroxyethyl methacylate to obtain the cationic group) (Uchida et al., 2003). The hydrogels were capable of storing azulene (anionic drug), by the effect of ion exchange reaction, and releasing the drug under physiological conditions. There was a problem relating to the size change of the hydrogel pre- and post- drug release; changes which were prevented by adding anionic monomers MAA and 2-methacryloyloxyethyl phosphate to the matrix (Uchida et al., 2003). These monomers were also added to pHEMA lenses which resulted in extended release of naphazoline (a cationic

vasoconstrictor). About 85% of the drug was released within 14 hours, with the uptake of drug increasing in turn with increasing the amount of anionic ligands within the matrix (Sato et al., 2005).

Copolymerisation of pHEMA soft lenses with functional monomers (different concentrations of MAA or N-vinyl-2-pyrrolidone) was used to assess the *in vitro* release kinetics of corticosteroid triamcinolone acetonide (Garcia-Millan et al., 2015). The modified lenses with MAA exhibited similar swelling behaviour in physiological condition. However, MAA-containing lenses demonstrated a higher degree of swelling with the change in pH as a result of repulsive forces contained by the hydrogel (generated by ionisation of carboxyl groups of MAA residues). Moreover, MAA lenses showed the best drug loading and the fastest drug release when compared with N-vinyl-2-pyrrolidone hydrogels (Garcia-Millan et al., 2015).

On basis of the ion-ligand mechanism, the *in vitro* uptake of antibiotic agents gatifloxacin and moxifloxacin was assessed (Kakisu et al., 2013). The drug uptake seemed to increase as percentage weight of anionic MAA increased. Initial burst release kinetics were observed from the modified lenses where *in vivo* studies exhibited greater drug concentration in cornea (gatifloxacin: 0.89 μg/mL, moxifloxacin: 2.22 μg/mL) and aqueous humour (gatifloxacin: 4.1 μg/mL, moxifloxacin: 9.35 μg/mL) after 24 hours when compared to antibacterial eye drops with the same antibacterial agents, which indicate an improvement in penetration into the eye.

Whilst previous studies focussed on incorporating ligands via copolymerisation, another novel concept was proposed which saw the use of surfactants to improve the release of ionic drugs for more than two hours. Generally, this can be done by creating a high surface charged lens by adsorbing an ionic surfactant on the hydrogel matrix increasing the sustained release of active for an extended time. For instance, pHEMA CLs were developed for the controlled release of anionic drug dexamethasone 21-disodium phosphate using the cationic surfactant cetalkonium chloride. The drug release time was significantly improved from 2 hours to 50 hours (Bengani and Chauhan, 2013).

Altering the composition of the matrix can also solve the issue of low oxygen permeability. Ocular hypotensive active (timolol) and the steroid (dexamethasone) have been released at a sustained rate from lenses when silicone polymers have been used to replace conventional lens

material (pHEMA) (J. Kim et al., 2008). Silicone polymers are highly advantageous with regards to O_2 permeability but can encounter problems with lack of patient compliance as a result of decreased water content leading to stiffness of the lens (Compan et al., 1999).

2.2.4.1.4 Colloidal Carriers and Nanocarriers

The arena of nanotechnology has already been successfully exploited in drug delivery for an array of therapeutic applications e.g. transdermal (Khan et al., 2014), nasal (Rassu et al., 2015) and ocular (Mehta et al., 2015). The concept has extended to ocular drug delivery via contact lenses in the form of nanoparticles (NPs), surfactants, liposomes and CDs. The nature of these nano-carriers can protect sensitive materials from harsh external environments and can prevent drug degradation; the drug can exist in an environment they would otherwise be unstable in. The sizes of these colloidal carriers also prove advantageous and patients' vision is not compromised upon administration whilst increasing drug loading. The most common types of NPs are either lipid-based or polymeric-based.

2.2.4.1.4.1 Liposomes

Liposomes are amphiphilic, closed bilayer phospholipid vesicles. They consist of a hydrophilic core and surface with an internal hydrophobic ring. Their amphiphilic nature enables them to encapsulate both hydrophilic and lipophilic drugs whilst their high thermodynamic stability can achieve high drug loading capacity providing subsequent extended drug release (Johannesson, Stefansson and Loftsson, 2016). Liposomes also have the ability to change their size (20nm to few µm), zeta potential and their surface charge, allowing these carriers to be customised for specific applications. They are usually incorporated into the pre lens or post lens region of the eye, retarding diffusion in both directions providing extended/sustained release (ElShaer et al., 2014). The interaction between liposomes and the cornea was first investigated by Schaeffer and Krohn in 1982. They found that corneal liposome uptake was greatest with positively charged liposomes, suggesting preliminary interaction is electrostatic adsorption; the uptake of water soluble penicillin G also increased four-fold when using positively charged unilamellar liposomes (Schaeffer and Krohn, 1982). One of the first attempts to use liposomes for ocular topical drug delivery was for the treatment of acute and chronic herpetic keratitis, where Smolin et al found the delivery of idoxuridine was more effective with liposomes than without (Smolin et al., 1981; Smolin et al., 1980).

Liposomes were first used in conjunction with soft CLs by Gulsen et al (Gulsen et al., 2005). Lidocaine was entrapped in the lipid bilayer of dimyristoyl-phosphatidylcholine liposomes, which were loaded into pHEMA lenses. The lenses remained transparent and exhibited initial burst release (due to free drug), followed by sustained release from entrapped drug for up to 8 days (Gulsen et al., 2005).

A group in Canada demonstrated sustained release of levofloxacin (6 days) by incorporating the drug into liposomes which were immobilized onto the surfaces of soft CLs (Danion et al., 2007). The same research team immobilized intact liposomes onto multi-layered CLs (Danion, Arsenault and Vermette, 2007). Polyethylenimine was first covalently bound to Hioxifilcon B lenses (via hydroxyl groups). NHS-PEG-biotin molecules were attached to the amide surface groups onto which protein Neutr-Avidin was bound. The intact liposomes (loaded with PEG-biothylated lipids were docked onto surface immobilized Neutr-Avidin; further exposure to Neutr-Avidin and liposomes yielded multi-layered soft CLs (Danion et al., 2007).

2.2.4.1.4.2 Polymeric Micelles

Surfactants are amphiphilic entities which have the ability to solubilise aqueous and lipophilic drugs/material. During polymerisation of polymeric matrix for CLs, the incorporated surfactants come together forming spherical micelles with a hydrophobic core and a hydrophilic shell. Hydrophobic molecules can occupy the space in the core of these structures during polymerisation, enabling the drug to remain in an environment in which it would otherwise be unstable. Entrapment of drug using this method retards drug diffusion; providing sustained release (Tran et al., 2012). Surfactant molecules consist of a hydrophilic head connected to a hydrophobic tail; which interacts with the CL matrix, creating lenses with charged surfaces. This can help enhance drug loading; charged drugs can adsorb onto these charged surfaces hence achieve extended drug release (Sahoo, Biswas and Guha, 2014).

A HG containing silica shell cross-linked methoxy micelles was developed in which polycaprolactone (PCL) formed the core and silica formed the shell of the micelles (Lu et al., 2013). The micelles were loaded with dexamethasone acetate (hydrophobic nature) before they were incorporated into HGs. The release rate of the drug from the HGs was observed for up to 30 days. About 97% of the drug was released within 10 hours with 60% being released within 8

hours. The same research group used Cyclosporine A to study the potential development of pHEMA lenses for the controlled release using various Brij® surfactants (Kapoor and Chauhan, 2008; Kapoor et al., 2009). Focussing on how chain length of surfactant affects the HG, Brij® 78 exhibited the longest release rate (70% after 50 days) compared to pure pHEMA (90% in less than 10 days) (Kapoor et al., 2009). Cyclosporine A was also used as a model ophthalmic drug to develop surfactant-laden lenses where the effect of thickness of the lens on drug release was also assessed (Kapoor and Chauhan, 2008). 100 µm thick lenses indicated extended release of 7-8 days (2% Brij® 78) and 16 days (8% Brij® 78) whilst with 200 µm thick lenses, the release rate was extended to 16-17 days and 40 days for 2% and 8% surfactant, respectively (Kapoor and Chauhan, 2008).

2.2.4.1.4.3 Nanoparticles

Nanoparticles are colloidal carriers on the nanoscale. Trapping API's within NPs before dispersion through the hydrogel matrix provides a degree of protection to the drug from interaction with the hydrogel itself during polymerisation. Gulsen et al developed lidocaine-loaded NPs using hexadecane microemulsions (stabilised with silica shell). These NPs enabled the initial burst release of lidocaine where 50% of drug was released within the first few hours. This was followed by 80% drug being released after 5 days (Gulsen and Chauhan, 2004).

More recently, silicone hydrogels have been loaded with propoxylated glyceryl triacrylate NPs containing timolol. It was observed that a HG with 5% drug loading was able to delivery timolol at the therapeutic concentration for 1 month at room temperature, preliminarily (Jung et al., 2013). *In vivo* testing in glaucomatous beagle dogs demonstrate a reduction in IOP but release was much faster at higher temperatures (>40°C), releasing almost 100% within 3-4 days. This is thought to be due to the ester links between the timolol and propoxylated glyceryl triacrylate (Jung et al., 2013).

Nanocrystals (100nm) of bovine serum albumin coated meloxicam (NSAID) were prepared and dispersed in pHEMA HG for the treatment of post cataract endophthalmitis. The gel released the meloxicam-nanoaggregates for approximately 5 days in which the thickness of the lens and degree of cross-linking were the dependent variables of drug release and by altering these, the drug release rate could be optimised (Zhang et al., 2014).

Silver NPs have also been embedded into lenses to enhance their antimicrobial properties. *In vitro* testing using *P. aeruginosa* and *S. aureus* demonstrated great antimicrobial effects against *P. aeruginosa* but only lenses with increased concentration of silver NPs were effective against *S. aureus* at 48 and 72 hours (Bazzaz et al., 2014).

More recently, anti-fungal agent voriconazole was loaded into lipid-based NPs (Füredi et al., 2017). The resulting NPs were 182±4.1 nm in size. The poorly water soluble drug was readily released from the nanocarrier and inhibited the reproduction of fungus.

Lipid NPs were also utilised to encapsulate indomethacin for delivery to anterior and posterior segment ocular tissues (Balguri, Adelli and Majumdar, 2016). The resulting particles (266±5nm) achieved encapsulation efficiency of 81±0.9%. Modifying the lipid NPs with chitosan chloride increased the ocular penetration of indomethacin, showing these nanocarriers as potential vehicles in ocular drug delivery.

2.2.4.1.4.4 Cyclodextrins

Cyclodextrins (CDs) are oligosaccharides made up of glucose units linked via α 1,4 –glycosidic bonds. These cyclic structures are categorised based on the number of glucopyranose units they possess: α-CDs, β-CDs or γ-CDs. Their cyclic structure enables the entrapment of hydrophobic drugs (e.g. puerarin (Xu, Li and Sun, 2010) and ethoxzolamide (Garcia-Fernandez et al., 2013; Ribeiro et al., 2012)) resulting in increased drug BA, stability as well as reducing the potential of undesirable side effects.

Ribeiro et al exploited the ability for natural β-CDs and γ-CDs to form inclusion complexes with carbonic anhydrase inhibitors acetazolamide and ethoxzolamide in aqueous solution and developed N-N-dimethylacrylate-co-N-vinylpyrrolidone lenses with these pendant CDs (Ribeiro et al., 2012). The incorporation of CDs had no lasting effect on optical transparency of the lenses or on the cytocompatiblity of the lenses. Acetazolamide-loaded HG sustained release for 3-6 hours whilst ethoxzolamide HGs sustained release for over a week. Ethoxzolamide was also loaded into poly-CDs which notably enhanced drug solubility and provided a much more delayed drug release rate compared to free CDs (Garcia-Fernandez et al., 2013). The poly-CDs also enhanced drug loading which resulted in sustained release for several weeks.

Puerarin β-CD complexes were successfully loaded into pHEMA lenses where *in vitro* and *in vivo* studies showed drug- β-CD complexes were 7.2 times and 4 times as effective as eye drops and isolated lenses, respectively (Xu et al., 2010). Drug loading was found to be dependent on the β-CD content; as was the *in vitro* release of puerarin. *In vivo* analysis showed that drug retention in the precorneal region was enhanced with greater BA using β-CD loaded pHEMA lenses (Xu et al., 2010). Puerarin was also used to synthesise cyclodextrin-containing hydrogels for ophthalmic drug delivery. The amount of puerarin loaded into HG matrix using a crosslinkable chitosan derivative containing β-CD was greatly increased and the release was much more controlled with the addition of the CD (Hu et al., 2013).

More recently, conventional and silicone lenses (synthesized with methacrylated β-CD and methacrylated 2-hydroxypropyl-β CD) were loaded with natamycin and its release was assessed. These lenses improved drug release up to a threshold despite not extending the drug release duration (Chau-Minh Phan, Subbaraman and Jones, 2014).

2.2.4.2 Advantages and Limitations of Contact Lens Drug Loading Mechanisms

Whilst these methods of loading drug into or onto contact lenses have shown potential, there are some limitations relating to the feasibility and the use of the developed devices and the ability to control drug loading and release. **Table 2.2** summarises the advantages and limitations of each mechanism.

Table 2.2 Summary of the advantages and limitations of current drug loading mechanisms for contact lenses

Mechanism	*Advantages*	*Disadvantages*
Soak and Release and Vitamin E Barriers	• Extends release duration • Ease of implementation • UV Blocking	• Vitamin E can increase size of formulation and decrease ion permeability • Drug loading depends on drug solubility in matrix and duration of soaking • Most of the drug is released within a few hours therefore cannot be used for prolonged delivery
Molecular Imprinting	• Increased Drug Loading capacity • Increased Release duration	• Time Consuming (extensive testing) • Limited to one drug • High Degree of cross linking is required which affects O_2 permeability
Colloidal Carriers	• Provides extended drug release • Size of carriers	• Can cause loss of lens transparency due to particle aggregation • Decaying release rate • Rate controlling carriers can cause burst release for free drug due to diffusion during long storage periods
Ionic Interactions	• Extends release duration and drug loading capacity • Increases stability of the implantation device	• Drug release can cause volume changes • Cannot be used for neutral drugs or mix of cationic and anionic drugs

The ability to control drug loading and drug release from contact lenses stands to be the most important drawback when using contact lenses as drug delivery devices. Addressing this and the other limitations stated in **Table 2.2** to be able to develop a method which ca increase drug loading capacity and extend drug release without affect stability in a one-step, on demand process would be extremely advantageous. Here, I propose using a novel engineering process to develop medicated contact lenses which will ultimately act as a safe and efficacious drug delivery device.

2.2.4.3 Engineering Methods to Coat Contact Lenses

Rather than incorporation of drug into the lens matrix, there have been attempts to coat the surface of lenses in a bid to revolutionise ocular topical drug delivery. This approach has been met with promising results (Liu et al., 2009; Garty et al., 2011; Anderson et al., 2009; Manju and Kunnatheeri, 2010; Mehta et al., 2015). For instance, rapamycin is an immunosuppressant agent used for prevention of organ transplant rejection. It was incorporated into a poly (lactic-glycolic acid) (PLGA)-chloroform solution, which was subsequently sprayed on the edge of poly-(methyl methacrylate) (PMMA) lens in an attempt to prevent formation and development of posterior capsular opacification (PCO). Unmodified lenses (group A) and PLGA lenses (group B) served as controls and group C was the rapamycin-sprayed lenses. After 7 days, the mean concentration of rapamycin in aqueous humour reached 1.10±0.3 µg/ml after peaking to 14.57±0.99 µg/ml after 24 hours after administration to albino rabbits. *In vivo* analysis showed that the initial detection of PCO in rabbits in group C was much later than in groups A and demonstrating effective prevention of PCO formation and development (Liu et al., 2009).

Anderson et al have exposed HEMA lenses to an octadecyl isocyanate solution where it was established that the polyurethane bonds between the hydroxyl groups on the HEMA lenses and the isocyanate groups retarded norfloxacin release. Immersion of lenses in octadecyl isocyanate solution for 60 minutes led to more than 90% of the drug being released within 2 hours; although this is rapid, it is slower than non-coated lenses (Anderson et al., 2009). Coating of PMMA lenses (with amino groups) with poly (sodium 4-styrene sulfonate) and ampicillin enhanced drug release with a 6-layer coating provided sustained release for 7 days (105µg of ampicillin) (Manju and Kunnatheeri, 2010).

EHDA is a novel technique that has been utilised to develop multi-functional ocular lenses. It was used to produce PVP NPs (50-130 nm) and PVP fibres (130-250 nm) to coat both sides of the contact lens (Mehta et al., 2015). As PVP is a rapidly dissolving polymer, the release was over 80% within 2 minutes with fibres demonstrating slightly longer sustained release due to lower surface area EHDA is a one step, on demand process which can bypass many of the limitations stated earlier with regards to other approaches to yield drug eluting contact lenses.

2.3 Glaucoma

Glaucoma is the term given to a group of complex ocular disorders associated with ocular hypertension.

2.3.1 Pathophysiology and Epidemiology

Glaucoma is the second leading cause of blindness in the world, affecting 60 million people worldwide. It is a multi-factorial progressive optic neuropathy that often results in visual loss due to fluid imbalance in the eye. This imbalance leads to the characteristic degeneration of the optic nerve, the structure responsible for relaying information from the retina and eye to the brain (Morrison and Pollack, 2002; Healey and Thomas, 2010). The progressive damage initiates with peripheral vision loss, leading to subsequent central vison loss and ultimately full blindness in severe cases.

Glaucoma affects 2% of the worlds' population over the age of 40 (**Figure 2.3**); with an estimated 8.4 million cases resulting in irreversible damage and permanent blindness (Tham et al., 2014).

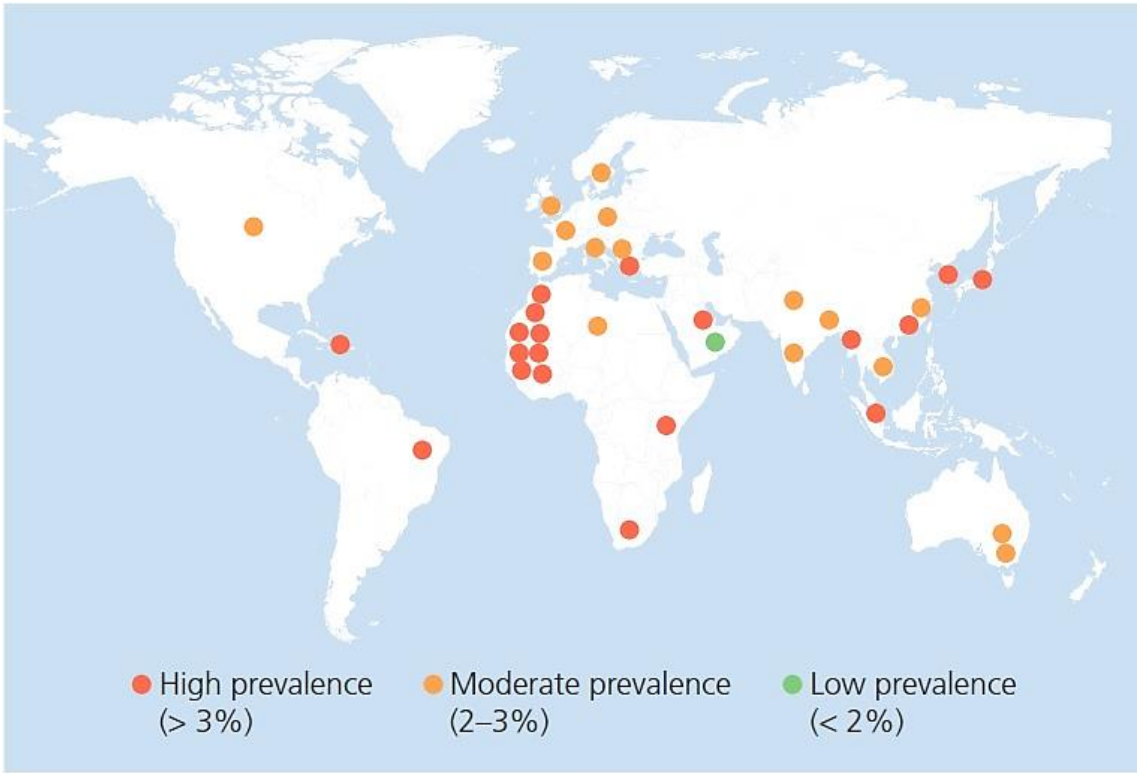

Figure 2.3 Prevalence of glaucoma in people over 40 years of age by geographic region. Figure and caption extracted from (Healey and Thomas, 2010)

In 2010, the World Health Organisation (WHO) estimated glaucoma was liable for 15% of vision loss cases globally. Approximately, 60 million people currently suffer from glaucoma (Kapetanakis et al., 2016) with this figure estimated to increase to 79.6 million by 2020 (Quigley and Broman, 2006) and 111.8 million by 2040 (Tham et al., 2014).

2.3.2 Aetiology

As glaucoma is a multi-factorial condition, there is no definitive cause for it, although a majority of cases do involve elevation of IOP. This increase in IOP is a result of insufficient drainage of AH via the trabecular meshwork. The AH is usually drained from the eye to the bloodstream via these tubes at the same rate as it is produced hence maintaining the correct IOP; 12-22 mmHg (Barranco Esporcatte and Tavares, 2016). If the meshwork becomes damaged or is blocked, the AH cannot drain efficiently and remains in the synapse between the cornea and iris. An accumulation of fluid causes the IOP to increase damaging retinal nerves and optic nerves. It has not yet been fully established why morphological changes occur in the trabecular meshwork but it has been the focus of glaucoma-related research in recent years.

2.3.3 Types of Glaucoma

Glaucoma can be subcategorised into 5 main classes all of which are still classed as optic neuropathies.

2.3.3.1 Primary Open Angle Glaucoma

Primary Open Angle Glaucoma (POAG) is the most common type of glaucoma where the slow blockage of the trabecular meshwork causes a slow increase in IOP (Allingham, Liu and Rhee, 2009). This chronic condition develops very slowly and is painless which makes detecting and diagnosing the disease very difficult. The patient can lose up to 40% of their vision before noticing any changes, as the peripheral vision is the first to be affected. It is thought the obstruction in the tubes within the trabecular meshwork causes an increase in outflow resistance consequently requiring an elevated IOP to maintain AH flow through the anterior chamber. This increase in IOP is thought to lead to the apoptosis of retinal ganglion cells. The rate at which this degeneration occurs is dependent on the hydrostatic pressure on the optic nerve and the compromisation of local ocular microvascularity.

POAG is more prevalent in adults over the age of 65 years. It is 3 more times likely to occur in African–Americans (Abdu, 2013) **(Figure 2.2)**; for whom glaucoma is the leading cause of blindness. Research has also concluded that those with a family history of POAG are more susceptible to developing glaucoma due to the fact that characteristics such as eye size, IOP and AH outflow competency are inherited (Wiggs and Pasquale, 2017; Swierkowska and Gajecka, 2017). Patients who suffer from diabetes and ocular refractive error conditions such as myopia are also at increased risk of developing this type of glaucoma.

2.3.3.2 Angle-Closure Glaucoma

Angle Closure Glaucoma (ACG) occurs due to rapid blockage of the draining canals, causing a sudden increase in IOP (Lai, Choy and Shum, 2016). This elevation in pressure reduces the synapse between the iris and cornea, hindering the drainage of the AH through the trabecular meshwork. This space in a healthy working eye usually houses the trabecular meshwork. The junction at the edge of the anterior chamber is known as the anterior chamber angle. The name ACG comes from the reduction of this angle because of the reduced distance between the iris and cornea. ACG is a chronic condition where the patient experiences great amount of pain and requires immediate medical attention and treatment to prevent blindness.

Whilst age and family history can increase the risk of ACG, ethnicity also plays a big role. ACG is very common in South East Asians, especially the Chinese population. Females are also more susceptible to developing ACG than men, at a 4 to 1 ratio (International Glaucoma Association 2017).

2.3.3.3 Normal Tension Glaucoma

Normal Tension Glaucoma, also known as low-tension glaucoma, differs from other types of glaucoma because neurodegeneration occurs at normal IOP conditions (Barranco Esporcatte and Tavares, 2016). The aetiology of normal tension glaucoma is still unknown; research is still prominent in ascertaining why the optic nerves are damaged regardless of regular IOP.

People who have a family history of normal tension glaucoma are more at risk. Those of Japanese ancestry are also more prone to developing this type of glaucoma (Anderson, 2017).

Although a significant connection has not been identified, patients with history of systemic heart diseases such as arrhythmia are also at risk of getting normal tension glaucoma.

2.3.3.4 Secondary Glaucoma

Glaucoma can also occur due to pre-existing ocular disorders. Certain conditions can cause an increase in IOP, compromising the optic nerve structure and function. Reduction in AH outflow can also occur due to inflammatory residue and growth of new blood vessels in the anterior chamber as a result of vascular ocular diseases.

2.3.3.5 Congenital Glaucoma

Incomplete development of the trabecular meshwork (and in turn increase in outflow resistance) in babies during the prenatal period can result in congenital glaucoma (Samant, Medsinge and Nischal, 2016). Although this class of glaucoma is very rare (1 in 10,000 births), it is very severe. It has also been linked with gene abnormalities concerning the CYPIBI gene; the gene that is responsible for the production of the enzyme P450IBI. The CYPIBI gene is present in many structures in the eye, however, its function in eye development is yet to be established. One hypothesis is that it may aid the formation of the anterior segment of the eye and may be involved in the regulation of fluid secretion inside the eye.

2.3.4 Treatment

A majority of treatments developed for glaucoma appertain to lowering IOP in the eye. Therapy can be classed into 3 main approaches: topical medical treatment, laser therapy and surgical treatment.

2.3.4.1 Topical Therapeutics

The most common approach to treating glaucoma is topical drug administration in the form of eye drops. There are five main classes of drugs used to lower IOP (Arthur and Cantor, 2011; Cheema et al., 2016). These drugs work in one of two ways: improving the outflow of AH from the eye or reducing AH production. **Table 2.3** summarizes examples of each category and the mode of action.

2.3.4.1.1 Beta Blockers

Beta blockers work by decreasing AH production from the trabecular meshwork. Systemic side effects can be avoided by closing the eye after administration to prevent drug drainage into systemic circulation. Systemic absorption can cause a decrease in cardiac output and bronchial constriction. These actives can also lower blood pressure and rare effects such as reduced libido and depression can also occur.

2.3.4.1.2 Prostaglandin Analogues

Prostaglandin Analogues are a class of drugs that work by improving the outflow of AH from the eye. They are usually prescribed to patients suffering from Primary Open Angle Glaucoma. Side effects include change in iris colour, growth of eye lashes, itching, redness and blurred vision. No or few systemic effects are seen with prostaglandin analogues.

2.3.4.1.3 Alpha Agonists

Like beta blockers, alpha agonists (also known as sympathomimetics) work by reducing AH production. Side effects include burning upon administration, headaches, fatigue, drowsiness and minimal cardiovascular effect.

2.3.4.1.4 Cholinergics

Cholinergics (miotics) work by improving the outflow of AH from the eye. The mode of action involves the contraction of the cillary muscle in the eye (shrinking of pupil), constricting the trabecular meshwork, increasing outflow of fluid. Cholinergics can be used alone or in conjunction with beta-blockers or carbonic anhydrase inhibitors.

2.3.4.1.5 Carbonic Anhydrase Inhibitors

Carbonic Anhydrase Inhibitors reduce AH production via inhibition of carbonic anhydrase in the ciliary body. These actives are usually administered topically in patients with POAG but systemic administration (tablets) is preferred with ACG. Those administered topically have been found to be less effective and not have a therapeutic effect for a long period of time. Topically applied drugs have found to cause stinging and burning in the eye whilst tablets haven been reported to cause tingling in hands and feet with the possibility of developing kidney stones or depression.

Table 2.3 Examples of the different drug classes used in treatment of glaucoma and the mechanism of action of the active

Drug Class	*Generic Name*	*Brand*	*Mode of Action*
Prostaglandin Analogues	Latanoprost 0.005%	Xalatan®	An ester prodrug activated to free acid in the cornea; selective agonist
	Travaprost 0.004%	Travatan ® Z	Prostaglandin F2-alpha analogue
	Tafluprost Ophthalmic Solution 0.0025%	Zioptan™	Selective Agonist at prostaglandin F receptor
Beta Blockers	Timolol Maleate Ophthalmic 0.5%	Istalol	Non-selective beta adrenergic blocking agent
	Betaxolol HCl 0.25%, 0.5%	Betopic® S	Selectively blocks beta 1-adrenergic receptor with little effect on beta 2-receptors
	Levobunolol HCl Ophthalmic Solution USP 0.25%	Betaga®	Non-cardio selective beta-adrenergic blocking agent
Alpha Agonists	Brimonidine Tartrate 0.1%, 0.15%	Alphagan® P	Selective alpha 2-receptor
	Apraclonidine HCl 0.5%, 1%	Iopidine®	Potent alpha-adrenergic agent
Cholinergics	Pilocarpine HCl 1%, 2%, 4%	Isopto® Carpine	Alkaloid that mimics muscarinic effects an acetylcholine at post-ganglionic parasympathetic nerves. Directly stimulates cholinergic receptors in the eye
	Carbachol 0.75%, 1.5%, 4%	Isopto ® Carbachol	Binds and activates acetylcholine receptor; a parasympathomimetic that stimulates muscarinic and nicotinic receptors
Carbonic Anhydrase Inhibitors	Dorzolamide HCl 2%	Trusopt®	Reversibly inhibits carbonic hydrase; reduces proton secretrion and increases renal excretion of sodium, potassium, carbonate ions and water to decrease AH production
	Acetazolamide	Diamox®	Inhibits carbonic hydrase
	Methazolamide	Neptazane®	Inhibits carbonic hydrase

2.3.4.2 Surgery

While most cases of glaucoma can be treated using topical medication, more severe cases may require surgery in order to alleviate the increased IOP to a safe platform/threshold (Ansari, 2017).

Trabeculectomy involves a surgical incision and partial removal of the trabecular meshwork; creating new drainage tubes to improve fluid outflow (Ansari, 2017; Januleviciene et al., 2015; Saheb and Ahmed, 2012; Matlach and Klink, 2015). This is the most common procedure when the use of topical medication is rendered inadequate. The incision in the trabecular meshwork creates a permanent canal between the cornea and sclera; allowing the controlled release/removal of fluid from the eye; the fluid that had built up around the scleral flap is absorbed by blood vessels and drained away into the bloodstream. Another similar procedure, called a trabeculotomy, can also be carried out which involves surgical incisions without the

removal of trabecular tissue. This is not as effective as trabeculectomy but minimises infection risk and post-operative complications.

Laser surgery can help to improve outflow of AH by focussing a light beam onto eye tissue; creating a hole or burn in the tissue, depending on the strength of the beam (Ianchulev et al., 2017). There are two types of laser surgeries. Selective Laser Trabeculoplasty is a simple technique which is often used in the treatment of POAG (Zhou and Aref, 2017). This process utilises a low strength, wide beam to "selectively" treat trabecular meshwork cells; leaving most of the drainage tubes intact. This procedure is often for the treatment of POAG (Richter and Coleman, 2016).

Argon Laser Trabeculoplasty works by activating the trabecular meshwork cells by focussing a beam onto the canals using a lens (Samples et al., 2011). The laser beam creates an opening in drainage canals; helping fluid outflow.

Those that suffer from ACG can benefit from laser peripheral iridotomy. As the anterior chamber angle between the iris and the cornea is significantly reduced, a laser is used to create a new drainage canal on top of the iris, improving liquid outflow.

2.4 Electrohydrodynamic Atomization

2.4.1 Introduction

EHDA, in recent years, has shown to be a versatile technique with great potential in the pharmaceutical industry. The fundamental principle involves using electrical forces for liquid atomization to produce micrometre and nanometre structures suitable for DD. The maturing area of nanotechnology (in regenerative medicine, tissue engineering and DD) has great potential to benefit from such enabling platform technologies. The generation of nano-sized entities, in particular those with complex release kinetics and multi-functional capabilities, is currently of great interest for pharmaceutical application with respect to DD.

EHDA is a one-step process which can be employed at ambient temperatures and is easily amended to achieve optimum conditions for the production of nanoparticles applicable to numerous pharmaceutical applications (Mehta et al., 2017).

2.4.2 The EHDA Process

2.4.2.1 Defining the Principle Process

EHDA utilises electrical forces to atomise liquids. An electrically imposed (electro) liquid (hydro) jet (dynamic) exits a nozzle in the form of particles or fibers (Grace and Marijnissen, 1994). These structures are then collected on a ground electrode positioned under the tip of the nozzle, usually 10-12 cm below the tip **(Figure 2.4).** Several factors influence the resultant structures: process parameters (flow rate (FR), applied voltage (AV) working distance (WD)) and liquid properties (surface tension (ST), electro-conductivity (EC) and viscosity) (Kim and Kim, 2011). As a consequence, there are two main recognised forms of EHD processing; electrospraying (Esy) (particle production) and electrospinning (ES) (fiber production).

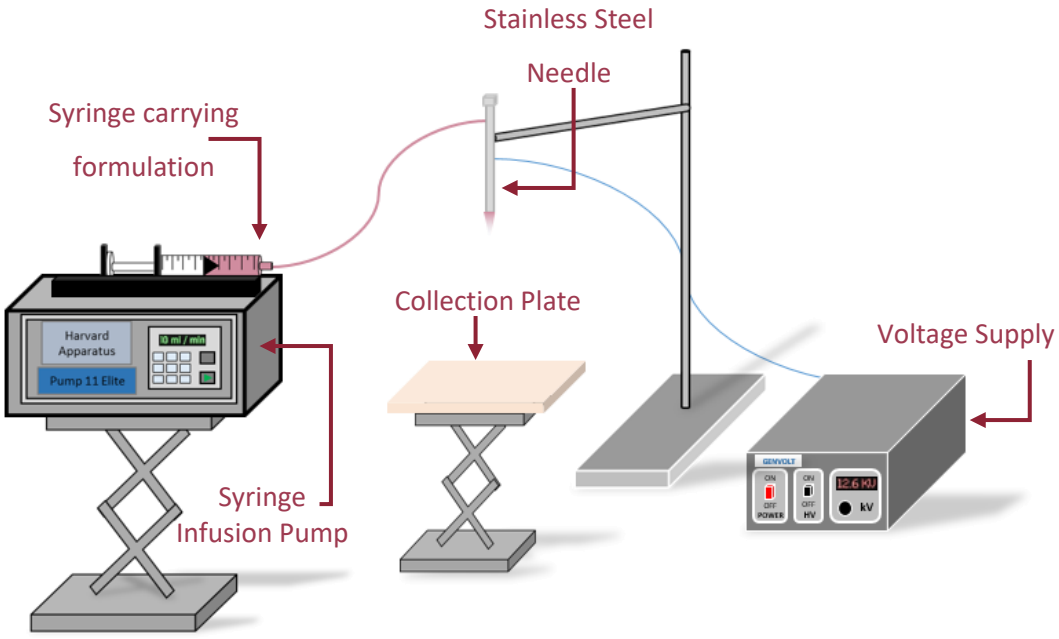

Figure 2.4 Schematic diagram of the EHD system

2.4.2.1.1 Electrospraying

Esy is a cost-effective, one-step process used for the fabrication of micro and nano particles. In the late 16th century, William Gilbert demonstrated the very first concept of electrostatic phenomena (Gilbert, 1628). By exposing a droplet of water to charged amber, it was observed that the droplet deformed into a cone. More than 200 years later, physicist Lord Rayleigh proposed using electrostatic forces to atomise liquids. He hypothetically predicted that a liquid droplet would become unstable when a threshold charge is reached. He correctly predicted the maximum charge a droplet could "hold" before forming an unstable jet of liquid (Rayleigh, 1878). This threshold was confirmed a century later and is now known as Rayleigh's Limit (Taylor, 1964a; Tang and Gomez, 1995). Rayleigh found that a droplet exposed to an electrical charge would deform due to repulsion of like electrostatic charge. Once this repulsion exceeds the ST keeping the drop intact, the droplet would breakdown into more stable, finer droplets i.e. coulomb fission occurs (Tu and Ray, 2005). John Zeleny, a Czech-American physicist, exploited this theory by using a capillary-plate configuration to demonstrate how electrostatics affects the behaviour of liquids (Zeleny, 1917); a configuration similar to the set up used in the

present day. His work involved experimental research which provided evidence for several Esy modes recognised today including dropping, pulsating and cone jetting (Zeleny, 1914).

Half a century later, Sir Geoffrey Taylor experimented with the balance between the ST of liquid and electrical forces, developing the underlying theory of electrospraying (Taylor, 1964a). Taylor found there was a threshold where the electrical field was in equilibrium with the ST of the liquid which resulted in a stable jet of liquid (Taylor, 1964b). This characteristic jet is now known as the Taylor Cone and is a prerequisite for the production of small, uniform spherical structures.

Esy is an explicit method used for the production of near monodispersed particles. Its application to various research disciplines has been of great interest as of late, especially in the maturing area of nanotechnology for the delivery of APIs including anti-cancer therapeutics (Luo et al., 2012), proteins (Suksamran et al., 2009) and NSAIDs (Bohr et al., 2012).

2.4.2.1.2 Electrospinning

The first concept of utilising electrostatic forces established by Gilbert along with Rayleigh's work on droplet destabilisation influenced Morton's theory of developing one dimensional structures using ES in the early 20th century. Extensive research was carried out by a number of scientists and many patents filed; the first by John Francis Cooley (Cooley, 1900). Cooley, an inventor and electrician from New York, filed a patent that described various charged spinning heads including a coaxial head, an air assisted model and a rotating spinneret (Cooley, 1902). Another crucial patent issued was filed by Anton Formhals who demonstrated the use of electrodes to focus the cone jet to a rotating cylinder. For more than a decade, Formhals dedicated his research to the concept of ES; evolving the configuration of the system, resulting in a number of patents being issued (Formhal 1934, Formhals 1938). The interest in the ES process began to increase dramatically in the 1980's in sync with the growing significance of nanotechnology research. This is reflected in the number of publications that were produced which more than tripled in the period of 2005-2010.

ES uses comparable set-ups to Esy to produce continuous fibers. However, rather than the jet breaking up, the electrical field stretches the visco-elastic (polymeric) solutions at the capillary exit to form fine strands of nanometre width (Zhang, Jayasinghe and Edirisinghe, 2006). The

novel physiochemical and biological characteristics of the electrospun structures is a credit to the unique morphology of the structures which can be utilised in a wide range of applications, including bioengineering (tissue engineering) (Frohbergh et al., 2013), ophthalmics (Tonsomboon and Oyen, 2013) and DD (Jiang et al., 2005). Various controllable morphologies have been produced using ES (fibers, filled, hollow tubes) and this, combined with the fact that it is an easy to operate, cheap, on-demand process renders ES a common method for the production of nanofibers (NFs).

2.4.2.2 Characterising the Electrohydrodynamic jet

During the EHD spraying process, the solution is imposed through a conductive needle that leads to jet formation at the needle exit. Subsequently, the atomised structures can be collected. The process can be altered to produce structures with the desired particle morphology, surface charge, porosity and size (with narrow size distribution). This is achieved by varying the process parameters and liquid properties. EHD spraying jets are established and characterised by evaluating two parameters: intensity and droplet diameter, both of which are affected by the physical properties of the liquid being sprayed and the process parameters FR, AV and WD.

2.4.2.2.1 Modes of EHDA

Different spraying modes of EHDA have been established based on two principles: i) how the liquid exits the needle and ii) how the liquid jet breaks up into droplets (Jaworek and Krupa, 1999); and these have been classified into two different modes; dripping mode and jetting mode. Dripping mode occurs when only fragments of liquid exit from the nozzle. The atomised structures tend to be larger due to gravitational and electrical forces on the liquid attempting to overcome liquid ST (**Figure 2.5**). Jetting mode occurs when the liquid breaks up into fine droplets some distance from the end of the nozzle, causing a continuous jet at the nozzle tip.

Subdivisions in each category of spraying modes have also been observed upon altering the WD between the capillary and the collecting platform and the applied voltage. Both process parameters (AV and FR) and physical properties of liquids need to be optimised for mono-dispersed droplets and a stable jet (Yao et al., 2008). The cone jet mode is the most prominent, stable jet, where the liquid forms an axisymmetric cone at the capillary tip. Taylors' work to

establish this cone; aptly named "Taylor Cone" is the most stable of EHD modes and is a prerequisite for easily controllable, uniform PS production.

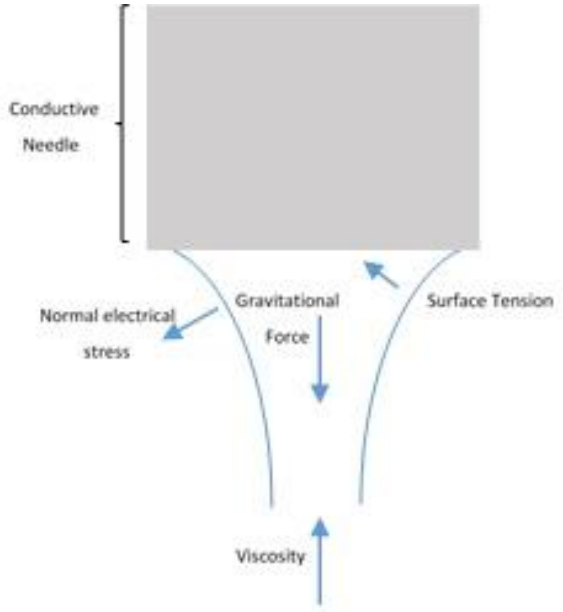

Figure 2.5 Schematic Illustration of forces acting in the liquid cone at the needle exit

With respect to ES, a Taylor cone jet is established but the jet experiences some instability causing the jet to solidify much faster than it normally would (i.e. during electrospraying), thus stretching the solution; producing fibrous structures (H. B. Zhang et al., 2006). In this regards, there are three types of instabilities which have been distinguished; Rayleigh instability, axisymmetric instability and non-axisymmetric instability (Wu and Clark, 2008). The latter was found to be the most crucial as it is the main cause of fibrous structure generation (Hohman et al., 2001). With non-axisymmetric instability, rather than the jet splitting into multiple jets, an inverse cone can be seen consisting of a single rapidly bending strand. These fibers have been found to reach several metres in length whilst maintaining their nano-scale widths (Laudenslager and Sigmund, 2011).

2.4.2.2.2 Criteria for EHDA

Liquid physical properties can significantly affect the EHDA process, hence material selection should focus on the viscosity, EC, and ST of the formulation to be processed. The voltage applied to the solution as well as the rate at which the liquid is expelled are significantly important to

assess and quantify as these also impact on the jetting stability and the outcome of the EHDA process (Xie et al., 2008; Ahmad et al., 2008).

2.4.2.2.2.1 Physical Properties of Liquids

The physical properties of liquids are critically important in EHDA. These factors help to determine the shape, morphology and characteristics of the resulting structures. The EHDA process requires the electrical forces to overcome the ST of the liquid in order for the liquid to be atomised; ergo the ST needs to be low enough for the AV to overcome it so a stable cone jet can be produced. The ST of the liquid cannot exceed 50mNm^{-1}, as liquids with higher ST than this cannot be atomised; the electrical field would be exceeded when voltage is applied (Smith, 1986; Tang and Gomez, 1995).

Due to the introduction of the electrical field, there is an accumulation of charge at the cone-jet, resulting in jet break up. Due to this, the EC of the materials and solvent used in the EHDA process are critical parameter to consider. Materials with low EC (less than 10^{-10}Sm^{-1}) would not be able to produce a stable cone jet. For example, heptane, a straight-chain hydrocarbon, has an EC of 0.03pSm^{-1} at 20°C. In such cases of low EC, additives known as anti-statics can be added to increase the EC of the solvent. Liquids with high EC can also experience similar problems due to competition between the EC and ST during the spraying process. The ideal range for EC is between 10^{-4} and 10^{-8} Sm^{-1}.

The viscosity of the formulations being processed is another vital physical property as this allows the differentiation between electrospraying and electrospinning (Bock, Dargaville and Woodruff, 2012). Low viscosity liquids are ideal for stable cone jet production, which results in small, uniform (with respect to size and morphology) particles when sprayed. With regards to electrospinning, polymeric viscosity is directly proportional to the polymer concentration. The higher the polymer concentration, the more difficult it may become to control and maintain the liquid infusion from the nozzle and fibers can be produced (Bock et al., 2012; Jayasinghe and Edirisinghe, 2002).

2.4.2.2.2.2 Processing parameters of EHDA

The FR at which the liquid is expelled from the needle and the AV are crucial during the EHDA process as these parameters can control both the jetting mode and the electrical field that exists between the tip of the needle and the collecting platform. The AV also has a substantial effect on the resulting particle size. Typically, the upper-most limit for AV is 30 kV but this value is dependent on the configuration of the device (e.g. single or coaxial arrangement) and the formulation. By increasing the AV, the atomization effect on the jet is enhanced resulting in smaller particles (below 270 nm) (Moghadam et al., 2009). Altering the voltage results in various jetting modes (dropping, Taylor cone, spindle (Wu et al., 2012)), which depend on the electrical force applied as well as the flow rate of the liquid. High voltage causes multi-jet spraying resulting in poly-disperse particles whereas low voltages result in intermittent jet formation, causing dripping mode to occur. Some research has suggested that the higher the voltage, the more repulsive forces that are present, resulting in a decrease in particle/fiber diameter. However, some have found that a higher voltage encouraged the increase in diameter; hence, the voltage needs to be optimised for specific formulations for uniform, stable production of particles or fibers (Jayasinghe and Edirisinghe, 2002).

In order to form a stable Taylor Cone jet, it is imperative to optimise the flow rate of the liquid. FR is inversely proportional to the viscosity of the fluid, as flow rate increases, viscosity reduces. The rate at which the liquid is expelled through the needle also affects diameter of the resulting structures, the slower the rate, the smaller the diameter (Wu et al., 2012). The flow rate needs to be slow enough for the solvent to evaporate so spherical particles are generated.

It has become increasingly noted that the WD (distance between the needle exit and the collection plate) can affect the results of the EHDA process as WD directly affects the electrical field strength (Hossain, Gong and Rigout, 2015). It has been reported that the WD can affect the morphologies of the resulting structures. If the WD is too short, there is insufficient solvent evaporation; leading to “wet” particles (not fully dry) resulting in poly-disperse size distribution. If the collection plate is too far from the needle exit, the particles may be lost to the surrounding atmosphere. The ideal WD range is between 12 and 15 cm (Moghadam et al., 2009).

2.4.2.2.2.3 Scaling Laws

The minimum FR of the solution can be calculated based on the properties of the liquid. Barreo and Loscertales, in 2007, found that for high conductive liquids with low viscosity, the minimum FR can be scaled as:

$$Q_{min} \sim \frac{\varepsilon_r \gamma}{\rho K} \tag{2.1}$$

where Q_{min} is the minimum flow rate, γ is the surface tension, ρ is the density of the liquid, K is the concentration of the liquid, ε_r is the permittivity of the liquid. Due to the concept of EHDA evolving and advancing in material development, minimum FR scaling has recently been updated to include process parameters as well as physical liquid properties (Scheideler and Chen, 2014). As **Equation 2.1** does not take into account the nozzle diameter, Scheideler and Chen approximated the minimum FR of highly viscous liquids (**Equation 2.2):**

$$Q_{min} \sim \frac{\gamma D^2}{\mu} \tag{2.2}$$

where D is the nozzle diameter and μ is liquid viscosity. Several studies concluded that highly conductive liquids or highly viscous liquids behaved very differently to low viscosity liquids. Solutions that have high viscosities have a relatively low ratio between the change in kinetic energy of the liquid jet (in the axial direction) over the change in viscous stress (in the centrifugal direction) resulting in fibrous structures (Yurteri, Hartman and Marijnissen, 2010).

2.4.3 Applications of EHDA

As mentioned earlier, the technological advancement of EHDA has allowed the process to be utilised in an array of applications and yielded numerous experimental systems (coaxial, multi-needle, needleless, and printing); with the most simple and most common being single needle EHDA.

2.4.3.1 Single Needle Electrospraying

The first EHDA configuration consisted of a single stainless steel nozzle through which the formulation is infused. The API is usually dissolved into a polymeric-solvent solution, but additives have also been incorporated to modify functionality. During the process of single needle (SN) Esy, the solvent evaporates at the nozzle exit resulting in the API being uniformly distributed through the polymeric matrix. This is turn enhances the amorphous form of crystalline drugs, enhancing the solubility of the drug in question. (Jafari-Nodoushan, Barzin and Mobedi, 2015). With applications extending to protein delivery, anticancer therapeutics and gene therapy, it is clear to see the abundant potential of SN Esy.

2.4.3.1.1 Protein Delivery

One of the first biomolecules to be employed by the Esy process was insulin. The hormone-loaded NPs produced ranged between 98 and 117 nm; with smaller particles being fabricated by using a low insulin concentration and by reducing the flow rate (from 0.38 µl/min to 0.17 µl/min (Gomez et al., 1998).

The delivery of thermoresponsive materials such as proteins and peptides like insulin has always posed challenges due to the physical and chemical lability of these biomacromolecules (Zamani et al., 2014). Conventional methods of encapsulating proteins require processing conditions that cause the temperature or stress to be increased leading to denaturation altering the functionality of the protein (Zamani, Prabhakaran and Ramakrishna, 2013). Esy offers a means of successfully encapsulating biomacromolecules without damaging the material in a simple one-step process at ambient temperatures.

Bovine serum albumin (BSA) has served as a model protein to demonstrate protein encapsulation using SN Esy, yielding particles 937±158 nm in diameter using high viscosity alginate (Suksamran et al., 2009). Poly (lactic-co-glycolic acid) (PLGA) NPs loaded with amino acid n-acetylcysteine were fabricated to overcome its poor oral BA of the amino acid (Zarchi et al., 2015). The NPs were spherical in shape with some as small as 122 nm and also exhibited biphasic release in *in vitro* release studies. More recently, peptide angiotensin II was encapsulated into N-octyl-o-sulphate chitosan particles which demonstrated triphasic release profile with an EE of 92±1.8% and average diameter of 105.7±4 nm (Rasekh et al., 2015b).

2.4.3.1.2 Gene Therapy

DNA-based pharmaceutical preparations have been developed for medical treatment of several diseases e.g. asthma, cancer and cystic fibrosis. However, the delivery of genes as a pharmaceutical dosage form currently results in instability problems such as losing DNA molecular integrity upon processing (Zeles-Hahn et al., 2011). It is vital to conserve either the super coiled or the open circle form of plasmid DNA in order to accomplish robust gene expression (Kimoto and Taketo, 1996).

Delivery of DNA based drugs to the desirable organ in the body can be achieved in 3 different ways: i) intravenous injection, ii) direct injection and iii) topical application by aerolization. The latter is most commonly used due to the advantage of non-invasively targeting the affected cells, reducing any toxic effect on other body organs (Bennett et al., 2002; Zeles-Hahn et al., 2011). The nature of Esy allows sensitive material to be handled and processed without the integrity of the materials being compromised. Zeles-Hahn et al demonstrated that Esy is a reliable method for administering DNA-based therapeutics to the epithelium cells in the pulmonary system (Zeles-Hahn et al., 2011). Stable plasmid DNA-polyethyleneimine aerosols were sprayed using a SN without any signs of structural alteration or loss of integrity of the DNA. The electrical field applied was found to cause temporary mild toxicity which reverted to normal conditions within a few hours of administration to the tissue. Further *in vivo* investigation combined with these results demonstrates potential for administering DNA-based therapy to the pulmonary epithelium and various other tissues using this technology.

Lee et al successfully improved the transformation efficiency (5-7 fold) of gold NPs (50nm) loaded with PET30a-GFP plasmid DNA. The transformation of the plasmid using Esy did not require the preparation and time needed for conventional methods, which is often the limiting step in such DNA transformation methods (Lee et al., 2011). Similarly, Park et al showed the Esy process has the capability to produce adenovirus carriers for effective transduction efficiency in cancer cells (Park, Kim et al., 2012). Beads produced using 0.5% alginate concentration demonstrated high encapsulation activity and sustained release for 7 days; with high transduction efficiency in U343 glioma cells. These cross-linked alginate structures show the potential of Esy beads to overcome the limitation of liver accumulation and immune response.

2.4.3.1.3 Cancer Treatment

Due to lack of effectiveness of existing therapeutic approaches, treatment for cancer is still a major challenge. Despite various chemotherapy drugs available (both orally and intravenously), current treatment still has numerous limitations. Physical properties (e.g. drug solubility) and poor pharmacodynamics of the drug and physiological conditions (i.e. pH 7.4) lead to ineffective therapeutic concentrations at the target site. Current approaches commonly involve frequent radiation application after surgical removal of the tumour. By producing anti-cancer loaded Esy structures, a much more effective dose of drug can be delivered directly to the tumour (i.e. local drug delivery), halting the need for repetitive drug and radiation administration.

Various drugs used for an array of cancers (including breast, ovarian, retinoblastoma) have already been incorporated into polymeric particles yielding promising results. Tamoxifen, a lipophilic drug used for breast cancer treatment, was loaded into poly (amidoamine)-cholesterol carriers, producing particles in powder form with an average diameter of 500 nm (Cavalli et al., 2011). Wu et al incorporated active doxorubicin (DOX) into elastin-like polypeptides, producing biocompatible NPs ranging from 300 nm to 400 nm in diameter (Wu et al., 2009).

Cancer treatment using cyclophosphamide is advantageous due to the mode of action interfering with DNA replication of cancer cells. A study by Gulfam found 7% gliadin polymer entrapped 72.02% of cyclophosphamide following Esy deposition (Gulfam et al., 2012). Gradual release of the drug from the gliadin NPs was observed for 48 hours and the homogenous NPs (218.66±5.1nm) demonstrated down regulation of BCC-2 protein in breast cancer cells following exposure for 24 hours. Luo et al also demonstrated high encapsulation using Esy to load hydroxycamptothecin into poly (benzyldehyde poly ethylene glycol) poly (D,L-lactide) NPs (Luo et al., 2014). These biodegradable, acid-labile NPs showed fewer side effects (e.g. tissue necrosis, tumour growth) in *in vivo* testing with Hepa2 cells and H22 tumour-bearing mice; a substantial improvement compared to existing methods (Venditto and Simanek, 2010).

More recently, Lee et al developed hyaluronic acid derivative nanocomposites to entrap the drug reservatol for local tumour treatment (Lee et al., 2016). The amphiphilic nature of hyaluronic-ceramide combined with Soluplus (a solubility enhancer) in this study enabled more than 80% of drug to be loaded into the nanocomposites. Compared to Soluplus alone, the

combination of solubility enhancer and hyaluronic acid derivatives demonstrated higher cellular uptake efficiency in CD44 receptor and positive human breast cancer cells. The nanocomposites had an average diameter of 230 nm and showed sustained, pH dependant release whilst showing decrease in *in vivo* clearance, highlighting the potential of Esy in theranostic nano-systems for receptor expressed cancers.

2.4.3.1.4 Non-Steroidal Anti-Inflammatory Drugs

NSAIDs are actives known for their role in pain mitigation and reduction of inflammation. The mode of action involves interfering with cyclo-oxygenase, an enzyme which controls the production of prostaglandins. Esy can bypass the time consuming manufacture of tablets and develop NSAID-loaded structures on demand with increased drug loading reducing the need for frequent dosage.

Yu et al prepared naproxen, a non-selective COX inhibitor, and lecithin-loaded PVP microparticles (MPs) as templates for molecular self-assembly for *in situ* liposome synthesis (Yu et al., 2012). Using Esy, an EE of 91.2% was achieved and *in vitro* release analysis from the self-assembled liposomes from Esy composites exhibited high EE (91.3%) and 80.7% drug release over 24 hours via Fickian diffusion.

Piroxicam is an analgesic NSAID described as a class 2 drug in the Biopharmaceutical Classification System, an active displaying low aqueous solubility and high permeability. A research group in Finland found that by electrospraying piroxicam, an unknown polymeric form of the NSAID could be yielded (Nyström et al., 2015). 3 polymorphs (I, II, III) have been found to date; with Esy now presenting yet another polymorph. X-ray Diffraction (XRD) analysis of the resulting structures demonstrated an unknown crystal structure of piroxicam. Comparison of Fourier Transform Infrared (FTIR) spectra of generated particles to that of form I of piroxicam showed evident changes with new functional groups and chemical bonds present in the atomised particles (11.4 µm). Various analytical methods (Scanning Electron Microscopy (SEM), Differential Scanning Calorimetry (DSC), High Pressure Liquid Chromatography (HPLC)) found the particles were spherical in shape and showed no signs of degradation during 127 days of storage.

Biodegradable PLGA microspheres loaded with celecoxib were developed to help improve the oral solubility of the drug (Bohr et al., 2012). Celecoxib remained in its amorphous state and the microspheres (28 µm) remained stable for up to 3 months.

2.4.3.1.5 Miscellaneous

PLGA has been utilised to encapsulate antibiotic metronidazole using trifluoroethanol, yielding microspheres 1774±167 nm in diameter (Prabhakaran et al., 2015). PLGA has also been used as a carrier for statin simvastatin (Imanparast et al., 2016). The biocompatible NPs (160 nm) developed here possessed high encapsulation (90.3%) and demonstrated enhanced aqueous solubility.

Hia et al attempted to produce a self-healing composite system incorporating epoxy resin into alginate microcapsules (Hia et al., 2016). Although SN Esy was used in this study, the capsules that were produced presented core-shell structures commonly seen with a coaxially arranged system. The stable particles had an average diameter 320±20 µm and possessed the ability to heal up to 3 times more due to multi-core capsule structure, demonstrating the first sustainable, eco-friendly self-healing system.

2.4.3.2 Single Needle Electrospinning

As mentioned earlier, ES is the production of fibers using an electrical field. SN ES uses a similar device set-up to that of Esy i.e. a polymeric solution is fed through a conductive needle via a syringe pump. The drug is dissolved or dispersed into the polymer and solvent, achieving a homogenous distribution once fibers are formed. When the electrical force is applied and reaches the critical threshold at which the ST of the polymeric solution is overcome, rather than breaking up into particles (as with Esy), the jet becomes unstable. This results in a whipping motion of the liquid jet in the synapse between the needle and collection plate due to the applied voltage trying to overcome solution ST. This rapid whipping causes the solvent to evaporate, yielding polymeric fibers, which over time form fibrous mats. Over the past 2-3 decades, the interest in ES has spiked, allowing research to discover new applications for these fibrous structures including protein delivery (Li et al. 2005, Xu et al, 2013, Ozcan, Ertul and Maltas, 2016), anticancer therapy (Xie and Wang, 2006, Zhang et al, 2015) and bioengineering (Zakaria et al 2013, Dash et al 2011, Li et al 2014).

2.4.3.2.1 Protein delivery

Maintaining the bioactivity of sensitive materials like proteins can be challenging during processing or encapsulation. By optimising material properties and the EHD process, the bioactivity of biomacromolecules can be preserved whilst achieving high encapsulation efficiency.

Electrospun fibrous scaffolds have been developed which successfully incorporate biomacromolecules providing structural support as well as to stimulate tissue regeneration. A research group from Philadelphia, Pennsylvania fabricated PLGA, gelatin and elastin scaffolds with the ability to support dense cell growth (Li et al., 2005). Common limitations often seen with engineering of macroscopic tissue, such as necrotic cores, were absent with these fibers with the scaffolds showing high porosity, facilitating sufficient nutrient transport to a high number of cells as well waste removal.

BSA is a common protein used to model the potential of ES for protein delivery. Along with myoglobin, BSA has been incorporated into PLGA NFs (468±139 nm) forming scaffolds with a loading efficiency of around 80%. This dual-protein delivery system can be utilised and has potential for controlled tissue engineering application (Xu et al., 2013). Zeng et al demonstrated the encapsulation of BSA and enzyme luciferase into poly (vinyl acid) (PVA) fibers with both molecules retaining their bioactivity once electrospun (Zeng et al., 2005). BSA has also been used to develop fiber scaffolds with the ability to mimic tissue (Ozcan, Ertul and Maltas, 2016). Ozcan et al fabricated BSA, globulin, and haemoglobin fiber mats (75 nm, 117 nm and 220 nm in diameter, respectively) which had high surface area and were potential substrates for regenerative tissue growth.

Kim et al reported multi-functionalised electrospun scaffolds containing PCL fibers ranging from 100 nm to 200 nm in diameter (Kim, Choi and Cha, 2012). These fibers were loaded with mussel adhesive protein and exhibited apt mechanical strength with the ability to encapsulate protein without surface modification. *In vivo* analysis using a rat model showed the hydrophilicity of protein-PCL fibers facilitated keratinocyte growth demonstrating accelerated skin regeneration. The blended nanofibrous scaffolds also possessed an entrapment efficiency three times higher

than non-blended structures thereby increasing growth factor residence time in the wound. This allowed the activation of adjacent cells and hence improved skin regeneration (Kim et al., 2017).

2.4.3.2.2 Gene Therapy

Gene therapy has also benefitted from the ES process. The formulation, handling and logistics of DNA based formulations require great attention due to the sensitivity of the structure of DNA molecules and preservation of the DNA is vital for optimum treatment/delivery of DNA based drugs. The process parameters of ES enable such sensitive formulations to be handled without the integrity of the material being compromised.

One of the first studies which used the electrospinning process for DNA based application was in the late 1990s where DNA fibers using calf thymus-NA with diameters between 50 nm and 80 nm were observed (Fang and Reneker, 1997). Following this, experiments were directed towards preparing fibrous matrices incorporating lambda DNA, an *Escherichia coli* bacteriophage. Bellan et al isolated stretched DNA molecules and loaded them into polyethylene oxide (PEO) NFs (100-350 nm) (Bellan et al., 2006). Modifying the process parameters yielded fibers with smaller diameters, ranging from 50 nm to 250 nm.

DNA plasmids have also successfully been incorporated into fibrous polymer scaffolds using biodegradable co-block polymers (PLGA, Poly (lactic acid) (PLA) - poly (ethylene glycol) (PEG)). 10% copolymer block formulation gave fibers with diameter average of 250 to 875 nm. *In vitro* assessment of DNA release showed the plasmid was released from the scaffold intact with bioactive capabilities, highlighting the possibility of using ES for gene therapy (Luu et al., 2003).

The potential of DNA-based molecules small interfering RNA (siRNA), up until recently, have not been exploited fully with respect to silencing genes. siRNA are molecules comprising of 2 RNA strands, which can be integrated into “RNA induced silencing complexes” (Tokatlian and Segura, 2010) which controls mRNA binding and cleavage. However, delivery of siRNA has its limitations; both extracellular (degradation, specific cell targeting) and intracellular (endosomal escape, mRNA targeting) (Grabow and Jaeger, 2014). The therapeutic application of siRNA often takes the form of nanoparticles, however, for fundamental applications such as tissue regeneration, electrospun fiber production offers a cheap and simple alternative.

Cao et al encapsulated siRNA in a PCL shell to form polymeric nanofibers (300-400 nm in diameter) which achieved controlled release for 28 days under physiological conditions (Cao et al., 2010). The siRNA remained bioactive for this duration, showing potential for sustained gene delivery. Copolymeric nanofibers (caprolactone and ethyl ethylene phosphate) has also been used a platform to alter siRNA kinetics for siRNA delivery and gene silencing (Rujitanaroj et al., 2011).

2.4.3.2.3 Anticancer Therapy

Physiological conditions (pH 7.4, temperature 37°C) pose challenges with respect to administering a sustainable amount of drug to achieve a therapeutic effect at the site of action. By loading such drugs into electrospun fibrous mats, the amount and release of drug delivered to the site of the tumour can be controlled. The fibrous mat can be administered directly to the tumour site following surgery or for treating the tumour, ensuring almost all of the drug loaded into the matrix will be delivered at the desired site.

Cisplatin is one of the most potent anticancer drugs in medicine. It has been used extensively to treat various cancers including testicular, ovarian and bladder cancer. Although efforts to understand the exact mode of action of cisplatin still advance, it is clear that drug - DNA interaction is a key component. Mechanisms such as binding to the purine bases in the DNA double helix structure and the cisplatin interfering with the DNA repair mechanism (resulting in damage to DNA) have been associated with the mode of action. Xie et al developed optimised cisplatin-loaded PLA/PLGA fibers for the *in vitro* treatment of C6 glioma (Xie, Tan and Wang, 2008). SEM analysis showed the fibers (0.5 µm-1.7 µm) were interlocked, increasing the strength of the resulting fibrous mat produced in turn improving the efficacy of the scaffold. Paclitaxel-loaded fibers have also been produced to analyse its potential in treating C6 glioma (Xie and Wang, 2006). These PLGA fibers (30nm) had EE over 90% and provided sustained release for more than 60 days. Cytotoxicity tests were carried out to obtain the half maximal inhibitory concentration (IC_{50}) of the drug in this formulation. An IC_{50} value of 36 mg/mL was observed, a value comparable to Taxol®, a commercial paclitaxel formulation (W. Xie, Marijnissen and Wang, 2006).

DOX hydrochloride (DHCl) (an anticancer, bacterial antibiotic active) was used as a model drug to demonstrate the feasibility of drug delivery from electrospun PEG/Poly (L-lactic acid (PLLA) (di-block copolymer) fibers; using an emulsion rather than a solution (Xu et al., 2005). The fibers ranged from 300 nm to 1 µm in diameter with 1-5% drug content within the fibers. Using MTT methods (C6 cell lines) it was established that DHCl could be released without any detriment to its cytotoxicity. The encapsulated DHCl also had the same chemical structure and exhibited comparable antitumor activity to pure DOX, highlighting the EHDA process does not affect the drug in any way. PEG/PLA and PEO/water water-oil-emulsion was electrospun to create core-shell fibers, with average size of 749 µm (Xu et al., 2006). The resulting composite fibers exhibited a water-soluble polymeric core. In an extended study, Xu et al incorporated paclitaxel into the oil phase of a w/o emulsion and DHCl into the aqueous phase, creating a multi-drug delivery system (Xu et al., 2009). SEM images showed smooth surfaces on the fibers (730 nm) with crystal formation, indicating both drugs were finely incorporated within the nanofibers.

DOX was also loaded into carbon nanotubes which were successfully electrospun into PLLA fibers (326±63 nm) (Zhang et al., 2015). Combining ES with photothermal therapy induced cancer cell death as well as promoting increased diffusion of DOX to the tumour site, consequently demonstrating enhanced inhibitory effect on tumour growth.

2.4.3.2.4 Antibiotic Delivery

There are a wide variety of antibiotics available to prevent or treat bacterial infections. However, to maintain their antibacterial activity constant administration of the drug is required. Failure to do so can result in a concentration lower than the Minimum Inhibition Concentration (MIC), leading to antibiotic resistance. Maintaining the drug concentration above MIC can achieve the desired therapeutic effect over an extended period of time whilst preventing antibiotic resistance.

Incorporating the antibiotics into NFs has been found to extend the release of drug when ES fibrous mats are applied as wound dressings, accelerating the rate of wound healing as well as preventing infection. A research group in the USA developed a biodegradable gauze made of poly (lactic-co-glycolide) (PLAGA) NFs (Katti et al., 2004). These NFs were loaded with cefazolin, a broad spectrum bactericidal antibiotic. This API works by attaching to penicillin binding

proteins resulting in inhibition of cell wall synthesis for that bacterium. The electrospun fibers ranged from 470 nm to 490 nm. By modifying the process parameters the PLAGA fibers could be tailored for personalised for wound healing depending on the type and location of the wound.

More recently, PLGA fibers containing multiple antibiotics were developed for the prevention of orthopaedic implant associated infections (Gilchrist et al., 2013). The NFs (loaded with fusidic acid and rifampicin) had an average diameter of 612±32.2 nm with an EE exceeding 75%. Fibers loaded with 10% fusidic acid and 5% rifampicin caused a reduction of more than 99% of the adherent cells in a rodent model of implant associated infections.

Fluoroquinolone antibiotics (ciprofloxacin hydrochloride, levofloxacin hemihydrate or moxifloxacin hydrochloride) have been entrapped into poly (L-lactic-co-D,L-lactide)/PEG) matrix for wound dressings (Toncheva et al., 2012). The electrospun fibers exhibited a biphasic release profile with an initial burst release followed by sustained release, a fundamental prerequisite for wound treatment.

Zupancic et al incorporated ciprofloxacin into poly (methyl methacrylate) (PMMA) and PVA blended fibers or chitosan fibers which demonstrated drug release over 18 days (Zupancic et al., 2016). Ciprofloxacin loaded-PEO fibers in the same study showed the highest burst release whereas chitosan fibers showed the slowest release. Zupancic also loaded metronidazole into chitosan/PEO NFs for treatment for local infections. The biocompatible and biodegradable fibers were smaller than 80nm in diameter when using high drug loading (15%). Release kinetics of metronidazole varies with the fluid at the therapeutic site; areas with limited volume (e.g. chronic wounds) exhibited slower drug release whilst at sites with larger volumes of bodily fluids, such as the buccal mucosa, the fibers showed greater drug release.

A research group from Egypt produce gelatin electrospun fibers loaded with chloramphenicol 150-450nm in diameter (Nada et al., 2016). The resulting biocompatible, biodegradable fibers demonstrated strong inhibitory activity against gram positive *S. aureus*, gram negative *P. aeruginosa* and fungus *Candida albicans* whilst presenting sufficient EE of chloramphenicol.

2.4.3.2.5 Bioengineering

Material development and the continuous evolution of the ES process has allowed the process to be used in much more critical applications such as biomaterial engineering. Biomaterial electrospun systems can be developed to mimic bone extracellular matrix to repair primarily degenerated bone functionality (Liu et al., 2013).

Hydroxyapatite (HA) is a biomaterial largely used for bone replacement and regeneration. HA-loaded-fibers with diameters ranging from <100 nm to 20 µm have been produced using various polymeric matrices such as polyurethane (A. S. Khan et al., 2008), polyvinyl butyal (Zakaria et al., 2013), chitosan (Frohbergh et al., 2013) and PCL (Zakaria et al., 2013). For example, HA-loaded chitosan fibers were fabricated by Frohbergh et al for bone tissue engineering. The electrospun NFs were 227±154 nm in diameter and supported adhesion, proliferation and osteogenic differentiation of mouse 7F2 osteoblast-like cells. Crosslinking HA-loaded chitosan fibers with genipin yielded scaffolds useful in the repair and regeneration of maxillofacial defects and injuries (Frohbergh et al., 2013).

Chitosan along with collagen has been used extensively in this area due to their biocompatibility and resemblance to structures in the body such as skin, bone and muscle. Chitosan is a semi-synthetic versatile polymer that has a number of biomedical uses (Dash et al., 2011), whilst collagen is structural protein found in abundance in animal connective tissue which has been utilised in treating various bone and skin impediments (Matthews et al., 2002). Electrospun chitosan and collagen nanofibers have been used to produce novel matrices for wound dressings to encourage/promote skin regeneration. Type 1 collagen, chitosan and PEO were used to fabricate thin membranes of nanofibers (134±42 nm) (Chen, Chang and Chen, 2008). SEM images showed that a flow rate of 0.5 ml/h and an AV of 30 kV were the optimised electrospinning processing conditions to obtain nanofibers. *In vitro* studies showed good biocompatibility while *in vivo* animal studies proved the nanofiber membranes were sufficiently better than gauze and commercial collagen sponge wound dressings with respect to the rate of wound healing (Chen et al., 2008).

Chitosan has also been used in conjunction with polyurethane to fabricate silver sulfadiazine loaded fibers to enhance antibacterial activity and mechanical strength of wound dressings. The

fiber sheets exhibited strong antimicrobial activity by inhibition of bacterial growth of both gram positive *(S. aureus*) and gram negative (*P. aeruginosa*) bacteria whilst preventing infection of the wound (Lee et al., 2014).

Recent studies have also fabricated nanofibers combining chitosan with PEO to encapsulate multi-cancer treating drug 5 Fluorouracil, (5FU) to achieve controlled drug release for biomedical application (Li et al., 2014). 5FU has also been electrospun into nanofibers for use in tissue scaffolds and novel controlled drug delivery systems for multiple drugs using nanomicelles (Hu et al., 2014) as well as multifunctional PEO fibers containing amphiphilic vesicles for the encapsulation of hydrophobic 5FU and hydrophobic paeonolum (Li et al., 2015). The operating parameters of ES can evidently create systems that can efficiently encapsulate and potentially deliver "environmentally demanding" materials/actives.

Collagen micro and nanofibers have successfully been used as artificial skin support and as bone scaffolds highlighting the potential of using ES nanofibers as future material for tissue engineering (Matthews et al., 2002). Biodegradable poly(esteramides) (derived from L-alanine) scaffolds were fabricated to show potential for biomedical engineering. The nanofibers (average of 400 nm) proved to be a strong candidate for vascular tissue engineering (Srinath et al., 2012).

2.4.3.3 Complex EHDA Systems

An increase in material knowledge, material development and process understanding has enabled the EHDA process to evolve yielding complex and innovative systems for an array of applications.

Coaxial EHDA (Co EHDA) is the term used to describe when two conductive needles are used in conjunction in a coaxial arrangement. This configuration can be utilised for one-step encapsulation of APIs and therapeutic agents within a polymeric shell. The solutions used with this system are immiscible, therefore, the coaxially aligned needles produce particles with a defined shell and a defined core. As with single needle, this mode of EHDA can produce structures with narrow size distribution in the micro-/nano-meter range. Loscertales et al were the first to propose the use of two conjunctive needles. Using a coaxial set-up, capsules (inner needle: water, outer needle: olive oil) ranging between 150 nm and 10 µm were produced

(Loscertales et al., 2002). Chen et al found that when encapsulating cooking oil in a shell of ethanol, glycerol and tween, the outer liquid flow rate determined the properties of the spray itself (the viscosity, EC of the liquid) (Chen et al., 2005).

Co EHDA, like single needle, has been used to produce structures, encapsulating biomacromolecules such as peptides and proteins without denaturation and degradation. Angiotensin II was successfully encapsulated into N-octyl-O-Sulphate chitosan and tristearin, respectively; yielding NPs 100-300 nm in diameter, with peptide EE of 92±1.8%. A triphasic release profile is indicative of the emerging potential of Co EHDA (Rasekh et al., 2015b). model protein BSA has been encapsulated within a PLGA shell where the core-shell particles had diameters between 3 and 5.5 µm. The EE of BSA was 15.7% and 25.1% higher than emulsion Esy particles for high and low molecular PLGA, respectively (Zamani et al., 2014). BSA has also been encapsulated into biodegradable PLGA particles (3.4 µm) along with lysozyme which retained more than 90% of its bioactivity during release (more than 30 days), highlighting structure and function was not compromised by the Esy process (Xie et al., 2008).

A distinguishing aspect of EHDA is being able to produce structures with a large array of structures valuable for poorly soluble materials such as quercetin, a poorly soluble pigment used in the treatment of high blood pressure and diabetes. 3 formulations with various drug loadings with a PVP:Quercetin core and PVP:sodium shell were atomised at different flow rates. Quercetin remained in its amorphous form; unaffected by the EHD process. The interactions between the components increase the dissolution and permeability of quercetin, a theory easily applicable to other poorly water-soluble drugs for novel drug delivery systems (Li et al., 2014).

Laelorspoen et al developed zein microparticles consisting of an alginate and *Lactobacillus acidophilus* core to assess the ability to produce EHD delivery vehicles for microorganisms. The core-shell structures provided sufficient protection from harsh physiological conditions. The capsules (259±62 µm in diameter) improved the survival of the probiotic bacterium five-fold (Laelorspoen et al., 2014).

The evolving development and optimisation of process parameters and liquid properties has made the concept of producing nanocapsules a reality (Ghayempour and Mortazavi, 2013; Hao et al., 2015; Cao et al., 2014). Alginate nanocapsules as small as 80 nm where generated for the

encapsulation of an essential oil (Ghayempour and Mortazavi, 2013), whilst antibiotic agent metronidazole was loaded into Eudragit RS/PMMA core-shell particles, 60 nm in diameter. The amphiphilic (hydrophobic shell, hydrophilic core) metronidazole nanocapsules exhibited EE of 100.2±0.92% at 2% PMMA and sufficient controlled release, highlighting potential in an array of clinical applications (Hao et al., 2015).

Microbubbles (MBs) have successfully been developed and utilised in a vast array of application in the pharmaceutical industry e.g. ultrasound imaging and biomedical engineering (Li et al., 2008). Hollow microparticles (filled with air) are produced using a similar set-up to Co EHDA except air is passed through the inner needle. Farook et al prepared MB suspensions using a glycerol-air system. These MBs were less than 10 μm in diameter with narrow size distribution (Farook et al., 2007). By adapting this process it was possible to develop MBs with phospholipid coating. These MBs were produced at high yield rate (10^9 bubbles/min) and were found to decrease in size at physiological temperature. The size and shape reduced and maintained shape at 1-2 μm after 20 minutes, showing an increase in temperature increased the diffusion of air through the phospholipid shell (Farook, Stride and Edirisinghe, 2009).

Coaxial configuration of EHDA has also been used to develop protein (BSA) MBs and porous films (Ekemen, Ahmad et al., 2011; Ekemen, Chang et al., 2011; Ekemen et al., 2013; Mahaingam, Meinders and Edirisinghe, 2014) suggesting a novel tool in protein and peptide delivery. A combination of high production yield and uniform production with easily amendable size modifications show the potential for multiple biomedical applications including tissue engineering. For example, Ekemen et al developed silk fibroin bubbles (240-1000 μm) where the hollow bubbles also served as porous material when dehydrated; advantageous in bio-coatings and tissue engineering (Ekemen et al., 2013).

Coaxial configuration in ES is particularly useful for materials/solutions that cannot be electrically atomised (e.g. non-conductive); they can be passed through the inner nozzle and be entrapped in a polymeric shell to produce hollow or “core-sheath” structures (Jarusuwannapoom et al., 2005). For susceptible materials, the shell structure of fibres can protect the contents of the core whilst providing sustained release of the encapsulated material. The first work in producing unique core-sheath structures was done using w/o emulsion (Xu et

al., 2006). Coaxial Es (COES) has been used in developing drug delivery systems and has initiated various novel devices in nanotechnology.

Generation of core-shell fibres encapsulating anticancer drugs have exhibited controlled, sustained drug release and have demonstrated prohibition of cancer cells (Huang et al., 2009; Yan et al., 2014; Yang et al., 2015). Yang et al developed an implantable device which exploited the amphiphilic nature of micelles and broad application of polymeric NFs. Hydrophobic DOX was entrapped into micelles which formed the core of gelatin fibres along with PVA. The development of this biodegradable device reduced the drug dose required to be administered as well as administration frequency whilst still having a sufficient therapeutic effect against cancerous tissue (Yang et al., 2015).

PCL, like PVA, is a biodegradable polymer and has been commonly used for shell material for biodegradable NF scaffolds. It has been found to provide sustained release of various antibiotics (Huang et al., 2006; Park, Yoo et al., 2012). Chitosan-PCL core-shell fibres exhibited sustained release of levofloxacin; beneficial for prevention of bacterial infections stemming from post-operative surgery (Park et al., 2012). Antibiotic gentamycin sulphate and antioxidant resveratrol were encapsulated into PCL fibres to form double-layered ultrafine fibres (208-1585 nm for gentamycin-loaded fibres, 153-1317 nm for Resveratrol-loaded fibres) (Huang et al., 2006). Novel sustained ibuprofen delivery systems have also been developed in the form of triple component nanocomposites (Qian et al., 2013) and nanofibers (W. Huang et al., 2013). Zein (a prolamine protein) was used to evenly distribute ibuprofen (the core) into N,N-dimethylformamide fibres. Qian et al developed triple component nanocomposites (ibuprofen/PVA/ polyacrylonitrile (PAN)) with average diameter of 620±120 nm with 10.5% PVP content. Compared to double component nanocomposites (ibuprofen/PAN), the triple component structures significantly improved *in vitro* ibuprofen release kinetics, preventing the drug from being entrapped in the insoluble PAN molecules (Qian et al., 2013).

BSA has been frequently used as a model protein to demonstrate the delivery of proteins using COES (Xu et al., 2013, Jiang et al., 2005; Raheja et al., 2013). Electrospun fibrous scaffolds have been developed in which two proteins have been incorporated to provide structural support as well as for the stimulation of tissue regeneration. BSA and myoglobin were integrated into PLGA-

PF127 fibrous scaffolds (423±209 nm) with a loading efficiency of around 80% proving to be a useful dual protein delivery system for tissue engineering applications (Xu et al., 2013). BSA has also been incorporated into poly(l-lactide-co-ε-caprolactone) (PLLACL) NFs in conjunction with rhodamine B to develop novel dual drug release tissue engineering and drug delivery carriers (Su et al., 2012). More recently, electrospun PLLA/gum tragacanth NFs exhibited promising capabilities as grafts for nerve tissue regeneration showing high cell differentiation as well as higher proliferation. The addition of gum tragacanth increased the hydrophilicity of PLLA scaffolds as well as NF diameter (226±73 nm) (Ranjbar-Mohammadi et al., 2016).

The use of coaxial EHDA configuration has also extended to more complex routes of application, for example transdermal administration. PVP particles (100nm-3µm) were sprayed onto the tips of microneedles; providing a rapidly dissolving coating for burst release of drug in the dermis of the skin (Khan et al., 2014).

Systems using more than 2 needles arranged concentrically have successfully produced multi-layered structures, enabling the resulting products to have much more complex release kinetics. Biodegradable multi-layered fibres having been fabricated by Lui et al using triaxial (3 needle) electrospinning set up (Liu et al., 2013). PCL (intermediate layer) and gelatin (sheath and core) were electrospun and fibres of 25µm were generated, revealed by Field Emission Scanning electron microscopy (FESEM), showing the ability of preparing materials for application in biotechnology. PCL was also used to produce 3-layered NFs exhibiting sustained release of probes from the core and a burst release from the sheath, highlighting the potential use of dual-drug triaxial NF membranes for wound treatment, externally and internally (Han and Steckl, 2013).

An ongoing issue with ES is the rate of fiber production. To overcome this, research has diverted towards the use of multi-needle devices (Regele et al., 2002). Utilising a multi-needle electrospinning system is a cost effective, convenient, one-step method to fabricate specific structured nanofibres at a high production rate (Jiang et al., 2014). The use of several needles and syringes within the process allows the fabrication of fibrous mats such as tissues, electrospun from a multi-jet. This system is more complex than single needle or coaxial (2 needle) spinning as repulsion may occur between similarly charged jets. Multi-needle systems

require well thought out configuration of needles in order to optimise electrospinning productivity. Needles can be configured in various ways for example circular, triangular or hexagonal as demonstrated by Yang el al (Yang et al., 2010). Preliminary simulations studies showed that using outer needles in a hexagonal shape assisted in the creation of a uniform electric field near the tips of the nozzles; yielding finer PEO fibres (as small as 200 nm).

A novel approach for ES was developed by Yarin et al; utilising a needleless system with a magnetic suspension and magnetic field to force the suspension through a polymer solution, resulting in fibers which ranged from 200-800 nm in size. Perturbation of the polymer layer by the ferromagnetic suspension led to a 12-fold enhancement of the production rate of the ES process (Yarin and Zussman, 2004). Bocanegra et al also developed a needleless system which used orifices rather than nozzle capillaries to achieve a steady jet for atomization of liquids (Bocanegra et al., 2005). The system (consisting of up to 37 pores) was found to increase the stability and reliability of the EHDA process. The orifices were arranged in a planar hexagonal pattern with each delivering a cone-jet in the multi-spray system that behaved independently from adjacent jets. The multi-pore system was electrically stable, regardless of pore number or orifice diameter.

Jet-bending (from electrostatic interactions with neighbouring jets) has been demonstrated using a flute-like horizontal device for the high throughput production of PCL MPs (Zhang et al., 2015). The novel device utilised a multi-pore design instead of needle capillaries where modifying pore configuration and processing parameters yielded uniform MPs. The spatial location of these multiple pores found to have adverse effects on the stability of the jets with electrostatic forces between adjacent jets causing the jets to bend, generating particles with irregular morphologies. By manipulating the spatial locations, these inconsistences in morphology can be overcome.

Another recent development has moved away from concentric nozzles, and focused more on aligned or converging nozzles (also termed co-jetting). Here, atomised materials do not encapsulate one another, but rather form composites as segmented compartments. These have been useful for the preparation of several Janus particle systems, which are able to combine functional properties through precursor spraying (for further processing) (Mou et al., 2013), as

well as altering the shape and segment loading volume which has great potential in targeted drug delivery (Rahmani et al., 2015).

2.4.3.4 Utilising EHDA for Ocular Drug Delivery

Only in recent years has the potential of using EHDA for ocular application been recognised, with researchers producing fibrous structures for not only drug delivery but corneal tissue engineering. Lancina et al developed electrospun dendrimer nanofibers as a matrix to delivery anti-glaucoma drug brimonidine tartrate topically to the cornea (Lancina et al., 2017). Whilst IOP responses were similar between this developed system and pure drug solution, in a single dose test the dendrimer fibers demonstrated much improved efficacy over 3 weeks. This, along with the fibers exhibiting no toxicity or ocular irritation, indicates these electrospun fibers have great potential as drug vehicle for topical ocular drug delivery.

Antibiotic-eluting sutures for post-surgery treatment have been fabricated by a research team in the USA (Kashiwabuchi et al., 2017). Kashiwabuchi et al used a wet electrospinning process to develop levofloxacin sutures, which were 45.11 ± 7.7 µm in diameter and successfully inhibited the growth of *Staphylococcus epidermis*, an ocular infecting bacteria. The PLLA-PEG absorbable sutures were histologically equivalent to commercial available nylon used for the same application. Using ES in this manner yielded strong, absorbable sutures capable for delivery of not only antibiotics but also other ocular actives. Antibiotics acyclovir, ciprofloxacin and cyanocobalamin have also been loaded into PVP and PCL fibers yielding 2 sets of electrospun fibers which possessed half-lives of up to 6 days (Baskakova et al., 2016). This is greater than those of a pure drug solution using the same *in vivo* model, highlighting the potential for generation of intravitreal implants. PCL has also been used for an implantable scaffold, developed as a delivery system for cells and drugs to the eye (Irani et al., 2015). PCL fibers with pressed, nanostructured porous silicone MPs displayed successful attachment to human lens epithelial cells ($SRAOVG_4$) and proliferated the growth of these cells. To assess drug release, insulin was seeded onto the pressed porous composites and the insulin was released continuously over 6 days, with an initial burst release followed by subsequent slower release. Whilst these composites did not cause neovascularisation, they did trigger a mild foreign body response. The ability to support attachment and growth of ocular epithelial cells highlights the potential of this composite as a novel implantable device for treatment.

PCL has also been used as a matrix to deliver antibiotic ofloxacin for the treatment of ocular infections (Karatas et al., 2016). The yielded fibers released ofloxacin via burst release and microbiological activity was tested against *P. aeruginosa, S. epidermis* and *S. aureus* results showed the fibers released sufficient ofloxacin to successfully inhibit the growth of the tested bacteria.

The potential of using ES for ocular inserts has been scrutinised and compared to the technique of solvent casting (Bhattarai et al., 2017). The electrospun PLA/PVA fibers were found to be much thinner (1% PVA = 50 µm, 5% PVA = 62.5 µm) than brittle solvent cast polymer inserts (>200 µm) and were capable of releasing drug in a sustained manner.

With biocompatibility being a crucial prerequisite when developing novel ocular delivery systems, full *in vitro* and *in vivo* testing is essential. Da Silva et al demonstrated the biocompatibility of PCL NFs using M10-M1 and ARPE-19 cell cultures (*in vitro*) and rats (*in vivo*) using Optical Coherence Topography and Histology (Da Silva et al., 2015). They found the fibers proliferated in the *in vitro* cells and formed organised monolayers. The NFs also displayed great potential in the *in vivo* characterisation test by not producing an inflammatory reaction and the retinal cells did not express pro-inflammatory cytokines. This display of cellular biocompatibility highlights the potential of PCL as a carrier or matrix in ocular drug delivery.

In addition, PLGA has been electrospun to produce rapidly biodegrading membranes for cultural limbal stem cell transplantation (Sefat et al., 2013). These fibrous membranes were capable of supporting rLEC for at least 2-3 weeks, with subsequent breakdown due to uptake of water. What is noteworthy here is following 12 months of storage, the polymeric membrane was still able to support growth of limbal epithelial cells, highlighting the use of electrospun fibrous structures for long term cell delivery.

2.5 Conclusion

In this chapter I have reviewed the use of contact lenses as drug delivery devices and a number of methods of drug loading for said devices. A thorough review into EHDA and its current uses has allowed me to decipher the fundamental principles of the process and summarise the successful applications of this engineering process. By researching glaucoma and criticising methods currently used to treat and manage ocular conditions, I have chosen to select and take forward EHDA and contacts lenses with the aim to combine two well-known avenues to develop a novel, efficacious ocular drug delivery device.

2.6 References

ABDU, L., 2013. Epidemiological Properties of Primary Open Angle Glaucoma in Nigeria. *Journal of Ophthalmology,* , pp. 402739.

ACHEAMPONG, A., TANG-LIU, D., SHACKLETON, M., LAM, S., ANGELOV, O. and DING, S., 1996. Ocular absorption of cyclosporine from an aqueous emulsion: Comparison to other eyedrop formulations. *Investigative Ophthalmology and Visual Science,* 37(3), pp. S1026-S1026.

ACOTT, T.S. and KELLEY, M.J., 2008. Extracellular matrix in the trabecular meshwork. *Experimental Eye Research,* 86(4), pp. 543-561.

AGRAHARI, V., MANDAL, A., AGRAHARI, V., TRINH, H.M., JOSEPH, M., RAY, A., HADJI, H., MITRA, R., PAL, D. and MITRA, A.K., 2016. A comprehensive insight on ocular pharmacokinetics. *Drug Delivery and Translational Research,* 6(6), pp. 735-754.

AHMAD, Z., ZHANG, H.B., FAROOK, U., EDIRISINGHE, M., STRIDE, E. and COLOMBO, P., 2008. Generation of multilayered structures for biomedical applications using a novel tri-needle coaxial device and electrohydrodynamic flow. *Journal of the Royal Society Interface,* 5(27), pp. 1255-1261.

ALLINGHAM, R.R., LIU, Y. and RHEE, D.J., 2009. The genetics of primary open-angle glaucoma: A review. *Experimental Eye Research,* 88(4), pp. 837-844.

ALVAREZ-LORENZO, C., HIRATANI, H., GOMEZ-AMOZA, J.L., MARTINEZ-PACHECO, R., SOUTO, C. and CONCHEIRO, A., 2002. Soft contact lenses capable of sustained delivery of timolol. *Journal of Pharmaceutical Sciences,* 91(10), pp. 2182-2192.

ALVAREZ-LORENZO, C., YANEZ, F., BARREIRO-IGLESIAS, R. and CONCHEIRO, A., 2006. Imprinted soft contact lenses as norfloxacin delivery systems. *Journal of Controlled Release,* 113(3), pp. 236-244.

AMMAR, H.O., SALAMA, H.A., GHORAB, M. and MAHMOUD, A.A., 2010. Development of dorzolamide hydrochloride in situ gel nanoemulsion for ocular delivery. *Drug Development and Industrial Pharmacy,* 36(11), pp. 1330-1339.

ANDERSON, D.R., 2017-last update, Normal-Tension Glaucoma. Available: https://www.glaucoma.org/glaucoma/normal-tension-glaucoma.php.

ANDERSON, E.M., NOBLE, M.L., GARTY, S., MA, H., BRYERS, J.D., SHEN, T.T. and RATNER, B.D., 2009. Sustained release of antibiotic from poly(2-hydroxyethyl methacrylate) to prevent blinding infections after cataract surgery. *Biomaterials,* 30(29), pp. 5675-5681.

ANDRADE-VIVERO, P., FERNANDEZ-GABRIEL, E., ALVAREZ-LORENZO, C. and CONCHEIRO, A., 2007. Improving the loading and release of NSAIDs from pHEMA hydrogels by copolymerization with functionalized monomers. *Journal of Pharmaceutical Sciences,* 96(4), pp. 802-813.

ANSARI, E., 2017. An Update on Implants for Minimally Invasive Glaucoma Surgery (MIGS). *Ophthalmology and Therapy,* 6(2), pp. 233-241.

ANUMOLU, S.S., SINGH, Y., GAO, D., STEIN, S. and SINKO, P.J., 2009. Design and evaluation of novel fast forming pilocarpine-loaded ocular hydrogels for sustained pharmacological response. *Journal of Controlled Release,* 137(2), pp. 152-159.

ARTHUR, S. and CANTOR, L.B., 2011. Update on the role of alpha-agonists in glaucoma management. *Experimental Eye Research,* 93(3), pp. 271-283.

BALGURI, S.P., ADELLI, G.R. and MAJUMDAR, S., 2016. Topical ophthalmic lipid nanoparticle formulations (SLN, NLC) of indomethacin for delivery to the posterior segment ocular tissues. *European Journal of Pharmaceutics and Biopharmaceutics,* 109, pp. 224-235.

BAR-ILAN, A., BARU, H., BEILIN, M., FRIEDMAN, D., AMSELEM, S. and NEUMANN, R., 1994. Extended activity and increased bioavailability of indomethacin formulated in submicron emulsion, compared to commercially available formulation. *Regional Immunology,* 6(1-2), pp. 166-168.

BARRANCO ESPORCATTE, B.L. and TAVARES, I.M., 2016. Normal-tension glaucoma: an update. *Arquivos Brasileiros de Oftalmologia,* 79(4), pp. 270-276.

BASKAKOVA, A., AWWAD, S., JIMENEZ, J.Q., GILL, H., NOVIKOV, O., KHAW, P.T., BROCCHINI, S., ZHILYAKOVA, E. and WILLIAMS, G.R., 2016. Electrospun formulations of acyclovir, ciprofloxacin and cyanocobalamin for ocular drug delivery. *International Journal of Pharmaceutics,* 502(1-2), pp. 208-218.

BAZZAZ, B.S.F., KHAMENEH, B., JALILI-BEHABADI, M., MALAEKEH-NIKOUEI, B. and MOHAJERI, S.A., 2014. Preparation, characterization and antimicrobial study of a hydrogel (soft contact lens) material impregnated with silver nanoparticles. *Contact Lens & Anterior Eye,* 37(3), pp. 149-152.

BELLAN, L.M., CROSS, J.D., STRYCHALSKI, E.A., MORAN-MIRABAL, J. and CRAIGHEAD, H.G., 2006. Individually resolved DNA molecules stretched and embedded in electrospun polymer nanofibers. *Nano Letters,* 6(11), pp. 2526-2530.

BENGANI, L.C. and CHAUHAN, A., 2013. Extended delivery of an anionic drug by contact lens loaded with a cationic surfactant. *Biomaterials,* 34(11), pp. 2814-2821.

BENNETT, W.D., BROWN, J.S., ZEMAN, K.L., HU, S.C., SCHEUCH, G. and SOMMERER, K., 2002. Targeting delivery of aerosols to different lung regions. *Journal of Aerosol Medicine-Deposition Clearance and Effects in the Lung,* 15(2), pp. 179-188.

BHATTARAI, R.S., DAS, A., ALZHRANI, R.M., KANG, D., BHADURI, S.B. and BODDU, S.H.S., 2017. Comparison of electrospun and solvent cast polylactic acid (PLA)/polyvinyl alcohol) (PVA) inserts as potential ocular drug delivery vehicles. *Materials Science & Engineering C-Materials for Biological Applications,* 77, pp. 895-903.

BOCANEGRA, R., GALAN, D., MARQUEZ, M., LOSCERTALES, I.G. and BARRERO, A., 2005. Multiple electrosprays emitted from an array of holes. *Journal of Aerosol Science,* 36(12), pp. 1387-1399.

BOCK, N., DARGAVILLE, T.R. and WOODRUFF, M.A., 2012. Electrospraying of polymers with therapeutic molecules: State of the art. *Progress in Polymer Science,* 37(11), pp. 1510-1551.

BOHR, A., KRISTENSEN, J., DYAS, M., EDIRISINGHE, M. and STRIDE, E., 2012. Release profile and characteristics of electrosprayed particles for oral delivery of a practically insoluble drug. *Journal of the Royal Society Interface,* 9(75), pp. 2437-2449.

CAO, H., JIANG, X., CHAI, C. and CHEW, S.Y., 2010. RNA interference by nanofiber-based siRNA delivery system. *Journal of Controlled Release,* 144(2), pp. 203-212.

CAO, Y., WANG, B., WANG, Y. and LOU, D., 2014. Dual Drug Release from Core-Shell Nanoparticles with Distinct Release Profiles. *Journal of Pharmaceutical Sciences,* 103(10), pp. 3205-3216.

CAO, Y., ZHANG, C., SHEN, W., CHENG, Z., YU, L.(. and PING, Q., 2007. Poly(N-isopropylacrylamide)–chitosan as thermosensitive in situ gel-forming system for ocular drug delivery. *Journal of Controlled Release,* 120(3), pp. 186-194.

CAVALLI, R., BISAZZA, A., BUSSANO, R., TROTTA, M., CIVRA, A., LEMBO, D., RANUCCI, E. and FERRUTI, P., 2011. Poly(amidoamine)-Cholesterol Conjugate Nanoparticles Obtained by Electrospraying as Novel Tamoxifen Delivery System. *Journal of Drug Delivery,* 2011, pp. 587604.

CHAU-MINH PHAN, SUBBARAMAN, L.N. and JONES, L., 2014a. In vitro drug release of natamycin from beta-cyclodextrin and 2-hydroxypropyl-beta-cyclodextrin-functionalized contact lens materials. *Journal of Biomaterials Science-Polymer Edition,* 25(17), pp. 1907-1919.

CHAU-MINH PHAN, SUBBARAMAN, L., LIU, S., GU, F. and JONES, L., 2014b. In vitro uptake and release of natamycin Dex-b-PLA nanoparticles from model contact lens materials. *Journal of Biomaterials Science-Polymer Edition,* 25(1), pp. 18-31.

CHEEMA, A., CHANG, R.T., SHRIVASTAVA, A. and SINGH, K., 2016. Update on the Medical Treatment of Primary Open-Angle Glaucoma. *Asia-Pacific Journal of Ophthalmology,* 5(1), pp. 51-58.

CHEN, J., CHANG, G. and CHEN, J., 2008. Electrospun collagen/chitosan nanofibrous membrane as wound dressing. *Colloids and Surfaces A-Physicochemical and Engineering Aspects,* 313, pp. 183-188.

CHEN, X.P., JIA, L.B., YIN, X.Z., CHENG, J.S. and LU, J., 2005. Spraying modes in coaxial jet electrospray with outer driving liquid. *Physics of Fluids,* 17(3), pp. 032101.

CHENG, Y., HUNG, K., TSAI, T., LEE, C., KU, R., CHIU, A.W., CHIOU, S. and LIU, C.J., 2014. Sustained delivery of latanoprost by thermosensitive chitosan-gelatin-based hydrogel for controlling ocular hypertension. *Acta Biomaterialia,* 10(10), pp. 4360-4366.

COMPAN, V., LOPEZ, M.L., ANDRIO, A., LOPEZ-ALEMANY, A. and REFOJO, M.F., 1999. Determination of the oxygen transmissibility and permeability of hydrogel contact lenses. *Journal of Applied Polymer Science,* 72(3), pp. 321-327.

CONWAY, B.R., 2008. Recent patents on ocular drug delivery systems. *Recent Patents on Drug Delivery & Formulation,* 2(1), pp. 1-8.

COOLEY, J.F., 1902. *Apparatus for electrically dispersing fluids.*

COOLEY, J.F., 1900. *Improved methods of and apparatus for electrically separating the relatively volatile liquid component from the component of relatively fixed substances of composite fluids.*

COUTO, A.S., VIEIRA, J., FLORINDO, H.F., VIDEIRA, M.A. and CABRAL-MARQUES, H.M., 2014. Characterisation of DM-beta-cyclodextrin:prednisolone complexes and their formulation as eye drops. *Journal of Inclusion Phenomena and Macrocyclic Chemistry,* 80(1-2), pp. 155-164.

DA SILVA, G.R., LIMA, T.H., OREFICE, R.L., FERNANDES-CUNHA, G.M., SILVA-CUNHA, A., ZHAO, M. and BEHAR-COHEN, F., 2015. In vitro and in vivo ocular biocompatibility of

electrospun poly(epsilon-caprolactone) nanofibers. *European Journal of Pharmaceutical Sciences,* 73, pp. 9-19.

DANION, A., ARSENAULT, I. and VERMETTE, P., 2007. Antibacterial activity of contact lenses bearing surface-immobilized layers of intact Liposomes loaded with Levofloxacin. *Journal of Pharmaceutical Sciences,* 96(9), pp. 2350-2363.

DANION, A., BROCHU, H., MARTIN, Y. and VERMETTE, P., 2007. Fabrication and characterization of contact lenses bearing surface-immobilized layers of intact liposomes. *Journal of Biomedical Materials Research Part a,* 82A(1), pp. 41-51.

DASH, M., CHIELLINI, F., OTTENBRITE, R.M. and CHIELLINI, E., 2011. Chitosan-A versatile semi-synthetic polymer in biomedical applications. *Progress in Polymer Science,* 36(8), pp. 981-1014.

DAULL, P., BUGGAGE, R., LAMBERT, G., FAURE, M., SERLE, J., WANG, R. and GARRIGUE, J., 2012. A Comparative Study of a Preservative-Free Latanoprost Cationic Emulsion (Catioprost) and a BAK-Preserved Latanoprost Solution in Animal Models. *Journal of Ocular Pharmacology and Therapeutics,* 28(5), pp. 515-523.

DAULL, P., LALLEMAND, F. and GARRIGUE, J., 2014. Benefits of cetalkonium chloride cationic oil- in- water nanoemulsions for topical ophthalmic drug delivery. *Journal of Pharmacy and Pharmacology,* 66(4), pp. 531-541.

DAVE, V. and PALIWAL, S., 2014. A novel approach to formulation factor of aceclofenac eye drops efficiency evaluation based on physicochemical characteristics of in vitro and in vivo permeation. *Saudi Pharmaceutical Journal,* 22(3), pp. 240-245.

DJEBLI, N., KHIER, S., GRIGUER, F., COUTANT, A., TAVERNIER, A., FABRE, G., LERICHE, C. and FABRE, D., 2017. Ocular Drug Distribution After Topical Administration: Population Pharmacokinetic Model in Rabbits. *European Journal of Drug Metabolism and Pharmacokinetics,* 42(1), pp. 59-68.

DO, M.P., NEUT, C., METZ, H., DELCOURT, E., SIEPMANN, J., MAEDER, K. and SIEPMANN, F., 2015. Mechanistic analysis of PLGA/HPMC-based in-situ forming implants for periodontitis treatment. *European Journal of Pharmaceutics and Biopharmaceutics,* 94, pp. 273-283.

DUBEY, A. and PRABHU, P., 2014. Formulation and evaluation of stimuli-sensitive hydrogels of timolol maleate and brimonidine tartrate for the treatment of glaucoma. *International Journal of Pharmaceutical Investigation,* 4(3), pp. 112-118.

EKEMEN, Z., AHMAD, Z., EDIRISINGHE, M. and STRIDE, E., 2011. Forming of Protein Bubbles and Porous Films Using Co-Axial Electrohydrodynamic Flow Processing. *Macromolecular Materials and Engineering,* 296(1), pp. 8-13.

EKEMEN, Z., AHMAD, Z., STRIDE, E., KAPLAN, D. and EDIRISINGHE, M., 2013. Electrohydrodynamic Bubbling: An Alternative Route to Fabricate Porous Structures of Silk Fibroin Based Materials. *Biomacromolecules,* 14(5), pp. 1412-1422.

EKEMEN, Z., CHANG, H., AHMAD, Z., BAYRAM, C., RONG, Z., DENKBAS, E.B., STRIDE, E., VADGAMA, P. and EDIRISINGHE, M., 2011. Fabrication of Biomaterials via Controlled Protein Bubble Generation and Manipulation. *Biomacromolecules,* 12(12), pp. 4291-4300.

ELSHAER, A., GHATORA, B., MUSTAFA, S. and ALANY, R.G., 2014. Contact lenses as drug reservoirs & delivery systems: the successes & challenges. *Therapeutic Delivery,* 5, pp. 1085-1100.

FANG, X. and RENEKER, D.H., 1997. DNA fibers by electrospinning. *Journal of Macromolecular Science-Physics,* B36(2), pp. 169-173.

FAROOK, U., STRIDE, E. and EDIRISINGHE, M.J., 2009. Preparation of suspensions of phospholipid-coated microbubbles by coaxial electrohydrodynamic atomization. *Journal of the Royal Society Interface,* 6(32), pp. 271-277.

FAROOK, U., ZHANG, H.B., EDIRISINGHE, M.J., STRIDE, E. and SAFFARI, N., 2007. Preparation of microbubble suspensions by co-axial electrohydrodynamic atomization. *Medical Engineering & Physics,* 29(7), pp. 749-754.

FORMHALS, A., 1934. Process and apparatus for preparing artificial threads.

FORMHALS, A., 1938. Method and apparatus for the production of fibers.

FORRESTER, J.V., 2008. *The eye: basic sciences in practice.* 3rd edn. Edinburgh: Saunders Elsevier.

FORRESTER, J.V., DICK, A.D., MCMENAMIN, P.G., ROBERTS, F. and PEARLMAN, E., 2015. Anatomy of the eye and orbit. *The Eye: Basic Sciences in Practice.* 4th Edition edn. Saunders Ltd, pp. 1-102.

FROHBERGH, M.E., KATSMAN, A., BOTTA, G.P., LAZAROVICI, S.C.L.P., WEGST, U.G.K. and LELKES, P.I., 2013. Electrospun hydroxyapatite-containing chitosan nanofibers cross linked with genipin for bone tissue engineering. *Biomaterials,* 33, pp. 9167-9178.

FUREDI, P., PAPAY, Z.E., KOVACS, K., KISS, B.D., LUDANYI, K., ANTAL, I. and KLEBOVICH, I., 2017. Development and characterization of the voriconazole loaded lipid-based nanoparticles. *Journal of Pharmaceutical and Biomedical Analysis,* 132, pp. 184-189.

GARCIA-FERNANDEZ, M.J., TABARY, N., MARTEL, B., CAZAUX, F., OLIVA, A., TABOADA, P., CONCHEIRO, A. and ALVAREZ-LORENZO, C., 2013. Poly-(cyclo)dextrins as ethoxzolamide carriers in ophthalmic solutions and in contact lenses. *Carbohydrate Polymers,* 98(2), pp. 1343-1352.

GARCIA-MILLAN, E., KOPRIVNIK, S. and JAVIER OTERO-ESPINAR, F., 2015. Drug loading optimization and extended drug delivery of corticoids from pHEMA based soft contact lenses hydrogels via chemical and microstructural modifications. *International Journal of Pharmaceutics,* 487(1-2), pp. 260-269.

GARTY, S., SHIRAKAWA, R., WARSEN, A., ANDERSON, E.M., NOBLE, M.L., BRYERS, J.D., RATNER, B.D. and SHEN, T.T., 2011. Sustained Antibiotic Release from an Intraocular Lens-Hydrogel Assembly for Cataract Surgery. *Investigative Ophthalmology & Visual Science,* 52(9), pp. 6109-6116.

GASCO, M., GALLARATE, M., TROTTA, M., BAUCHIERO, L., GREMMO, E. and CHIAPPERO, O., 1989. Microemulsions as Topical Delivery Vehicles - Ocular Administration of Timolol. *Journal of Pharmaceutical and Biomedical Analysis,* 7(4), pp. 433-439.

GASMI, H., WILLART, J.-., DANEDE, F., HAMOUDI, M.C., SIEPMANN, J. and SIEPMANN, F., 2015. Importance of PLGA microparticle swelling for the control of prilocaine release. *Journal of Drug Delivery Science and Technology,* 30, pp. 123-132.

GHAYEMPOUR, S. and MORTAZAVI, S.M., 2013. Fabrication of micro–nanocapsules by a new electrospraying method using coaxial jets and examination of effective parameters on their production. *Journal of Electrostatics,* 71, pp. 717-727.

GIANNACCARE, G., FRESINA, M. and VERSURA, P., 2016. A Novel Osmoprotectant Tear Substitute for the Treatment of Dry Eye Disease. *International Journal of Ophthalmology and Clinical Research,* 3(2), pp. 1-6.

GILBERT, W., 1628. *De Magnete, Magneticisque Corporibus, et de Magno Magnete Tellure.* London:

GILCHRIST, S.E., LANGE, D., LETCHFORD, K., BACH, H., FAZLI, L. and BURT, H.M., 2013. Fusidic acid and rifampicin co-loaded PLGA nanofibers for the prevention of orthopedic implant associated infections. *Journal of Controlled Release,* 170(1), pp. 64-73.

GOMEZ, A., BINGHAM, D., DE JUAN, L. and TANG, K., 1998. Production of protein nanoparticles by electrospray drying. *Journal of Aerosol Science,* 29(5-6), pp. 561-574.

GONZALEZ-CHOMON, C., CONCHIERO, A. and ALVAREZ-LORENZO, C., 2013. Soft Contact Lensesfor controlled ocular delivery: 50 years in the making. *Therapeutic Delivery.,* 4, pp. 1141-1161.

GRABOW, W.W. and JAEGER, L., 2014. RNA Self-Assembly and RNA Nanotechnology. *Accounts of Chemical Research,* 47(6), pp. 1871-1880.

GRACE, J.M. and MARIJNISSEN, J.C.M., 1994. A Review of Liquid Atomization by Electrical Means. *Journal of Aerosol Science,* 25(6), pp. 1005-1019.

GUDMUNDSDOTTIR, B.S., PETURSDOTTIR, D., ASGRIMSDOTTIR, G.M., GOTTFREDSDOTTIR, M.S., HARDARSON, S.H., JOHANNESSON, G., KURKOV, S.V., JANSOOK, P., LOFTSSON, T. and STEFANSSON, E., 2014. gamma-Cyclodextrin Nanoparticle Eye Drops with Dorzolamide: Effect on Intraocular Pressure in Man. *Journal of Ocular Pharmacology and Therapeutics,* 30(1), pp. 35-41.

GUIDI, G., KOROGIANNAKI, M. and SHEARDOWN, H., 2014. Modification of timolol release from silicone hydrogel model contact lens materials using hyaluronic acid. *Eye and Contact Lens,* 40(5), pp. 269-276.

GULFAM, M., KIM, J., LEE, J.M., KU, B., CHUNG, B.H. and CHUNG, B.G., 2012. Anticancer Drug-Loaded Gliadin Nanoparticles Induce Apoptosis in Breast Cancer Cells. *Langmuir,* 28(21), pp. 8216-8223.

GULSEN, D., LI, C. and CHAUHAN, A., 2005. Dispersion of DMPC Liposomes in Contact Lenses for Ophthalmic Drug Delivery. *Current Eye Research,* 30, pp. 1071-1080.

GULSEN, D. and CHAUHAN, A., 2005. Dispersion of microemulsion drops in HEMA hydrogel: a potential ophthalmic drug delivery vehicle. *International Journal of Pharmaceutics,* 292(1-2), pp. 95-117.

GULSEN, D. and CHAUHAN, A., 2004. Ophthalmic drug delivery through contact lenses. *Investigative Ophthalmology & Visual Science,* 45(7), pp. 2342-2347.

GUPTA, H., JAIN, S., MATHUR, R., MISHRA, P., MISHRA, A.K. and VELPANDIAN, T., 2007. Sustained ocular drug delivery from a temperature and pH triggered novel in situ gel system. *Drug delivery,* 14(8), pp. 507-515.

HAN, D. and STECKL, A.J., 2013. Triaxial Electrospun Nanofiber Membranes for Controlled Dual Release of Functional Molecules. *Acs Applied Materials & Interfaces,* 5(16), pp. 8241-8245.

HAO, S., WANG, B. and WANG, Y., 2015. Porous hydrophilic core/hydrophobic shell nanoparticles for particle size and drug release control. *Materials Science and Engineering: C,* 49, pp. 51-57.

HEALEY, P.R. and THOMAS, R., 2010. Diagnosis and Clinical Features. In: P.R. HEALEY and R. THOMAS, eds, *Fast Facts: Glaucoma.* Oxford, UK: Health Press Limited, pp. 30-68.

HIA, L., PASBAKHSH, P., CHAN, E.S. and CHAI, S.P., 2016. Electrosprayed Multi-Core Alginate Microcapsules as Novel Self-Healing Containers. *Scientific Reports,* 6.

HILLMAN, J.S., 1974. Management of Acute Glaucoma with Pilocarpine-Soaked Hydrophilic Lens. *British Journal of Ophthalmology,* 58(7), pp. 674-679.

HIRATANI, H. and ALVAREZ-LORENZO, C., 2004. The nature of backbone monomers determines the performance of imprinted soft contact lenses as timolol drug delivery systems. *Biomaterials,* 25(6), pp. 1105-1113.

HIRATANI, H. and ALVAREZ-LORENZO, C., 2002. Timolol uptake and release by imprinted soft contact lenses made of N,N-diethylacrylamide and methacrylic acid. *Journal of Controlled Release,* 83(2), pp. 223-230.

HOHMAN, M.M., SHIN, M., RUTLEDGE, G. and BRENNER, M.P., 2001. Electrospinning and electrically forced jets. II. Applications. *Physics of Fluids,* 13(8), pp. 2221-2236.

HOSSAIN, M.F., GONG, R. and RIGOUT, M., 2015. Optimization of the process variables for electrospinning of poly(ethylene oxide)-loaded hydroxypropyl-β cyclodextrin nanofibres. *Journal of the Textile Institute,* 107 (10) pp. 1-11

HSU, K.-., GAUSE, S. and CHAUHAN, A., 2014. Review of ophthalmic drug delivery by contact lenses. *Journal of Drug Delivery Science and Technology,* 24(2), pp. 123-135.

HSU, K., FENTZKE, R.C. and CHAUHAN, A., 2013. Feasibility of corneal drug delivery of cysteamine using vitamin E modified silicone hydrogel contact lenses. *European Journal of Pharmaceutics and Biopharmaceutics,* 85(3), pp. 531-540.

HSU, K., LAZON DE LA JARA, P., ARIYAVIDANA, A., WATLING, J., HOLDEN, B., GARRETT, Q. and CHAUHAN, A., 2015. Release of betaine and dexpanthenol from vitamin e modified silicone-hydrogel contact lenses. *Current eye research,* 40(3), pp. 267-273.

HU, X.H. and LI, D., 2013. Facile way to synthesise hydrogel contact lenses with good performance for ophthalmic drug delivery. *Materials Technology,* 28(4), pp. 192-198.

HU, X., QIU, J., TAN, H., LI, D. and MA, X., 2013. Synthesis and Characterization of Cyclodextrin-containing Hydrogel for Ophthalmic Drugs Delivery. *Journal of Macromolecular Science Part A-Pure and Applied Chemistry,* 50(9), pp. 983-990.

HUANBUTTA, K., SANGNIM, T., LIMMATVAPIRAT, S., NUNTHANID, J. and SRIAMORNSAK, P., 2016. Design and characterization of prednisolone-loaded nanoparticles fabricated by electrohydrodynamic atomization technique. *Chemical Engineering Research & Design,* 109, pp. 816-823.

HUANG, H., HE, C., WANG, H. and MO, X., 2009. Preparation of core-shell biodegradable microfibers for long-term drug delivery. *Journal of Biomedical Materials Research Part a,* 90A(4), pp. 1243-1251.

HUANG, W., ZOU, T., LI, S., JING, J., XIA, X. and LIU, X., 2013. Drug-Loaded Zein Nanofibers Prepared Using a Modified Coaxial Electrospinning Process. *Aaps Pharmscitech,* 14(2), pp. 675-681.

HUANG, Z.M., HE, C.L., YANG, A.Z., ZHANG, Y.Z., HANG, X.J., YIN, J.L. and WU, Q.S., 2006. Encapsulating drugs in biodegradable ultrafine fibers through co-axial electrospinning. *Journal of Biomedical Materials Research Part a,* 77A(1), pp. 169-179.

HUI, A., SHEARDOWN, H. and JONES, L., 2012. Acetic and Acrylic Acid Molecular Imprinted Model Silicone Hydrogel Materials for Ciprofloxacin-HCl Delivery. *Materials,* 5(1), pp. 85-107.

HUI, A., WILLCOX, M. and JONES, L., 2014. In Vitro and In Vivo Evaluation of Novel Ciprofloxacin-Releasing Silicone Hydrogel Contact Lenses. *Investigative Ophthalmology & Visual Science,* 55(8), pp. 4896-4904.

IANCHULEV, T., AHMED, I.I.K., STAMPER, R.L., CHANG, D.F., SAMUELSON, T.W. and LINDSTROM, R.L., 2017. Innovative alternatives in the surgical management of glaucoma with cataract surgery. *Expert Review of Ophthalmology,* 12(5), pp. 403-419.

IMANPARAST, F., FARAMARZI, M.A., PAKNEJAD, M. and KOBARFARD, F., 2016. Preparation, optimization and characterisation of simvastatin nanoparticles by electrospraying: An artificial neural networks study. *Journal of Applied Polymer Science,* 133(28),

INTERNATIONAL GLAUCOMA ASSOCIATION, 2017-last update, Primary angle closure (acute) glaucoma. Available: https://www.glaucoma-association.com/about-glaucoma/types-of-glaucoma/acute-glaucoma/.

IRANI, Y.D., TIAN, Y., WANG, M., KLEBE, S., MCINNES, S.J., VOELCKER, N.H., COFFER, J.L. and WILLIAMS, K.A., 2015. A novel pressed porous silicon-polycaprolactone composite

as a dual-purpose implant for the delivery of cells and drugs to the eye. *Experimental Eye Research,* 139 pp: 123-131

ISMAIL, D., AMRANE, M., GARRIGUE, J.S. and BUGGAGE, R., 2011. A phase 2, randomized study evaluating the safety and efficacy of Catioprost® (unpreserved latanoprost 0.005% emulsion) compared to Travatan Z® in subjects with glaucoma and ocular surface disease. *Acta Ophthalmologica.* 89 (248)

JAFARI-NODOUSHAN, M., BARZIN, J. and MOBEDI, H., 2015. Size and morphology controlling of PLGA microparticles produced by electro hydrodynamic atomization. *Polymers for Advanced Technologies,* 26(5), pp. 502-513.

JANULEVICIENE, I., SIAUDVYTYTE, L., DILIENE, V., BARSAUSKAITE, R., SIESKY, B. and HARRIS, A., 2015. Effect of Trabeculectomy on Ocular Hemodynamic Parameters in Pseudoexfoliative and Primary Open-angle Glaucoma Patients. *Journal of Glaucoma,* 24(5), pp. e52-e56.

JARUSUWANNAPOOM, T., HONGROIJANAWIWAT, W., JITJAICHAM, S., WANNATONG, L., NITHITANAKUL, M., PATTAMAPROM, C., KOOMBHONGSE, P., RANGKUPAN, R. and SUPAPHOL, P., 2005. Effect of solvents on electro-spinnability of polystyrene solutions and morphological appearance of resulting electrospun polystyrene fibers. *European Polymer Journal,* 41(3), pp. 409-421.

JAWOREK, A. and KRUPA, A., 1999. Classification of the modes of EHD spraying. *Journal of Aerosol Science,* 30(7), pp. 873-893.

JAYASINGHE, S.N. and EDIRISINGHE, M.J., 2002. Effect of viscosity on the size of relics produced by electrostatic atomization. *Journal of Aerosol Science,* 33(10), pp. 1379-1388.

JIANG, H.L., HU, Y.Q., LI, Y., ZHAO, P.C., ZHU, K.J. and CHEN, W.L., 2005. A facile technique to prepare biodegradable coaxial electrospun nanofibers for controlled release of bioactive agents. *Journal of Controlled Release,* 108(2-3), pp. 237-243.

JIANG, S., DUAN, G., ZUSSMAN, E., GREINER, A. and AGARWAL, S., 2014. Highly Flexible and Tough Concentric Triaxial Polystyrene Fibers. *Acs Applied Materials & Interfaces,* 6(8), pp. 5918-5923.

JOHANNESSON, G., MOYA-ORTEGA, M.D., ASGRIMSDOTTIR, G.M., LUND, S.H., THORSTEINSDOTTIR, M., LOFTSSON, T. and STEFANSSON, E., 2014. Kinetics of gamma-cyclodextrin nanoparticle suspension eye drops in tear fluid. *Acta Ophthalmologica,* 92(6), pp. 550-556.

JOHANNESSON, G., STEFANSSON, E. and LOFTSSON, T., 2016. Microspheres and Nanotechnology for Drug Delivery. *Developments in ophthalmology,* 55, pp. 93-103.

JUNG, H.J., ABOU-JAOUDE, M., CARBIA, B.E., PLUMMER, C. and CHAUHAN, A., 2013. Glaucoma therapy by extended release of timolol from nanoparticle loaded silicone-hydrogel contact lenses. *Journal of Controlled Release,* 165(1), pp. 82-89.

KACZMAREK, J.C., TIEPPO, A., WHITE, C.J. and BYRNE, M.E., 2014. Adjusting biomaterial composition to achieve controlled multiple-day release of dexamethasone from an extended-wear silicone hydrogel contact lens. *Journal of Biomaterials Science-Polymer Edition,* 25(1), pp. 88-100.

KAKISU, K., MATSUNAGA, T., KOBAYAKAWA, S., SATO, T. and TOCHIKUBO, T., 2013. Development and Efficacy of a Drug-Releasing Soft Contact Lens. *Investigative Ophthalmology & Visual Science,* 54(4), pp. 2551-2561.

KANG-MIELER, J.J. and MIELER, W.F., 2016. Thermo-Responsive Hydrogels for Ocular Drug Delivery. *Developments in Ophthalmology,* 55, pp. 104-11.

KAPETANAKIS, V.V., CHAN, M.P.Y., FOSTER, P.J., COOK, D.G., OWEN, C.G. and RUDNICKA, A.R., 2016. Global variations and time trends in the prevalence of primary open angle glaucoma (POAG): a systematic review and meta-analysis. *British Journal of Ophthalmology,* 100(1), pp. 86-93.

KAPOOR, Y. and CHAUHAN, A., 2008. Drug and surfactant transport in Cyclosporine A and Brij 98 laden p-HEMA hydrogels. *Journal of Colloid and Interface Science,* 322(2), pp. 624-633.

KAPOOR, Y., THOMAS, J.C., TAN, G., JOHN, V.T. and CHAUHAN, A., 2009. Surfactant-laden soft contact lenses for extended delivery of ophthalmic drugs. *Biomaterials,* 30(5), pp. 867-878.

KARATAS, A., ALGAN, A.H., PEKEL-BAYRAMGIL, N., TURHAN, F. and ALTANLAR, N., 2016. Ofloxacin Loaded Electrospun Fibers for Ocular Drug Delivery: Effect of Formulation Variables on Fiber Morphology and Drug Release. *Current Drug Delivery,* 13(3), pp. 433-443.

KARLGARD, C.C.S., WONG, N.S., JONES, L.W. and MORESOLI, C., 2003. In vitro uptake and release studies of ocular pharmaceutical agents by silicon-containing and p-HEMA hydrogel contact lens materials. *International Journal of Pharmaceutics,* 257(1-2), pp. 141-151.

KASHIWABUCHI, F., PARIKH, K.S., OMIADZE, R., ZHANG, S., LUO, L., PATEL, H.V., XU, Q., ENSIGN, L.M., MAO, H., HANES, J. and MCDONNELL, P.J., 2017. Development of

Absorbable, Antibiotic-Eluting Sutures for Ophthalmic Surgery. *Translational Vision Science & Technology,* 6(1), pp. 1.

KATTI, D.S., ROBINSON, K.W., KO, F.K. and LAURENCIN, C.T., 2004. Bioresorbable nanofiber-based systems for wound healing and drug delivery: Optimization of fabrication parameters. *Journal of Biomedical Materials Research Part B-Applied Biomaterials,* 70B(2), pp. 286-296.

KHADKA, P., RO, J., KIM, H., KIM, I., KIM, J.T., KIM, H., CHO, J.M., YUN, G. and LEE, J., 2014. Pharmaceutical particle technologies: An approach to improve drug solubility, dissolution and bioavailability. *Asian Journal of Pharmaceutical Sciences,* 9(6), pp. 304-316.

KHAJAVI, R. and ABBASIPOUR, M., 2012. Electrospinning as a versatile method for fabricating coreshell, hollow and porous nanofibers. *Scientifica Iranica,* 19(6), pp 2029-2034

KHAN, A.S., AHMAD, Z., EDIRISINGHE, M.J., WONG, F.S. and REHMAN, I.U., 2008. Preparation and characterization of a novel bioactive restorative composite based on covalently coupled polyurethane-nanohydroxyapatite fibres. *Acta Biomaterialia,* 4, pp. 1275-1287.

KHAN, H., MEHTA, P., MSALLAM, H., ARMITAGE, D. and AHMAD, Z., 2014. Smart Microneedle coatings for controlled delivery and biomedical analysis. *Journal of Drug Targeting,* 22, pp. 790-795.

KHAN, N., AQIL, M., AMEEDUZZAFAR, IMAM, S.S. and ALI, A., 2015. Development and evaluation of a novel in situ gel of sparfloxacin for sustained ocular drug delivery: in vitro and ex vivo characterization. *Pharmaceutical Development and Technology,* 20(6), pp. 662-669.

KIM, B.J., CHEONG, H., CHOI, E., YUN, S., CHOI, B., PARK, K., KIM, I.S., PARK, D. and CHA, H.J., 2017. Accelerated skin wound healing using electrospun nanofibrous mats blended with mussel adhesive protein and polycaprolactone. *Journal of Biomedical Materials Research Part a,* 105(1), pp. 218-225.

KIM, B.J., CHOI, Y.S. and CHA, H.J., 2012. Reinforced Multifunctionalized Nanofibrous Scaffolds Using Mussel Adhesive Proteins. *Angewandte Chemie-International Edition,* 51(3), pp. 675-678.

KIM, J., CONWAY, A. and CHAUHAN, A., 2008. Extended delivery of ophthalmic drugs by silicone hydrogel contact lenses. *Biomaterials,* 29(14), pp. 2259-2269.

KIM, J., PENG, C. and CHAUHAN, A., 2010. Extended release of dexamethasone from silicone-hydrogel contact lenses containing vitamin E. *Journal of Controlled Release,* 148(1), pp. 110-116.

KIM, W. and KIM, S.S., 2011. Synthesis of biodegradable triple-layered capsules using a triaxial electrospray method. *Polymer,* 52(15), pp. 3325-3336.

KIMOTO, H. and TAKETO, A., 1996. Studies on electrotransfer of DNA into Escherichia coli: Effect of molecular form of DNA. *Biochimica Et Biophysica Acta-Gene Structure and Expression,* 1307(3), pp. 325-330.

KOROGIANNAKI, M., GUIDI, G., JONES, L. and SHEARDOWN, H., 2015. Timolol maleate release from hyaluronic acid-containing model silicone hydrogel contact lens materials. *Journal of Biomaterials Applications,* 30(3), pp. 361-376.

LAELORSPOEN, N., WONGSASULAK, S., YOOVIDHYA, T. and DEVAHASTIN, S., 2014. Microencapsulation of Lactobacillus acidophilus in zein–alginate core–shell microcapsules via electrospraying. *Journal of Functional Foods,* 7(0), pp. 342-349.

LAI, J., CHOY, B.N.K. and SHUM, J.W.H., 2016. Management of Primary Angle-Closure Glaucoma. *Asia-Pacific Journal of Ophthalmology,* 5(1), pp. 59-62.

LALLEMAND, F., DAULL, P., BENITA, S., BUGGAGE, R. and GARRIGUE, J., 2012. Successfully improving ocular drug delivery using the cationic nanoemulsion, novasorb. *Journal of Drug Delivery,* 2012, pp. 604204.

LANCINA,MICHAEL G.,,III, SINGH, S., KORNPELLA, U.B., HUSAIN, S. and YANG, H., 2017. Fast Dissolving Dendrimer Nanofiber Mats as Alternative to Eye Drops for More Efficient Antiglaucoma Drug Delivery. *Acs Biomaterials Science & Engineering,* 3(8), pp. 1861-1868.

LAUDENSLAGER, M.J. and SIGMUND, W.M., 2011. Developments in electrohydrodynamic forming: Fabricating nanomaterials from charged liquids via electrospinning and electrospraying. *American Ceramic Society Bulletin,* 90(2), pp. 22-26.

LEE, S.J., HEO, D.N., MOON, J., PARK, H.N., KO, W., BAE, M.S., LEE, J.B., PARK, S.W., KIM, E., LEE, C.H., JUNG, B. and KWON, I.K., 2014. Chitosan/Polyurethane Blended Fiber Sheets Containing Silver Sulfadiazine for Use as an Antimicrobial Wound Dressing. *Journal of Nanoscience and Nanotechnology,* 14(10), pp. 7488-7494.

LEE, S.Y., LEE, J., PARK, J., LEE, J., KO, S., SHIM, J., LEE, J., HEO, M.Y., KIM, D. and CHO, H., 2016. Electrosprayed nanocomposites based on hyaluronic acid derivative and Soluplus

for tumor-targeted drug delivery. *Colloids and Surfaces B: Biointerfaces,* 145, pp. 267-274.

LEE, Y., WU, B., ZHUANG, W., CHEN, D. and TANG, Y.J., 2011. Nanoparticles facilitate gene delivery to microorganisms via an electrospray process. *Journal of Microbiological Methods,* 84(2), pp. 228-233.

LI, K.Y., TU, H. and RAY, A.K., 2005. Charge limits on droplets during evaporation. *Langmuir,* 21(9), pp. 3786-3794.

LI, M., MONDRINOS, M.J., CHEN, X. and LELKES, P.I., 2005. Electrospun blends of natural and synthetic polymers as scaffolds for tissue engineering. *Conference proceedings: ...Annual International Conference of the IEEE Engineering in Medicine and Biology Society.IEEE Engineering in Medicine and Biology Society.Annual Conference,* 6, pp. 5858-5861.

LI, W., LUO, T., YANG, Y., TAN, X. and LUI, L., 2015. Formation of Controllable Hydrophilic/Hydrophobic Drug Delivery Systems by Electrospinning of Vesicles. *Langmuir,* 31, pp. 5141-5146.

LI, C., YU, D., WILLIAMS, G.R. and WANG, Z., 2014. Fast-Dissolving Core-Shell Composite Microparticles of Quercetin Fabricated Using a Coaxial Electrospray Process. *Plos One,* 9(3), pp. e92106.

LI, Q., LI, Z., ZENG, W., GE, S., LU, H., WU, C., GE, L., LIANG, D. and XU, Y., 2014. Proniosome-derived niosomes for tacrolimus topical ocular delivery: In vitro cornea permeation, ocular irritation, and in vivo anti-allograft rejection. *European Journal of Pharmaceutical Sciences,* 62, pp. 115-123.

LI, W., LUO, T., SHI, Y., YANG, Y., HUANG, X., XING, K., LIU, L. and WANG, M., 2014. Preparation, Characterization, and Property of Chitosan/Polyethylene Oxide Electrospun Nanofibrous Membrane for Controlled Drug Release. *Integrated Ferroelectrics,* 151(1), pp. 164-178.

LI, Y., LI, J., ZHANG, H.B. and SU, Y.S., 2008. Microbubble suspensions prepared via electrohydrodynamic jetting process, Y.Z. PENG Y., ed. In: *Microbubble suspensions prepared via electrohydrodynamic jetting process.*, Sanya, PEOPLES R CHINA2008, pp. 445-449.

LIAO, I.C., CHEW, S.Y. and LEONG, K.W., 2006. Aligned core-shell nanofibers delivering bioactive proteins. *Nanomedicine,* 1(4), pp. 465-471.

LIN, M.C. and SVITOVA, T.F., 2010. Contact Lenses Wettability In Vitro: Effect of Surface-Active Ingredients. *Optometry and Vision Science,* 87(6), pp. 440-447.

LIU, H., DING, X., ZHOU, G., LI, P., WEI, X. and FAN, Y., 2013. Electrospinning of Nanofibers for Tissue Engineering Applications. *Journal of Nanomaterials,* , pp. 495708.

LIU, H., WU, L., FU, S., HOU, Y., LIU, P., CUI, H., LIU, J., XING, L. and ZHANG, X., 2009. Polylactide-glycoli acid and rapamycin coating intraocular lens prevent posterior capsular opacification in rabbit eyes. *Graefes Archive for Clinical and Experimental Ophthalmology,* 247(6), pp. 801-807.

LIU, W., GRIFFITH, M. and LI, F., 2008. Alginate microsphere-collagen composite hydrogel for ocular drug delivery and implantation. *Journal of Materials Science-Materials in Medicine,* 19(11), pp. 3365-3371.

LIU, W., NI, C., CHASE, D.B. and RABOLT, J.F., 2013. Preparation of Multilayer Biodegradable Nanofibers by Triaxial Electrospinning. *Acs Macro Letters,* 2(6), pp. 466-468.

LIU, Y., LIU, J., ZHANG, X., ZHANG, R., HUANG, Y. and WU, C., 2010. In Situ Gelling Gelrite/Alginate Formulations as Vehicles for Ophthalmic Drug Delivery. *Aaps Pharmscitech,* 11(2), pp. 610-620.

LOSCERTALES, I.G., BARRERO, A., GUERRERO, I., CORTIJO, R., MARQUEZ, M. and GANAN-CALVO, A.M., 2002. Micro/nano encapsutation via electrified coaxial liquid jets. *Science,* 295(5560), pp. 1695-1698.

LU, C., YOGANATHAN, R.B., KOCIOLEK, M. and ALLEN, C., 2013. Hydrogel containing silica shell cross-linked micelles for ocular drug delivery. *Journal of pharmaceutical sciences,* 102(2), pp. 627-637.

LUO, X., JIA, G., SONG, H., LIU, C., WU, G. and LI, X., 2014. Promoting Antitumor Activities of Hydroxycamptothecin by Encapsulation into Acid-Labile Nanoparticles Using Electrospraying. *Pharmaceutical research,* 31(1), pp. 46-59.

LUO, X., XU, G., SONG, H., YANG, S., YAN, S., JIA, G. and LI, X., 2012. Promoted antitumor activities of acid-labile electrospun fibers loaded with hydroxycamptothecin via intratumoral implantation. *European Journal of Pharmaceutics and Biopharmaceutics,* 82(3), pp. 545-553.

LUU, Y.K., KIM, K., HSIAO, B.S., CHU, B. and HADJIARGYROU, M., 2003. Development of a nanostructured DNA delivery scaffold via electrospinning of PLGA and PLA-PEG block copolymers. *Journal of Controlled Release,* 89(2), pp. 341-353.

MAHAINGAM, S., MEINDERS, M.B.J. and EDIRISINGHE, M., 2014. Formation, Stability, and Mechanical Properties of Bovine Serum Albumin Stabilized Air Bubbles Produced Using Coaxial Electrohydrodynamic Atomization. *Langmuir,* 30(23), pp. 6694-6703.

MALAKOOTI, N., ALEXANDER, C. and ALVAREZ-LORENZO, C., 2015. Imprinted Contact Lenses for Sustained Release of Polymyxin B and Related Antimicrobial Peptides. *Journal of Pharmaceutical Sciences,* 104(10), pp. 3386-3394.

MANDAL, S., THIMMASETTY, M.K., PRABHUSHANKAR, G. and GEETHA, M., 2012. Formulation and evaluation of an in situ gel-forming ophthalmic formulation of moxifloxacin hydrochloride. *International Journal of Pharmaceutical Investigation,* 2(2), pp. 78-82.

MANJU, S. and KUNNATHEERI, S., 2010. Layer-by-Layer modification of Poly (methyl methacrylate) intra ocular lens: Drug delivery applications. *Pharmaceutical Development and Technology,* 15(4), pp. 379-385.

MARTIN, X.D., 1992. Normal Intraocular Pressure in Man. *Ophthalmologica,* 205(2), pp. 57-63.

MATLACH, J. and KLINK, T., 2015. Trabeculectomy versus canaloplasty. *Ophthalmologe,* 112(4), pp. 325-331.

MATTHEWS, J.A., WNEK, G.E., SIMPSON, D.G. and BOWLIN, G.L., 2002. Electrospinning of collagen nanofibers. *Biomacromolecules,* 3(2), pp. 232-238.

MAULVI, F.A., SONI, T.G. and SHAH, D.O., 2015. Extended release of hyaluronic acid from hydrogel contact lenses for dry eye syndrome. *Journal of Biomaterials Science. Polymer edition,* 26(15), pp. 1035-1050.

MCGHEE, C.N.J., DEAN, S. and DANESH-MEYER, H., 2002. Locally administered ocular corticosteroids - Benefits and risks. *Drug Safety,* 25(1), pp. 33-55.

MEHTA, P., HAJ-AHMAD, R., RASEKH, M., ARSHAD, M.S., SMITH, A., VAN DER MERWE, S.M., LI, X., CHANG, M. and AHMAD, Z., 2017. Pharmaceutical and biomaterial engineering via electrohydrodynamic atomization technologies. *Drug Discovery Today,* 22, pp. 157-165.

MEHTA, P., JUSTO, L., WALSH, S., ARSHAD, M.S., WILSON, C.G., O'SULLIVAN, C.K., MOGHIMI, S.M., VIZIRIANAKIS, I.S., AVGOUSTAKIS, K., FATOUROS, D.G. and AHMAD, Z., 2015. New platforms for multi-functional ocular lenses: engineering double-sided functionalized nano-coatings. *Journal of Drug Targeting,* 23(4), pp. 305-310.

MITRA, A.K., ANAND, B.S. and DUVVURI, S., 2005. Drug Delivery to the Eye. *Advances in Organ Biology,* 10, pp. 307-351.

MOGHADAM, H., SAMIMI, M., SAMIMI, A. and KHORRAM, M., 2009. Study of Parameters Affecting Size Distribution of Beads Produced from Electro-Spray of High Viscous Liquids. *Chemical. Engineering,* 6, pp. 88-98.

MOISSEIEV, E. and LOEWENSTEIN, A., 2017. Drug Delivery to the Posterioir Segment of the Eye. *Developments in Ophthalmology,* 58, pp. 87-101.

MORRISON, J. and POLLACK, I., 2002. *Glaucoma: Science and Practice.* 1 edn. Hong Kong: Thieme Medical Publishers.

MOU, F., CHEN, C., GUAN, J., CHEN, D.R. and JING, H., 2013. Oppositely Charged twin-head electrospray: a general strategy for building Janus Particles with controlled structures. *Nanoscale,* 5, pp. 2055-2064.

MUCHTAR, S., ALMOG, S., TORRACCA, M.T., SAETTONE, M.F. and BENITA, S., 1992. A Submicron Emulsion as Ocular Vehicle for Delta-8-Tetrahydrocannabinol - Effect on Intraocular-Pressure in Rabbits. *Ophthalmic research,* 24(3), pp. 142-149.

NADA, A.A., MONTASER, A.S., AZEEM, R.A.A. and MOUNIER, M.M., 2016. Eco-Friendly Gelatin-based Electrospun Fibers to Control the Release of Chloramphenicol. *Fibers and Polymers,* 17(12), pp. 1985-1994.

NANJWADE, B.K., DESHMUKH, R.V., GAIKWAD, K.R., PARIKH, K.A. and MANVI, F.V., 2012. Formulation and evaluation of micro hydrogel of Moxifloxacin hydrochloride. *European journal of drug metabolism and pharmacokinetics,* 37(2), pp. 117-123.

NIJHAWAN, R. and AGARWAL, S.P., 2003. Development of an ophthalmic formulation containing ciprofloxacin-hydroxypropyl-b-cyclodextrin complex. *Bollettino chimico farmaceutico,* 142(5), pp. 214-219.

NYSTRÖM, M., ROINE, J., MURTOMAA, M., SANKARAN, R.M., SANTOS, H.A. and SALONEN, J., 2015. Solid State transformations in consequence of electrospraying - A novel polymorphic form of piroxicam. *European Journal of Pharmaceutics and Biopharmaceutics,* 89, pp. 182-189.

OJEDA, E., PURAS, G., AGIRRE, M., ZARATE, J., GRIJALVO, S., ERITJA, R., MARTINEZ-NAVARRETE, G., SOTO-SANCHEZ, C., DIAZ-TAHOCES, A., AVILES-TRIGUEROS, M., FERNANDEZ, E. and PEDRAZ, J.L., 2016. The influence of the polar head-group of synthetic cationic lipids on the transfection efficiency mediated by niosomes in rat retina and brain. *Biomaterials,* 77, pp. 267-279.

OZCAN, F., ERTUL, S. and MALTAS, E., 2016. Fabrication of protein scaffold by electrospin coating for artificial tissue. *Materials Letters,* 182, pp. 359-362.

PARK, H., KIM, P., HWANG, T., KWON, O., PARK, T., CHOI, S., YUN, C. and KIM, J.H., 2012. Fabrication of cross-linked alginate beads using electrospraying for adenovirus delivery. *International Journal of Pharmaceutics,* 427(2), pp. 417-425.

PARK, H., YOO, H.H., HWANG, T., PARK, T., PAIK, D., 최성욱 and HYUN, K.I.M.J.U.N.G., 2012. Fabrication of levofloxacin-loaded nanofibrous scaffolds using coaxial electrospinning. *Journal of Pharmaceutical Investigation,* 42(2), pp. 89-93.

PATEL, P.B., SHASTRI, D.H., SHELAT, P.K., SHUKLA, A.K. and SHAH, G.B., 2012. Design and characterization of ofloxacin mucoadhesive in situ hydrogel. *African Journal of Pharmacy and Pharmacology,* 6(23), pp. 1644-1652.

PENG, C., BEN-SHLOMO, A., MACKAY, E.O., PLUMMER, C.E. and CHAUHAN, A., 2012. Drug Delivery by Contact Lens in Spontaneously Glaucomatous Dogs. *Current Eye Research,* 37(3), pp. 204-211.

PENG, C., BURKE, M.T., CARBIA, B.E., PLUMMER, C. and CHAUHAN, A., 2012. Extended drug delivery by contact lenses for glaucoma therapy. *Journal of Controlled Release,* 162(1), pp. 152-158.

PENG, C., BURKE, M.T. and CHAUHAN, A., 2012. Transport of Topical Anesthetics in Vitamin E Loaded Silicone Hydrogel Contact Lenses. *Langmuir,* 28(2), pp. 1478-1487.

PENG, C., KIM, J. and CHAUHAN, A., 2010. Extended delivery of hydrophilic drugs from silicone-hydrogel contact lenses containing Vitamin E diffusion barriers. *Biomaterials,* 31(14), pp. 4032-4047.

POKHARKAR, V., PATIL, V. and MANDPE, L., 2015. Engineering of polymer-surfactant nanoparticles of doxycycline hydrochloride for ocular drug delivery. *Drug delivery,* 22(7), pp. 955-968.

PRABHAKARAN, M.P., ZAMANI, M., FELICE, B. and RAMAKRISHNA, S., 2015. Electrospraying technique for the fabrication of metronidazole contained PLGA particles and their release profile. *Materials Science and Engineering: C,* 56, pp. 66-73.

PRABHU, P., DUBEY, A., PARTH, V. and GHATE, V., 2015. Investigation of hydrogel membranes containing combination of gentamicin and dexamethasone for ocular delivery. *International Journal of Pharmaceutical Investigation,* 5(4), pp. 214-225.

PRATT, N.L., RAMSAY, E.N., ELLETT, L.M.K., NGUYEN, T.A. and ROUGHEAD, E.E., 2015. Association between Ophthalmic Timolol and Hospitalisation for Bradycardia. *Journal of Ophthalmology,* pp. 567387.

PURAS, G., MARTINEZ-NAVARRETE, G., MASHAL, M., ZARATE, J., AGIRRE, M., OJEDA, E., GRIJALVO, S., ERITJA, R., DIAZ-TAHOCES, A., AVILES-TRIGUEROS, M., FERNANDEZ, E. and PEDRAZ, J.L., 2015. Protamine/DNA/Niosome Ternary Nonviral Vectors for Gene Delivery to the Retina: The Role of Protamine. *Molecular Pharmaceutics,* 12(10), pp. 3658-3671.

PURAS, G., MASHAL, M., ZARATE, J., AGIRRE, M., OJEDA, E., GRIJALVO, S., ERITJA, R., DIAZ-TAHOCES, A., MARTINEZ NAVARRETE, G., AVILES-TRIGUEROS, M., FERNANDEZ, E. and PEDRAZ, J.L., 2014. A novel cationic niosome formulation for gene delivery to the retina. *Journal of Controlled Release,* 174, pp. 27-36.

QIAN, W., YU, D., LI, Y., LI, X., LIAO, Y. and WANG, X., 2013. Triple-Component Drug-Loaded Nanocomposites Prepared Using a Modified Coaxial Electrospinning. *Journal of Nanomaterials,*pp. 826471.

QUIGLEY, H. and BROMAN, A.T., 2006. The Number of People with Glaucoma Worldwide in 2010 and 2020. *British Journal of Ophthalmology,* 90, pp. 262-267.

RAHEJA, A., AGARWAL, A., MUTHUVIJAYAN, V., CHANDRA, T.S. and NATARAJAN, T.S., 2013. Studies on Encapsulation of Bovine Serum Albumin, Lysozyme and Insulin Through Coaxial Electrospinning. *Journal of Biomaterials and Tissue Engineering,* 3(6), pp. 669-672.

RAHMANI, S., VILLA, C.H., DISHMAN, A.F., GRABOWSKI, M.E., PAN, D.C., DURMAZ, H., MISRA, A.C., COLÓN-MELÉNDEZ, L., SOLOMON, M.J., MUZYKANTOV, V.R. and LAHANN, J., 2015. Long-circulating Janus Nanoparticles made by electrohydrodynamic co-jetting for systemic drug delivery applications. *`Journal of Drug Targetting,* 23, pp. 750-758.

RANJBAR-MOHAMMADI, M., PRABHAKARAN, M.P., BAHRAMI, S.H. and RAMAKRISHNA, S., 2016. Gum tragacanth/poly(l-lactic acid) nanofibrous scaffolds for application in regeneration of peripheral nerve damage. *Carbohydrate Polymers,* 140, pp. 104-112.

RASEKH, M., YOUNG, C., ROLDO, M., LANCIEN, F., LE MEVEL, J., HAFIZI, S., AHMAD, Z., BARBU, E. and GORECKI, D., 2015. Hollow-layered nanoparticles for therapeutic delivery of peptide prepared using electrospraying. *Journal of Materials Science-Materials in Medicine,* 26(11), pp. 256.

RASSU, G., COSSU, M., LANGASCO, R., CARTA, A., CAVALLI, R., GIUNCHEDI, P. and GAVINI, E., 2015. Propolis as lipid bioactive nano-carrier for topical nasal drug delivery. *Colloids and surfaces.B, Biointerfaces,* 136, pp. 908-917.

RATHOD, L.V., KAPADIA, R. and SAWANT, K.K., 2017. A novel nanoparticles impregnated ocular insert for enhanced bioavailability to posterior segment of eye: In vitro, in vivo

and stability studies. *Materials Science & Engineering C-Materials for Biological Applications,* 71, pp. 529-540.

RAYLEIGH, L., 1878. On The Instability Of Jets. *Proc. London Math. Soc,* 11, pp. 4-13.

REGELE, J.D., PAPAC, M.J., RICKARD, M.J.A. and DUNN-RANKIN, D., 2002. Effects of capillary spacing on EHD spraying from an array of cone jets. *Journal of Aerosol Science,* 33(11), pp. 1471-1479.

RIBEIRO, A., VEIGA, F., SANTOS, D., TORRES-LABANDEIRA, J.J., CONCHEIRO, A. and ALVAREZ-LORENZO, C., 2012. Hydrophilic acrylic hydrogels with built-in or pendant cyclodextrins for delivery of anti-glaucoma drugs. *Carbohydrate Polymers,* 88(3), pp. 977-985.

RICHTER, G.M. and COLEMAN, A.L., 2016. Minimally invasive glaucoma surgery: current status and future prospects. *Clinical Ophthalmology,* 10, pp. 189-206.

RUJITANAROJ, P., WANG, Y., WANG, J. and CHEW, S.Y., 2011. Nanofiber-mediated controlled release of siRNA complexes for long term gene-silencing applications. *Biomaterials,* 32(25), pp. 5915-5923.

SAHEB, H. and AHMED, I.I.K., 2012. Micro-invasive glaucoma surgery: current perspectives and future directions. *Current Opinion in Ophthalmology,* 23(2), pp. 96-104.

SAHOO, R.K., BISWAS, N. and GUHA, A., 2014. Nonionic Surfactant Vesicles in Ocular Delivery : Innovative Approaches and Perspectives. *Biomedical Research International,* 2014, pp. 263-304.

SAMANT, M., MEDSINGE, A. and NISCHAL, K.K., 2016. Pediatric Glaucoma: Pharmacotherapeutic Options. *Pediatric Drugs,* 18(3), pp. 209-219.

SAMPLES, J.R., SINGH, K., LIN, S.C., FRANCIS, B.A., HODAPP, E., JAMPEL, H.D. and SMITH, S.D., 2011. Laser Trabeculoplasty for Open-Angle Glaucoma. *Ophthalmology,* 118(11), pp. 2296-2302.

SATO, T., UCHIDA, R., TANIGAWA, H., UNO, K. and MURAKAMI, A., 2005. Application of polymer gels containing side-chain phosphate groups to drug-delivery contact lenses. *Journal of Applied Polymer Science,* 98(2), pp. 731-735.

SCHAEFFER, H.E. and KROHN, D.L., 1982. Liposomes in Topical Drug Delivery. *Investigative Ophthalmology and Visual Science,* 22, pp. 220-227.

SCHEIDELER, W.J. and CHEN, C.H., 2014. The minimum flow rate scaling of Taylor cone-jets issued from a nozzle. *Applied Physics Letters,* 104.

SCHOPF, L.R., POPOV, A.M., ENLOW, E.M., BOURASSA, J.L., ONG, W.Z., NOWAK, P. and CHEN, H., 2015. Topical Ocular Drug Delivery to the Back of the Eye by Mucus-Penetrating Particles. *Translational Vision Science and Technology,* 4, pp. 11.

SEFAT, F., MCKEAN, R., DESHPANDE, P., RAMACHANDRAN, C., HILL, C.J., SANGWAN, V.S., RYAN, A.J. and MACNEIL, S., 2013. Production, sterilisation and storage of biodegradable electrospun PLGA membranes for delivery of limbal stem cells to the cornea. *3rd International Conference on Tissue Engineering (Icte2013),* 59, pp. 101-116.

SHASTRI, D., PATEL, L. and PARIKH, R., 2010. Studies on In situ Hydrogel: A Smart Way for Safe and Sustained Ocular Drug Delivery. *Journal of Young Pharmacists : JYP,* 2(2), pp. 116-120.

SHULMAN, S., JOHANNESSON, G., STEFANSSON, E., LOEWENSTEIN, A., ROSENBLATT, A. and HABOT-WILNER, Z., 2015. Topical dexamethasone-cyclodextrin nanoparticle eye drops for non-infectious Uveitic macular oedema and vitritis - a pilot study. *Acta Ophthalmologica,* 93(5), pp. 411-415.

SMITH, D., 1986. The Electrohydrodynamic Atomization of liquids. *IEEE Transactions on Industry Applications,* 22 (3), pp. 527-535.

SMOLIN, G., OKUMOTO, M., CONDON, D. and FEILER, L.S., 1980. Liposomes for Drug Delivery in Herpetic Keratitis. *Investigative Ophthalmology and Visual Science,* (SUPPL), pp. 158-158.

SMOLIN, G., OKUMOTO, M., FEILER, S. and CONDON, D., 1981. Idoxuridine-Liposome Therapy for Herpes Simplex Keratitis. *American Journal of Ophthalmology,* 91(2), pp. 220-225.

SRINATH, D., LIN, S., KNIGHT, D.K., RIZKALLA, A.S. and MEQUANINT, K., 2012. Fibrous Biodegradable l-alanine-based scaffolds for vascular tissue engineering. *Journal of Tissue Engineering and Regenerative Medicine* 8 (7), pp. 578-588.

SU, Y., SU, Q., LIU, W., JIN, G., MO, X. and RAMAKRISHNA, S., 2012. Dual-Drug Encapsulation and Release from Core-Shell Nanofibers. *Journal of Biomaterials Science-Polymer Edition,* 23 (7), pp. 861-871.

SUKSAMRAN, T., OPANASOPIT, P., ROJANARATA, T., NGAWHIRUNPAT, T., RUKTANONCHAI, U. and SUPAPHOL, P., 2009. Biodegradable alginate microparticles developed by electrohydrodynamic spraying techniques for oral delivery of protein. *Journal of Microencapsulation,* 26 (7), pp. 563-570.

SWIERKOWSKA, J. and GAJECKA, M., 2017. Genetic factors influencing the reduction of central corneal thickness in disorders affecting the eye. *Ophthalmic Genetics,* 38(6), pp. 501-510.

TAMILVANAN, S. and BENITA, S., 2004. The potential of lipid emulsion for ocular delivery of lipophilic drugs. *European Journal of Pharmaceutics and Biopharmaceutics,* 58(2), pp. 357-368.

TANG, K.Q. and GOMEZ, A., 1995. Generation of Monodisperse Water Droplets from Electrosprays in a Corona-Assisted Cone-Jet Mode. *Journal of Colloid and Interface Science,* 175(2), pp. 326-332.

TASHAKORI-SABZEVAR, F. and MOHAJERI, S.A., 2015. Development of ocular drug delivery systems using molecularly imprinted soft contact lenses. *Drug Development and Industrial Pharmacy,* 41(5), pp. 703-713.

TAYLOR, G., 1964a. Disintegration of Water Droplets in an Electric Field. *Proceedings of the Royal Society A,* 280 (1382), pp. 383.

TAYLOR, G., 1964b. The force exerted by an electric field on a long cylindrical conductor. *Proceedings of the Royal Society A,* 280 (1425), pp. 383.

THAM, Y., LI, X., WONG, T.Y., QUIGLEY, H.A., AUNG, T. and CHENG, C., 2014. Global Prevalence of Glaucoma and Projections of Glaucoma Burden through 2040 A Systematic Review and Meta-Analysis. *Ophthalmology,* 121(11), pp. 2081-2090.

THOMAS, N., LÄHDESMÄKI, I. and PARVIZ, B.A., 2012. A contact lens with an integrated lactate sensor. *Sensors and Actuators B: Chemical,* 162(1), pp. 128-134.

THRIMAWITHANA, T.R., YOUNG, S., BUNT, C.R., GREEN, C. and ALANY, R.G., 2011. Drug Delivery to the posterior segment of the eye. *Drug Discovery Today,* 16 (5-6), pp. 270-277.

TOKATLIAN, T. and SEGURA, T., 2010. siRNA applications in nanomedicine. *Wiley Interdisciplinary Reviews-Nanomedicine and Nanobiotechnology,* 2 (3), pp. 305-315.

TONCHEVA, A., PANEVA, D., MAXIMOVA, V., MANOLOVA, N. and RASHKOV, I., 2012. Antibacterial fluoroquinolone antibiotic-containing fibrous materials from poly(L-lactide-co-D,L-lactide) prepared by electrospinning. *European Journal of Pharmaceutical Sciences,* 47(4), pp. 642-651.

TONSOMBOON, K. and OYEN, M.L., 2013. Composite electrospun gelatin fiber-alginate gel scaffolds for mechanically robust tissue engineered cornea. *Journal of the Mechanical Behavior of Biomedical Materials,* 21 , pp. 185-194.

TRAN, V.B., SUNG, Y.S., COPLEY, K. and RADKE, C.J., 2012. Effects of aqueous polymeric surfactants on silicone-hydrogel soft- contact-lens wettability and bacterial adhesion of Pseudomonas aeruginosa. *Contact Lens & Anterior Eye,* 35(4), pp. 155-162.

UCHIDA, R., SATO, T., TANIGAWA, H. and UNO, K., 2003. Azulene incorporation and release by hydrogel containing methacrylamide propyltrimenthylammonium chloride, and its application to soft contact lens. *Journal of Controlled Release,* 92(3), pp. 259-264.

VANDERLAAN, D.G., NUNEZ, I.M., HARGISS, M., ALTON, M.L. and WILLAMS, S., 1999. *Soft Contact Lenses.*

VENDITTO, V.J. and SIMANEK, E.E., 2010. Cancer Therapies Utilizing the Camptothecins: A Review of the in Vivo Literature. *Molecular Pharmaceutics,* 7(2), pp. 307-349.

VIDAL-ROHR, M., WOLFFSOHN, J.S., DAVIES, L.N. and CERVINO, A., 2018. Effect of contact lens surface properties on comfort, tear stability and ocular physiology. *Contact Lens & Anterior Eye,* 41(1), pp. 117-121.

WALTMAN, S.R. and KAUFMAN, H.E., 1970. Use of Hydrophilic Contact Lenses to Increase Ocular Penetration of Topical Drugs. *Investigative ophthalmology,* 9(4), pp. 250-&.

WEI, J., HE, H., ZHENG, C. and ZHU, J., 2011. Chitosan-coated ophthalmic submicro emulsion for pilocarpine nitrate. *Acta pharmaceutica Sinica,* 46(8), pp. 990-6.

WHEELER, J., WOODS, J., COX, M., CANTRELL, R., WATKINS, F. and EDLICH, R., 1996. Evolution of hydrogel polymers as contact lenses, surface coatings, dressings, and drug delivery systems. *Journal of Long-Term Effects of Medical Implants,* 6(3-4), pp. 207-217.

WIGGS, J.L. and PASQUALE, L.R., 2017. Genetics of glaucoma. *Human Molecular Genetics,* 26(R1), pp. R21-R27.

WILSON, C.G., SEMENOVA, E.M., HUGHES, P.M. and OLEJNIK, O., 2011. Eye Structure and Physiological Functions. *Enhancement in Drug Delivery.* 1st edn. Florida: Taylor & Francis Group, pp. 473-486.

WILSON, C., 2004. Topical drug delivery in the eye. *Experimental eye research,* 78(3), pp. 737-743.

WU, Y. and CLARK, R.L., 2008. Electrohydrodynamic atomization: a versatile process for preparing materials for biomedical applications. *Journal of Biomaterial Science: Polymer Edition,* 19 (5), pp. 573-601.

WU, Y., DUONG, A., JAMES, L.L. and WYSLOUZIL, B.E., 2012. Electrospray Production of Nanoparticles for Drug/Nucleic Acid Delivery. In: DR ABBASS A. HASHIM, ed, *The Delivery of Nanoparticles.* pp. 223-242.

XIE, J.W., MARIJNISSEN, J.C.M. and WANG, C.H., 2006. Microparticles developed by electrohydrodynamic atomization for the local delivery of anticancer drug to treat C6 glioma in vitro. *Biomaterials,* 27(17), pp. 3321-3332.

XIE, J., TAN, R.S. and WANG, C., 2008. Biodegradable microparticles and fiber fabrics for sustained delivery of cisplatin to treat C6 glioma in vitro. *Journal of Biomedical Materials Research Part a,* 85A(4), pp. 897-908.

XIE, J. and WANG, C., 2006. Electrospun micro- and nanofibers for sustained delivery of paclitaxel to treat C6 glioma in vitro. *Pharmaceutical Research,* 23(8), pp. 1817-1826.

XU, J., LI, X. and SUN, F., 2010. Cyclodextrin-containing hydrogels for contact lenses as a platform for drug incorporation and release. *Acta Biomaterialia,* 6(2), pp. 486-493.

XU, W., ATALA, A., YOO, J.J. and LEE, S.J., 2013. Controllable dual protein delivery through electrospun fibrous scaffolds with different hydrophilicities. *Biomedical Materials,* 8(1), pp. 014104.

XU, X.L., YANG, L.X., XU, X.Y., WANG, X., CHEN, X.S., LIANG, Q.Z., ZENG, J. and JING, X.B., 2005. Ultrafine medicated fibers electrospun from W/O emulsions. *Journal of Controlled Release,* 108(1), pp. 33-42.

XU, X., CHEN, X., WANG, Z. and JING, X., 2009. Ultrafine PEG-PLA fibers loaded with both paclitaxel and doxorubicin hydrochloride and their in vitro cytotoxicity. *European Journal of Pharmaceutics and Biopharmaceutics,* 72(1), pp. 18-25.

XU, X., ZHUANG, X., CHEN, X., WANG, X., YANG, L. and JING, X., 2006. Preparation of core-sheath composite nanofibers by emulsion electrospinning. *Macromolecular Rapid Communications,* 27(19), pp. 1637-1642.

XU, X., WENG, Y., XU, L. and CHEN, H., 2013. Sustained release of avastin® from polysaccharides cross-linked hydrogels for ocular drug delivery. *International Journal of Biological Macromolecules,* 60, pp. 272-276.

YAN, E., FAN, Y., SUN, Z., GAO, J., HAO, X., PEI, S., WANG, C., SUN, L. and ZHANG, D., 2014. Biocompatible core-shell electrospun nanofibers as potential application for chemotherapy against ovary cancer. *Materials Science & Engineering C-Materials for Biological Applications,* 41, pp. 217-223.

YANG, G., WANG, J., WANG, Y., LI, L., GUO, X. and ZHOU, S., 2015. An Implantable Active-Targeting Micelle-in-Nanofiber Device for Efficient and Safe Cancer Therapy. *Acs Nano,* 9(2), pp. 1161-1174.

YANG, Y., JIA, Z., LI, Q., HOU, L., LIU, J., WANG, L., GUAN, Z. and ZAHN, M., 2010. A Shield Ring Enhanced Equilateral Hexagon Distributed Multi-needle Electrospinning Spinneret. *IEEE Transactions on Dielectrics and Electrical Insulation,* 17(5), pp. 1592-1601.

YAO, J., LIM, L.K., XIE, J., HUA, J. and WANG, C., 2008. Characterization of electrospraying process for polymeric particle fabrication. *Journal of Aerosol Science,* 39(11), pp. 987-1002.

YARIN, A.L. and ZUSSMAN, E., 2004. Upward needleless electrospinning of multiple nanofibers. *Polymer,* 45(9), pp. 2977-2980.

YU, D.G., YANG, J.H., WANG, X. and TIAN, F., 2012. Liposomes self-assembled from electrosprayed composite microparticles. *Nanotechnology,* 23(10), pp. 105606.

YURTERI, C.U., HARTMAN, R.P.A. and MARIJNISSEN, J.C.M., 2010. Producing Pharmaceutical Particles via Electrospraying with an Emphasis on Nano and Nano Structured Particles - A Review. *KONA Powder and Particle,* 28 , pp. 91-115.

ZAKARIA, S.M., SHARIF, Z.S.H., OTHMAN, M.R. and JANSEN, J.A., 2013. Hydroxyapatite nanoparticles: electrospinning and calcination of hydroxyapatite/polyvinyl butyral nanofibers and growth kinetics. *J Biomed Mater Res A,* 101, pp. 1977-1985.

ZAMANI, M., PRABHAKARAN, M.P. and RAMAKRISHNA, S., 2013. Advances in drug delivery via electrospun and electrosprayed nanomaterials. *International Journal of Nanomedicine,* 8, pp. 2997-3017.

ZAMANI, M., PRABHAKARAN, M.P., THIAN, E.S. and RAMAKRISHNA, S., 2014. Protein encapsulated core–shell structured particles prepared by coaxial electrospraying: Investigation on material and processing variables. *International Journal of Pharmaceutics,* 473(1–2), pp. 134-143.

ZARCHI, A.A.K., ABBASI, S., FARAMARZI, M.A., GILANI, K., GHAZI-KHANSARI, M. and AMANI, A., 2015. Development and Optimisation of N-Acetylcysteine-loaded poly(lactic-co-glycolic acid) nanoparticles by electrospray. *International Journal of Biological Macromolecules,* 72, pp. 764-770.

ZELENY, J., 1917. Instability of electrified liquid surfaces. *Physical Review,* 10, pp. 1-6.

ZELENY, J., 1914. The Electrical discharge from liquid points, and a hydrostatic method of measuring the electric intensity at their surfaces. *Physical Review,* 10, pp. 1-6.

ZELES-HAHN, M.G., LENTZ, Y.K., ANCHORDOQUY, T.J. and LENGSFELD, C.S., 2011. Effect of electrostatic spray on human pulmonary epithelial cells. *Journal of Electrostatics,* 69(1), pp. 67-77.

ZENG, J., AIGNER, A., CZUBAYKO, F., KISSEL, T., WENDORFF, J.H. and GREINER, A., 2005. Poly(vinyl alcohol) nanofibers by electrospinning as a protein delivery system and the retardation of enzyme release by additional polymer coatings. *Biomacromolecules,* 6(3), pp. 1484-1488.

ZHANG, C., CHANG, M., AHMAD, Z., HU, W., ZHAO, D. and LI, J., 2015. Stable single device multi-pore electrospraying of polymeric microparticles via controlled electrostatic interactions. *RSC Advances,* 5(107), pp. 87919-87923.

ZHANG, H.B., JAYASINGHE, S.N. and EDIRISINGHE, M.J., 2006. Electrically forced microthreading of highly viscous dielectric liquids. *Journal of Electrostatics,* 64(6), pp. 355-360.

ZHANG, W., ZU, D., CHEN, J., PENG, J., LIU, Y., ZHANG, H., LI, S. and PAN, W., 2014. Bovine serum albumin-meloxicam nanoaggregates laden contact lenses for ophthalmic drug delivery in treatment of postcataract endophthalmitis. *International Journal of Pharmaceutics,* 475(1-2), pp. 25-34.

ZHANG, Z., LIU, S., XIONG, H., JING, X., XIE, Z., CHEN, X. and HUANG, Y., 2015. Electrospun PLA/MWCNTs composite nanofibers for combined chemo- and photothermal therapy. *Acta Biomaterialia,* 26, pp. 115-123.

ZHOU, Y. and AREF, A.A., 2017. A Review of Selective Laser Trabeculoplasty: Recent Findings and Current Perspectives. *Ophthalmology and Therapy,* 6(1), pp. 19-32.

ZUPANCIC, S., SINHA-RAY, S., SINHA-RAY, S., KRISTL, J. and YARIN, A.L., 2016. Long-Term Sustained Ciprofloxacin Release from PMMA and Hydrophilic Polymer Blended Nanofibers. *Molecular Pharmaceutics,* 13(1), pp. 295-305.

Chapter 3 Materials and Methods

This chapter will outline all the materials used in this research project alongside detailed descriptions of the methods and characterisation techniques utilised throughout the project.

3.1 Materials

3.1.1 Polyvinylpyrrolidone

Polyvinylpyrrolidone (PVP) (**Figure 3.1**) is a versatile, biocompatible, non-ionic polymer commonly used in the pharmaceutical industry often as a tablet binder or filler. Its hydrophilic nature enables PVP to form complexes with proton donors resulting in rapid dissolution as well as enhanced drug/API solubility in aqueous environments. Formation of complexes with proton donors can also contribute to uniform distribution of other excipients (e.g. APIs) enabling controlled release of APIs. PVP was sourced from Ashland (Worcestershire, UK) and was used at a molecular weight of $4.4x10^4$ g/mol.

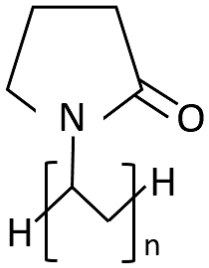

Figure 3.1 Structure of PVP

3.1.2 Poly (N-isopropylacrylamide)

Poly (N-isopropylacrylamide) (PNIPAM) (**Figure 3.2**) is a biocompatible, thermo-responsive polymer synthesised from N-isopropylacrylamide (Lima, Morales and Cabral, 2016). This polymer undergoes a reversible Lower Critical Solution Temperature (LCST) transition above 32°C in water. At this critical temperature, the 3D hydrogel expels at least 90% of its volume transitioning into a dehydrated state from a solute state. Due to this transition occurring at a

temperature close to physiological conditions, there are many advantages in using PNIPAM in the healthcare remit; especially as a drug carrier matrix and in bioengineering. PNIPAM was sourced from Sigma Aldrich (Dorset, UK) and 2-4x10^4 g/mol molecular weight was used.

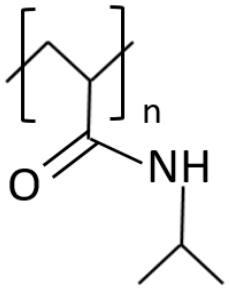

Figure 3.2 Structure of PNIPAM

3.1.3 Chitosan

Chitosan is a bioadhesive cationic polysaccharide **(Figure 3.3)** derived from the alkaline deacetylation of chitin, a naturally occurring polysaccharide. It is a widely used polymer due to its biocompatibility, biodegradability and non-toxicity (Muxika et al., 2017). Chitosan has been found to have multiple uses including as a haemostatic agent, a mucoadhesive agent and a permeation enhancer. The cationic nature of chitosan promotes molecular pull towards negatively charged mucosal membranes (e.g. corneal surfaces) due to electrostatic attraction. The amino groups can also protonate easily at low pH, a characteristic that can be exploited in targeted drug delivery (Shastri, 2017). Chitosan was sourced from Sigma Aldrich (Dorset, UK) and used at a concentration 5 x10^4 g/mol – 1.0x 10^5 g/mol.

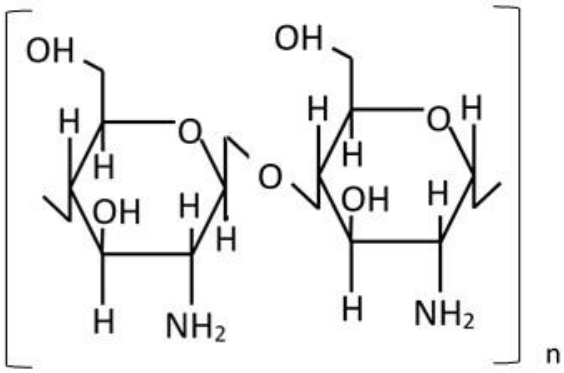

Figure 3.3 Structure of Chitosan

3.1.4 Surfactants

Surfactants are compounds that are able to lower the surface tension between solid-liquid interfaces or liquid-liquid interfaces. They are naturally present in low concentrations in the lipid bilayer in epithelial cells. At these low concentrations, the surfactants can modify the physical properties of the cell membrane. However, upon saturation, membrane solubilisation occurs because of micelle formation, removing phospholipids from the cell membrane. All surfactants used in this research were sourced from Sigma Aldrich (Dorset, UK)

Brij® 78 is a biodegradable, non-ionic surfactant **(Figure 3.4**) used as an absorption promoter in ocular DD (Kapoor et al., 2009). It possesses good thermal and chemical stability and supposedly enhances drug permeation transcellularly as opposed to via the paracellular pathway like calcium chelators.

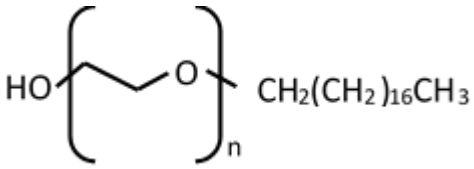

Figure 3.4 Structure of Brij® 78

BAC is a quaternary ammonium compound (**Figure 3.5**) typically used as an antimicrobial agent and preservative in many pharmaceutical and personal care products. BAC is a cationic surfactant that acts as a permeation enhancer by breaking down anatomical and physiological barriers of the corneal epithelial layer, creating an increase in intercellular space by opening tight junctions between cells (Saettone et al., 1996).

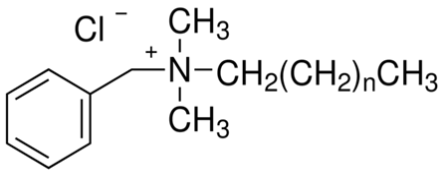

Figure 3.5 Structure of BAC

3.1.5 Ethylenediaminetetraacetic acid

Ethylenediaminetetraacetic acid (EDTA) (**Figure 3.6**) is a calcium chelating agent which is used to loosen tight junctions between corneal epithelial cells. Chelating agents are typically used to inhibit unwanted side effects of specific heavy metals or drugs. Chelating agents work by binding to metal ions or minerals such as calcium (Ca^{2+}) and remove them from the bloodstream for excretion via kidneys (Kaur and Smitha, 2002). A reduction in Ca^{2+} in the corneal epithelium causes not only disturbance of adherent junctions but also actin filaments. Depletion of Ca^{2+} also activates protein kinases; integral in the formation and barrier properties of tight junctions.

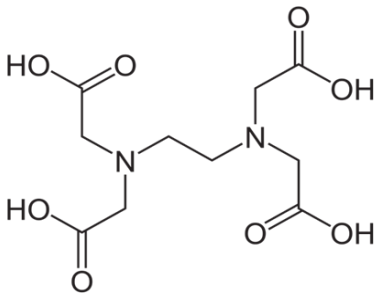

Figure 3.6 Structure of EDTA

3.1.6 Borneol

Borneol (**Figure 3.7**) is a naturally occurring compound derived from the resin of the *Dryobalanops aromatica,* also known as Borneo Camphor (Yi et al., 2016). It is commonly used in Chinese herbal formulations but has also been found to have potential in the pharmaceutical industry in ocular formulations such as topical eye drops (Huang et al., 2015; Yang et al., 2009; Wu Chun-Jie et al., 2006). Although poorly water soluble, the long term clinical safety of the compound is advantageous in ocular drug delivery.

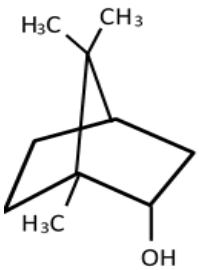

Figure 3.7 Structure of Borneol

3.1.7 Timolol Maleate

Timolol Maleate (TM) (tert-butyl (2-hydroxy-3-{[4-(morpholin-4-yl-)-1, 2, 4-thiadiazole-3-yl)oxy}propan-2-ol) (**Figure 3.8**) is a non-selective beta-adrenergic blocking agent which competes with adrenergic neurotransmitters to block the action of the sympathetic nervous system (Sah and Suresh, 2017).

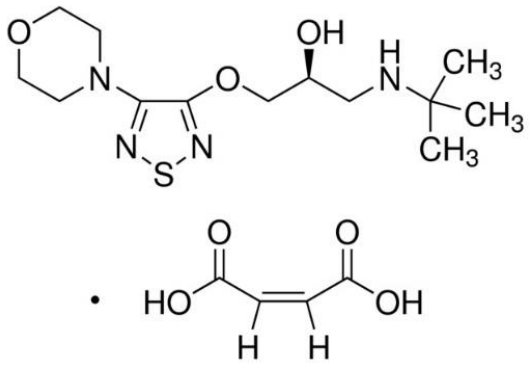

Figure 3.8 Structure of Timolol Maleate

In a clinical setting, TM is used to treat hypertension, angina pectoris (Vedoya and Schena, 1974), myocardial infarction (Anderson, Jones and Evanko, 2003) and most commonly glaucoma. Although the mechanism of action for the treatment of glaucoma is not yet established, the leading theory is associated with the production of AH. TM is thought to block beta- receptors found on the ciliary body, reducing the amount of AH produced and secreted. There is also research that suggests timolol binds to receptors on the blood vessels that nourish the ciliary body, resulting in vasoconstriction, hence reducing the volume of fluid and its flow out of the vessels that later produces AH (Stamper, Lieberman and Drake, 2009). The blockage of beta-adrenergic receptors decreases cardiac activity (slows heart rate, in both healthy and heart-disease patients) and can also increase airway resistance from the parasympathetic system. TM was approved by the FDA for ocular use in 1978 and has since been used widely for the treatment of glaucoma (Jung and Chauhan, 2013). It is typically administered topically as eye drops, although commercial *in situ* gels have also been approved. Timolol maleate eye drops usually contain 0.25%w/v timolol and are administered twice daily, approximately 12 hours apart with one drop in each affected eye. TM is a hydrophilic drug and the products and formulations it is incorporated into are hydrophilic to aid penetration through the cornea once topically applied.

3.2 Methods

3.2.1 Solution Characterisation

3.2.1.1 Viscosity

Viscosity is defined as a fluid's thickness or a fluid's resistance to flow. This liquid property is primarily quantified using a viscometer. A sine-wave vibra viscometer (A&D SC-10) was used to determine the viscosity (mPa.s) of the polymeric solutions used during all studies, as seen in **Figure 3.9**. The mechanism for measuring viscosity here involves identifying the driving electric current required to resonate two gold-plated sensors maintained at a constant frequency of 30 Hz. The difference in the viscous drag between the pair of plates and the sample is detected as the driving current, with the viscosity being measured by exploiting the proportional relationship between the driving current and viscous resistance. The sample container was filled with 10 ml of the formulation and the gold-plated sensor plates were submerged into the container. The experiments were carried out in triplicate at room temperature (23°C±0.5°C)

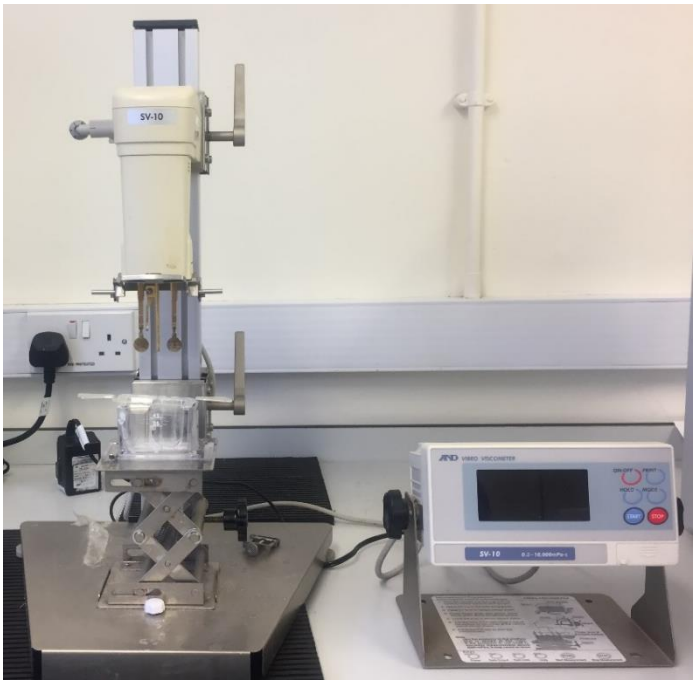

Figure 3.9 Digital Image of an A&D SV-10 sine-wave vibra viscometer

3.2.1.2 Surface Tension

The ST of formulations were measured using the du Noüy ring method (du Noüy, 1925), (**Figure 3.10)**. The force required to remove or withdraw a platinum ring from one phase (often the surface of a liquid) into another phase (air/gas) is measured. The ring is lowered onto the surface of the liquid and upon external forces, the ring is lifted away from the liquid surface. This force required is what is ultimately used to calculate the liquids' surface tension based on the following equation:

$$\sigma = \frac{F}{L.\cos\theta} \tag{3.1}$$

Where σ is surface tension (N/m), F is the force (Newtons) and L is the wetting length of the ring (sum of the inner and outer circumference) (meters), θ is the contact angle between the liquid and the ring. ST experiments were conducted using a torsion balance by White Elec Inst Co Ltd. Experiments were carried out in triplicate at ambient temperatures (23°C±0.5°C).

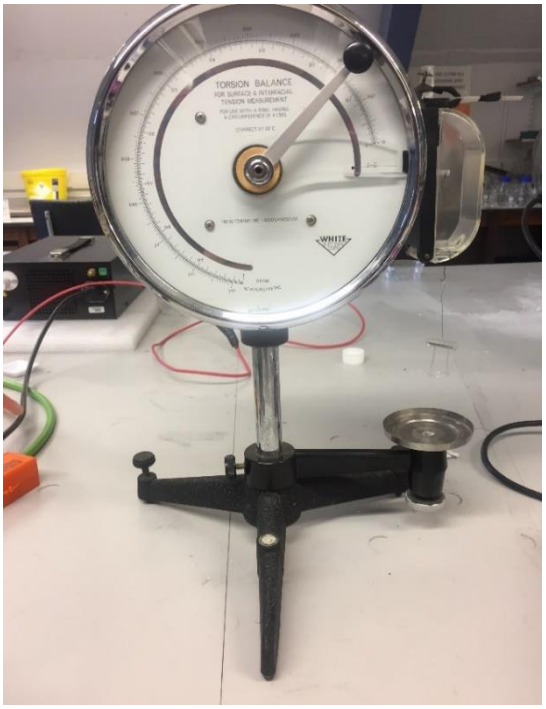

Figure 3.10 Digital Image of a While Elec Ltd Torsion balance

3.2.1.3 Electro-conductivity

The ability of a solution to transmit an electrical current is analysed using a conductive meter. The conductive meter consists of a probe that holds 4 electrodes (the probe is as seen in **Figure 3.11)**. An alternating current is initiated by the probe once inserted into the liquid sample and its current is passed between the four electrodes. The distance between the probes' electrodes alongside the potential between the electrodes is used to calculate the conductivity of the liquid using Ohm's Law:

$$I = \frac{V}{R} \tag{3.2}$$

Where I is the current (in Amperes), V is the voltage (in volts) and R is the resistance (in Ohms).

The electro-conductivity of formulations were quantified using a Mettler Toledo LE73 Conductivity Meter. The probe was submersed in 20 ml of formulation at room temperature. The experiments were carried out in triplicate and an average was taken.

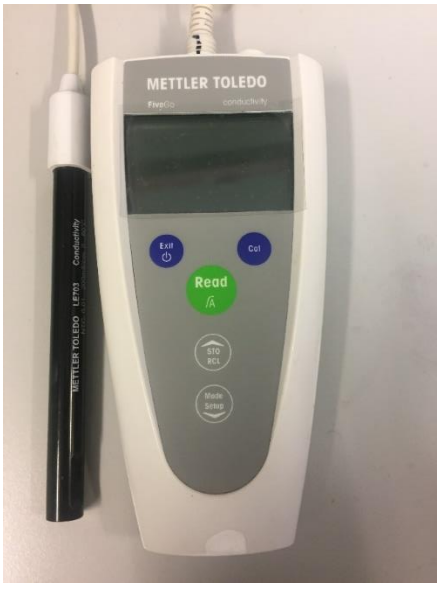

Figure 3.11 Digital Image of a Mettler Toledo Electrical Conductivity Meter

3.2.2 Electrohydrodynamic atomization

The basic EHDA set-up consists of 5 key components: a syringe holding the formulation, a syringe infusion pump, a conductive stainless steel needle, a voltage supply and a collection plate (**Figure 3.12**).

The infusion pump allows the flow rate of the formulation to be regulated through the system whilst the voltage supply can control the applied voltage to the system. The formulation is infused through silicone tubing to the needle. Introduction of the voltage to the system overcomes the surface tension of the liquid at needle exit, resulting in solvent evaporation and ultimately the production of particles or fibers. **Section 2.4.2** outlines the EHDA process in more detail, summarising the factors that affect the process.

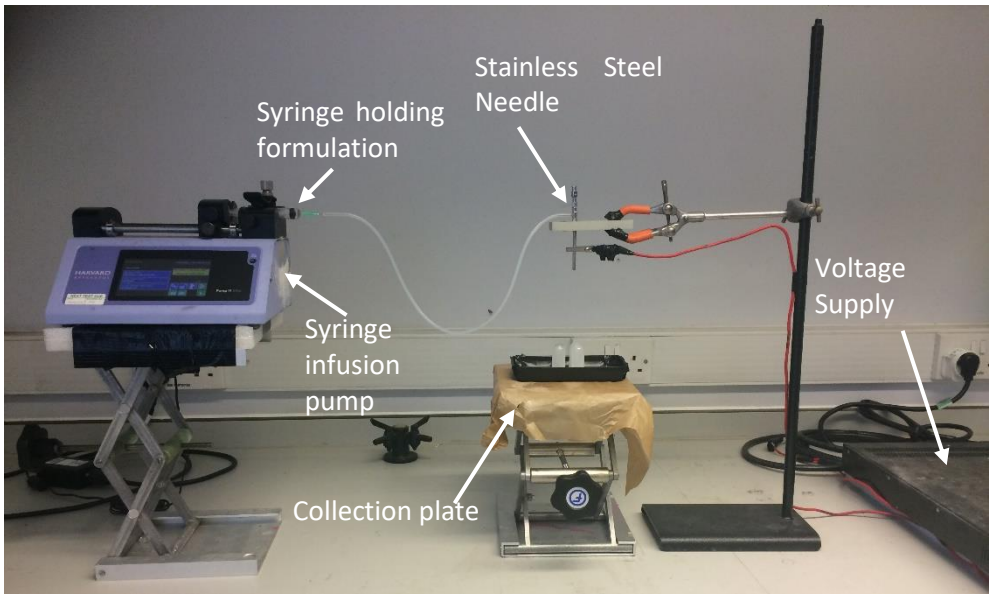

Figure 3.12 Digital Image of the EHDA system

3.2.3 Scanning Electron Microscopy

Scanning Electron Microscopy (SEM) (**Figure 3.13**) is a microscopic technique that utilises an electron beam rather than the conventional light beam to create an image of a samples surface. The electron beam scans the sample surface in a raster pattern, producing signals displayed as 3D images. The electrons are produced at the top of the SEM column and the electron gun emits the electrons, accelerating them in a powerful electromagnetic field. The electrons pass through a series of condenser lenses and apertures, focusing the electron beam onto the samples' surface. Upon interaction with the surface, the electrons either reflect back off the sample (backscatter detection) or they transfer some of their energy to atoms in the sample. The latter is known as secondary electron detection. In practise, the sample may have to be gold or carbon coated to make the sample conductive. The sample is then loaded onto aluminium stubs with copper tape which are mounted on to a stage in the main chamber. SEM is a popular microscopic technique due to the ability to achieve high resolution (1 nm) 3D images and highly detailed topographical, morphological and compositional information about the sample in question.

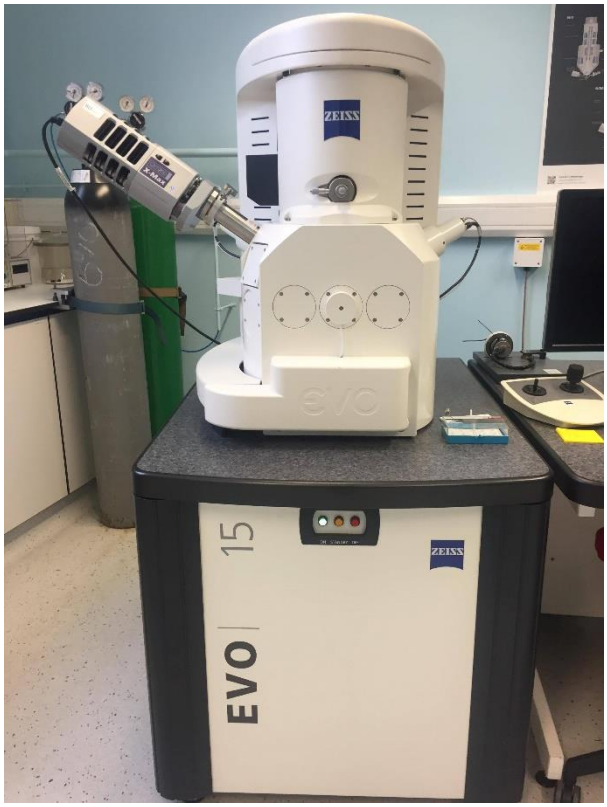

Figure 3.13 Digital Image of a Zeiss Evo HD-15 Scanning Electron Microscope

3.2.4 Differential Scanning Calorimetry

DSC is a thermal analytical method used to measure the energy changes within a sample as it is heated. The study of thermal transitions of materials can establish the thermal stability of the sample in question. In practise, DSC measures the heat flow to the sample and an inert reference as they are both subjected to the same temperature and heated at the same rate, ensuring there is no temperature difference between the sample and reference. During application of heat the sample can undergo changes, for example, chemical reactions such as hydrolysis or physical changes like melting. These changes either emit heat (exothermic) or require heat to occur (endothermic). In order to maintain the equal temperatures between the sample and the reference, the heat flow is adjusted; it is this difference in heat flow which is analysed in DSC. Any adjustments in heat flow are established and observed as peaks and troughs in a thermogram. A Perkin Elmer Jade differential scanning calorimeter is shown in **Figure 3.14**.

Figure 3.14 Digital Image of a Perkin Elmer Jade differential scanning calorimeter

3.2.5 Thermogravimetric Analysis

Thermogravimetric Analysis (TGA) is a thermal analytical technique which observes the physical changes in mass of a sample as the sample is subjected to a controlled heating programme. TGA can be used to analyse the thermal stability and oxidative stability of materials along with analysing the decomposition kinetics of samples. In practise, the sample is heated in a controlled manner in an inert atmosphere (commonly nitrogen) and the changes in mass are measured as a function of temperature. During heating, the changes in mass can result due to a number of reasons. Weight loss can be a result of decomposition (chemical bonds breaking), evaporation of volatile solvents or desorption. Weight gain can be an outcome of oxidation or absorption. These mass changes are represented by peaks and troughs in TGA thermograms as a function of temperature. A Pyris 1 TG analyser can be seen in **Figure 3.15.**

Figure 3.15 Digital Image of a Perkin Elmer Pyris 1 thermogravimetric analyser

3.2.6 Goniometry

Goniometry is the observation of liquid droplet morphology when in contact with a solid surface. The quantitative analysis of this wetting of a solid is known as the contact angle (CA), θ. A droplet of liquid is introduced to a sample on a microscope slide via a precision syringe (**Figure 3.16a).** A camera is used to continually monitor the liquid drop and sample over time. Computer software is used to help analyse drop morphology and is used for quantitative analysis. The CA is defined as the angle produced by the liquid drop at the intersection of the 3 phases; liquid (drop), solid (sample) and gas (atmosphere). The contact between these three phases can be defined by the Young equation:

$$\gamma_{SG} = \gamma_{SL} + \gamma_{LG} \cos\theta \qquad (3.3)$$

Where:
- γ_{SG} is the solid-gas interfacial energy
- γ_{SL} is the solid-liquid intefacial energy
- γ_{LG} is the liquid-gas interfacial energy
- θ is the equilibrium contact angle

Based on the contact angle, there are 3 degrees of wetting ability. If θ < 90°, the liquid "wets" the sample. If θ = 0° indicates complete spreading of the liquid droplet whilst θ>90°, the surface is said to be non-wetting with the liquid as illustrated in **Figure 3.16b** .

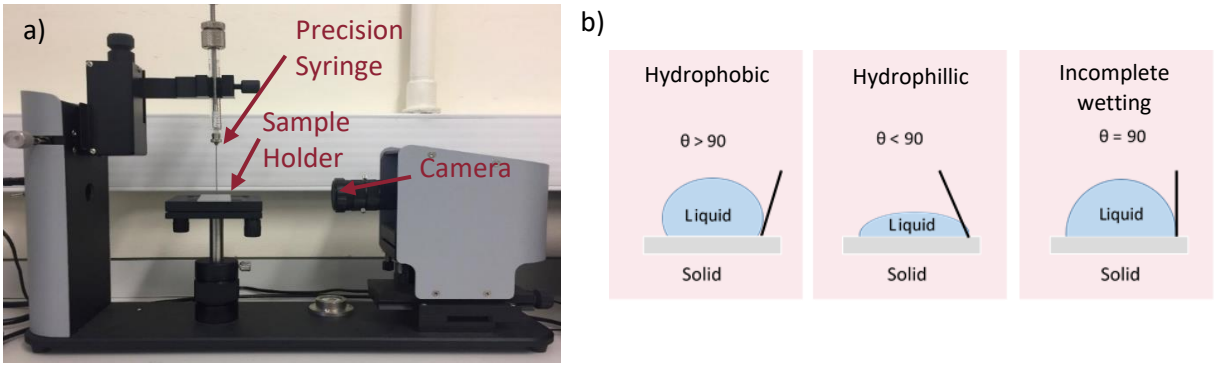

Figure 3.16 a) Annotated Digital Image of a Thetalite TL100 goniometer, b) a schematic diagram of the three degrees of wetting ability

3.2.7 Fourier Transform Infrared Spectroscopy

FTIR spectroscopy is most commonly used to identify unknown samples or confirm structures of molecules or compounds based on the samples' characteristic absorption of infrared (IR) radiation. When an IR beam passes through a sample, some energy is absorbed and some is transmitted. The absorbed radiation by selective molecules causes changes in dipole moment of the sample molecules. Due to this, the vibrational energy level of the sample transitions to an excited state. This transfer from ground state is depicted as an absorption peak on a "fingerprint" of the sample and the intensity of these peaks correlates with the change of dipole moment (Gaffney and Marley, 2012). The wavelength region of 4000-400 cm^{-1} is used for FTIR as most organics absorb within this range. Attenuated Total Reflection (ATR) is a side branch of FTIR which utilises an optically dense crystal and internal IR beam which reflects upon contact with the sample (**Figure 3.17**). The IR beam is concentrated onto the highly refractive crystal and the internal reflectance causes an evanescent wave. This wave passes not only through the crystal but through the sample too. If the energy is absorbed within the range (4000-400cm^{-1}), the wave attenuates and this altered energy is transferred to the IR beam. It continues to pass through the optical dense crystal and to a detector, creating a fingerprint spectrum unique to that sample (Minnes et al., 2017). It is useful with samples that produce strong and intense transmission peaks. ATR is advantageous over FTIR due to its ease of operation and ability to analyse samples in their natural state (liquid, solid). High resolution fingerprints are also yielded. Appendix A shows characteristic infrared absorption wavenumbers for common functional groups (Berthomieu and Hienerwadel, 2009).

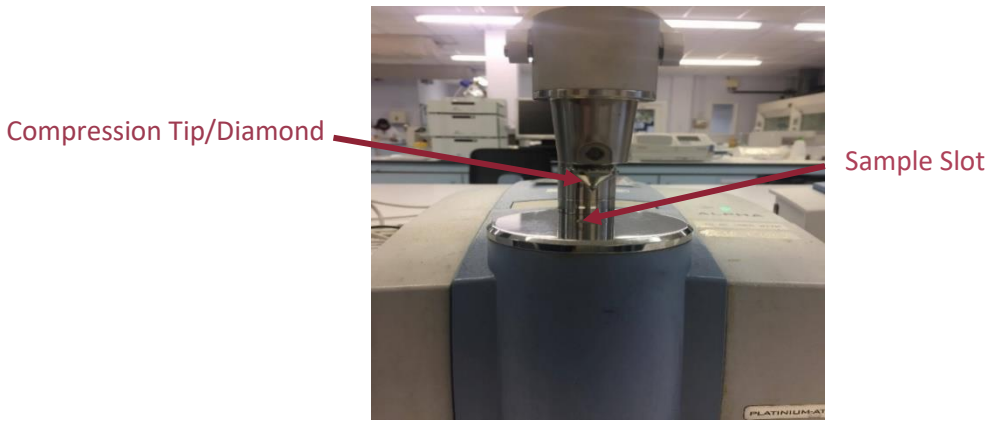

Figure 3.17 Digital Image of a ATR-FTIR spectrophotometer fitted with Bruker Alpha Opus 27 FT-IR

3.2.8 Drug Release and Drug Permeability

To overcome the challenges met with using animal models to assess drug release and drug permeability in the ocular pharmaceutical remit, *in vitro* release testing (using cellulose acetate as a dialysis membrane) and *ex vivo* permeability testing (using freshly excised ocular tissue) is vital and extremely useful in drug delivery device development as they are able to predict/forecast *in vivo* behaviour.

3.2.8.1 *In Vitro* Testing

3.2.8.1.1 In Vitro Drug Release

In vitro testing refers to experiments carried out in a controlled environment or atmosphere mimicking physiological conditions. *In vitro* drug release testing involves quantifying or measuring the release of drug from a matrix or carrier in an environment simulating physiological conditions. Whilst these studies are typically carried out at physiological conditions (temperature: 37°C, pH: 7.1-7.4), customised or personalised dosage forms may require elevated or dropped temperatures and/or pH.

In vitro Elution Testing is used to assess the release of drug from an eluting device that is subject to a continuously stirred medium. The sample is introduced to system in the donor compartment which is separated from the receptor compartment by a dialysis membrane (e.g. cellulose acetate). At pre-determined time points, the medium in the receptor compartment is sampled and quantified to produce a release profile as a function of time. The conditions at which this type of testing is carried out is solely dependent on the application of the device/product being tested. The cumulative drug release data obtained from such studies can be scrutinized to produce release profiles as a function of time which can then be used to determine release kinetics and the mechanism of drug release (e.g. Fickian Diffusion).

3.2.8.1.2 Release Kinetic Modelling

Drug release following zero-order kinetics demonstrates a release independent to the drug concentration (**Equation 3.4**) whilst first-order kinetics indicate the release of drug is concentration dependent (**Equation 3.5**).

$$C_t = C_0 + k_0 t \quad (3.4)$$

Where C_t is the amount of drug released at time t, C_0 is the initial amount of drug in solution and k_0 is the zero-order rate constant. In order to determine if the release of TM was zero order, the cumulative percentage release of TM was plotted against time.

$$\log C = \log C_0 - Kt/2.303 \quad (3.5)$$

Where C_0 is the initial concentration of drug and K is the first order release constant and 2.303 is a constant. Here, log percentage drug remaining was plotted as a function of time.

Hixson-Cromwell cube root law describes the release of drug due to change in particle surface area and diameter (Hixson and Cromwell, 1931), where the cube root of the percentage of drug remaining in the matrix is plotted versus time, according to **Equation 3.6**:

$$W_0^{\frac{1}{3}} - W_t^{\frac{1}{3}} = kt \quad (3.6)$$

The Higuchi model describes drug dissolution from various types of modified release from polymeric matrices. The model was originally intended for planar systems but evolved to extend to different geometries and porous matrices. The Higuchi model has been generalised to yield the simplified Higuchi Model (Siepmann and Peppas, 2011) and was used here. (**Equation 3.7**):

$$Mt = k_H \sqrt{t} \quad (3.7)$$

where M_t is the quantity of cumulative drug released (µg) at time t, and k_H is the Higuchi constant. This model is based on several hypotheses: i) initial drug concentration in the matrix is much higher than drug solubility; ii) drug diffusion is only in one plane; iii) drug particles are much smaller than the system matrix; iv) the matrix swelling and dissolution is negligible; v) drug diffusivity is constant; vi) perfect sink conditions in release environment are reached. The cumulative drug release of TM from all 3 samples was plotted as function of square root of time.

The Korsmeyer-Peppas model was devised to explain the type of diffusive mechanism from polymeric matrix. The Korsmeyer-Peppas model is helpful when there are multiple possible release mechanisms. **Equation 3.8** shows the Korsmeyer-Peppas model;

$$\frac{M_t}{M_\infty} = k\, t^n \tag{3.8}$$

Where M_t/M_∞ is the proportion of drug released at time, t; k is the release rate constant and n is the release exponent, the factor that determines the mechanism of drug release. **Equation 3.9** shows how to derive the release exponent.

$$\log\left(\frac{M_t}{M_\infty} \times 100\right) = n \log t + \log k \tag{3.9}$$

For spherical/cylindrical matrices, various n values depict specific release mechanisms; n≤0.45 corresponds to quasi-Fickian drug transport: n=0.5 shows Fickian diffusion (molecular diffusion of drug due to a chemical potential gradient), while 0.45<n<0.89 relates a Non- Fickian diffusion mechanis; n=0.89 relates to the case II transport, with n>0.89 corresponds to the super case II transport (Riger and Peppas, 1987) (drug transport mechanism associated with stresses and state transition in hydrophilic glassy polymers which swell in water and other biological fluids) (Korsmeyer et al., 1983). Log cumulative release (%) was plotted as a function of log t; here only the first 60% cumulative release was fitted to the Korsmeyer-Peppas model

3.2.8.2 Ex Vivo Testing

Quantifying the rate of drug permeation through a biological membrane is vital as its impact is key in the absorption and distribution of the released drug. The most common model used for *ex vivo* permeation studies is Vertical Franz Diffusion Cells (**Figure 3.18**). The donor compartment and receptor compartment are separated by freshly excised animal tissue, as opposed to a synthetic membrane in *in vitro* studies. Samples are removed from the sampling port and the cumulative amount of API is measured over time. From these results, the apparent permeability coefficient (P_{app}) can be derived and compared to known established values in literature. P_{app} (or flux) is the rate of drug permeated or accumulated in the receptor compartment scaled per surface area of the tissue membrane used in the study.

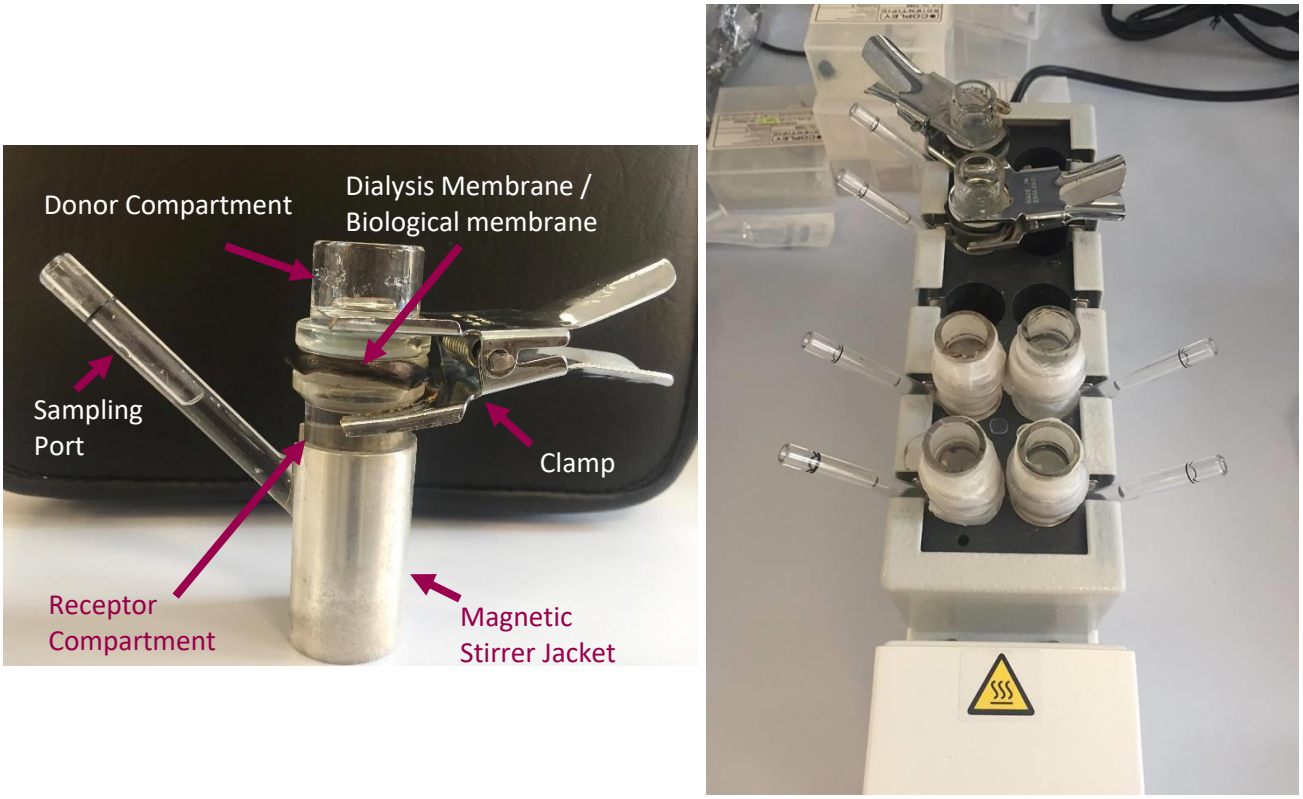

Figure 3.18 A typical Franz Cell prepared for an ex vivo permeability study

3.2.9 Bovine Corneal Opacity and Permeability Testing

The Bovine Corneal Opacity and Permeability (BCOP) test is an *in vitro* test utilised as an alternate ocular irritation assay (Gautheron et al. 1992). Damage to freshly excised bovine cornea due to exposure to test sample can be defined using the BCOP test. The corneal opacity aspect of the test can detect protein denaturation or stromal swelling; the cornea is a transparent structure hence any opacity is indicative of damage. An increase in corneal permeability shows the cellular structure of the cornea has been compromised; losing the protective barrier function. The bovine cornea is freshly excised from the eye and is treated with phosphate buffer saline (PBS) before the sample is introduced (**Figure 3.19a**). Corneal Permeability is assessed by analysing the penetration/permeation of sodium fluorescein dye following introduction of sample (**Figure 3.19c**). Visual observation was used to analyse the extent of damage for corneal opacity; a cloudy appearance reveals some damage has occurred as a result of the sample, highlighting some ocular toxicity.

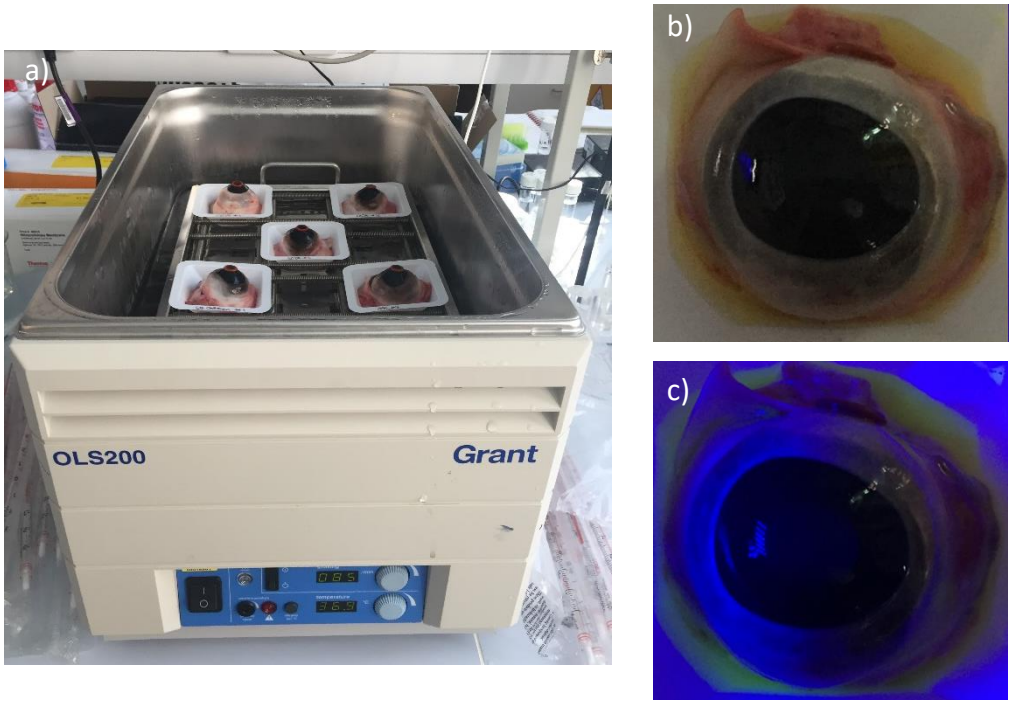

Figure 3.19 Digital Image showing a) incubation of freshly excised bovine eyes, b) Digital image of treated bovine cornea, c) Fluorescent image of treated bovine cornea

3.3 References

ANDERSON, S., JONES, W. and EVANKO, T., 2003. Dosage of beta-adrenergic blockers after myocardial infarction. *American Journal of Health-System Pharmacy,* 60(23), pp. 2471-2474.

BERTHOMIEU, C. and HIENERWADEL, R., 2009. Fourier transform infrared (FTIR) spectroscopy. *Photosynthesis Research,* 101, pp. 157-170.

DU NOÜY, P.L., 1925. An Interfacial Tensiometer for Universal Use. *Journal of General Physiology,* 7, pp. 625-633.

GAFFNEY, J.S. and MARLEY, N.A., 2012. Fourier Transform Infrared (FTIR) Spectroscopy. In: E KAUFMAN, ed, *Characterization of Materials.* 2nd edn. John Wiley & Sons, pp. 57.

GAUTHERON, P., DUKIC, M., ALIX, D. and SINA, J.F., 1992. Bovine Corneal Opacity and Permeability Test: an in Vitro Assay of Ocular Irritancy. *Fundamental and Applied Toxicology,* 18, pp. 442-449.

HIXSON, A.W. and CROMWELL, J.H., 1931. Dependence of Reaction Velocity upon Surface Agitation. *Ind, Eng, Chem.,* 23, pp. 923-931.

HUANG, L., BAI, J., YANG, H., LIU, J. and CUI, H., 2015. Combined use of borneol or menthol with labrasol promotes penetration of baicalin through rabbit cornea in vitro. *Journal of pharmaceutical sciences,* 28, pp. 1-7.

JUNG, H.J. and CHAUHAN, A., 2013. Extended Release of Timolol from Nanoparticle-Loaded Fornix Insert for Glaucoma Therapy. *Journal of Ocular Pharmacology and Therapeutics,* 29(2), pp. 229-235.

KAPOOR, Y., THOMAS, J.C., TAN, G., JOHN, V.T. and CHAUHAN, A., 2009. Surfactant-laden soft contact lenses for extended delivery of ophthalmic drugs. *Biomaterials,* 30(5), pp. 867-878.

KAUR, I.P. and SMITHA, R., 2002. Penetration Enhancers and Ocular Bioadhesives: Two New Avenues for Ophthalmic Drug Delivery. *Drug Dev.Ind.Pharm.,* 28, pp. 353-369.

KORSMEYER, R.W., GURNY, R., DOELKER, E., BURI, P. and PEPPAS, N.A., 1983. Mechanisms of solute release from porous hydrophilic polymers. *Int.J.Pharm.,* 15, pp. 25-35.

LIMA, L.H., MORALES, Y. and CABRAL, T., 2016. Ocular Biocompatibility of Poly-N-Isopropylacrylamide (pNIPAM). *Journal of Ophthalmology,* , pp. 5356371.

MINNES, R., NISSINMANN, M., MAIZELS, Y., GERLITZ, G., KATZIR, A. and RAICHLIN, Y., 2017. Using Attenuated Total Reflection-Fourier Transform Infra-Red (ATR-FTIR) spectroscopy to distinguish between melanoma cells with a different metastatic potential. *Scientific Reports,* 7, pp. 4381.

MUXIKA, A., ETXABIDE, A., URANGA, J., GUERRERO, P. and DE LA CABA, K., 2017. *Chitosan as a bioactive polymer: Processing, properties and applications.*

RIGER, P.L. and PEPPAS, N.A., 1987. A simple equation for description of solute release: II. Fickian and anomalous release from swellable devices. *J. Controlled Release,* , pp. 37-42.

SAETTONE, M., CHETONI, P., CERBAI, R., MAZZANTI, G. and BRAGHIROLI, L., 1996. Evaluation of ocular permeation enhancers: In vitro effects on corneal transport of four beta-blockers, and in vitro in vivo toxic activity. *International journal of pharmaceutics,* 142(1), pp. 103-113.

SAH, A.K. and SURESH, P.K., 2017. Medical management of glaucoma: focus on ophthalmologic drug delivery systems of timolol maleate. *Artificial Cells Nanomedicine and Biotechnology,* 45(3), pp. 448-459.

SHASTRI, D.H., 2017. Thiolated Chitosan: A Boon to Ocular Drug Delivery of Therapeutics. *MOJ Bioequiv Availab,* 3, pp. 00029.

SIEPMANN, J. and PEPPAS, N.A., 2011. Higuchi Equation: Derivation, applications, use and misuse. *International .Journal of Pharmaceutics,* 418, pp. 6-12.

STAMPER, R.L., LIEBERMAN, M.F. and DRAKE, M.V., 2009. CHAPTER 25 - Adrenergic antagonists. In: R.L. STAMPER, M.F. LIEBERMAN and M.V. DRAKE, eds, *Becker-Shaffer's Diagnosis and Therapy of the Glaucomas (8th Edition).* Edinburgh: Mosby, pp. 392-406.

VEDOYA, R. and SCHENA, R., 1974. Timolol Maleate, a New Adrenergic Blocking Agent without Quinidine Action for Treatment of Angina Pectoris. *Prensa medica argentina,* 61(4), pp. 136-143.

WU CHUN-JIE, HUANG QIN-WAN, QI HONG-YI, PING, G. and HOU SHI-XIANG, 2006. Promoting effect of borneol on the permeability of puerarin eye drops and timolol maleate eye drops through the cornea in vitro. *Pharmazie,* 61(9), pp. 783-788.

YANG, H., XUN, Y., LI, Z., HANG, T., ZHANG, X. and CUI, H., 2009. Influence of Borneol on In Vitro Corneal Permeability and on In Vivo and In Vitro Corneal Toxicity. *Journal of International Medical Research,* 37(3), pp. 791-802.

YI, Q., YAN, J., TANG, S., HUANG, H. and KANG, L., 2016. Effect of borneol on the transdermal permeation of drugs with differing lipophilicity and molecular organization of stratum corneum lipids. *Drug Development and Industrial Pharmacy,* 42(7), pp. 1086-1093.

Chapter 4 Finding a suitable polymeric matrix for on-demand electrically atomised coatings

4.1 Introduction

This chapter scrutinises the properties of various atomised polymeric contact lens coatings with the aim of finding the most suitable matrix for TM encapsulation and release.

4.2 Background

With glaucoma being the 2nd leading cause of visual impairment globally (after cataracts) (World Health Organisation., 2015), it is vital to understand the aetiology and pathophysiology of the ocular condition for appropriate and successful treatment. Currently there is no ultimate cure for glaucoma due to the fact the definitive cause for the condition has not yet been identified. Hence, research in this field is still very much active and is thriving. Many of the approaches to treatment of glaucoma involve the use of eye drops, requiring multiple dosing throughout the day. For example Timoptol® (0.25 % or 0.5 %w/v TM) eye drops are to be administered twice a day; one drop in each affected eye (MHRA., 2015) whilst Trusopt® (20 mg/ml dorzolamide) eye drops are administered 3 times a day (morning, afternoon and night) (MHRA., 2017).

Regardless of the ease of formulating and developing liquid formulations like eye drops, there are some limitations with such dosage forms. The short residence time in the eye due to drainage mechanisms such as nasolacrimal drainage and tear dilution leads to poor drug bioavailability; with only 5% of the active reaching the target site (Schopf et al., 2015).

As a result of these confines, many researchers have explored the developments of new drug delivery devices. The most extensive device to emerge from this shift in research are CLs (ElShaer et al., 2014). While being typically used for vision correction, the uses of these lenses have now extended to cosmetics, pharmaceutics and theranostics (Peng, Kim and Chauhan, 2010; Thomas, Lähdesmäki and Parviz, 2012; Kaczmarek et al., 2014; Tashakori-Sabzevar and Mohajeri, 2015). Even though the first concept of using CLs as drug delivery devices was first proposed half a

century ago, it was only in the last two decades that the full potential of drug-eluting lenses was considered. Since the 1990s, the delivery of many classes of actives using CLs have been assessed including antibiotics (Hui, Sheardown and Jones, 2012), NSAIDs (Andrade-Vivero et al., 2007) and antiglaucoma drugs (Hollo and Katsanos, 2015; Bengani and Chauhan, 2013).

To eradicate the need for frequent dosing and to improve drug bioavailability, EHDA was used here to produce drug-loaded coatings for commercial lenses which would provide controlled and sustained release of TM. Polymers PVP and PNIPAM were used as matrices with TM as the active to develop the novel coatings. Following thorough research in this field, to date, this application of EHDA has not yet been exploited thereby introducing a novel, on-demand engineering process for drug delivery to the eye.

4.3 Materials and Methods

4.3.1 Materials

PVP ($4.4x10^4$ g/mol) was sourced from Ashland, UK. PNIPAM ($2\text{-}4x10^4$ g/mol), methanol, TM (>98%), acetone, sodium hydroxide, and rhodamine B dye were all obtained from Sigma Aldrich, Dorset, UK. PureVision® Balafilcon A silicone hydrogel contact lenses were supplied by Bausch and Lomb, New York, USA. All reagents used were of analytical grade.

4.3.2 Methods

4.3.2.1 Timolol Maleate Calibration Curve

A stock solution (SS1) was prepared by weighing 10 mg of TM on an analytical balance and dissolving this in 100 ml of freshly prepared phosphate buffer saline (PBS) at pH 7.4. 10 ml was taken from SS1 and made up to 100 ml to make a second stock solution (SS2).

Both stock solutions were used to achieve a range of TM concentrations from 0 µg/ml to 50 µg/ml (**Table 4.1**). UV spectroscopy was used to firstly determine the wavelength of maximum absorbance (in scanning mode) and then consequently to read the absorbance of the range of TM solutions (in fixed mode). A calibration curve of TM was plotted using these absorbance values. Readings were taken in triplicate and an average was taken.

Table 4.1 The volumes required from stock solutions to make up a range of TM concentrations and the corresponding absorbance readings

	Concentration (µg/ml)	*Volume taken (ml)*	*Absorbance*
Using SS1	50	5	0.94
	45	4.5	0.857
	40	4	0.766
	35	3.5	0.678
	30	3	0.583
	25	2.5	0.491
	20	2	0.396
	15	1.5	0.295
Using SS2			
	10	SS2	0.202
	5	5	0.119
	2	2	0.072
	1	1	0.03

4.3.2.2 Solution Preparation

20 ml solutions containing 5 %w/v of each polymer and composite of both PVP and PNIPAM at a 1:1 ratio were prepared using methanol as the vehicle. Each solution also contained TM at a concentration of 5 %w/w of the polymer. All excipients were added to 20 ml of methanol and were prepared by magnetic stirring for 10 minutes at ambient temperatures. **Table 4.2** shows the composition of each formulation.

Table 4.2 Formulation Composition

Formulation	*Polymer*	*Polymer Concentration (%w/v)*	*TM Concentration (%w/w of polymer)*
F1	*PVP*	*5*	*5*
F2	PNIPAM	5	5
F3	Composite	2.5 (PVP)	5
		2.5 (PNIPAM)	

4.3.2.3 Characterisation of Polymeric Solutions

Each formulation was characterised based on three physical liquid properties; viscosity, surface tension and electro-conductivity. These experiments were carried out as specified in **Section 3.2.1.**

4.3.2.4 EHDA Set-Up

Figure 3.12 shows the set-up of a single needle electrospraying system. A BD Plastipak™ Luer syringe containing 5 ml of solution was mounted on to a Pump11 Elite syringe infusion pump (Harvard Apparatus, USA) which was used to precisely control the flow of solution through the EHDA system. The syringe was connected to a BD Microlance™ 3 needle (21G, 1 ½ inch) which in turn was inserted into silicone tubing. The formulation was infused through the tube to a stainless steel conductive coaxial needle device, where only the outer needle was used. The coaxial device was also coupled to a high power voltage supply from Glassman High Voltage Supply, UK. A collector plate was placed 12 cm under the needle exit; this was the working distance (determined via exploratory experiments). All atomization processes were carried out at ambient temperatures; 23 °C±0.5 °C.

4.3.2.5 Optimisation of EHDA process

Firstly, the EHDA process was optimised for each formulation as each possessed varying physical liquid properties. Each formulation was atomised at flow rates in increasing increments of 1 µl/min from 0 µl/min up to 20 µl/min. At each flow rate, the voltage required to produce a stable jet, an unstable jet and to achieve dripping mode were recorded. These values were utilised to

construct jetting mode maps enabling the optimum flow rate and voltage ranges to be identified for each formulation. A flow rate of 15 µl/min was used for atomising F1, 10 µl/min for F2 and 10 µl/min for F3. A voltage between 13 kV and 20 kV sufficed for establishing a stable jet.

4.3.2.6 EHDA Coating Application

The resulting atomised coatings were initially collected on glass microscope slides for preliminary analysis, with subsequent characterisation carried out on coated commercial contact lenses. PureVision® Balafilcon A lenses were dried in a desiccator on a novel lens holder (to maintain lens shape) for 30 minutes and were weighed before and following the coating process to determine the weight of the coating sample. Controlled deposition of coating was achieved by using a modified lens holder (which held 4 lenses) with an additional mask arm which enabled deposition onto peripheral regions keeping central regions clear for vision.

4.3.2.7 Coating Characterisation

4.3.2.7.1 Imaging and Size Distribution

Exploratory analysis of morphology and size of the nanostructures that made up the atomised coatings were conducted using SEM. Coated microscope slides were gold coated (S150B, Edwards, Crawley, UK) and mounted onto aluminium stubs before being analysed using a Zeiss Evo HD-15 microscope. High resolution images at both x5k and x50k magnification were obtained using a working distance between 9.5 mm and 10.5 mm, respectively, with a voltage between 10kV and 18kV.

Smart Tiff software was used in conjunction with SEM to gather data on average diameter size and size distribution information of the atomised structures. These samples were further analysed on CLs to ensure the lenses (i.e. the surface the coatings were collected on) did not affect the resulting atomised structures. Digital images were also taken of an uncoated lens and a coated lenses using a Samsung NX200 mirrorless digital camera. An Evos Fluorescence microscope was utilised to exhibit probe encapsulation within the atomised polymer nanostructures at x40 magnification.

4.3.2.7.2 Drug Encapsulation

Atomised coatings were collected, weighed and dissolved in methanol and left for 1 week. **Equation 4.1** was used to calculate encapsulation efficiency (EE):

$$EE = \frac{Drug\ added - free\ drug}{Drug\ added} \qquad (4.1)$$

Calculating the amount of drug that is present within the atomised coatings aids the analysis of subsequent *in vitro* and *ex vivo* testing.

4.3.2.7.3 DSC

DSC studies were carried out using a Jade Differential Scanning Calorimeter, (PerkinElmer, US) (**Figure 3.14**). Indium, with a known melting point, T_m, of 156.6 °C was used as a standard to calibrate the temperature scale of the calorimeter. 2-4 mg of coating samples were sealed in aluminium pans and heated at a rate of 20 °C/min under a flow of nitrogen gas.

4.3.2.7.4 TGA

Pyris 1 TGA Thermogravimetric analyser (PerkinElmer, USA) was used to carry out TGA analysis (**Figure 3.15**). Similar to DSC, this thermoanalytical technique was carried out under a flow of nitrogen gas along with air. Sealed pans containing 8-10 mg of sample were heated from 20 °C to 700 °C in increasing increments of 20 °C/min.

4.3.2.7.5 Goniometry

The wetting ability of the coatings was quantitatively analysed using Thetalite TL100 goniometer and OneAttention software (Biolin Scientific, Sweden) (**Figure 3.16**). Distilled water droplets (10 µl) were used and each sample was ran 5 times in Sessile Drop Mode and an average was taken.

4.3.2.7.6 Spectroscopy

Any interactions between the polymers and TM was studied using ATR-FTIR. Spectras were obtained using FTIR Platinum-ATR spectrophotometer fitted with Bruker Alpha Opus 27 FT-IR (**Figure 3.17**). Raw materials and atomised coatings were scanned over the range of 400-4000 cm^{-1} at an average of 10 scans with 4 cm^{-1} resolution.

4.3.2.7.7 In vitro Release and Kinetics

4.3.2.7.7.1 *In Vitro* Drug Release

A lens holder was designed and developed to carry the coated lenses and to maximise surface contact between the lens and the synthetic dialysis membrane. The cellophane membrane separated the donor compartment from the receptor compartment, which contained PBS at pH 7.4 (which acted as the release medium). The coated lens were fixed into the holder and exposed to vials filled with 10 ml PBS at 37 °C. At fixed time intervals, the holder was removed and placed into fresh vials of PBS. This *in vitro* drug release method was adapted from Mehta et al (Mehta et al., 2015). Drug release into the medium was quantified using UV spectroscopy (λ=295nm).

4.3.2.7.7.2 *In Vitro* Probe Release

Probe release was demonstrated using a similar set-up to the process described above. Contact lenses were coated with polymeric nanostructures containing rhodamine B, 5 %w/w of the polymer as opposed to TM. Five lenses were coated and exposed to PBS at 37 °C. Each lens was removed at specific predetermined time points: 0 minutes, 10 minutes, 1 hour, 6 hours and 24 hours. Fluorescence microscopy was used to determined dye intensity (DI) on the lens and UV spectroscopy to determine DI in the receptor medium (PBS) at λ=560 nm. Experiments were carried out in triplicate for all 3 formulations.

4.3.2.7.7.3 Release Kinetic Modelling

The mechanism of TM release from the polymeric coatings was determined by utilising *in vitro* data and applying it to various kinetic models; as outlined in **Section 3.2.8.1.2.**

4.3.2.7.8 Ocular Irritancy Testing

Any damage the atomised coating could cause to the eye was evaluated using BCOP assay. This test can assess ocular tolerability by investigating corneal integrity. Six samples were tested; normal saline (as a negative control), acetone (mild positive control), sodium hydroxide (positive control), F1, F2 and F3. Freshly excised bovine eyes (source from ABP Food Groups Abattoir) were primarily checked for epithelial detachment and/or corneal damage and were then incubated at 37 °C in a water bath for 10 minutes. A drop of saline was applied to the corneal surface before incubating for a further 5 minutes. 100 µl of sample (control or coating dissolved

in PBS) was introduced to the corneal surface and left for 30 seconds before the bovine eyes were washed with normal saline (10 ml) and left to incubate for a further 10 minutes. The degree of corneal damage was visually gauged by extent of opacification and was further assessed using a staining method; using sodium fluorescein dye (2% w/v) under a cobalt blue light (465-490 nm).

4.3.2.7.9 Ex Vivo Testing

TM release from the atomised coatings and permeation through freshly excised bovine cornea was studied using vertical diffusion cells. **Figure 4.1** shows the process of *ex vivo* analysis; from excising the cornea to fixing it between the donor and receptor compartment. Freshly excised bovine eyes were checked for any corneal damage before dissection to obtain the cornea with a 2 mm sclera border to preserve corneal structure. The cornea-sclera tissue was washed with PBS and mounted in between glass donor compartment (surface area =1.77 cm^2) and receptor compartment; corneal endothelium facing the latter. The receptor was filled with 12 ml PBS and contained a mini magnetic stirrer to ensure constant stirring. The temperature of the cells was maintained at 37 °C via a heating block. At pre-determined times, 400 µl of receptor medium was removed from the receptor compartment and replaced with fresh PBS. Cumulative drug permeation was analysed using UV spectroscopy (λ=295 nm). The cumulative amount of TM permeating through the cornea was plotted as function of time and the linear slope of the resulting plot was used to calculate the steady state flux.

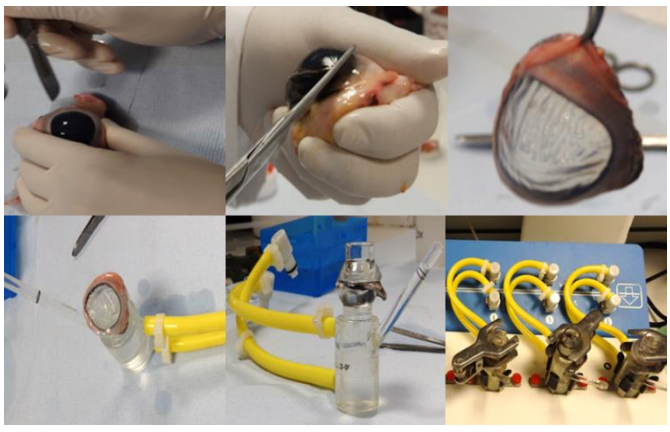

Figure 4.1 Preparation of bovine cornea for *ex vivo* drug permeation study using vertical Franz Cells

4.3.2.7.10 Statistical Analysis

All experiments (unless stated otherwise) were carried out in triplicate. Statistical analysis (one –way analysis of variance, ANOVA) was performed. Differences in results between formulations were considered significant at a level of $p<0.05$.

4.4 Results and Discussion

The two polymers investigated in this study were PVP and PNIPAM. PVP was selected for its biocompatibility and hydrophilic nature, allowing for rapid dissolution in an aqueous environment. The hydroxyl groups on the polymer backbone enables the PVP to form complexes with materials capable of donating protons. The hydrogen bonds result in not only rapid dissolution of the polymeric matrix but also increased API solubility in an aqueous environment. Mehta et al 2015 used PVP to demonstrate the rapid dissolution of electrically atomised multifunctional particles and fibers loaded with probe and antibacterial API (Mehta et al., 2015). The polymeric matrix dissolved within two minutes when exposed to PBS, pH 7.4; releasing 100% of the active and probe. Wang et al found as a result of the incorporation of PVP in 3D film patches produced using EHDA printing, the release of antibacterial tetracycline hydrochloride was expedited (Wang et al., 2017). Based on these observations, PVP was chosen to achieve rapid drug release.

PNIPAM is a polymer which has exceptional potential in the pharmaceutical industry with respect to controlled and self-regulating drug delivery. It is one of the most extensively researched stimuli-responsive polymers. Above 32°C, PNIPAM undergoes a reversible phase transition, transforming from a swollen state to a dehydrated state. At physiological temperatures (37°C) PNIPAM loses up to 90% of its original weight due to expelling of its contents i.e. any material the polymeric matrix is holding. This property can and has been exploited in temperature-modulated drug release in the human body. PNIPAM has been used as a microgel in the form of microbeads (Chen et al., 2013; Jia et al., 2014), particles (Hanga and Holdich, 2014; Inoue et al., 2018; Tempesti et al., 2018; Chen et al., 2018; Luckanagul et al., 2018), 2D films (Weng et al., 2017; Weng et al., 2016) and 3D structures (Iwata, Miyashita and Iwase, 2017; Lee et al., 2017; Dosh et al., 2017; Ma et al., 2016).

Using PNIPAM for temperature controlled drug delivery using EHDA was first proposed by a research group from Newarke, USA. Rockwood et al developed fibrous PNIPAM mats which were stable with no compromise of PNIPAM structure during the engineering process (Rockwood et al., 2008). The LCST of PNIPAM was exploited by Schoolaert et al who produced continuous, bead-free PNIPAM NFs from water (Schoolaert et al., 2017). Waterborne ES of PNIPAM yielded structurally strong fibers which were stable in water at temperatures above 32°C in an ecological manner. These research groups yielded positive findings using EHDA however, to date there is no research published using PNIPAM alongside PVP in ocular drug delivery as electrospun dual-polymer matrices for contact lenses.

4.4.1 Timolol Maleate Calibration Curve

To obtain a calibration curve for TM, various concentrations of TM solutions with PBS were made. The most concentrated solution (50 µg/ml) was first analysed by the spectrophotometer in scanning mode, giving a wavelength of maximum absorbance (λmax) of 295 nm, as found in literature (Mohammedi, Shyale and Shanta Kumar, 2011). All following solutions were measured in fixed UV mode, at a wavelength 295nm. The absorbance values were plotted against concentration resulting in the calibration curve shown in **Figure 4.2.** A coefficient (R^2) of 0.9975 was determined indicating strong linearity.

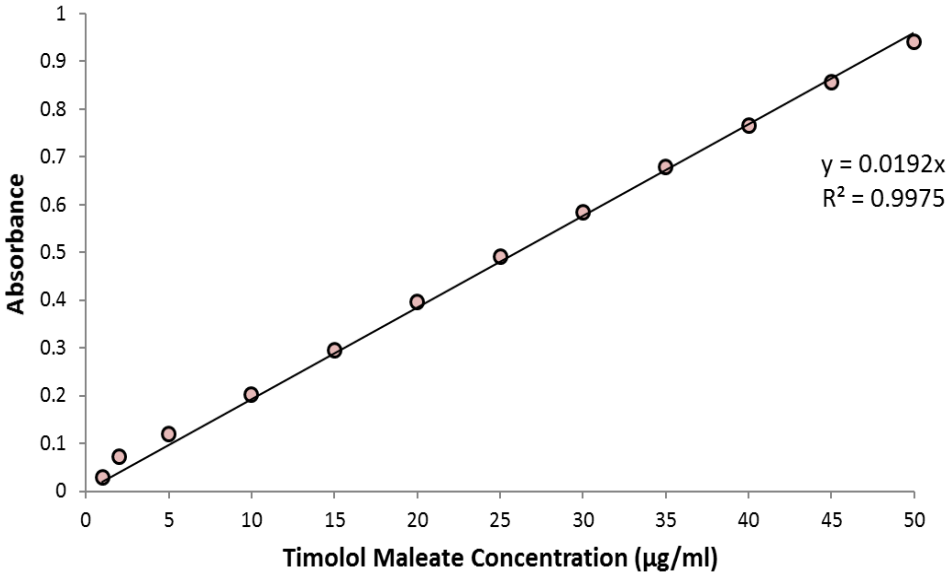

Figure 4.2 Calibration Curve of Timolol Maleate

4.4.2 Solution Characterisation

4.4.2.1 Viscosity

It is imperative to determine the viscosity of the formulations being atomised as it allows the prediction or differentiation between electrospraying and electrospinning (Bock, Dargaville and Woodruff, 2012). **Figure 4.3** shows the average readings for all 3 formulations as well as the solvent, methanol. It is clear to see the addition of polymer to the solvent increases the viscosity of the resulting solution. The addition of PVP to methanol increased the viscosity from 0.6 mPa.s to 1.4 mPa.s; a 2.33 fold increase. The incorporation of PNIPAM to methanol saw an increase to 3.09 mPa.s; over 5 times as viscous as that of methanol alone. Dissolving both PVP and PNIPAM in the methanol gave an average viscosity reading of 4.29 mPa.s.

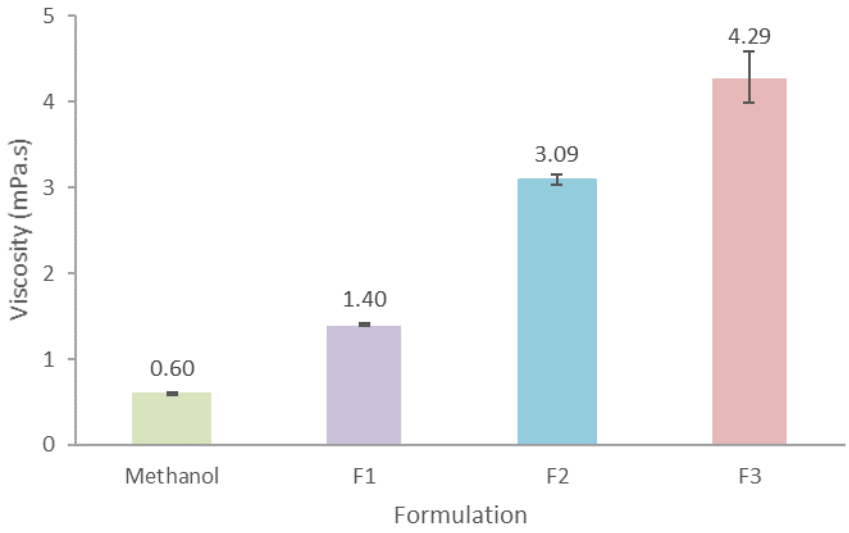

Figure 4.3 Average Viscosity of Pure Methanol, F1, F2 and F3

A hypothesis can be made on this observation of increased viscosity with formulations that contain PNIPAM: upon EHD processing, these formulations will produce fibers. Utilising a high molecular weight of PNIPAM means there is the presence of more polymeric chains, causing them to entangle and become more disordered in solution. Consequently, the mobility of the polymeric chains is reduced/limited, increasing the viscosity (Ganan-Calvo, Davila and Barrero, 1997; Jayasinghe and Edirisinghe, 2002). Due to the increased viscosity, the liquid at the exit of the stainless steel needle will not break up into droplets, but instead will stretch. This results in

rapid whipping of the unstable elongated liquid stream in the synapse between the needle and the collection plate which in turn causes evaporation of the volatile solvent. The remaining excipients in the formulation form continuous fibrous structures. Lower solution viscosities are ideal for the formation of a stable Taylor cone jet, which will result in small, uniform particles (Jayasinghe and Edirisinghe, 2002).

4.4.2.2 Surface Tension

Atomization during EHD processing is principally due to the ST of the liquid being overcome by the applied electrical field. The ST essentially "competes" with the electrical forces in the atomising process. As a result, the electrical potential needs to overcome the ST in order for atomization to occur. The ST of all 3 formulations were very similar with an average reading of 22.91, 23.53 and 20.88 mN/m for F1, F2 and F3, respectively (**Figure 4.4**). These values are close to that of pure methanol, showing the addition of a polymer (PVP, PNIPAM or Composite) did not appear to have an effect on ST.

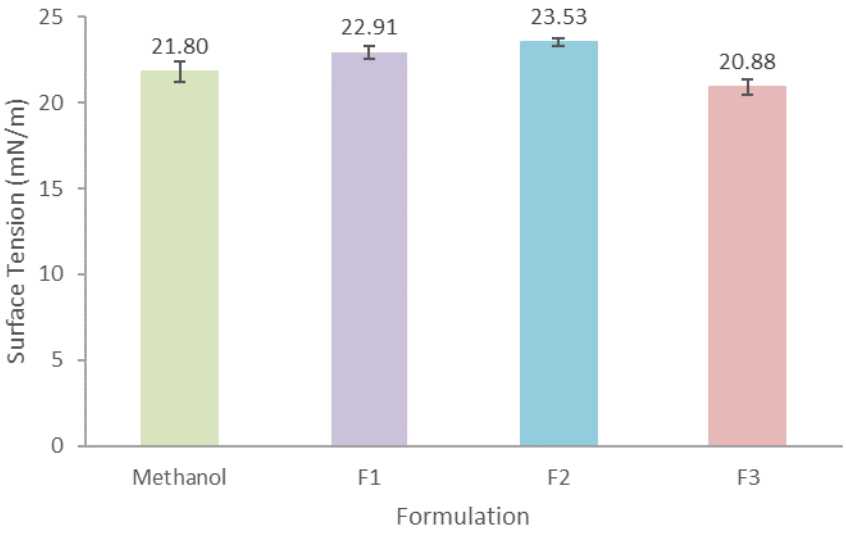

Figure 4.4 Average Surface Tension of Pure Methanol, F1, F2 and F3

This is expected due to methanol making up a large majority of the formulations with the polymer not making a drastic difference. Tang and Gomez found a stable cone jet is most likely not going to take effect if the ST of the liquid is too high due to the fact that it would exceed the electrical field when the voltage is applied thus not allowing the liquid to atomise (Tang and Gomez, 1995). Solutions with ST higher than 50^{-2} N/m will not be able to be atomised, so to

overcome this, organic solvents with low ST such as methanol are often used in the EHDA process (Smith, 1986).

4.4.2.3 Electro-conductivity

The formulations subjected to EHD processing must be conductive due to the principle driving force for EHDA being the electrical field (Larriba-Andaluz and de la Mora, 2010). Previous research has found materials or solutions with an EC below 10^{-11} Sm^{-1} were unable to carry sufficient charge, leading to an unstable jet and therefore yielding poly-dispersed atomised nanostructures (Smith, 1986; Smeets, Clasen and Van der Mooter, 2017). **Figure 4.5** demonstrates the differences in electrical conductivity between pure methanol and the three formulations. Upon introduction of polymer to methanol, the EC of the resulting solution greatly increased; with F3 having the highest EC reading (199.20 µS/cm). This considerable increase in EC places all three formulations within the ideal range for EC: between 10 μSm^{-1} and 100,000 μSm^{-1} (Kelly, 1990).

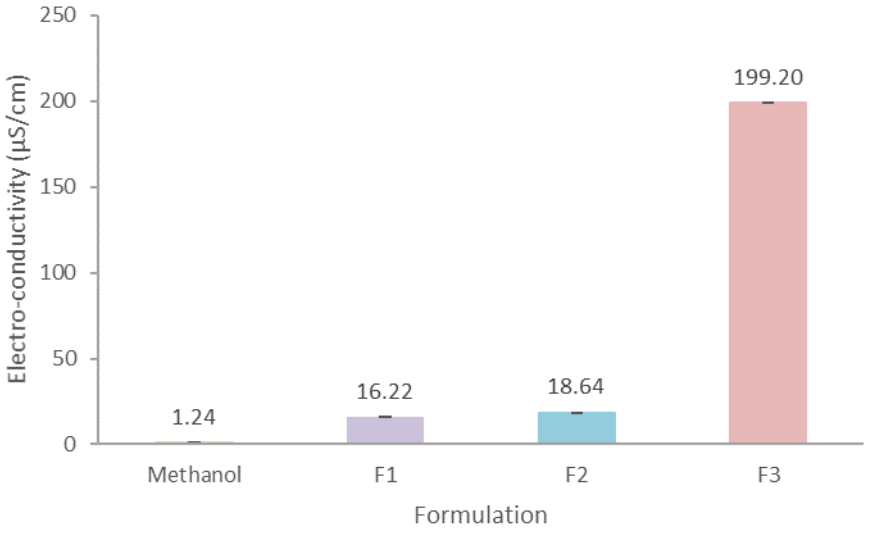

Figure 4.5 Average electrical conductivity of Pure Methanol, F1, F2 and F3

4.4.3 Optimising the EHD Process

The manner in which the liquid formulation exits the stainless steel needle and how the liquid breaks up will determine the EHD spraying mode. Every EHD system starts in "Dripping Mode." Here, the liquid breaks up into fragments giving rise to poly-dispersed atomised structures. Upon

application of electrostatic forces, the liquid will start to stabilise as it is infused through the needle. At the optimum voltage, a stable cone forms at the needle exit, known as the Taylor Cone. This EHD mode is known as “Jetting Mode”.

The mono-dispersed atomised droplets undergo rapid drying to form nanostructures such as particles, fibers or beaded fibers. To obtain a Taylor Cone, it was vital to optimise the system. There are two main approaches to this; i) modify the liquid physical properties or ii) alter the process parameters. In this research, a simplistic polymeric matrix was imperative to establish a suitable carrier hence the latter approach was taken. Due to the vast combinations of liquid physical properties the formulations in this study had (**Figures 4.3 – 4.5**), the optimised process parameters required to produce a stable jet must be identified in order to yield near uniform particle/fiber production.

Generating jetting mode maps enables the EHDA process to be optimised for specific formulations. The resulting maps (achieved by looking at the relationship between flow rate and applied voltage) presents an operating window within which a stable Taylor Cone jet is produced. **Figure 4.6** shows the maps produced for F1, F2, and F3. Each solution was subject to flow rates ranging from 0 to 20 µl/min (in 1 µl/min increments) to determine the optimum voltage for each flow rate. Voltages between 13 kV and 20 kV were found to produce a stable jet yielding atomised structures within the nanometre range in the form of particles and beaded structures. The working distance is also a critical process parameter to optimise; too short a distance between the needle exit and the collection plate and the solvent (methanol) does not have enough spatial span to evaporate before reaching the collection plate. Too long a distance can result in losing the atomised structures to the external surrounding environment. By performing exploratory experiments that involved altering the working distance alongside the jetting map studies, an ideal deposition distance for particle engineering was determined. This was found to be 12 cm. **Figure 4.7** illustrates the flow of liquid in various modes alongside the stable cone jet formed at the needle exit when atomising F1, F2 and F3 and the optimised process parameters deciphered using the jetting maps.

a)

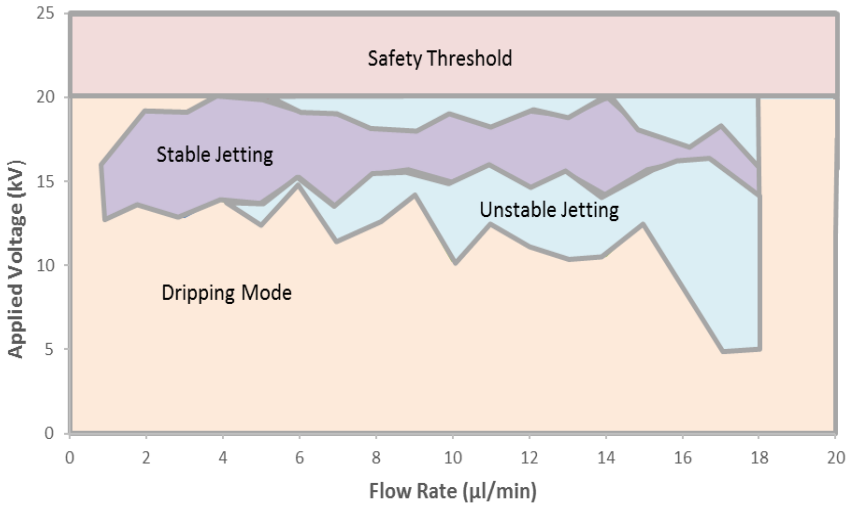

b)

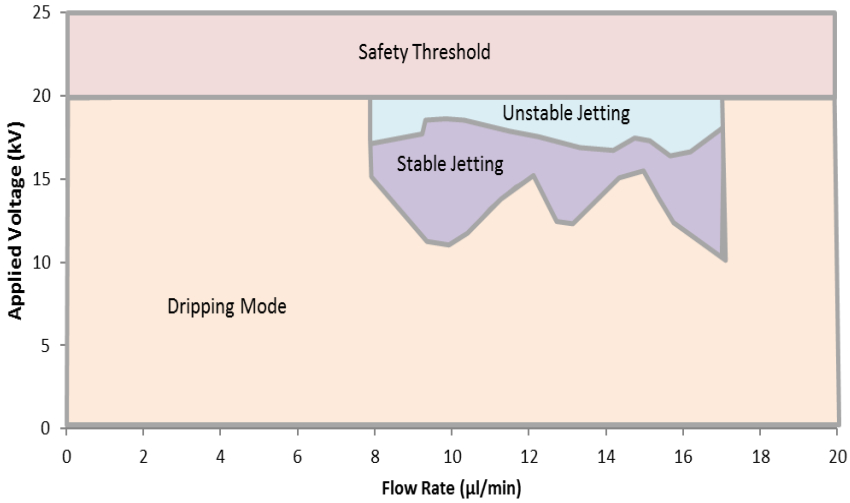

c)

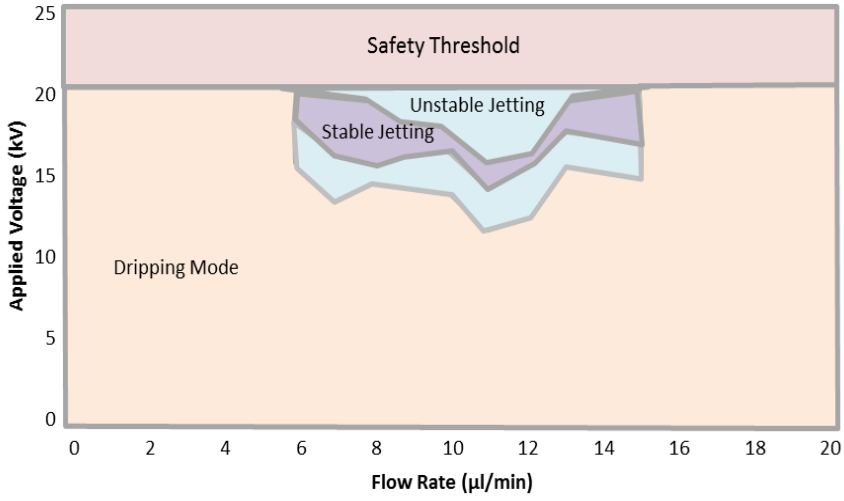

Figure 4.6 Jetting Maps to determine the relationship between flow rate and applied voltage for a) F1, b) F2 and c) F3

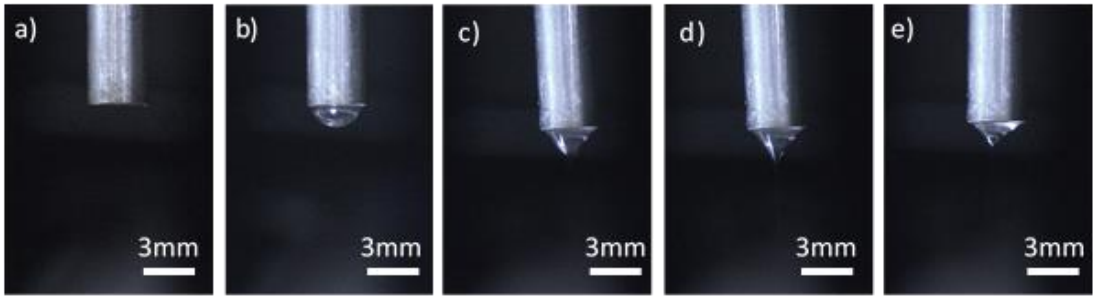

Figure 4.7 Flow of liquid under an electrical field using a single conductive needle under a) no flow, b) dripping mode. Stable cone jet formation when spraying c) F1, d) F2, e) F3.

4.4.4 Coating Characterisation

4.4.4.1 Imaging

Figure 4.8 presents digital images of dehydrated lenses: an uncoated lens (**Figure 4.8a**) and an example of a coated lens (**Figure 4.8b**). The atomised coatings can be identified by observing the fine white "mist" on the outer surface of the lens. A mask arm used in the atomization process successfully permitted the lenses to only be coated on the peripheral regions; allowing the central region to be vacant for vision.

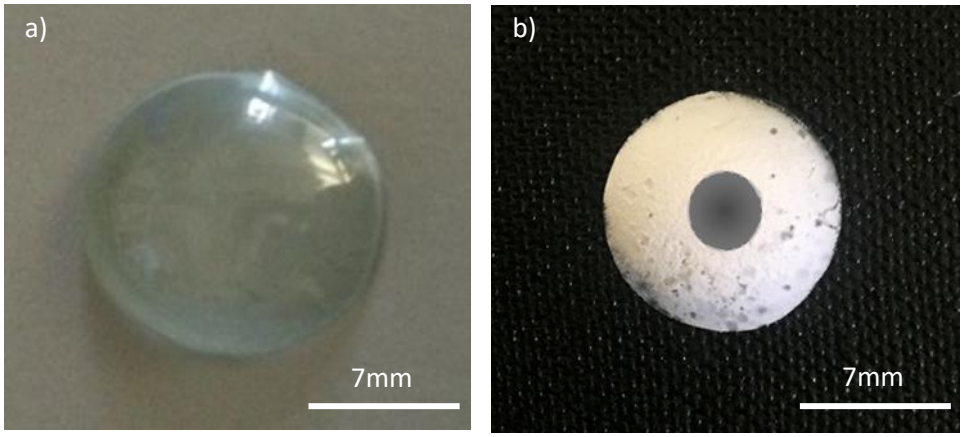

Figure 4.8 Digital Images of a) an uncoated lens and b) a lens coated with a typical electrically atomised coating

4.4.4.1.1 Morphology

Determining the morphology of nanostructures and, more significantly, controlling nanomaterial morphology is critical when exploiting the functional characteristics in emerging pharmaceutical technologies. EHDA has previously demonstrated its ability to produce atomised structures with an array of morphologies including (but not limited to) spherical structures (Huanbutta et al., 2016; Yuan et al., 2015), rods (Deotare and Kameoka, 2015), porous structures (Ekemen et al., 2013; Khajavi and Abbasipour, 2012; Kim and Lee, 2014), hollow structures (Chang, Stride and Edirisinghe, 2010; B. Wang et al., 2016; Rasekh et al., 2015), core-shell structures (Liao, Chew and Leong, 2006; Yan et al., 2014), triple-layered structures (Labbaf et al., 2013; Kim and Kim, 2011), red-blood cell shaped (Doshi et al., 2009) and strawberry-like structures (Z. Ma et al., 2011). **Table 4.3** shows the presence and morphology of the resulting particles after the EHD processing of all three formulations using SEM. Small (nanoscale), uniform structures (with respect to size and morphology) would be ideal here to ensure even distribution of drug and to aid reproducibility of the engineering process for this application.

Table 4.3 SEM images (at 2 magnifications) of EHD processed coatings at various flow rates

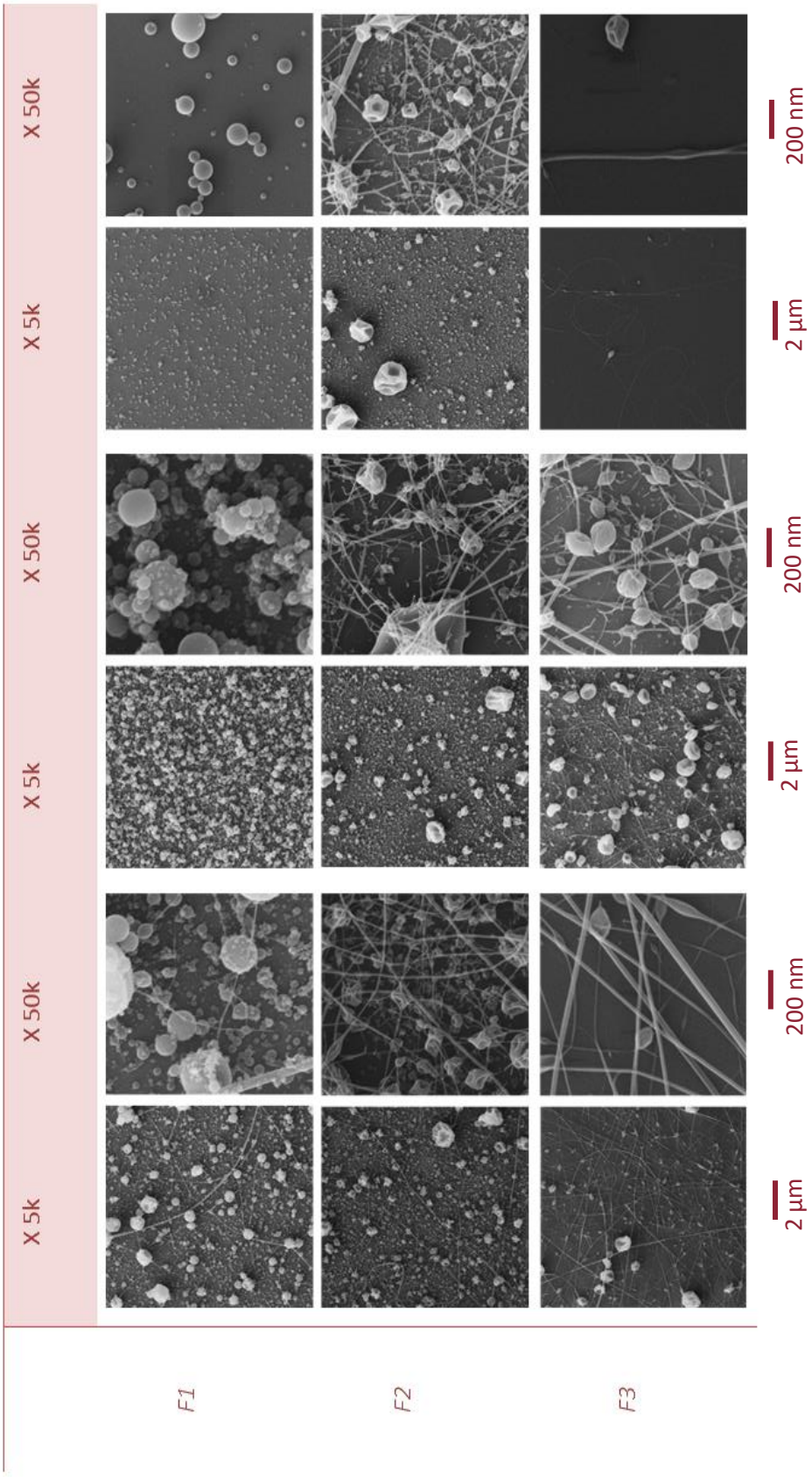

Using the jetting maps, a flow rate from dripping mode, unstable mode and stable mode was used primarily to demonstrate the difference in morphology as a resulting of the EHDA mode. At low flow rate for all three formulations, dripping mode was established. This resulted in extreme differences in particle/fiber morphology **(Table 4.3)**. Large globules varying in morphology and size can be observed at a flow rate of 5 µl/min**,** highlighting a stable cone jet was not formed at this flow rate; resulting in wet samples. **Table 4.3** shows spherical, uniform (with respect to shape size) particles were produced using F1 at a flow rate of 15 µL/min. The particle coatings (F1) produced with lower flow rates (10 µl/min) more poly-dispersed; which could eventually lead to uneven drug distribution and ultimately uncontrollable drug release (Nguyen, Clasen and Van den Mooter, 2016). Increasing the flow rate to a value within the stable zone of the jetting profiles saw a change in the morphology of the structures; coatings consisting of more uniform nanostructures were engineered. Another thing to note was the addition of fibrous structures when atomising F2 and F3; yielding beaded fibers. This was an early hypothesis proved correct due to the increased viscosity of the solutions containing PNIPAM. The increase in viscosity of the polymeric solutions upon incorporation of PNIPAM caused the stable cone jet to elongate rather than break-up into particles. The elongation of the viscoelastic solution at the nozzle tip results in fibrous structures being fabricated (Zhang, Jayasinghe and Edirisinghe, 2006).

The appearance of the deposited particles and fibers show that the TM-loaded structures were essentially dry before hitting the collection plate; the methanol had successfully evaporated. Nevertheless, for the electrosprayed particles using F2 and F3 also showed collapsed/porous particles, indicating the evaporation rate of the solvent from the particles may have been too fast (Ahmad et al., 2008).

4.4.4.1.2 Size and Size Distribution

The need for particles and structures on a nano scale has grown significantly in pharmaceuticals. This evolution enables the generation of particles which can be utilised for various routes of administration. Due to their size, the carrying capacity of the particles increases when within the nanometre range due to increased surface area to volume ratio hence more drug can be delivered.

To obtain particle/fiber size distribution, SmartTiff software was used in conjunction with SEM. **Figure 4.9** depicts the histograms following analysis of SEM images for all 3 formulations. All 3 formulations demonstrated positively skewed data, with more than 52% of the atomised structures having a diameter under 200 nm.

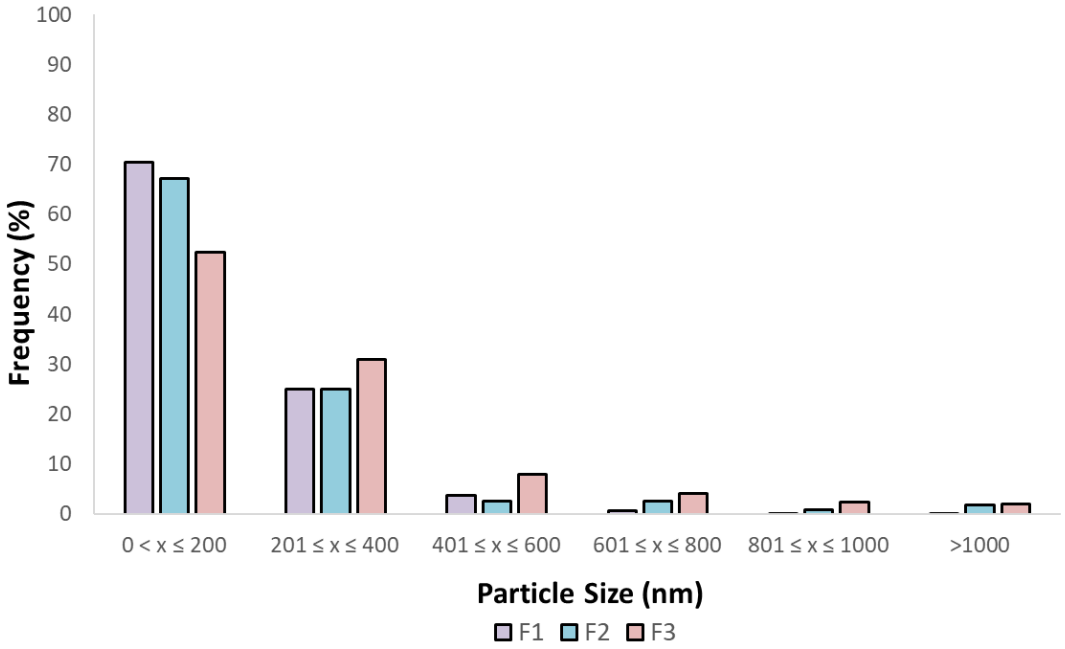

Figure 4.9 Size Distribution of Atomised Coatings

The average diameter for each formulation was 183 nm, 262 nm and 458 nm for F1, F2 and F3, respectively. 70% of the sampled particles from F1 had diameters under 200 nm with 24% between 201 and 400 nm. 67% of F2 atomised nanostructures were below 200 nm in diameter with 25% of the beaded fibers having a diameter between 201 and 400 nm. Over 45% of the beaded fibers produced by electrically atomising F3 were thicker than 201 nm. The increase in diameter could be attributed to the use/incorporation of PNIPAM into the formulation. As seen in **Table 4.3,** formulations containing PNIPAM yielded fibers fused to particles. As mentioned earlier, fibrous and spherical structures were produced simultaneously, resulting in beaded fibers due to the transition between electrospraying and electrospinning, hence the diameters of the atomised structures seem larger. Regardless, less than 2% of the structures were larger than 1 µm.

PVP has previously been electrospun to produce indomethacin-loaded fibers for wound dressings (Rasekh et al., 2014). Fibers with mean diameters of 2.58±0.3 µm were produced; much thicker than the beaded fibers produced with F3. As these structures are particles fused with fibers, the fibers are therefore much thinner. PVP has also been used to engineer coatings to develop smart microneedles (Khan et al., 2014). Particles (100 nm-3 µm) and fibers ranging between 400 nm and 1 µm were produced; a similar range to those yielded with F1, F2 and F3. Rockwood et al used a PNIPAM-acetone solution which led to the production of fibers (600 nm-1.7 µm in diameter) with "intermittent beads" (Rockwood et al., 2008). Here, 6 %w/v polymer concentration was used, a concentration similar to the one used in this study (5 %w/v); however when F2 was electrospun, much thinner beaded fibers were produced. Rockwood et al also found similar morphologies when electrospinning PNIPAM-tetrahydrofuran solutions; however these fibers were much thicker (13.5 µm).

By using low polymer concentrations in this study (5 %w/v), alongside a combination of polymers, much thinner fibers than previous studies have yielded have been produced (Garg and Bowlin, 2011); resulting in atomised coatings with larger surface area and therefore higher drug carrying capacity.

The preliminary studies of jet mapping and morphological analysis allowed the selection of an appropriate flow rate and voltage, using a flow rate of 15 µl/min, 10 µl/min and 10 µl/min for F1, F2 and F3, respectively.

4.4.4.1.3 Probe encapsulation

The ability of these electrically atomised coatings to encapsulate actives was demonstrated by replacing TM with model dye rhodamine B in all the formulations at the same concentration (5 %w/w of the polymer). The solutions were atomised, collected on microscope slides and were subjected to fluorescence microscopic analysis. **Figure 4.10** shows the entrapment of the probe within the polymeric matrix.

Figure 4.10a shows the encapsulation of rhodamine B in a PVP matrix. The excitation of the C=O bond in the PVP structure (**Figure 3.1**) emitted a long wavelength (green) whereas the conjugated double bonds within the ring structure in rhodamine B induced red-shift in absorption when exposed to RFP. The fluorescent images show structures with yellow cores and slightly darker shell; demonstrating probe encapsulation within the PVP matrix. PNIPAM does not fluoresce so when overlaid with rhodamine B under RFP, a speckled effect can be observed **(Figure 4.10b)** showing the probe within the particles. **Figure 4.10c** shows images of composite particles. Yellow structures can be seen due to the presence of PVP in the formulation. These results coincide with Khan et al findings when using PVP as the polymer matrix for NP coatings of solid microneedles for insertion in the skin (Khan et al., 2014).

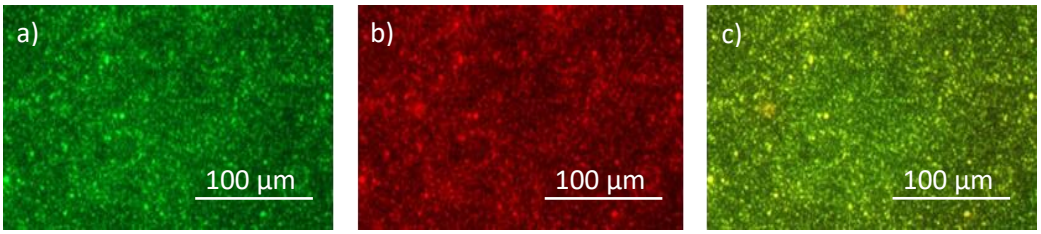

Figure 4.10 Fluorescence Microscopic Images confirming probe encapsulation in a) PVP coatings, b) PNIPAM coatings and c) Composite coatings

4.4.4.2 Drug Encapsulation

Table 4.4 displays information regarding the drug EE percentages of each formulation. F3 showed the highest EE with almost all of the drug (99.7%) being loaded into the atomised coating. The least efficient EE was exhibited with F1 (64.63%).

Table 4.4 Drug Encapsulation Efficiency of the 3 electrically atomised coatings

Formulation	*Encapsulation Efficiency*
F1	64.63%
F2	79.8%
F3	99.7%

These values were used to calculate the total amount of drug present in the samples used in *in vitro* and *ex vivo* studies.

4.4.4.3 Thermal Analysis

4.4.4.3.1 Differential Scanning Calorimetry

When using novel techniques within the pharmaceutical industry, it is imperative to ensure that the processing parameters do not affect the physical form of the active or materials used. DSC was utilised to analyse the thermal transitions of the raw materials within the electrically atomised particles to ensure the solvent (methanol) and the electrospraying process has not altered the crystallinity of the polymers and subsequently the properties of the resulting particles. **Figure 4.11** presents the DSC thermograms for all 3 formulations, including raw materials and pure drug.

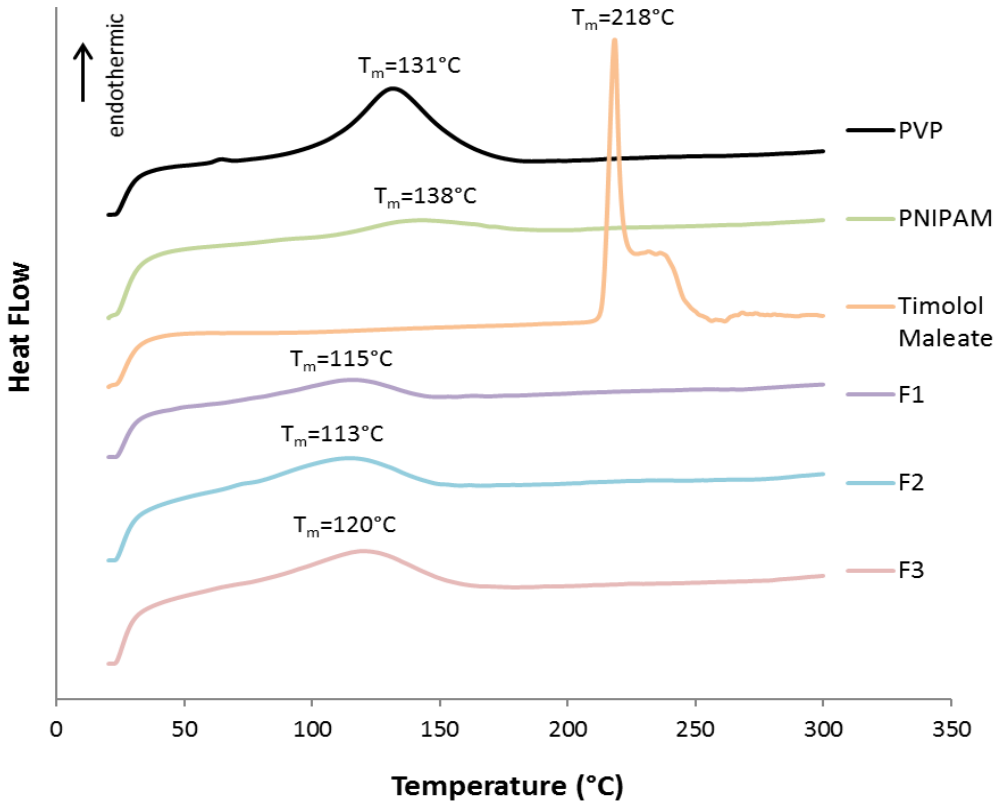

Figure 4.11 DSC thermograms of raw materials and atomised coatings

Pure TM is a crystalline drug with a defined melting point (T_m) of 218 °C as seen in **Figure 4.11**. **Figure 4.11** shows characteristic endothermic peaks at 131 °C and 138 °C for PVP and PNIPAM

respectively, corresponding to their melting point. The 3 formulations (polymer + drug) had similar broad endothermic peaks (60 °C-165 °C) with peaks at 115 °C, 113 °C and 120 °C for PVP, PNIPAM and the composite formulation respectively.

The thermograms comprise of one peak for each formulation, demonstrating that the original structures of the raw materials were not compromised, highlighting the materials formed polymer-drug complexes and are acting as one system rather than individual components. The resulting DSC scan for F3 particles show a lack of phase characteristic peaks of both PVP and PNIPAM as well as TM, except a broad peak with a maximum of 120 °C, (a higher melting point than PVP and PNIPAM alone), suggesting a single, more stable system. The absence of the sharp endothermic peak indicative of pure TM T_m in the thermograms of F1-F3 illustrates the drug is no longer present in crystalline form but now distributed in amorphous form within the polymeric matrix.

4.4.4.3.2 Thermogravimetric Analysis

TGA is a vital thermal characteristic to determine the degradation properties of samples. To investigate the thermal behaviour of raw materials and the resultant coatings, they were subjected to TGA. **Figure 4.12a and b** shows the TGA profile for raw materials and atomised samples. The trace for raw TM depicts a sharp weight loss (75.14%) between 201 °C and 370 °C that is shown as a significant decrease between this range. This decline is characteristic of drug degradation (Joshi et al., 2009).

Two major weight loss events can be observed with the TGA profiles for both raw polymers. The first weight loss reduction is seen between 40 °C and 140 °C and between 40 °C and 168 °C for PVP (11.19% loss) and PNIPAM (3.8% loss) respectively; corresponding to initial moisture loss of the surface-associated water within the polymer. The second weight loss event is characteristic of polymeric thermal degradation. Within the temperature interval 390 °C and 525 °C, a weight loss of 83.32% can be seen with the PVP TGA trace, where the PVP thermally degraded by release of pyrrolidone side group followed by decomposition of polyenic chains. These results coincide with Peniche's work (Peniche et al., 1993). Thermal degradation of PNIPAM can be observed at 342 °C-470 °C; a weight loss of 93.18%, which correlates to the degradation of PNIPAM found in literature (Bauri et al., 2013).

Figure 4.12b shows the TGA thermogram of the atomised coatings. The profile for all three samples are similar; all three formulations exhibited 2 major weight loss events between 20°C and 120°C and between 370°C and 485°C. The first weight loss occurrence corresponds to the dispelling of water and the second drastic weight loss is due to polymer degradation. F3 coatings degraded at a lower temperature compared to sole polymer-drug samples, which could be a result of the arrangement of polymeric chains during the atomization process. As with DSC, the presence of just two weight loss events for the coatings suggests the polymers and the drug are acting as one system rather than independent components.

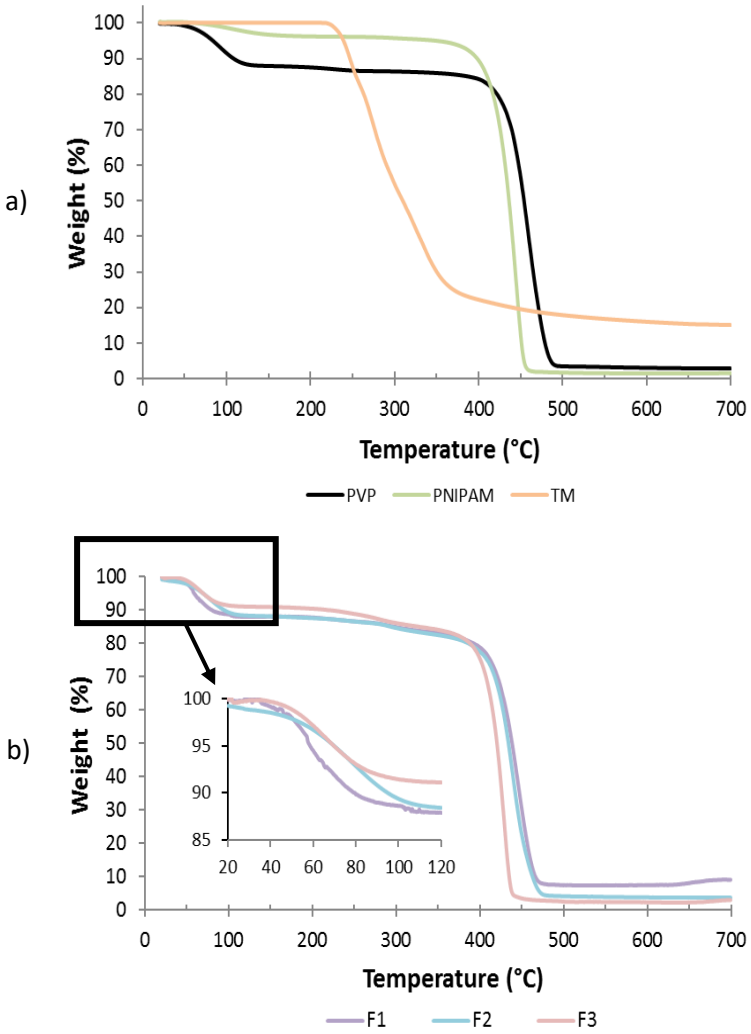

Figure 4.12 TGA thermograms for a) Raw Materials and b) Atomised Coatings

4.4.4.4 Contact Angle

CA is a quantitative measurement of the wetting of a solid by a liquid (usually water). Introducing a droplet of distilled water and analysing the droplet spreading kinetics can also provide data on the hydrophilicity of the material. Angles smaller than 90° indicate high wettability (hydrophilic) whilst angles larger than 90° indicate poor wettability and therefore are more hydrophobic. The wettability of the surface of the electrically atomised samples were characterised and analysed over time **(Figure 4.13).**

Upon dropping the water droplet, the highest static CA was observed with beaded fibers produced by atomising F2 and F3 (130.1° and 126.27°, respectively). At 0 seconds, the CA for TM-loaded PVP particles, an average CA of 83.02° was recorded using a trigger-sensor camera (**Figure 4.13d**). This difference in initial CA between particles and fibers could be due to the surface roughness of the structures.

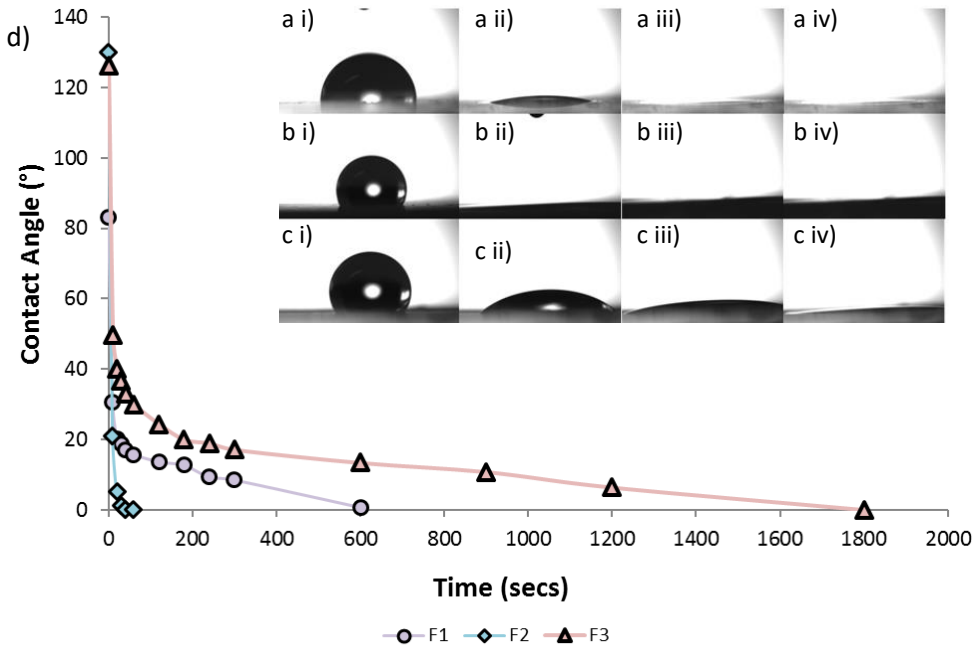

Figure 4.13 Contact Angle Analysis. Digital images taken during contact angle measurements over time for a) F1 samples, b) F2 samples, c) F3 samples at i) 0 s, ii) 30 s, iii) 10 mins, iv) 30 mins d) Contact Angle analysis over time for F1, F2 and F3.

The "featureless" surface of PVP particles (as confirmed through SEM) and high surface area of particles results in less air entrapment between the solid and liquid phases, ultimately resulting

in a low static CA as soon as the water droplet comes into contact with the sample (W. Ma et al., 2017). The water droplet applied to F2 samples completely disintegrated within 10 seconds indicating rapid penetration of water through the sample, dissolution of sample and/or the increase of degree of wettability with time **(Figure 4.13b).** This can be corroborated by the hydrophilic nature of PNIPAM (Ashraf et al., 2016). The CA for F1 and F3 samples were unmeasurable after 10 minutes and 30 minutes, respectively due to complete spreading of water after these time points. The polarity of PVP makes the polymer highly hydrophilic; indicating a low CA at 0 seconds. However, the density of the samples can cause particles to agglomerate, trapping air between the particles. This may prevent the water droplet penetrating and spreading. The dissolution of PVP and PNIPAM over time allows the water to penetrate the inter-particle pores and spread; with the droplet spreading completely within 10 minutes of application (Kim, Kim and Kim, 2013). The combination of particles and fibers with F3 samples increases the surface area and surface roughness of the sample; which in turn can contribute to the time it took for the CA to reduce from an average of 126° at 0 seconds to 0° after 1800 seconds, enabling the coating to be remain on the lens for longer; prolonging drug retention.

4.4.4.5 FTIR Spectroscopy Analysis

EHDA technologies have become more and more favoured due to the fact that the processing conditions do not seem to affect the structure of the materials being handled (Xie et al., 2015). FTIR is able to identify the presence of functional groups of materials. Following EHD processing, the resulting engineered products can be subjected to FTIR analysis to ensure the structure of the active and other additives have not been compromised. Here, FTIR was performed on raw materials (as obtained in powder form) and atomised structures (beaded fibers and particles). The fingerprint of PVP and PNIPAM can be observed using FTIR; as seen in **Figure 4.14** based on structural groups present.

With respect to PVP, peaks at 3469 cm^{-1} and 1664 cm^{-1} correspond to O-H stretching vibrations and C=O and N-C stretching vibration, respectively. Multiple peaks at 2948 cm^{-1}, 2918 cm^{-1} and 2875 cm^{-1} are present due to CH-CH_2 stretch vibrations. Evidence of C-H deformation of cyclic CH_2 groups can be seen at 1492 cm^{-1}, 1459 cm^{-1}, 1419 cm^{-1} and 1371 cm^{-1}. Amide III bond (C-N stretching vibration), amide V (CH_2 rocking vibrations) and amide IV bond are present at 1282 cm^{-1}, 732 cm^{-1} and 648 cm^{-1} respectively. Characteristic absorption peaks on the PNIPAM spectra

included amide II bond at 1550 cm^{-1}, C=O stretching and CH_3 asymmetric stretching vibrations at 1650 cm^{-1} and 2970 cm^{-1}, respectively.

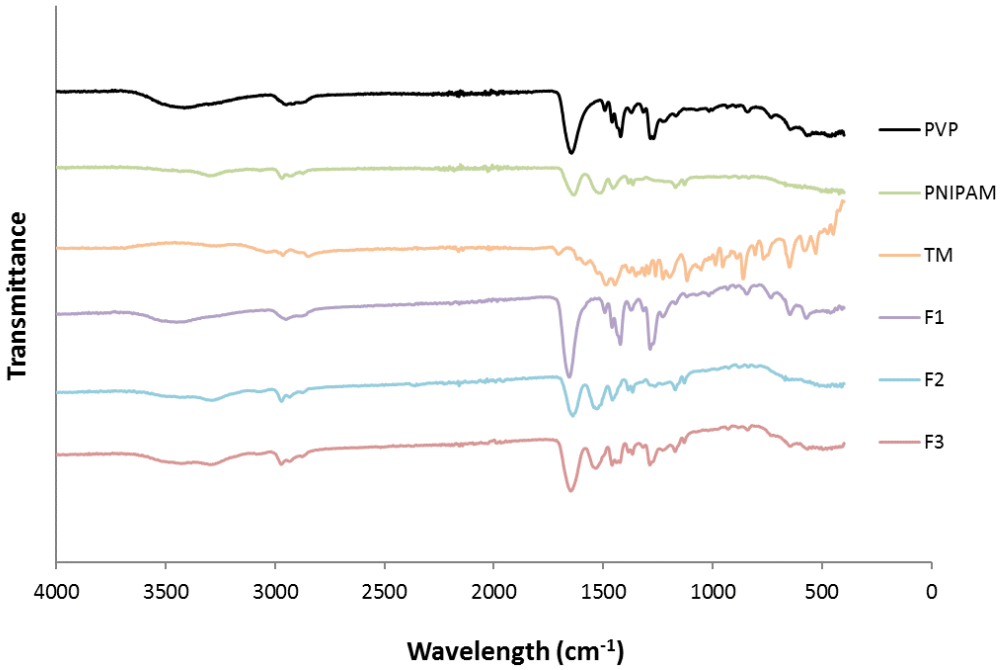

Figure 4.14 FTIR Spectra for raw materials and atomised structures

The stability of TM in the presence of PVP and PNIPAM (separately and as composite) and following EHDA process can be assessed by analysing the drug-polymer interactions in the resulting spectra from FTIR spectroscopy. A broad band in the spectrum for TM corresponds to O-H/N-H stretching vibrations whilst peaks at 2968 cm^{-1}, 2891 cm^{-1} and 2854 cm^{-1} are present due to aliphatic C-H stretching vibration. The acid carbonyl group of maleic acid and the N-H bending vibrations show peaks at 1707 cm^{-1} and 1496 cm^{-1}. Bands at 1229 cm^{-1} and 954 cm^{-1} are due to O-H bending and hydroxyl C-O stretching vibrations, respectively. Similar peaks in the spectra for the atomised formulations indicate the chemical structure of TM was not compromised and was unaffected by the EHDA process.

4.4.4.6 *In Vitro* Studies

4.4.4.6.1 Drug Release Studies

Drug release from polymeric matrices is a critical study to conduct with respect to establishing product behaviour during the numerous stages of drug product development. Establishing the drug release behaviour can provide extensive information on the dosage form alongside release mechanisms and kinetics. Nano-particulate structures and nanofibrous systems are considered to be complex dosage forms, hence monitoring and deciphering drug release from these systems is of great importance. *In vitro* drug release testing involves quantifying or measuring the release of drug from a matrix or carrier in an environment simulating physiological conditions. **Figure 4.15** shows cumulative release (%) of TM from polymeric coatings in PBS at physiological conditions (pH=7.4, 37 °C). The release study showed after 1 minute, 25.1%, 12.4% and 11% of TM was released from F1, F2 and F3 samples, respectively.

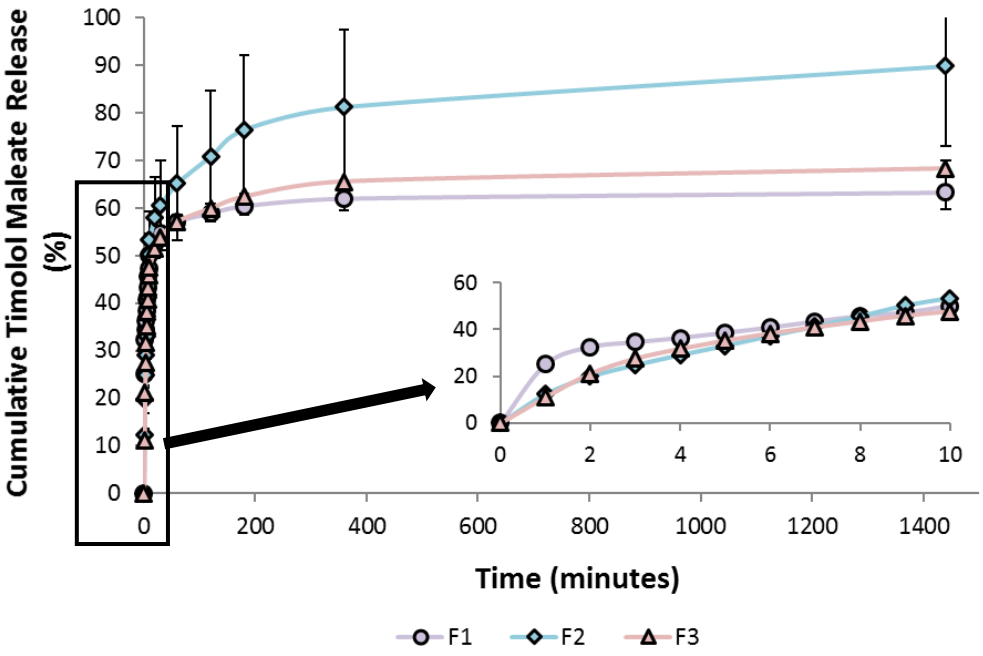

Figure 4.15 *In Vitro* cumulative TM release (%) from various polymeric coatings

After 30 minutes, over 50% of TM was released from all 3 samples. Readings taken at 24 hours, drug release was found to be 89.8% for F2 whereas for F1 and F3, only 63.2% and 68.2% of TM was released, respectively.

There is a noticeable general trend for all three formulations as similar release profiles can be observed. There is an initial burst release, followed by a sustained, controlled release phase that slowed but still increased with time eventually saturating at 24 hours. The rapidly dissolving nature of PVP could explain the initial burst release seen with F1 and F3. The morphology (combination of particles and fibers) of the atomised structures using F2 and F3 could account for the initial burst release observed, as particles tend to release drug more quickly due to higher total surface area. PVP has been used previously in ophthalmic formulations. For example, PVP was utilised as a rapidly dissolving matrix for the delivery of rifampicin (Braha et al., 2009) and in the manufacture of ocular films for delivery of anti-inflammatory drug diclofenac sodium which displayed controlled drug release. More than 50% of drug was released within 1 hour and the remaining drug was released within 4 hours (Jafariazar et al., 2015). Controlled release of drug using PNIPAM has been previously shown where PNIPAM was used as a nano-vesicular carrier for anticancer drug 5-fluorouracil (Li et al., 2015). Increasing the temperature to physiological temperature saw a more controlled sustained release with 35% of drug being released within 24 hours. The combination of a fast dissolving polymer (PVP) and a more sustained dissolving polymer (PNIPAM) here along with the novel technology of EHDA can be used to develop a polymeric device with controlled and prolonged release, as shown by these *in vitro* studies.

4.4.4.6.2 Probe Release Studies

To demonstrate the drug leaving the lens at a sustained rate as well as the coating remaining on the lens, lenses were coated with atomised probe-loaded polymeric coatings and exposed to PBS. **Table 4.5** shows the dye intensity on the lens using fluorescence microscopy and **Figure 4.16** displays the release profile of rhodamine B from the lens into PBS by showing DI in PBS, using UV-Spectroscopy.

Table 4.5 Fluorescence images of probe-loaded coatings over 24 hours when exposed to PBS medium

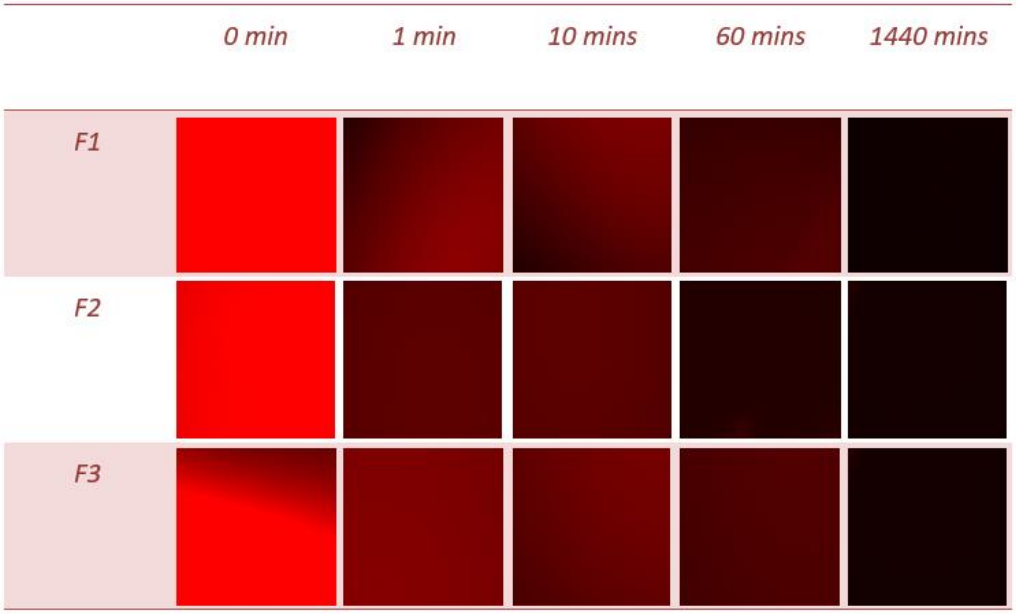

For PVP coated lenses, there is 100% DI on lens at 0 minutes and 0 DI in PBS. As time increased, the DI on lenses decreased (down to 8.7%) (**Figure 4.16a**) and the DI in PBS increased (up to 0.034). An initial burst release in the first 10 minutes (100% to 43% DI on Lens) was observed which gradually saturated after 6 hours (9.79% DI on lens). The data collated from UV spectroscopy reflected what was found with fluorescence microscopy: an initial burst release of probe into PBS from 0 to 0.0064 within the first 10 mins of exposure which then gradually increased to 0.034 after 24 hours. For the PNIPAM coated lens, a similar release profile was observed as with PVP: initial burst release followed by sustained release. **Table 4.6** shows fluorescence images of each contact lens after removal from PBS and **Figure 4.16b** shows the

release profiles of rhodamine B from the lens and into PBS. DI on the lens decreased rapidly within 10 minutes (65.5% of probe was released) and the profile of release into PBS showed a sudden initial increase (from 0 to 0.01) within 10 minutes with subsequent gradual increase after 1 hour (0.016) to 24 hours (0.047). With respect to the composite lenses an initial burst release with subsequent sustained release was observed with approximately 50% of the dye being released into the media and 50% remaining on the lens (**Figure 4.16c**). After 6 hours, 71% of the dye had been released from the polymeric sample and following the 24 hour mark, 89% of the dye had been released into the PBS. The sustained release of rhodamine B was exhibited from 10 mins (0.07667; absorbance in PBS) to 24 hours (0.0426). The results for all three formulations mirrored the outcomes found with *in vitro* TM release.

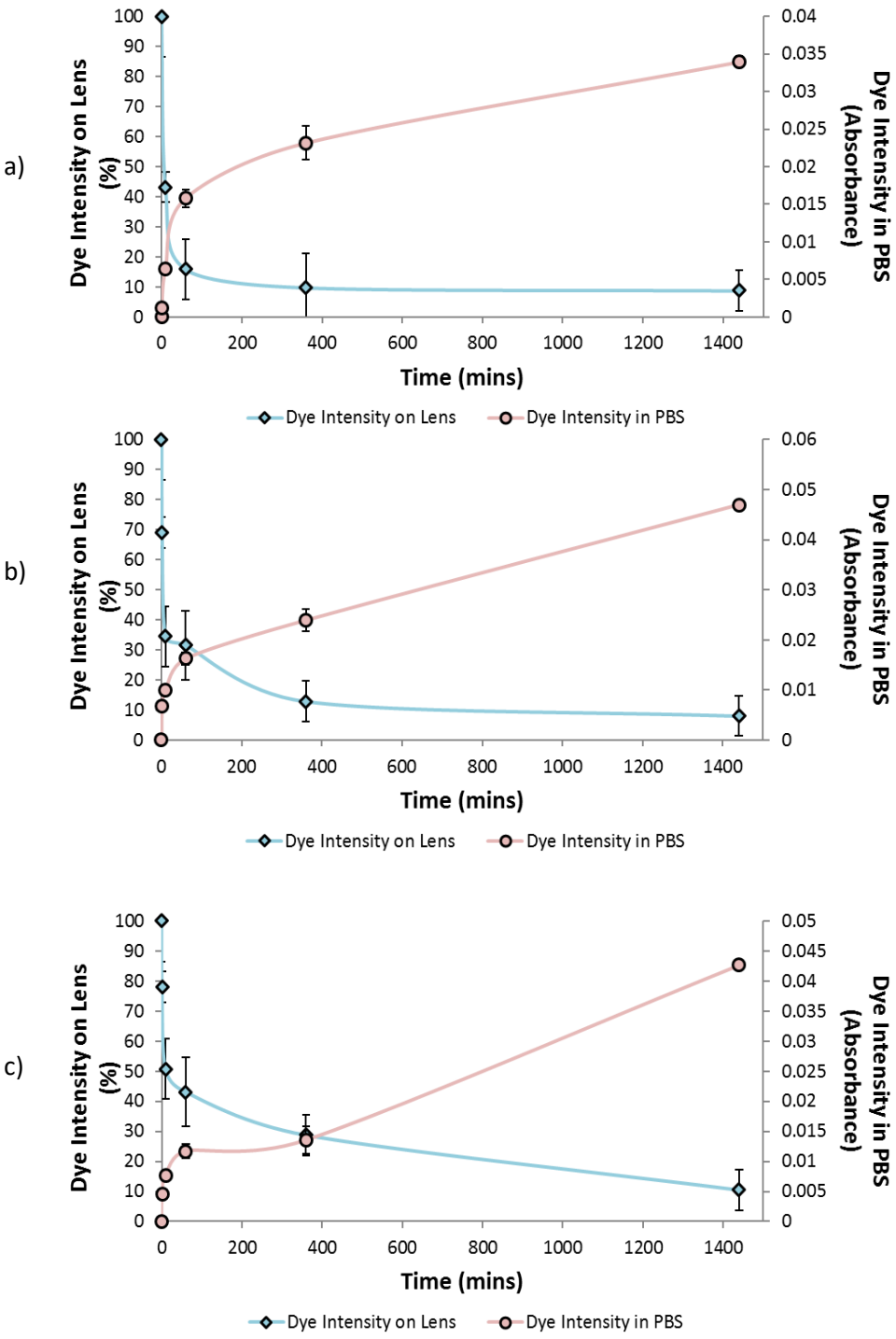

Figure 4.16 *In vitro* Probe detection from lens into PBS medium from a) F1 coatings, b) F2 coatings and c) F3 coatings

4.4.4.6.3 Drug Release Kinetic Modelling

To determine the mechanism by which TM was released from the atomised polymeric coatings, data from the *in vitro* release studies was fitted to various kinetic models to obtain graphical plots. The linearity of graphs was demonstrated by the regression co-efficient, R^2; the higher the R^2 value, the more linear the graph and subsequently, the better the correlation between the variables. Drug release following zero-order kinetics demonstrates a release independent to the drug concentration whilst first-order kinetics indicate the release of drug is concentration dependent .

In order to determine if the release of TM was zero order, the cumulative percentage release of TM was plotted against time (**Figure 4.17**). For analysis of first order kinetics, log cumulative percentage of TM remaining was plotted as a function of time (**Figure 4.18**).

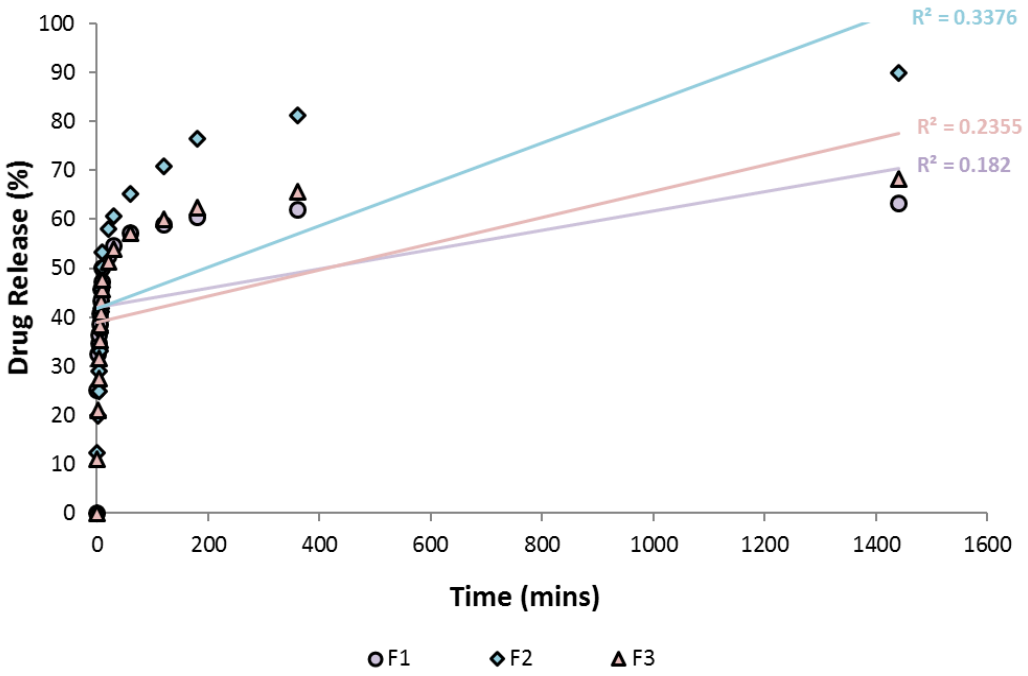

Figure 4.17 Timolol Maleate Release from atomised coatings according to zero-order model

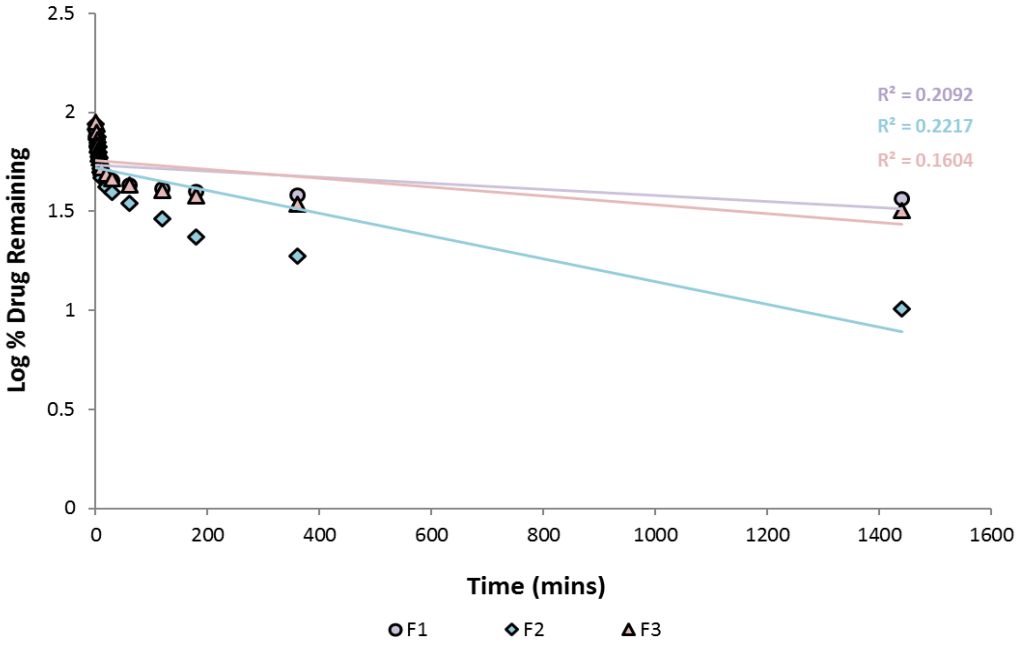

Figure 4.18 Timolol Maleate Release from atomised coatings according to first-order model

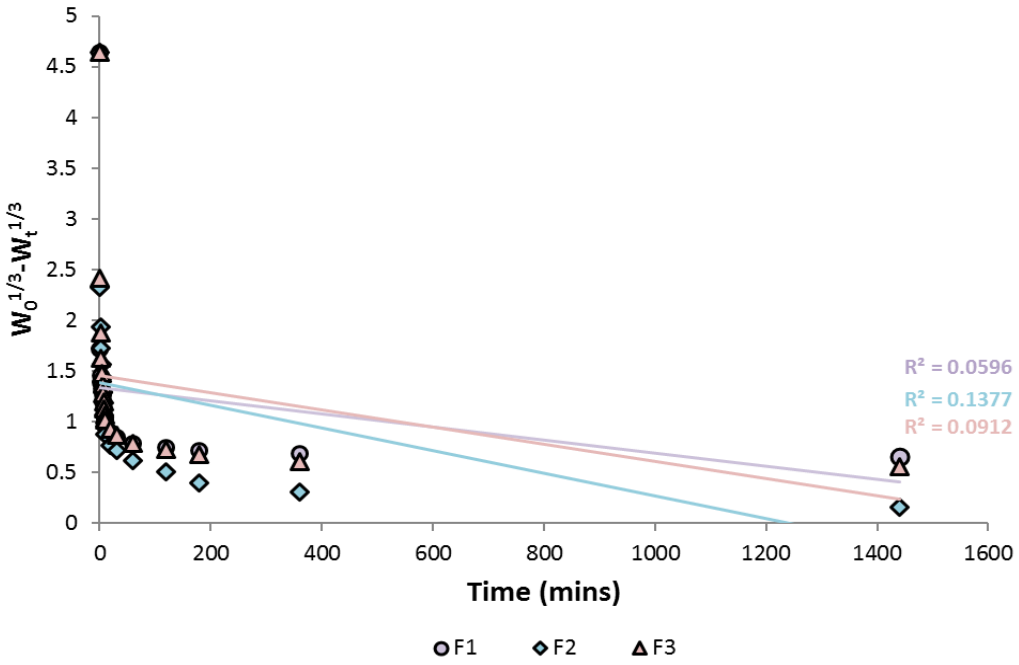

Figure 4.19 Timolol Maleate Release from atomised coatings according to the Hixson-Cromwell model

Hixson-Cromwell cube root law describes the release of drug due to change in particle surface area and diameter (Hixson and Cromwell, 1931), where the cube root of percentage of drug remaining in the matrix is plotted versus time (**figure 4.19**).

The Higuchi model describes drug dissolution from various types of modified release from polymeric matrices. The model was originally intended for planar systems but evolved to extend to different geometries and porous matrices. It has been generalised to yield the simplified Higuchi Model (Siepmann and Peppas, 2011). It is based on several hypotheses: i) initial drug concentration in the matrix is much higher than drug solubility; ii) drug diffusion is only in one plane; iii) drug particles are much smaller than the system matrix; iv) the matrix swelling and dissolution is negligible; v) drug diffusivity is constant; vi) perfect sink conditions in release environment are reached. The cumulative drug release of TM from all three samples was plotted as function of square root of time (**Figure 4.20**).

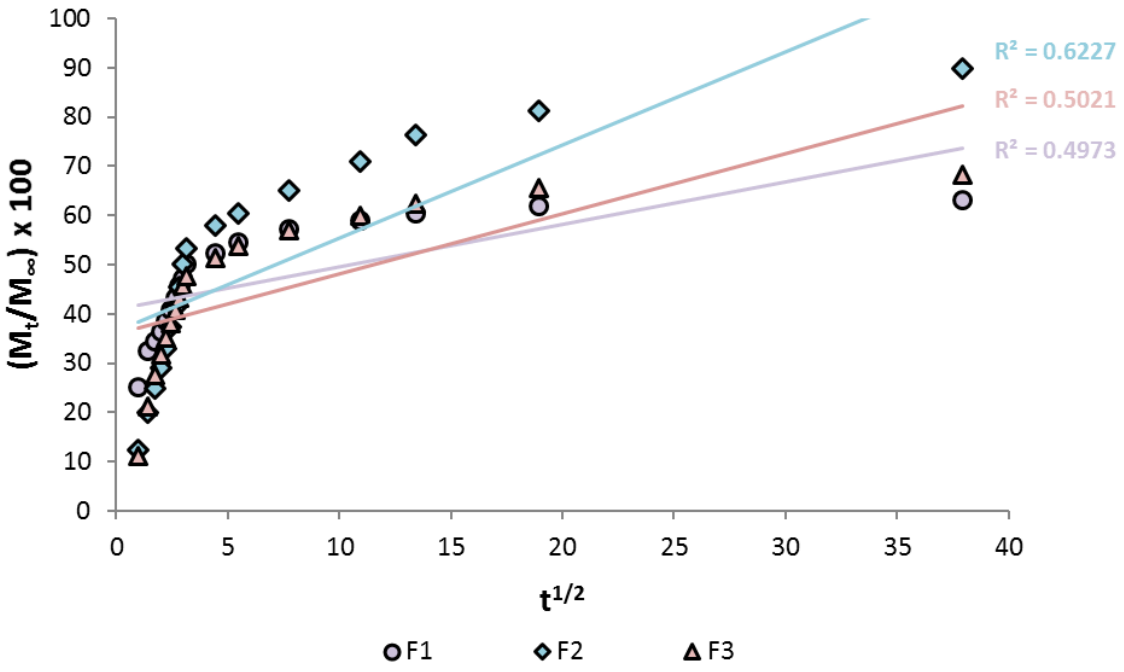

Figure 4.20 Timolol Maleate Release from atomised coatings according to the Higuchi model

All three formulations showed a poor fit for zero order and first order release kinetics, confirmed by low R^2 values (**Table 4.7**), showing drug concentration had no effect on the release of TM from the atomised coating.

Table 4.6 Kinetic Models for timolol maleate release expressed by regression coefficient, R^2

Formulation	*Zero-order*	*First-order*	*Hixson-Cromwell*	*Higuchi*
F1	0.1826	0.2092	0.0596	0.4973
F2	0.3376	0.2217	0.1377	0.6227
F3	0.2355	0.1604	0.0912	0.5021

Results from the Hixson Cromwell model indicate the release of TM was not limited by dissolution but by the transport of drug through the polymeric matrix. Adequate linearity (as classified by Siepmann and Peppas) across all 3 TM loaded polymeric samples were observed with the Higuchi Model (**Figure 4.20 and Table 4.6**); suggesting TM release was a diffusive mechanism, in particular it is likely to be quasi-Fickian Diffusion. This is mirrored in the coefficient of determination (R^2) of 0.5073, 0.6227 and 0.5021 for F1, F2 and F3 atomised formulations, respectively.

The Korsmeyer-Peppas model was devised to explain the type of diffusive mechanism from polymeric matrices. It is a logical kinetic model to use when there could be multiple possible release mechanisms. For spherical matrices, various n values depict specific release mechanisms stated in **section 3.2.8.1.2**. Log cumulative release (%) was plotted as a function of log t with only the first 60% was fitted to the Korsmeyer-Peppas model. The resulting parameters collated from the model given in **Table 4.7**. For F1, F2 and F3, the n values were 0.1588, 0.1964 and 0.4921, respectively, which, like the Higuchi model, indicated quasi-Fickian transport dominated the release of TM from polymeric nano-structures into PBS. Therefore the release mechanism of TM here was diffusion dominated (Riger and Peppas, 1987; Korsmeyer et al., 1983).

Table 4.7 Korsmeyer-Peppas model parameters for timolol maleate release

Formulation	*R^2*	*n*	*k*
F1	0.8107	0.1588	0.502
F2	0.7967	0.4921	0.2443
F3	0.6932	0.1964	0.3903

4.4.4.7 Ocular Irritancy Testing

The BCOP test is an organotypic assay utilised to assess the irritancy of test materials based on how corneal opacity and permeability is affected. An undamaged cornea is a clear structure, which acts as a protective barrier enabling the cornea to remain impermeable to a large array of materials including sodium fluorescein dye. Hence, any damage to the corneal cells following treatment with test substances can be associated with said substances (Abdelkader et al., 2015; Wilson, Ahearne and Hopkinson, 2015).

Figures 4.21a-c illustrates the response of bovine cornea opacity to TM-loaded nano-structures alongside controls. Visual observation (i.e. human eye) of the cornea confirms normal saline, the concurrent negative control, shows no damage to the cornea. There is also no change in the opacity of the cornea. In contrast, NaOH (the positive control), unmistakable opacification can be detected; indicating the most severe damage to the cornea. Application of NaOH to the cornea results in interactions with corneal cell membranes. Subsequently, fatty acids in these cells undergo saponification, compromising not only the tight junctions between the corneal epithelial cells but the whole epithelium layer; increasing the permeability of the cornea to the fluorescein dye (Reim, Schrage and Becker, 2001). Clear visual evidence under a cobalt blue filter (465-490nm) indicates that the fluorescein dye has permeated through the corneal layers in NaOH-treated cornea as seen in **Figure 4.21h**).

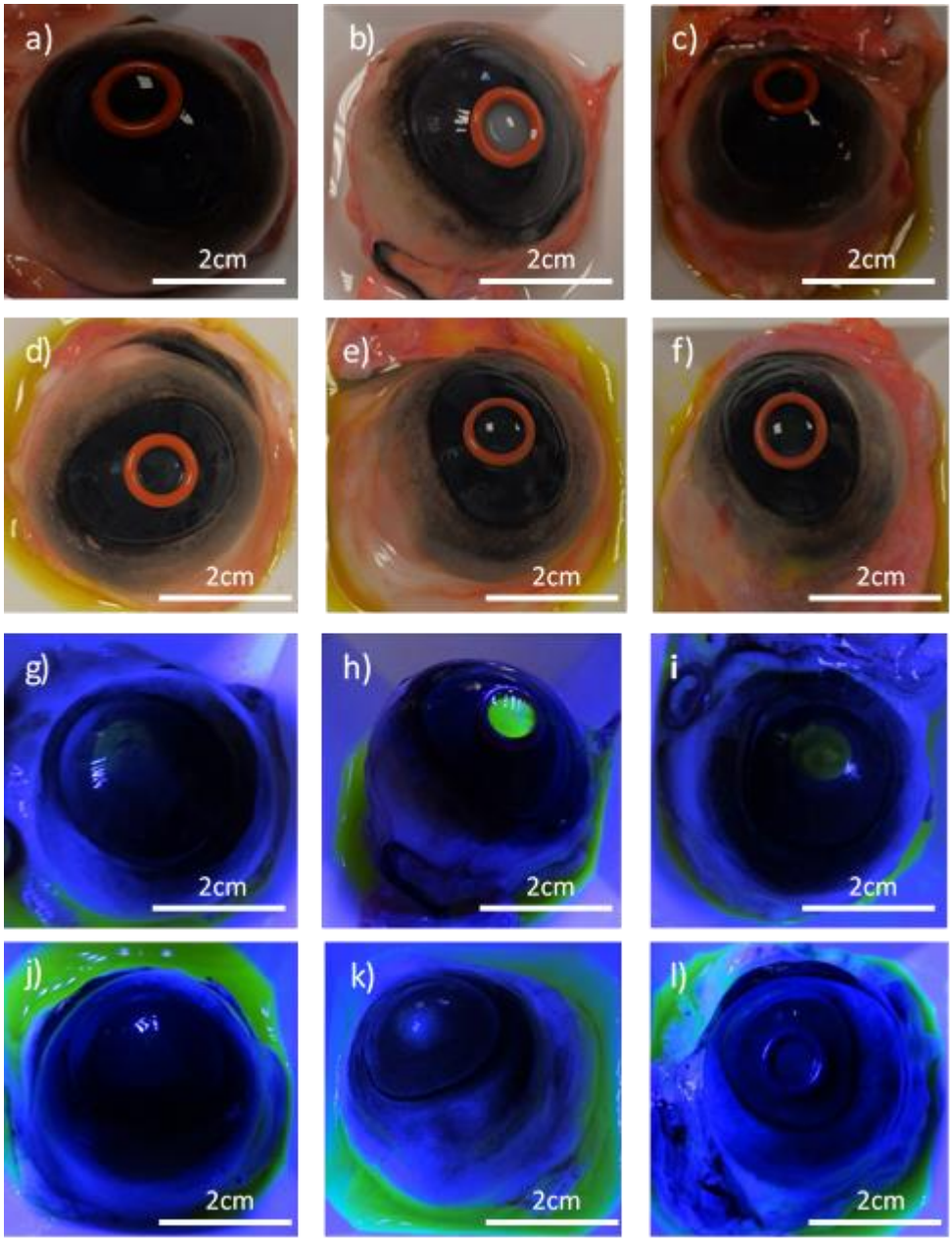

Figure 4.21 BCOP results of freshly excised bovine cornea. Digital images of treated cornea: a) negative control, b) positive control, c) mildly positive control, d) F1, e) F2, and f) F3. Fluorescence images under cobalt blue filter: g) negative control, h) positive control, i) mildly positive control, j) F1, k) F2 and l) F3

The mild positive control (acetone) exhibited a faint cloudy region, suggesting acetone to be a mild irritant to the eye. Acetone causes partial injury to epithelial cells because of lipid solvent interaction properties that can irritate mucosal membranes, ultimately resulting in eye irritation (demonstrated under a cobalt light filter as slight fluorescence) (**Figure 4.21i**). The bovine cornea

treated with normal saline exhibited no fluorescence, showing the dye had not permeated the cornea, highlighting the integrity of the cornea was not compromised. Staining of F1, F2 and F3 treated bovine cornea also showed no fluorescence, indicating there was no damage to the cornea and therefore these are biocompatible formulations for ocular drug delivery (**Figures 4.21j-l**).

4.4.4.8 *Ex Vivo* Testing

Ex vivo permeation studies can provide an insight to how the electrically atomised formulations release drug and how the active permeates through the corneal tissue. TM permeation was measured using freshly excised bovine corneas. By calculating the cumulative amount of TM that permeated through the cornea and using the dimensions of the vertical Franz cells used in this study, various parameters (steady state flux (J_{ss}), apparent permeation coefficient (P_{app})) can be derived. **Table 4.8** shows the J_{ss} and P_{app} values for all three atomised formulations.

Table 4.8 Summary of parameters derived from ex-vivo release studies

	F1			*F2*			*F3*		
	Lens 1	**Lens 2**	**Lens 3**	**Lens 1**	**Lens 2**	**Lens 3**	**Lens 1**	**Lens 2**	**Lens 3**
Sample Weight (mg)	1.3	1.3	1.4	3.9	2.8	4.1	1.3	1.3	2.3
% Permeated / Surface area (%/cm²) after 24 hrs	60.6	54.4	65.4	43.7	42.3	51.7	92.9	80.1	97.34
Steady State Flux (µg/cm²/min)	0.015	0.015	0.021	0.019	0.020	0.021	0.058	0.039	0.074
Apparent Permeability Coefficient (cm²/min)	0.0047	0.0048	0.0069	0.005	0.0053	0.0054	0.012	0.008	0.016

Statistical analysis (one way ANOVA) was conducted to report the statistical significance between the three formulations. The results showed a significant difference in ex vivo permeation between all three formulations ($p<0.05$) with regards to the amount of TM permeating through the excised cornea. The permeation rate of TM from F3 formulation was the highest (J_{ss}=4.431 µg/cm^2/h; P_{app} = 0.9334 cm/h) and was the lowest F1 (J_{ss}=0.86977 µg/cm^2/h; P_{app} = 0.2827 cm/h). This difference is due to the combination of rapidly dissolving polymer (PVP) and thermosensitive, slowly dissolving polymer (PNIPAM) allowing the facilitation of TM corneal drug delivery. Based on a study by Moosa the *in vivo* effect on TM release from

ocular inserts, marketed eye drops demonstrated P_{app} of $1.7x10^{-4}$ cm/min and J_{ss} = 0.00052 mg/cm^2/min in rabbit eyes. The values are contrastingly higher that those derived in this study suggesting atomised (coated) lenses could lead to a reduction in frequent dosing and medicated applications. This reduction, in turn, has the potential to minimise the risk of ocular toxicity because of lowered systemic drug absorption (Moosa et al., 2014). Furthermore, such systems provide greater potential for patient compliance; a challenge which current methods of treatment (e.g. eye drops) are met with.

4.5 Conclusion

This chapter looked at the potential of 3 different polymeric coatings for the effective loading, release and permeation of antiglaucoma drug TM. These coatings were engineered using EHD processing for the outer surface of soft contact lenses and were found to consist of particles or beaded fibers in the nanometre range. Probe encapsulation was demonstrated using fluorescence microscopy, FTIR analysis confirmed the structures of the raw materials, and drug was not compromised during EHD processing. *In vitro* release studies and kinetic modelling studies revealed that TM was released from the polymeric coatings in a biphasic manner via quasi-Fickian diffusion. BCOP testing confirmed the ocular tolerability of all three atomised coatings and *ex vivo* permeation studies indicated significant differences between the 3 polymeric matrices with respect to TM penetration through bovine cornea.

Following these experiments, I chose to focus on improving TM permeation through the cornea. Whilst *ex vivo* studies did show some promising results, long lag times were identified, indicating delayed drug action. *In vitro* studies suggested an initial burst release of TM followed by sustained release for 24 hours which is not mirrored in the *ex vivo* studies. While all three formulations assessed here had the potential to be further modified, F3 was selected due to the combination of PVP and PNIPAM as the polymeric matrix. This formulation presented a biphasic release profile with only approximately 68% of loaded TM being released after 24 hours. Therefore, attempting to improve TM permeation through the use of permeation enhancers felt like the natural progression of this current research.

4.6 References

ABDELKADER, H., PIERSCIONEK, B., CAREW, M., WU, Z. and ALANY, R.G., 2015. Critical appraisal of alternative irritation models: three decades of testing ophthalmic pharmaceuticals. *British Medical Bulletin,* 113(1), pp. 59-71.

AHMAD, Z., ZHANG, H.B., FAROOK, U., EDIRISINGHE, M., STRIDE, E. and COLOMBO, P., 2008. Generation of multilayered structures for biomedical applications using a novel tri-needle coaxial device and electrohydrodynamic flow. *Journal of the Royal Society Interface,* 5(27), pp. 1255-1261.

ANDRADE-VIVERO, P., FERNANDEZ-GABRIEL, E., ALVAREZ-LORENZO, C. and CONCHEIRO, A., 2007. Improving the loading and release of NSAIDs from pHEMA hydrogels by copolymerization with functionalized monomers. *Journal of Pharmaceutical Sciences,* 96(4), pp. 802-813.

ASHRAF, S., PARK, H., PARK, H. and LEE, S., 2016. Snapshot of Phase Transition in Thermoresponsive Hydrogel PNIPAM: Role in Drug Delivery and Tissue Engineering. *Macromolecular Research,* 24(4), pp. 297-304.

BAURI, K., ROY, S.G., ARORA, S., DEY, R.K., GOSWAMI, A., MADRAS, G. and DE, P., 2013. Thermal degradation kinetics of thermoresponsive poly(N-isopropylacrylamide-co-N,N-dimethylacrylamide) copolymers prepared via RAFT polymerization. *Journal of Thermal Analysis and Calorimetry,* 111(1), pp. 753-761.

BENGANI, L.C. and CHAUHAN, A., 2013. Extended delivery of an anionic drug by contact lens loaded with a cationic surfactant. *Biomaterials,* 34(11), pp. 2814-2821.

BOCK, N., DARGAVILLE, T.R. and WOODRUFF, M.A., 2012. Electrospraying of polymers with therapeutic molecules: State of the art. *Progress in Polymer Science,* 37(11), pp. 1510-1551.

BRAHA, S., GAFITANU, C., BRAHA, E., TUCHILUS, C., VASILESCU, M. and POIATA, A., 2009. Enhancement of Dissolution of Rifampicine and in Vitro/in Vivo Evaluation of Drug Release from Collyrium. *Farmacia,* 57(1), pp. 58-64.

CHANG, M.W., STRIDE, E. and EDIRISINGHE, M., 2010. Controlling the thickness of hollow polymeric microspheres prepared by electrohydrodynamic atomization. *Journal of Royal Society Interface,* 7(Supple 4), pp. S451-S460

CHEN, R., REN, N., JIN, X. and ZHU, X., 2018. Stabilization capacity of PNIPAM microgels as particulate stabilizer in dispersion polymerization. *Colloids and Surfaces A-Physicochemical and Engineering Aspects,* 538, pp. 789-794.

CHEN, Y., NURUMBETOV, G., CHEN, R., BALLARD, N. and BON, S.A.F., 2013. Multicompartmental Janus Microbeads from Branched Polymers by Single-Emulsion Droplet Microfluidics. *Langmuir,* 29(41), pp. 12657-12662.

DEOTARE, P.B. and KAMEOKA, J., 2015. Fabrication of Poly Lactic Acid (PLA) Nano/micro Particles and Rods by Electrospraying. *International Journal of Electrospun Nanofibers and Applications,* 1, pp. 123-130.

DOSH, R.H., ESSA, A., JORDAN-MAHY, N., SAMMON, C. and LE MAITRE, C.L., 2017. Use of hydrogel scaffolds to develop an in vitro 3D culture model of human intestinal epithelium. *Acta Biomaterialia,* 62, pp. 128-143.

DOSHI, N., ZAHR, A.S., BHASKAR, S., LAHANN, J. and MITRAGOTRI, S., 2009. Red blood cell-mimicking synthetic biomaterial particles. *Proceedings of the National Academy of Sciences of the United States of America,* 106(51), pp. 21495-21499.

DUONG NHAT NGUYEN, CLASEN, C. and VAN DEN MOOTER, G., 2016. Pharmaceutical Applications of Electrospraying. *Journal of Pharmaceutical Sciences,* 105(9), pp. 2601-2620.

EKEMEN, Z., AHMAD, Z., STRIDE, E., KAPLAN, D. and EDIRISINGHE, M., 2013. Electrohydrodynamic Bubbling: An Alternative Route to Fabricate Porous Structures of Silk Fibroin Based Materials. *Biomacromolecules,* 14(5), pp. 1412-1422.

ELSHAER, A., GHATORA, B., MUSTAFA, S. and ALANY, R.G., 2014. Contact lenses as drug reservoirs & delivery systems: the successes & challenges. *Therapeutic Delivery,* 5, pp. 1085-1100.

GANAN-CALVO, A., DAVILA, J. and BARRERO, A., 1997. Current and droplet size in the electrospraying of liquids. Scaling laws. *Journal of Aerosol Science,* 28(2), pp. 249-275.

GARG, K. and BOWLIN, G.L., 2011. Electrospinning jets and nanofibrous structures. *Biomicrofluidics,* 5(1), pp. 013403.

HANGA, M.P. and HOLDICH, R.G., 2014. Membrane emulsification for the production of uniform poly-N-isopropylacrylamide-coated alginate particles using internal gelation. *Chemical Engineering Research & Design,* 92(9), pp. 1664-1673.

HIXSON, A.W. and CROMWELL, J.H., 1931. Dependence of Reaction Velocity upon Surface Agitation. *Industrial & Engineering Chemistry,* 23(8), pp. 923-931.

HOLLO, G. and KATSANOS, A., 2015. Safety and tolerability of the tafluprost/timolol fixed combination for the treatment of glaucoma. *Expert Opinion on Drug Safety,* 14(4), pp. 609-17.

HUANBUTTA, K., SANGNIM, T., LIMMATVAPIRAT, S., NUNTHANID, J. and SRIAMORNSAK, P., 2016. Design and characterization of prednisolone-loaded nanoparticles fabricated by electrohydrodynamic atomization technique. *Chemical Engineering Research & Design,* 109, pp. 816-823.

HUI, A., SHEARDOWN, H. and JONES, L., 2012. Acetic and Acrylic Acid Molecular Imprinted Model Silicone Hydrogel Materials for Ciprofloxacin-HCl Delivery. *Materials,* 5(1), pp. 85-107.

INOUE, T., NORISUYE, T., SUGITA, K., NAKANISHI, H. and QUI TRAN-CONG-MIYATA, 2018. Size distribution and elastic properties of thermo-responsive polymer gel microparticles in suspension probed by ultrasonic spectroscopy. *Ultrasonics,* 82, pp. 31-38.

IWATA, Y., MIYASHITA, S. and IWASE, E., 2017. Self-rolling up micro 3D structures using temperature-responsive hydrogel sheet. *Journal of Micromechanics and Microengineering,* 27(12), pp. 124003.

JAFARIAZAR, Z., JAMALINIA, N., GHORBANI-BIDKORBEH, F. and MORTAZAVI, S.A., 2015. Design and Evaluation of Ocular Controlled Delivery System for Diclofenac Sodium. *Iranian Journal of Pharmaceutical Research,* 14, pp. 23-31.

JAYASINGHE, S.N. and EDIRISINGHE, M.J., 2002. Effect of viscosity on the size of relics produced by electrostatic atomization. *Journal of Aerosol Science,* 33(10), pp. 1379-1388.

JIA, X., HU, Y., WANG, K., LIANG, R., LI, J., WANG, J. and ZHU, J., 2014. Uniform Core-Shell Photonic Crystal Microbeads as Microcarriers for Optical Encoding. *Langmuir,* 30(40), pp. 11883-11889.

JOSHI, G.V., KEVADIYA, B.D., PATEL, H.A., BAJAJ, H.C. and JASRA, R.V., 2009. Montmorillonite as a drug delivery system: Intercalation and in vitro release of timolol maleate. *International Journal of Pharmaceutics,* 374(1-2), pp. 53-57.

KACZMAREK, J.C., TIEPPO, A., WHITE, C.J. and BYRNE, M.E., 2014. Adjusting biomaterial composition to achieve controlled multiple-day release of dexamethasone from an extended-wear silicone hydrogel contact lens. *Journal of Biomaterials Science-Polymer Edition,* 25(1), pp. 88-100.

KELLY, A.J., 1990. Charge Injection electrostatic atomization modeling. *Aerosol Science and Technology,* 12 (3), pp. 526-537

KHAJAVI, R. and ABBASIPOUR, M., 2012. Electrospinning as a versatile method for fabricating coreshell, hollow and porous nanofibers. *Scientifica Iranica,* 19(6) pp 2029-2034

KHAN, H., MEHTA, P., MSALLAM, H., ARMITAGE, D. and AHMAD, Z., 2014. Smart Microneedle coatings for controlled delivery and biomedical analysis. *Journal of Drug Targeting,* 22, pp. 790-795.

KIM, J., KIM, E. and KIM, S.S., 2013. Micro-nano hierarchical superhydrophobic electrospray-synthesized silica layers. *Journal of Colloid and Interface Science,* 392, pp. 376-381.

KIM, M.K. and LEE, K.H., 2014. Fabrication of Porous Silk Fibroin Microparticles by Electrohydrodynamic Spraying. *Polymer-Korea,* 38(1), pp. 98-102.

KIM, W. and KIM, S.S., 2011. Synthesis of biodegradable triple-layered capsules using a triaxial electrospray method. *Polymer,* 52(15), pp. 3325-3336.

KORSMEYER, R.W., GURNY, R., DOELKER, E., BURI, P. and PEPPAS, N.A., 1983. Mechanisms of solute release from porous hydrophilic polymers. *International Journal of Pharmaceutics,* 15(1), pp. 25-35.

LABBAF, S., DEB, S., CAMA, G., STRIDE, E. and EDIRISINGHE, M., 2013. Preparation of multicompartment sub-micron particles using a triple-needle electrohydrodynamic device. *Journal of Colloid and Interface Science,* 409, pp. 245-254.

LARRIBA-ANDALUZ, C. and DE LA MORA, J.F., 2010. Electrospraying insulating liquids via charged nanodrop injection from the Taylor cone of an ionic liquid. *Physics of Fluids,* 22(7), pp. 072002.

LEE, E., KIM, D., YANG, S.Y., OH, J. and YOON, J., 2017. Photo-crosslinkable comb-type copolymers bearing a benzophenone moiety for the enhanced swelling kinetics of hydrogels. *Polymer Chemistry,* 8(44), pp. 6786-6794.

LI, G., QI, M., YU, N. and TAO, Q., 2015. Polymer vesicles assembled from ALG-g-PNIPAM and β-cyclodextrin through inclusion complexation for drug release. *Journal of Controlled Release,* 213, pp. e35.

LIAO, I.C., CHEW, S.Y. and LEONG, K.W., 2006. Aligned core-shell nanofibers delivering bioactive proteins. *Nanomedicine,* 1(4), pp. 465-471.

LUCKANAGUL, J.A., PITAKCHATWONG, C., BHUKET, P.R.N., MUANGNOI, C., ROJSITTHISAK, P., CHIRACHANCHAI, S., WANG, Q. and ROJSITTHISAK, P., 2018. Chitosan-based polymer hybrids for thermo-responsive nanogel delivery of curcumin. *Carbohydrate Polymers,* 181 (, pp. 1119-1127.

MA, C., LE, X., TANG, X., HE, J., XIAO, P., ZHENG, J., XIAO, H., LU, W., ZHANG, J., HUANG, Y. and CHEN, T., 2016. A Multiresponsive Anisotropic Hydrogel with Macroscopic 3D Complex Deformations. *Advanced Functional Materials,* 26(47), pp. 8670-8676.

MA, W., GUO, Z., ZHAO, J., YU, Q., WANG, F., HAN, J., PAN, H., YAO, J., ZHANG, Q., SAMAL, S.K., DE SMEDT, S.C. and HUANG, C., 2017. Polyimide/cellulose acetate core/shell electrospun fibrous membranes for oil-water separation. *Separation and Purification Technology,* 177, pp. 71-85.

MA, Z., JI, H., TAN, D., DONG, G., TENG, Y., ZHOU, J., GUAN, M., QIU, J. and ZHANG, M., 2011. Large-scale preparation of strawberry-like, AgNP-doped SiO2 microspheres using the electrospraying method. *Nanotechnology,* 22(30), pp. 305307.

MEHTA, P., JUSTO, L., WALSH, S., ARSHAD, M.S., WILSON, C.G., O'SULLIVAN, C.K., MOGHIMI, S.M., VIZIRIANAKIS, I.S., AVGOUSTAKIS, K., FATOUROS, D.G. and AHMAD, Z., 2015. New platforms for multi-functional ocular lenses: engineering double-sided functionalized nano-coatings. *Journal of Drug Targeting,* 23(4), pp. 305-310.

MHRA., 2017-last update, Package leaflet: information for the user: TRUSOPT® 20 mg/ml eye drops, solution (dorzolamide). Available: http://www.mhra.gov.uk/spc-pil/?prodName=TRUSOPT%2020%20MG/ML%20EYE%20DROPS%20%20SOLUTION&subsName=&pageID=ThirdLevel&searchTerm=trusopt#retainDisplay.

MHRA., 2015-last update, PACKAGE LEAFLET: INFORMATION FOR THE USER Timoptol® Eye Drops 0.25% / Timolol Eye Drops 0.25% (timolol maleate),. Available: http://www.mhra.gov.uk/spc-pil/?prodName=TIMOPTOL%20EYE%20DROPS%200.25//&subsName=TIMOLOL%20MALEATE&pageID=SecondLevel.

MOHAMMEDI, H., SHYALE, S. and SHANTA KUMAR, S.M., 2011. Physio-chemical Characterization, UV Spectrophotometric Method Development and Validation Studies of Timolol Maleate. *International Journal of Pharmaceutical Sciences Review and Research,* 6(2), pp. 163-166.

MOOSA, R.M., CHOONARA, Y.E., DU TOIT, L.C., TOMAR, L.K., TYAGI, C., KUMAR, P., CARMICHAEL, T.R. and PILLAY, V., 2014. In vivo evaluation and in-depth pharmaceutical characterization of a rapidly dissolving solid ocular matrix for the topical delivery of timolol maleate in the rabbit eye model. *International Journal of Pharmaceutics,* 466(1–2), pp. 296-306.

PENG, C., KIM, J. and CHAUHAN, A., 2010. Extended delivery of hydrophilic drugs from silicone-hydrogel contact lenses containing Vitamin E diffusion barriers. *Biomaterials,* 31(14), pp. 4032-4047.

PENICHE, C., ZALDÍVAR, D., PAZOS, M., PÁZ, S., BULAY, A. and ROMÁN, J.S., 1993. Study of the thermal degradation of poly(N-vinyl-2-pyrrolidone) by thermogravimetry-FTIR. *Journal of Applied Polymer Science,* 50(3), pp. 485-493.

RASEKH, M., KARAVASILI, C., SOONG, Y.L., BOUROPOULOS, N., MORRIS, M., ARMITAGE, D., LI, X., FATOUROS, D.G. and AHMAD, Z., 2014. Electrospun PVP-indomethacin constituents for transdermal dressings and drug delivery devices. *International Journal of Pharmaceutics,* 473(1-2), pp. 95-104.

RASEKH, M., YOUNG, C., ROLDO, M., LANCIEN, F., LE MEVEL, J., HAFIZI, S., AHMAD, Z., BARBU, E. and GORECKI, D., 2015. Hollow-layered nanoparticles for therapeutic delivery of peptide prepared using electrospraying. *Journal of Materials Science-Materials in Medicine,* 26(11), pp. 256.

REIM, M., SCHRAGE, N.F. and BECKER, J., 2001. Interactions between ocular surface fluid and cornea related to contact lenses. *European Journal of Ophthalmology,* 11(2), pp. 105-115.

RIGER, P.L. and PEPPAS, N.A., 1987. A simple equation for description of solute release: II. Fickian and anomalous release from swellable devices. *Journal of Controlled Release,* 5(1) pp. 37-42.

ROCKWOOD, D.N., CHASE, D.B., AKINS, R.E., Jr. and RABOLT, J.F., 2008. Characterization of electrospun poly(N-isopropyl acrylamide) fibers. *Polymer,* 49(18), pp. 4025-4032.

SCHOOLAERT, E., RYCKX, P., GELTMEYER, J., MAJI, S., VAN STEENBERGE, P.H.M., D'HOOGE, D.R., HOOGENBOOM, R. and DE CLERCK, K., 2017. Waterborne Electrospinning of Poly(N-

isopropylacrylamide) by Control of Environmental Parameters. *ACS Applied Materials & Interfaces,* 9(28), pp. 24100-24110.

SCHOPF, L.R., POPOV, A.M., ENLOW, E.M., BOURASSA, J.L., ONG, W.Z., NOWAK, P. and CHEN, H., 2015. Topical Ocular Drug Delivery to the Back of the Eye by Mucus-Penetrating Particles. *Translational Vision Science and Technology,* 4(3), pp. 11.

SIEPMANN, J. and PEPPAS, N.A., 2011. Higuchi Equation: Derivation, applications, use and misuse. *International Journal of Pharmaceutics,* 418(1), pp. 6-12.

SMEETS, A., CLASEN and VAN DER MOOTER, G., 2017. Electrospraying of polymer solutions: Study of formulation and process parameters. *European Journal of Pharmaceutics and Biopharmaceutics,* 119, pp. 114-124.

SMITH, D., 1986. The Electrohydrodynamic Atomization of liquids. IEEE *Transactions on Industry Applications,* 22(3), pp. 527-535.

TANG, K.Q. and GOMEZ, A., 1995. Generation of Monodisperse Water Droplets from Electrosprays in a Corona-Assisted Cone-Jet Mode. *Journal of Colloid and Interface Science,* 175(2), pp. 326-332.

TASHAKORI-SABZEVAR, F. and MOHAJERI, S.A., 2015. Development of ocular drug delivery systems using molecularly imprinted soft contact lenses. *Drug Development and Industrial Pharmacy,* 41(5), pp. 703-713.

TEMPESTI, P., NICOTERA, G.S., BONINI, M., FRATINI, E. and BAGLIONI, P., 2018. Poly(N-isopropylacrylamide)-hydroxyapatite nanocomposites as thermoresponsive filling materials on dentinal surface and tubules. *Journal of Colloid and Interface Science,* 509, pp. 123-131.

THOMAS, N., LÄHDESMÄKI, I. and PARVIZ, B.A., 2012. A contact lens with an integrated lactate sensor. *Sensors and Actuators B: Chemical,* 162(1), pp. 128-134.

WANG, B., ZHENG, H., CHANG, M.W., AHMAD, Z. and LI, J.S., 2016. Hollow polycaprolactone composite fibers for controlled magnetic responsive antifungal drug release. *Colloids Surf B Biointerfaces,* 1(145), pp. 757-767.

WANG, J., ZHENG, H., CHANG, M.W., AHMAD, Z. and LI, J.S., 2017. Preparation of active 3D film patches *via* aligned fiber electrohydrodynamic (EHD) printing. *Scientific Reports,* 8(7), pp. 43924.

WENG, J., LI, X., GUAN, Y., ZHU, X.X. and ZHANG, Y., 2016. Large-area 2D microgel colloidal crystals fabricated via benzophenone-based photochemical reaction. *RSC Advances,* 6(85), pp. 82006-82013.

WENG, J., TANG, Z., GUAN, Y., ZHU, X.X. and ZHANG, Y., 2017. Assembly of highly ordered 2D arrays of silver-PNIPAM hybrid microgels. *Chinese Journal of Polymer Science,* 35(10), pp. 1212-1221.

WILSON, S.L., AHEARNE, M. and HOPKINSON, A., 2015. An overview of current techniques for ocular toxicity testing. *Toxicology,* 2(327), pp. 32-46

WORLD HEALTH ORGANISATION (WHO), 2015-last update, http://www.who.int/blindness/causes/priority/en/index6.html [01/05/2015].

XIE, J., JIANG, J., DAVOODI, P., SRINIVASAN, M.P. and WANG, C., 2015. Electrohydrodynamic atomization: A two-decade effort to produce and process micro-/nanoparticulate materials. *Chemical Engineering Science,* 125, pp. 32-57.

YAN, E., FAN, Y., SUN, Z., GAO, J., HAO, X., PEI, S., WANG, C., SUN, L. and ZHANG, D., 2014. Biocompatible core-shell electrospun nanofibers as potential application for chemotherapy against ovary cancer. *Materials Science & Engineering C-Materials for Biological Applications,* 41, pp. 217-223.

YUAN, W., WANG, Y., LI, W., WANG, J., ZHANG, X. and ZHANG, Y., 2015. Microencapsulation and characterization of polyamic acid microcapsules containing n-octadecane via electrospraying method. *Materials Express,* 5(6), pp. 480-488.

ZHANG, H.B., JAYASINGHE, S.N. and EDIRISINGHE, M.J., 2006. Electrically forced microthreading of highly viscous dielectric liquids. *Journal of Electrostatics,* 64(6), pp. 355-360.

Chapter 5 Improving timolol maleate permeation through the cornea

5.1 Introduction

This chapter looks at modifying the most suitable formulation identified in chapter 4- composite polymer loaded with 5% timolol maleate. The results shown in this chapter of work demonstrate the *in vitro* and *ex vivo* effect of incorporating 4 different permeation enhancers on i) the resulting electrically atomised coatings with respect to size, shape and stability , ii) the release of TM from the coatings and iii) the permeation of TM through the cornea.

Initially, the reason behind selecting and utilising PNIPAM was its unique thermoresponsive behaviour. In chapter 4, the results suggested the introduction of PNIPAM to PVP solution yielded beaded fibers when electrohydrodynamically processed which in turn found to contribute to a biphasic release profile of TM via a burst release from the PVP and more sustained release from PNIPAM fibers. Due to this, the reasoning behind continuing to use PNIPAM was its ability to provide sustained TM release as opposed to its thermoresponsive nature.

5.2 Background

The eye, whilst being an easily accessible organ, poses great challenges with respect to topical ocular drug delivery (Taskar, Tatke and Majumdar, 2017). More explicitly, the corneal structure is one of the most important barriers with ocular drug delivery. Its composition (ranging in degrees of hydrophilicity) can limit the topical delivery of ocular therapeutic actives (Kong and Mi, 2016).

Whilst the structure of the cornea is the most imperative anatomical barrier to drug delivery, there are an array of factors that can affect drug permeation through this tissue. These factors can be categorised into 3 groups: physiochemical factors (Mun et al., 2014), physiological factors and formulation factors (Malhotra and Majumdar, 2001), all of which have been summarised in **Table 2.1.** The approach taken in the work in this thesis was formulation based. From a

formulation point of view, these factors are arguably the most crucial due to patient safety. There have been many attempts to improve drug penetration but each are not without their downfalls. Increasing the concentration of the drug in question can increase the bioavailability of the active and consequently improve treatment; however, the maximum safety concentration threshold must not be breached. There is also the possibility of increasing drug particle size or using suspensions (for poorly soluble drugs) to increase residence time and provide sustained drug release. However, there is a maximum particle size which can be utilised (10μm) before they will be detected as foreign matter; initiating reflex tear production (Aldrich et al., 2013). Another approach taken to improve bioavailability by increasing residence time is increasing the viscosity of the formulation in question. This has been extremely successful and has led to commercialisation of many products such as Timoptic-XE®, a gel-forming solution. However, an increase in viscosity can lead to blurred vision, causing inconvenience to the patient and limiting the time at which the treatment can be used (i.e. at night). Other successful approaches include altering the pH and tonicity of the formulations, resulting in higher drug bioavailability and consequently extended drug delivery (Gupta, Samanta and Raichur, 2010; Reddy and Ahmed, 2013; Suresh and Abhishek, 2016).

The biggest hurdle research & development and formulation scientists experience in ODD is the poor bioavailability of ocular drugs. One approach to overcome this is to modify the formulation by incorporating permeation enhancers (PEs) (Kim et al., 2016). There are 5 main classes of PEs. Calcium chelators like EDTA work by weakening the tight junctions between epithelial cells in the corneal epithelium, enhancing the paracellular movement of active through the cornea (Kaur and Smitha, 2002; Morrison and Khutoryanskiy, 2014).

Unlike calcium chelators, surfactants enhance drug permeation via transcellular methods. Surfactants are molecules which lower the surface tension between 2 phases. It has been implied that surfactants interfere with the lipid bilayer of epithelial layers; forming micelles causing the phospholipids to be removed from the membrane (Abdelkader, Alani and Alany, 2014). Both non-ionic and cationic surfactants have been used to increase the permeability of various ocular drugs (Sahoo, Biswas and Guha, 2014) such as prednisolone, dexamethasone, atenolol and timolol. Non-ionic surfactants such as Brij®98 and Brij® 78 have been exploited as PEs showing promising results in ocular drug delivery, highlighting the safety and efficacy of

these surface active agents (Saettone et al., 1996). One of the most common surfactants used in ophthalmic formulations is BAC, a cationic surfactant, usually incorporated in ocular solutions at very low concentrations to act as preservative (de los Angeles Ramos-Cadena and Spaeth, 2016; Fukuda and Sasaki, 2015). The effects of this preservative have proven to be more effective in enhancing corneal permeation than other commonly used preservatives such as chlorobutanol and organomercurials. Borneol is a naturally occurring essential oil of *Cinnamonum camphora*. Although it does not fit into a defined category of PEs, it has shown potential in promoting corneal permeation of ocular drugs TM (Wu et al., 2006), dexamethasone (Yang et al., 2009), indomethacin (Yang et al., 2009) and ofloxacin (Yang et al., 2009).

The limitations of conventional methods to increasing BA can easily be overcome using implantable devices (i.e. CLs). By optimising formulations and combining EHDA with the use of CLs, it is possible to extend drug retention time whilst reducing the need of frequent administration. The utilization of nanocoatings engineered using EHDA can increase drug loading capacity due to increased surface area-to-volume ratio and hence reduce the need for multiple doses as with eye drops.

Here, four PEs were incorporated into composite-TM solution from chapter 4 which were subsequently electrohydrodynamically processed to engineer atomised contact lens coatings capable of increasing TM release and permeation through the cornea.

5.3 Materials and Methods

5.3.1 Materials

PVP ($4.4x10^4$ g/mol) was sourced from Ashland (Worcestershire, UK). PNIPAM ($2\text{-}4x10^4$ g/mol), ethanol, TM (>98%), acetone, sodium hydroxide, rhodamine B, BAC, EDTA, borneol and Brij®78 were all obtained from Sigma Aldrich (Dorset, UK). PureVision® Balafilcon A silicone hydrogel contact lenses were supplied by Bausch and Lomb (New York, USA). All reagents used were of analytical grade.

5.3.2 Methods

5.3.2.1 Solution Preparation

A base solution was prepared by dissolving PVP and PNIPAM in ethanol, yielding a 5%w/v polymeric solution. This base solution was used to prepare 8 different formulations, containing different drug concentrations and PE concentrations. **Table 5.1** shows the composition of each formulation. All solid excipients were weighed using an analytical balance and were mixed using a magnetic stirrer for 30 minutes to ensure solution homogeneity.

5.3.2.2 Solution Characterisation

Each formulation was characterised based on three physical liquid properties: viscosity, surface tension and electro-conductivity. The measurements were carried out as stated in **Section 3.2.1**, in triplicate, with an average reading taken.

5.3.2.3 EHDA Set-up and Optimisation

The system set-up was similar to that specified in **Section 4.3.2.4.** Briefly, polymeric solutions were drawn into 5 mL syringes that were attached to a syringe infusion pump. This pump enabled the flow of the polymer-drug-PE solution to be controlled throughout the atomization process. The solution was infused through silicone tubing to a single stainless steel conductive coaxial needle device (where only the outer needle was used) at various flow rates. This set-up was connected to a high power voltage supply. All atomization processes were carried out in ambient conditions (23°C).

Due to incorporation of new excipients to the composite formulation, new jetting mode maps need to be generated to determine the optimum process parameters for each formulation. Each formulation was processed at flow rates in increasing increments of 1 µl/min from 0 µl/min up to 20 µl/min. At each flow rate, the voltage that was required to produce various spraying modes (stable, unstable, dripping) were logged, providing data to generate jetting mode maps. **Table 5.1** shows the specific flow rates used and voltages applied to each formulation produce atomised coatings upon production of a stable jet.

Table 5.1 Formulation Composition and Optimum Process parameters for each formulation. Each formulation contained PVP and PNIPAM at 1:1 ratio to achieve 5 %w/v solution

Formulation	*TM Concentration (%w/w of the polymer)*	*Permeation Enhancer*	*Permeation Enhancer Concentration (%w/v)*	*Flow Rate (µl/min)*	*Applied Voltage (kV)*
Composite-TM	5	--	--	10	13.6
F1	5	BAC	0.01	8	14.5
F2	5	EDTA	0.5	10	15.6
F3	5	Borneol	0.1	8	13.2
F4	5	Brij® 78	1	15	14.7
F5	15	BAC	0.01	8	14.8
F6	15	EDTA	0.5	10	15.3
F7	15	Borneol	0.1	8	14.1
F8	15	Brij® 78	1	15	15.3

5.3.2.4 Coating Engineering

As with the experiments in chapter 4, microscope slides were used as a preliminary collection device for pilot characterisation studies. Thereafter, *in vitro* and *ex vivo* characterisation were conducted on coated commercial contact lenses. The lenses were dried in a desiccator on a novel lens holder (which helped maintain typical lens shape) for 30 minutes and were weighed before and after the coating process to ascertain the weight of the coating sample. Controlled deposition was again achieved using a modified lens holder and a mask arm producing peripherally coated lenses.

5.3.2.5 Characterisation of TM-Loaded Coatings

5.3.2.5.1 Imaging

Morphological and structure size analysis was carried out as stated in **Section 4.3.2.7.1.** Coatings on both microscope slides and dehydrated contacted lenses were analysed using SEM whilst fluorescence microscopy was used to demonstrate active encapsulation within the atomised coatings.

5.3.2.5.2 Drug Encapsulation Efficiency and Coating Composition

To determine TM encapsulation efficiency; weighed coating samples were dissolved in ethanol for 1 week. UV spectroscopy (λ=295 nm) was used to determine the amount of drug loaded into the weighed sample. **Equation 4.1** was used to calculate encapsulation efficiency. The encapsulation efficiency was then used to decipher the coating composition.

5.3.2.5.3 Thermal Behaviour

The stability and thermal behaviour (i.e. melting point) were assessed using TGA and DSC, respectively. Both studies were carried out as stated in **Section 4.3.2.7.3** (DSC) and **4.3.2.7.4** (TGA). Both raw materials and atomised coatings were analysed under the flow of nitrogen gas at a heating rate of 20 °C/min.

5.3.2.5.4 Goniometry

Contact angle hysteresis was determined using contacts lenses with the atomised coatings, as specified in **Section 4.3.2.7.5**. 10 µl of distilled water was introduced to the samples and each sample was measured in sessile mode at pre-determined time points. Readings were taken in triplicate and an average was derived.

5.3.2.5.5 FTIR

Any potential interactions between the raw excipients during and following electrohydrodynamic processing was assessed using FTIR. Both raw materials and atomised coatings were analysed over the range 400-4000 cm^{-1} using FTIR Platinum-ATR fitted with Bruker Alpha Opus 27 FT-IT at an average of 10 scans at a resolution of 4 cm^{-1}.

5.3.2.5.6 In vitro Release and Kinetics

Drug release and probe release was evaluated as stated in **Section 4.3.2.7.7.** Briefly, weighed contact lenses were introduced to the donor compartment; which had been specially designed to maximise surface contact between the lens and the synthetic dialysis membrane (which separated the donor compartment and the receptor compartment). Upon fixing the lenses in the holder, the entire device was submerged into the "receptor compartment"; a vial containing 10 ml PBS at pH 7.4. At predetermined time points, 1 ml of release medium was retracted and replaced with fresh 1ml PBS. Probe release from the coatings into the release medium was as described in **Section 4.3.2.7.7.2**. Both drug release and probe release studies were conducted in triplicate at 37 °C. *In vitro* drug release data was collated and plotted in various kinetic models to assess the release kinetics to ascertain the mechanism of TM release from the various polymeric coatings.

5.3.2.5.7 Biological Evaluation of Atomised Coatings

To ensure the formulations and ultimately the engineered coatings are biocompatible and display ocular tolerability, a BCOP test was performed as stated in **Section 4.3.2.7.8.**

5.3.2.5.8 *Ex Vivo* Testing

The release and permeation of TM from the atomised coatings was studied *ex vivo* using freshly excised bovine cornea as the membrane between the donor and receptor compartments when using Vertical Diffusion Cells. The method that was followed here is described in **Section 4.3.2.7.9.**

5.3.2.5.9 Statistical Analysis

ANOVA test was carried to compare the release of drug from polymer coatings containing different PEs. Derived *p* values less than 0.5 were considered statistically significant.

5.4 Results and Discussion

The effects of incorporating PEs into polymeric solutions containing TM was analysed here. In chapter 4, methanol was utilised as vehicle for the solutions. However, the solubility of the additional excipients used in this work was higher in ethanol; hence, this was the choice of solvent.

5.4.1 Solution Characterisation

The physical properties of liquids can greatly influence the structures that arise following EHD processing, especially in terms of morphology and size. Hence the viscosity, surface tension and electrical conductive nature of each formulation was investigated.

Table 5.2 shows the average viscosity, ST and EC readings of all 9 formulations alongside the vehicle ethanol. Compared to the vehicle, all the formulations show an increase in viscosity. The incorporation of PVP and PNIPAM to ethanol, (Composite-TM) showed an increase in viscosity; from 1.15 mPa.s to 4.01 mPa.s. This increase in viscosity may have an impact on the resulting atomized structures; leading to the production of fibrous coatings rather than particulate coatings (Barrero et al., 1999; Bock, Dargaville and Woodruff, 2012; Haider, Haider and Kang, 2015). This will be confirmed with subsequent morphological analysis using SEM. Upon addition of PEs there is no significant difference between the average viscosity readings (p= 0.687).

With respect to ST the incorporation of PEs lowered the overall surface tension of the formulations. Formulations that contained BAC and Brij® 78 found to have lower surface tension than Composite-TM; demonstrating these PEs also acted as surface active agents. BAC is found in over 70% of ocular formulations and is most commonly added as a preservative (Tu, 2014); however its cationic nature enables it to serve as a surfactant, lowering the formulations' surface tension. Brij® 78 is a non-ionic surfactant that has previously been researched in ocular DD (Montenegro, Bucolo and Puglisi, 2003), however, there have been no recent developments involving the use of this surface active agent.

Whilst mainly viewed as a chelating agent, EDTA can also be seen as an anionic surfactant. This conclusion can be drawn by observing the reduction in surface tension of formulations containing EDTA compared to PE-free formulations. Regardless of the small reduction; this will

aid the EHD process as the applied voltage can more easily overcome the surface tension on the liquid.

Table 5.2 Characterisation of Polymeric Solutions loaded with permeation enhancers. Data is shown as mean±S.D

Formulation	Viscosity (mPa.s)	Surface Tension (mN/m)	Electrical Conductivity (µS/cm)
Ethanol	1.15±0.0058	21.6±0.917	1.78±0.01
Composite-TM	4.01±0.061	21.24±0.21	199.20±0.02
BAC	4.25±0.60	19.03±0.097	195.02±0.42
EDTA	4.01±0.18	18.54±0.095	177.54.63±0.83
Borneol	3.93±0.086	21.05±1.35	221.94±0.19
Brij® 78	4.25±0.21	17.82±0.53	218.37±0.13

With respect to electro-conductivity, a large increase can be seen from 1.78 µS/cm to 199.20 µS/cm upon dissolving both polymers in ethanol. Upon introduction of PEs, there was no real difference in the average electrical conductivity readings. Due to these readings being within the ideal range for electro-conductivity for EHD processing (10^{-4} and 10^{-8} S/m), a stable jetting mode can be achieved with all 9 formulations.

5.4.2 EHDA Optimisation

Due to the varying physical liquid properties of the formulations used in this study, the flow rates and strength of electric field required to achieve various EHD jetting modes (dripping, unstable and stable) needs to be scrutinised to ensure the optimum process conditions are used during EHD processing. **Figure 5.1** shows the resulting jetting mode-maps that were generated. Due to the endless process parameter combinations, one parameter was kept constant for all 9 formulations from chapter 4. The working distance was kept at 12 cm. Maintaining this distance between the needle exit and collection plate ensured comparisons between the formulations would not be biased towards working distance.

The regions coloured lilac demonstrates the optimum window where any combination of applied voltage and flow rate will result in a stable cone forming at the needle exit. The dripping

mode (highlighted in peach) demonstrates at those specific combinations, the electrical field applied is not sufficient to overcome the surface tension of the liquid at that particular flow rate. The build up to achieving a stable jet often results in unstable jetting, as seen in **Figure 5.1** in blue. As a result of the positions of all three regions; flow rates and voltages utilised in this study were selected from the optimum working window. Selecting any other process parameters would result in polydisperse, non-uniform atomised structures which in turn could affect the release profile and kinetics of loaded therapeutic actives. **Figure 5.2** shows the formation of the stable cone jet at the nozzle exit upon processing each formulation.

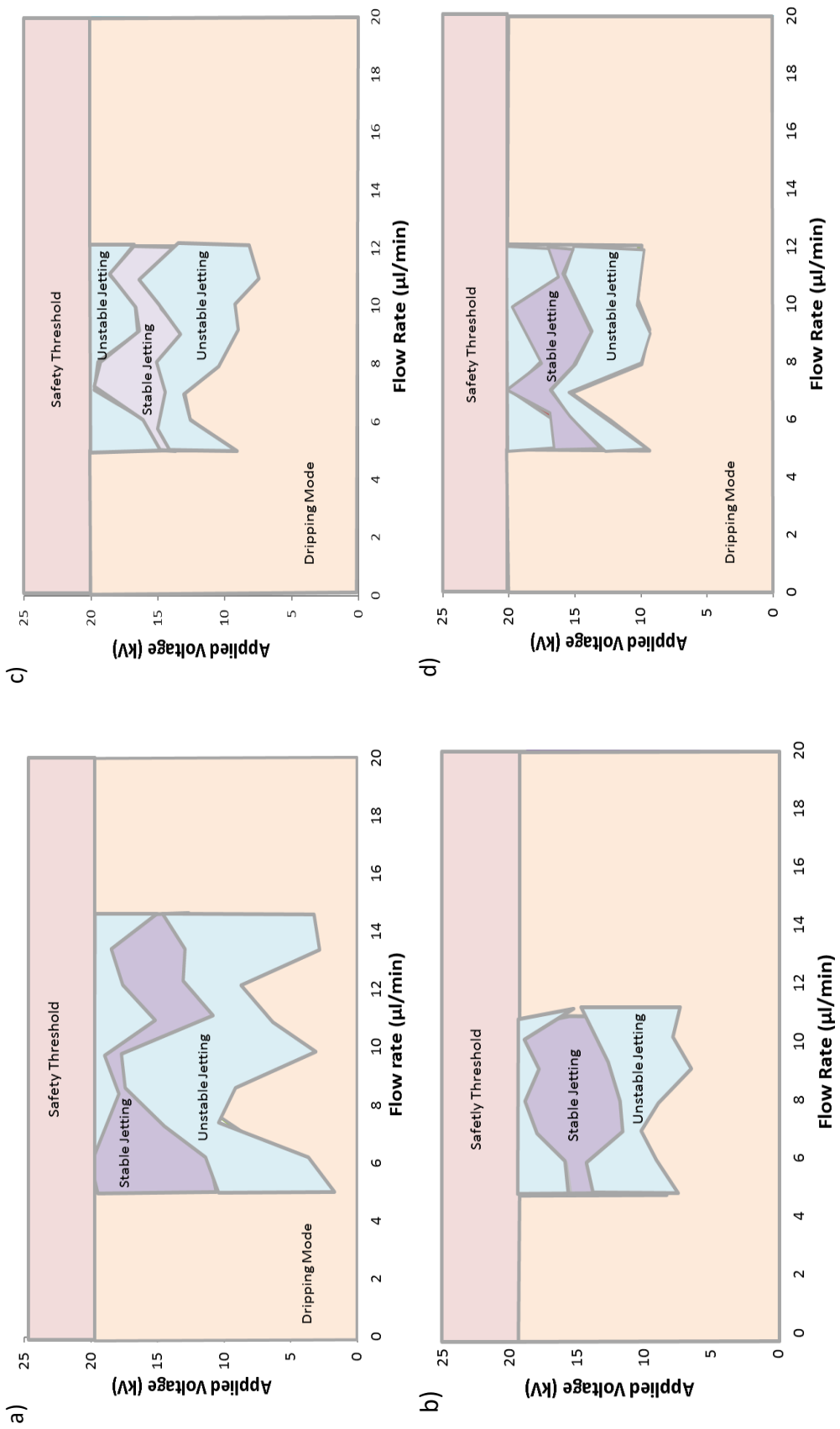

Figure 5.1 Jetting maps to determine the relationship between flow rate and applied voltage for formulations containing a) BAC, b) EDTA, c) borneol, and d) Brij® 78

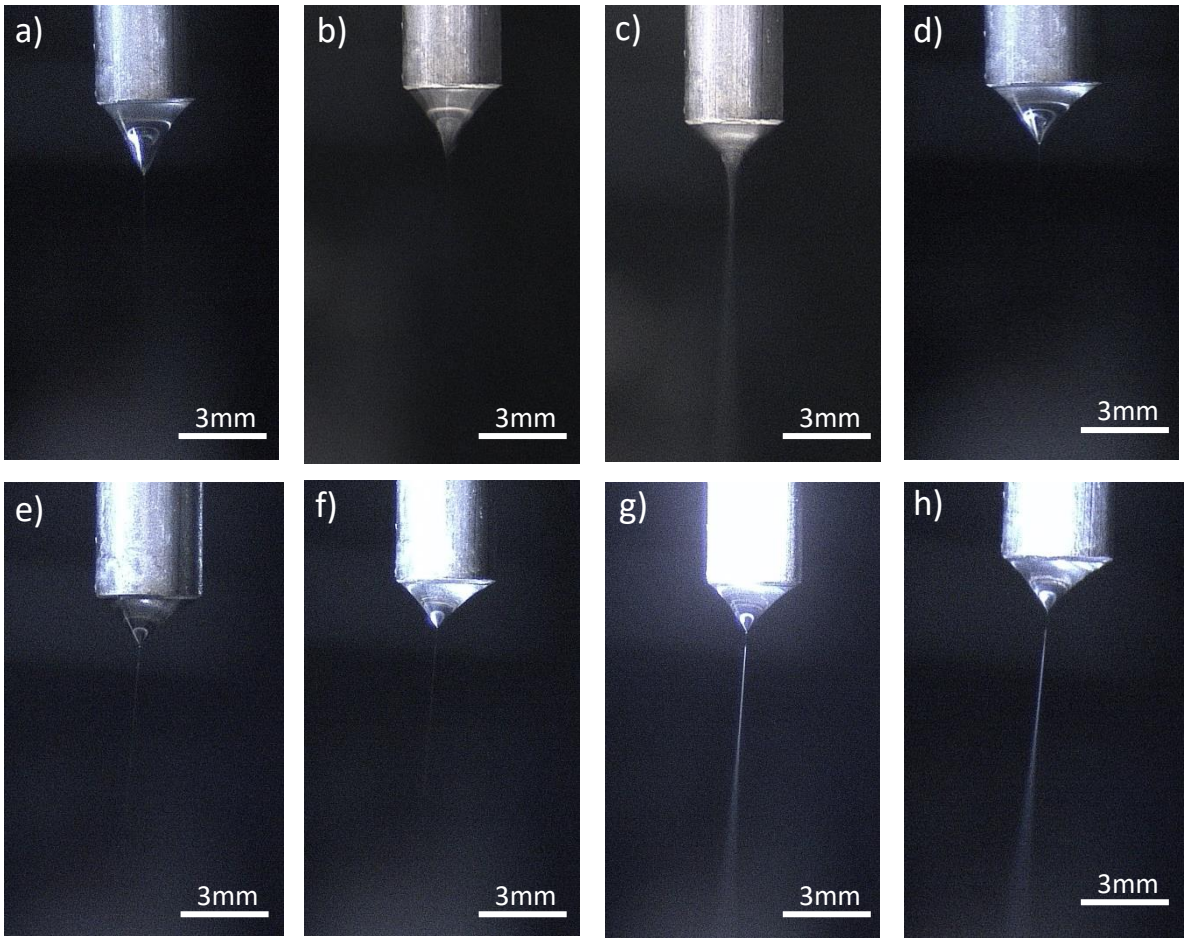

Figure 5.2 Stable Jet Formation when electrohydrodynamically processing each formulation at optimum process parameters. a) F1, b) F2, c) F3, d) F4, e) F5, f) F6, g) F7, h) F8

5.4.3 Coating Characterisation

5.4.3.1 Imaging and Size Distribution

Figure 5.3 shows the images derived from SEM analysis which were used to determine the morphology of the atomised structures that made up the contact lens coating. **Figure 5.4** shows the fiber size distribution for each formulation. Atomising the PE-free formulation seemed to yield beaded fibers similar to that found in chapter 4. The production of beaded fibers here could be as a result of insufficient synapse distance between the needle exit and the collection plate, hence there is insufficient space for the viscous formulation to "stretch" at the nozzle, causing inadequate solution evaporation to produce smooth fibers. The production of beaded fibers could also be due to the materials used. Electrohydrodynamic processing of low molecular weight PVP has previously reported to produce smooth, spherical particles (Mehta et al., 2015;

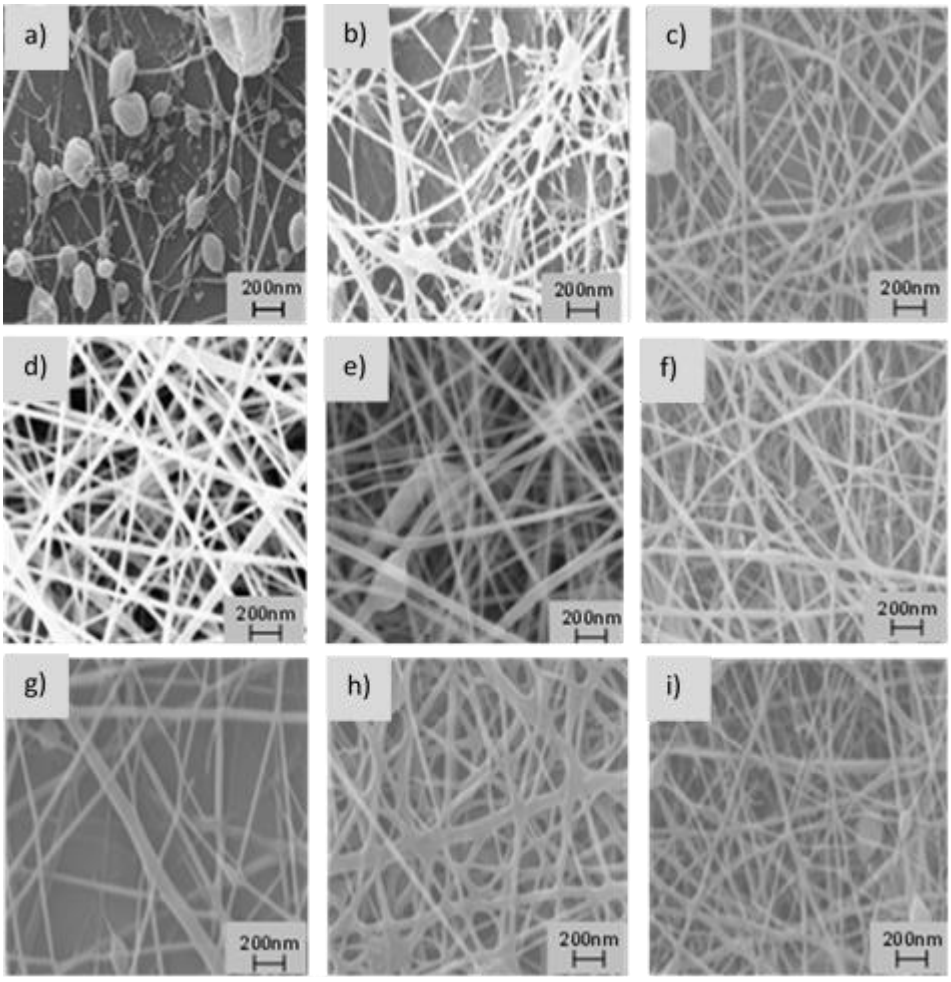

Figure 5.3 Scanning Electron Micrographs of atomised coatings at x50k magnification of a) Permeation free formulation, b) F1, c) F2, d) F3, e) F4, f) F5, g) F6, h) F7, i) F8

H. Khan et al., 2014). This could account for the "beads" of the resulting structures. The incorporation of PNIPAM increased the viscosity of the formulations; leading to the production of fibers upon atomization.

Electrically atomising F1 also produced visibly beaded fibers with some fibers as thin as 33 nm. BAC-containing fibers loaded with higher concentration of TM showed much smoother fibers than those with low drug concentration (5 %w/w with respect to the polymer). The increase in drug concentration distinctly had an effect on the morphology of the electrospun fibers, however, the average diameter increased to 90 nm as result of this increase in drug loading. F5 fibers demonstrated a positively skewed size distribution; with more than 65% of the NFs having a diameter less than 100 nm. Unlike PE-free NFs, F1 and F5, the incorporation of the remaining 3 PEs produced smooth fibers. SEM images revealed electrospun F2 fibers to have smooth surfaces with an average diameter of 55 nm with positively skewed data; almost half of NFs had a diameter between 1 and 50 nm. Electrospun F6 fibers demonstrated a non-uniform size distribution indicating high drug loading in the presence of EDTA does not achieve a narrow size distribution. F6 fibers had the largest average fiber diameter at 142±35 nm. This and the non-uniform size distribution could be attributed to the formation of a suspension when EDTA was incorporated into the formulation. As EDTA is insoluble in ethanol, a suspension was formed. As a result, EDTA would exist as its original particle size and therefore would not be completely homogenously dispersed throughout the matrix, even when electrohydrodynamically processed; hence possibly increasing the diameter of the resulting fibers.

Both F3 and F7 produced smooth-surfaced NFs with bell-shaped distribution; with drug loading not altering fiber diameter yielding fibers 74nm and 74nm respectively. These fibers are much thinner than those reported by Li et al when using just PVP as polymeric matrix. The borneol-PVP electrospun nanocomposites produced possessed smooth surfaces with an average fiber size of 610±120 nm (Li et al., 2012). Beaded NFs were produced when electrospinning F4 and F8, showing insufficient working distance as with F1 NFs. A negatively skewed distribution was observed with fibers engineered using F8 with 61% of fibers being above 100 nm in dimeter as opposed to 75% of F4 fibers being under 100 nm. This increase in diameter is associated with the incorporation of higher drug concentration encapsulated within the fibers.

PVP has been previously been electrospun to produce fibers with an average diameter of 305 nm (Huang et al., 2016); almost double that what has been fabricated here. Research involving the processing TM-loaded composite formulations for ocular delivery using EHDA is very scarce. However, TM has been electrospun into PVA and PCL fibers producing NF patches with fibers ranging between 200 nm and 400 nm (Gagandeep et al., 2014). PVP has been previously reported to produce contact lens coatings yielding both nanoparticles (50 nm-130 nm) and NFs (130-250 nm) (Mehta et al., 2015). The PE-loaded NFs produced here are reportedly much thinner than those previously stated in literature using single needle electrospinning (Huang et al., 2003; Braghirolli, Steffens and Pranke, 2014; Haider et al., 2015).

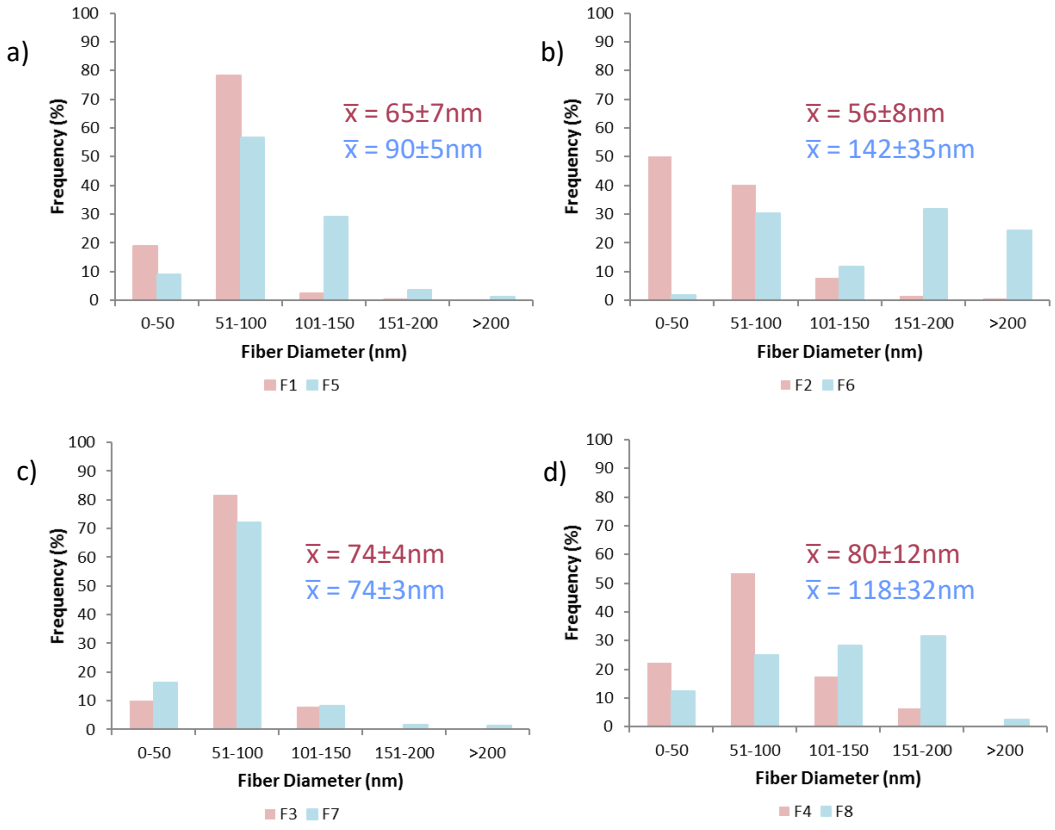

Figure 5.4 Fiber Diameter Distribution of formulations containing a) BAC, b) EDTA, c) borneol and d) Brij® 78. Pink is formulations containing 5% TM and blue is formulations containing 15% TM

5.4.3.2 Drug Encapsulation Efficiency and Coating Composition

Table 5.3 shows the theoretical compositions of the fibers produced. These calculations were based on the initial concentrations of materials and the TM encapsulation characteristics of the electrospun fibers are shown in **Table 5.3.** The highest encapsulation efficiency was found with F7 with almost all of the loaded TM (99.7%) being encapsulated within the matrix and the lowest with F4 (51.75%). For both drug loadings (5 %w/w and 15 %w/w), it seems the highest encapsulation was achieved with formulations containing borneol. The drug encapsulation efficiency was used to calculate how much of the weighted sample would be drug. Following this, the proportion of sample that is made up by polymer and permeation enhancer can be then interpreted as each concentration is known i.e. polymeric concentration is 5 %w/v.

Table 5.3 Fiber Composition and Drug Encapsulation Efficiency of each electrically atomised coating.

Formulation	**Theoretical Fiber Composition**			
	Polymer Composite (%w/w)	*Timolol Maleate (%w/w)*	*Permeation Enhancer (%w/w)*	*Drug Encapsulation Efficiency (%)*
F1	95.05	4.75	0.2	92.21
F2	86.96	4.35	8.69	60.92
F3	93.45	4.67	1.88	93.11
F4	80	4	16	51.75
F5	86.81	13.02	0.17	70.74
F6	80	12	8	57.01
F7	85.47	12.82	1.71	99.7
F8	74.1	11.1	14.8	82.45

5.4.3.3 Thermal Analysis

5.4.3.3.1 DSC Analysis

Figure 5.5 presents the DSC thermograms of all 8 formulations; including raw composite and pure drug. Due to electrospinning emerging as an imminent method of fiber production, it is important to demonstrate the process parameters do not affect the physical stability of the actives used as well as the resulting electrospun fibers. Pure TM is a crystalline drug with a defined T_m of 218 °C (**Figure 5.5**). The absence of this sharp endothermic peak in the thermograms of F1-F8 indicates the drug is no longer present in crystalline form but now in

amorphous form within the polymeric matrix. The T_m of each sample is expressed by a broad endothermic peak in each thermograms. Whilst the thermograms for electrospun fibers exhibited similar endothermic peaks to raw composite (131 °C), they all showed a lower melting point (114-125 °C), demonstrating the TM was evenly distributed throughout the fibers resulting in an increased dispersion of drug within the polymeric matrix. The presence of just a single, broad peak in each thermograms confirm the structure of the physical structures of raw polymer, drug and PE were not compromised during the EHD processing. This indicates the materials assembled into polymer-drug-PE complexes; acting as one "system" as opposed to individual excipients.

PVP and PNIPAM are predominantly amorphous polymers which experience a phase transition upon temperature changes at specific thresholds. During the transition, the polymer morphs from amorphous state to a partial rubber state-partial glassy state (Khan, Asmatulu and Eltabey, 2013; Pawar et al., 2015). The threshold at which this occurs is known as the Glass Transition Temperature (T_g). Whilst incorporation of solid materials (e.g. permeation enhancers) can significantly affect the T_g, our study shows there is insignificant effect of PE incorporation on T_g of the raw composite (depicted between approximately 55-65 °C) in the thermograms for raw composite and all 8 formulations. The lack of change in T_g may also be as a result of weak interactions (i.e. covalent bonds) between TM and the polymeric chains (W. S. Khan et al., 2013). The reported T_m of each PE used is as follows: BAC: 34-37 °C, EDTA: 237 °C, borneol: 208 °C, Brij® 78: 44-46 °C**.** In the case of no interaction between TM and polymer and PE, these T_m would be exposed as sharp endothermic peaks in the thermograms of each formulation at the respective temperatures. The absence of these peaks (and presence of solitary peaks) confirms the formation of drug-polymer-PE complexes to form stable systems in turn producing stable NFs.

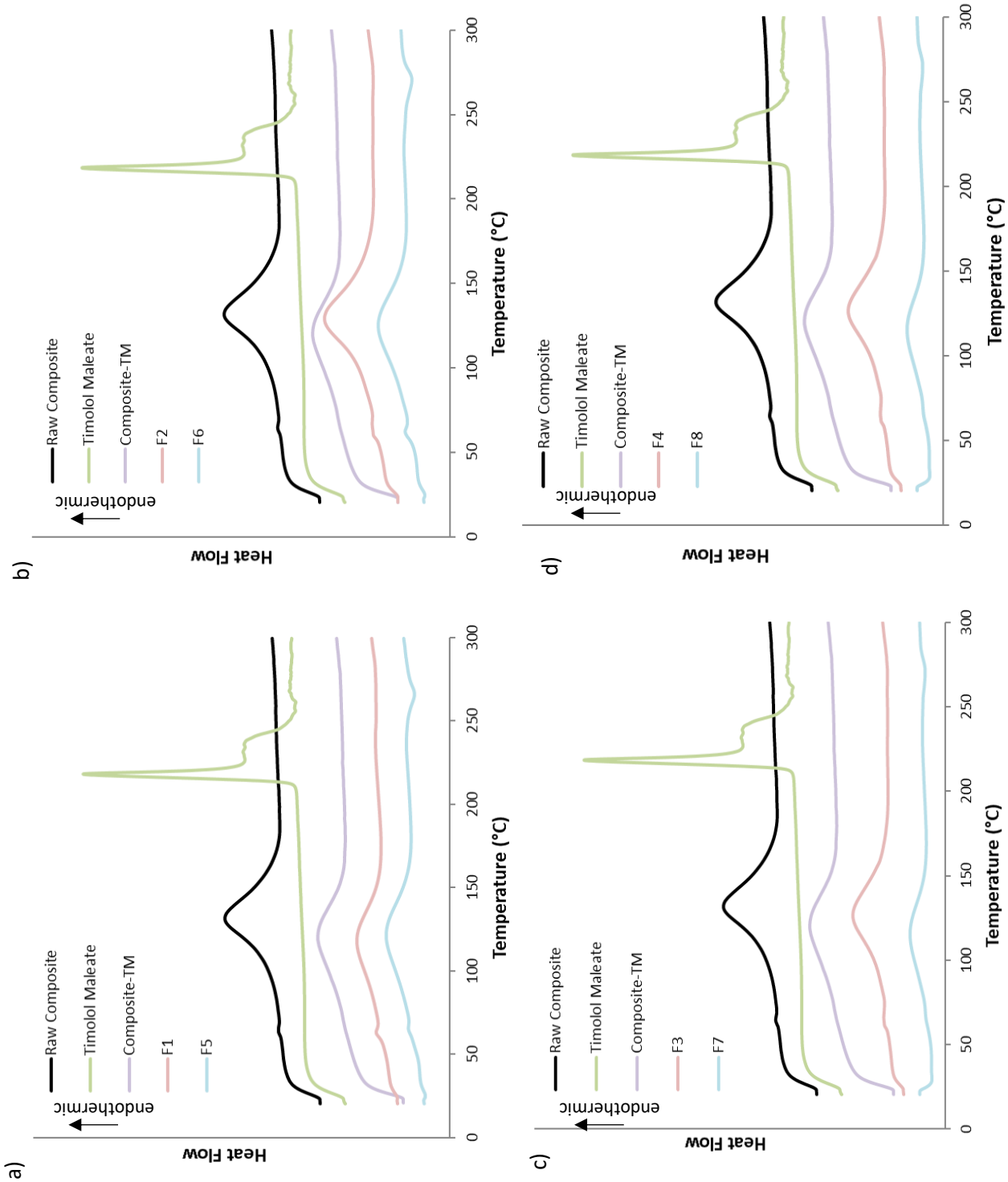

Figure 5.5 DSC Analysis of formulations containing a) BAC, b) EDTA, c) Borneol and d) Brij® 78

5.4.3.3.2 TGA Analysis

Figure 5.6 shows the TGA thermograms for pure TM, PE-free NFs and all 8 electrically atomised formulations. The thermogram for pure TM shows a single sharp endothermic weight loss event between 201 °C and 370 °C characteristic of drug degradation; also seen by Joshi et al (Joshi et al., 2009). Formulations F1-F8 exhibited a 2-step degradation profile; with initial weight loss (6-8%) due to moisture loss of surface-embedded water or even residual solvent within the polymeric matrix of the NFs. The second, more conspicuous decrease in weight loss is indicative of polymer degradation of PVP and PNIPAM. For all 8 formulations, the second weight loss event occurs between 300 °C and 540 °C (92-94%). The incorporation of PEs into the polymer-TM system causes this dominant weight loss to occur over a larger temperature range compared to PE-free fibers. Whilst this shift in degradation temperature may show encapsulation of drug and

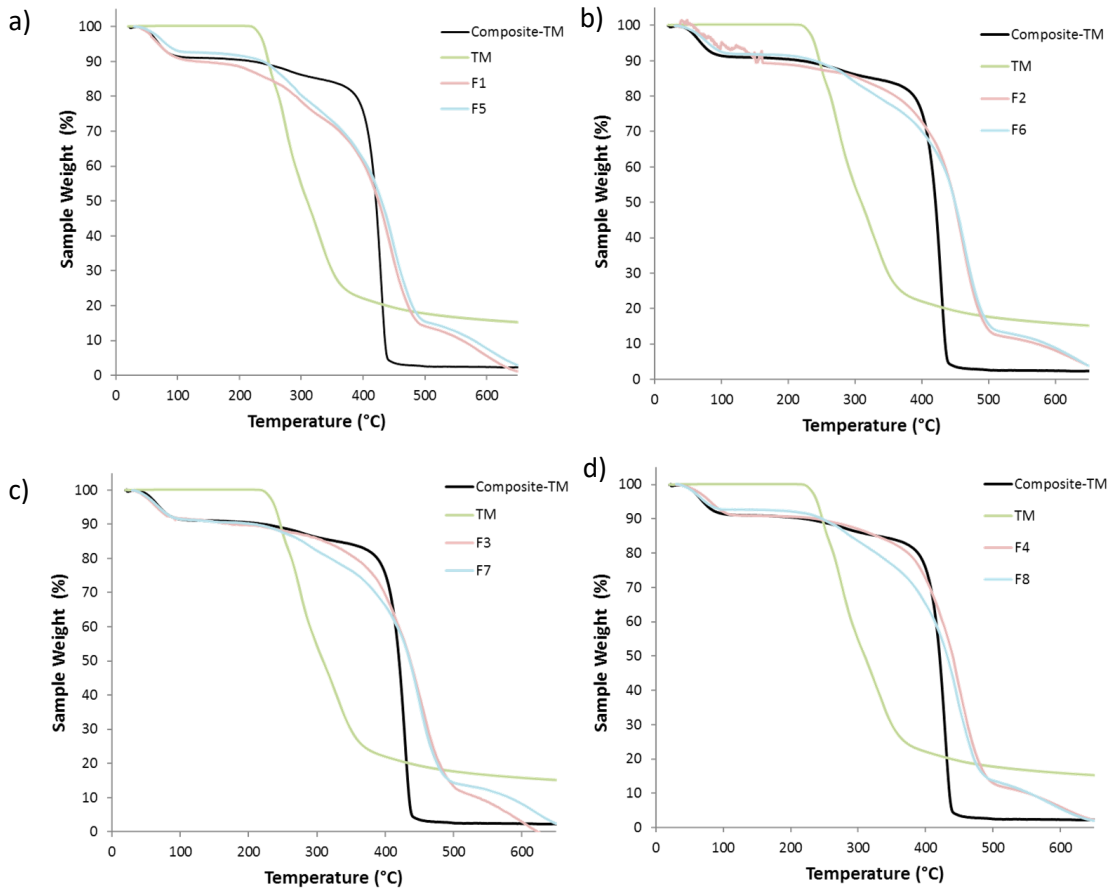

Figure 5.6 TGA analysis for formulations containing a) BAC, b) EDTA, c) Borneol and d) Brij® 78

PE (Nazari et al., 2017), it also implies formulations containing PEs are more stable and that polymer degradation was delayed by the incorporation of PE (Sundaray et al., 2008). One thing to note with these thermograms is there are no prominent physical or chemical changes at or over the narrow temperature of biological ocular temperature.

5.4.3.4 Goniometry

The wettability the electrospun coatings was characterised and analysed over time using CA analysis **(Figure 5.7).** CA is a critical measure as the interaction between the fibrous coatings and the lens material can determine detachment and release of coating and drug, respectively.

Upon application of water droplet, F2 demonstrated the highest static angle (79.91°) whilst F1 has the lowest (66.6°). This drastic difference in CA at 0 seconds compared to formulation without any permeation enhancers (CA=126.27°) shows the addition of PE (which all act as surfactants) lowered the surface tension of the formulations and in turn of the electrospun NFs (Stephansen et al., 2016). This consequently increases the wettability of the samples; indicating the samples have become more hydrophilic. This difference in CA could also be due to the change in morphology of the NFs of the formulations compared to the beaded-fibers of the formulation not containing PE. The presence of spherical structures with fibrous structures increases the amount of air entrapped between the solid and liquid droplet, in turn pinning the motion of the water droplet as it advances, causing an increase in CA. The combination of particles and fibers in Composite-TM samples (without PE) both increases surface area and surface roughness which can contribute to the increased time period required for the water droplet to completely disappear. Whilst the CA of electrospun NFs devoid of PE was still quantifiable for 1800 seconds (30 mins), the CA of all 8 formulations containing PEs were unmeasurable after 30 seconds as a result of complete spreading of water droplet within this time. The complete spreading of water within 20 seconds demonstrates the hydrophilicity of the fibrous coatings, highlighting an affinity to the hydrophilic soft contact lenses aiding the attachment of the electrospun coating to the lens.

One thing to note is the concentration of drug (5 %w/w or 15 %w/w with respect to the polymer) did not affect the initial CA or the CA profile. As seen in **Figure 5.7** those containing the same PE displayed almost identical CA profiles over time.

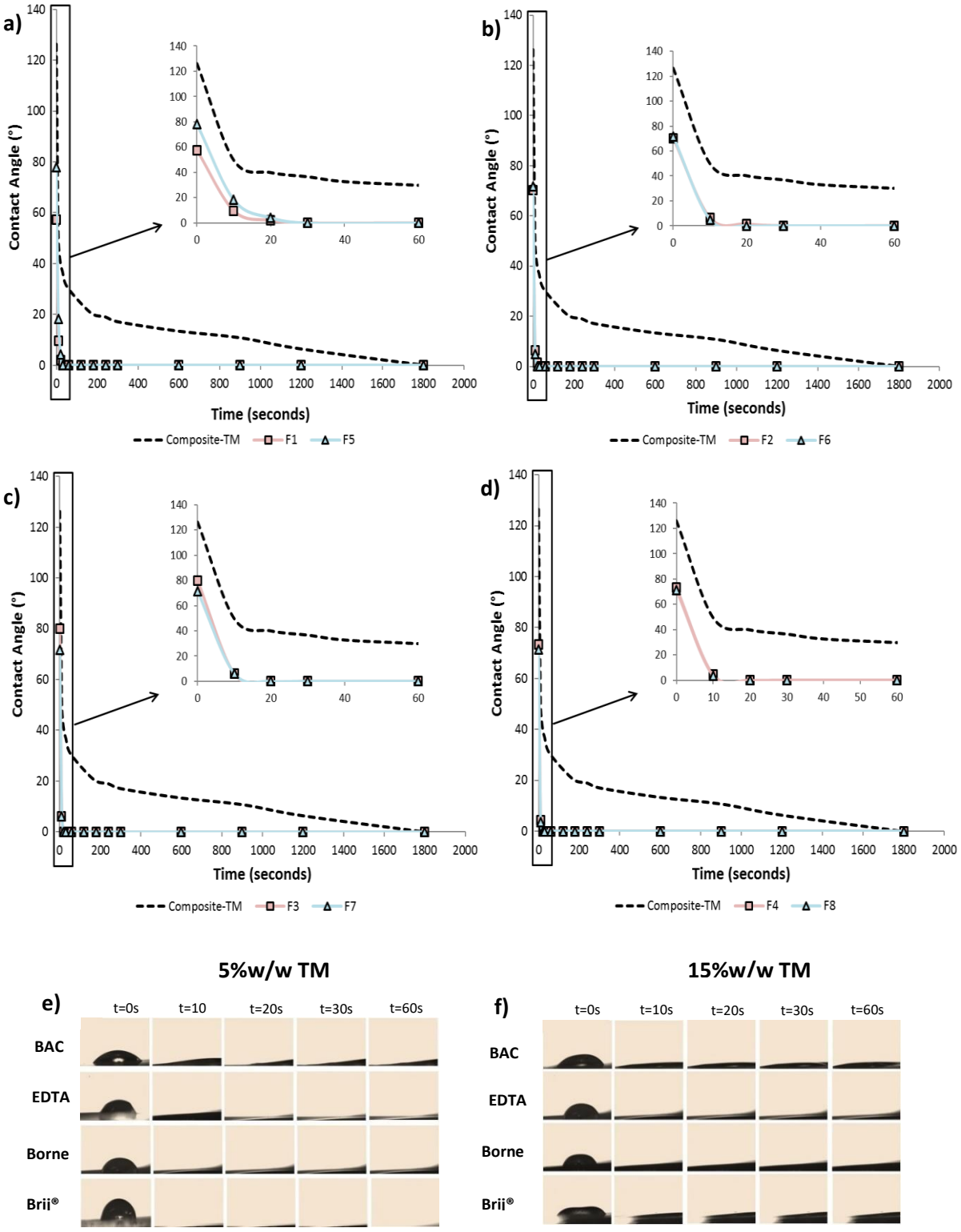

Figure 5.7 Contact angle analysis over time for formulations containing a) BAC b) EDTA c) Borneol d) Brij® 78 at two different drug loadings; 5 %w/w and 15%w/w. Digital Images of liquid droplet over time of formulations containing (e) 5%w/w TM and (f) 15%w/w

5.4.3.5 FTIR

Figure 5.8 shows the spectroscopic spectra derived from FTIR analysis of all 8 formulations and raw materials. FTIR was used here to show the stability of TM when processed in conjunction with polymer and PE. FTIR analysis is advantageous when trying to show compatibility between different excipients in a sample. Secondary interactions such as hydrogen bonding and Van der Waals (induced dipoles) often increase the stability of structures; interactions which can be detected by shifts in wavelength (cm^{-1}) in FTIR spectra.

Pure TM shows characteristic peaks at 2968 cm^{-1} (aliphatic C-H stretching), 3063 cm^{-1} (aromatic C-H stretching), 1718 cm^{-1} (C=O), 1229 cm^{-1} (O-H bending), 954 cm^{-1} (C-O stretching vibrations). These peaks are less prominent in the spectra for all 8 formulations; with some peaks shifting very slightly. These changes in the peaks confirms formation of hydrogen bonds with polymer and/or PE. Characteristic peak at 1651 cm^{-1} in all spectra for 8 formulations correspond C=O stretching vibrations in PVP. Multiple peaks at 2948 cm^{-1}, 2918 cm^{-1} and 2875 cm^{-1} are present due to CH-CH_2 stretch vibration. Evidence of C-H deformation of cyclic CH_2 groups can be seen at 1492 cm^{-1}, 1459 cm^{-1}, 1419 cm^{-1} and 1371 cm^{-1}. Amide III bond (C-N stretching vibration), amide V (CH_2 rocking vibrations) and amide IV bond are present at 1282 cm^{-1}, 732 cm^{-1} and 648 cm^{-1} respectively. Characteristic absorption peaks on the PNIPAM spectra included amide II bond at 1550 cm^{-1}, C=O stretching and CH_3 asymmetric stretching vibrations at 1650 cm^{-1} and 2970 cm^{-1}, respectively; all highlighted in **Figure 5.8**

In **Figure 5.8a**, a clear peak at 2927 cm^{-1} is present in the FTIR fingerprint of BAC (indicative of C-H_3 bending vibrations). However, this peak is less prominent in the spectra for F1 and F5; highlighting interaction between components within the sample. With samples containing EDTA, the distinctive peaks have shifted as a result of O-H groups being capable of forming hydrogen bonds with composite polymer and drug. A similar case is seen with F3 and F7 with the incorporation of borneol (**Figure 5.8c**). With respect to pure borneol, sharp peaks at 1054 cm^{-1}, 1456 cm^{-1} and 2950 cm^{-1} are observed; peaks which are absent in the fingerprint of F3 and F7. The presence of C=O bonds in PVP molecules and O-H group in borneol molecules enables them to act as proton receptor and proton donors, respectively, forming hydrogen bonds (Li et al., 2012). Brij® 78 is also able to form hydrogen bonds with the composite polymer and drug

with characteristic peaks at 2890 cm^{-1}, 1108 cm^{-1}, 1341 cm^{-1} and 1471 cm^{-1} (for pure Brij® 78) being omitted from the spectra for F4 and F8 (**Figure 5.8d).**

FTIR analysis was also carried out to observe any changes as a result of initial drug concentration. With all four PEs, the concentration of drug did not seem to have any effect on the FTIR fingerprints **(Figure 5.8a-d).**

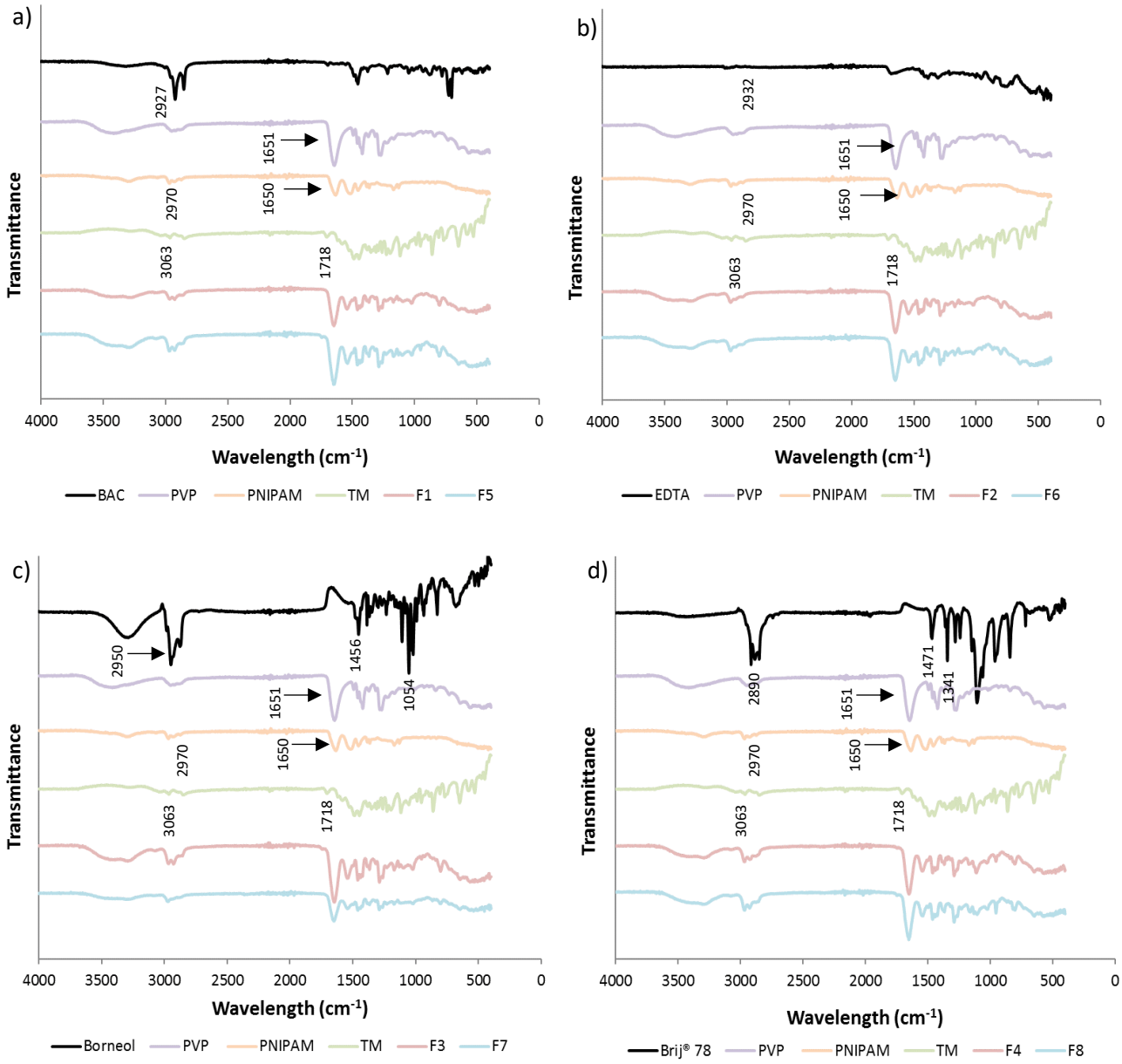

Figure 5.8 FTIR spectra for raw materials and electrospun fibers (a) NFs containing BAC, (b) NFs containing EDTA, (c) NFs containing Borneol, (d) NFs containing Brij® 78

5.4.3.6 *In Vitro* Release and Kinetics

5.4.3.6.1 In Vitro Drug Release

Understanding the release profile of TM from these electrospun coatings was crucial to see how the drug delivery device (i.e. the lens) would allow the fibrous coating to detach and allow for subsequent drug release. **Figure 5.9** shows the *in vitro* cumulative TM release from electrospun composite fibers. PE-free NFs presented a biphasic release profile; initial burst release (47% released within 10 minutes) followed by slow, sustained release; 68.24% after 24 hours. F1-F7 fibers exhibited triphasic release profile; initial burst release followed by gradual release and subsequent sustained release. The initial burst release is most likely to be due to the rapid release of surface-associated TM and PVP dissolution (Mehta et al., 2015). Subsequent gradual release is seemingly a result of breaking of PNIPAM polymer chains (dissolution of PNIPAM). The third phase of drug release (occurring at 300 mins) was caused by polymer erosion, releasing the drug in a more sustained fashion, with 20-32% of TM being released in the last 18 hours, depending on the PE used. The thermal transition of polymer from rubbery state to glassy state may account of this sustained release of TM. Some of the drug may be entrapped within the crystalline regions of the polymer and is therefore isolated from the release medium in the donor compartment. Only upon polymer degradation can the trapped drug be released resulting in gradual sustained release, forming the 3rd release phase (Natu, de Souza and Gil, 2011). The incorporation of PE may provide an extra barrier for drug molecule diffusion and these PE molecules may fill interfibrous voids, retarding drug diffusion through the matrix. This in turn slows the initial high burst release seen in the release from PE-free NFs. One exception to this was F8. As opposed to a triphasic release profile, F8 displayed a biphasic system with slow initial release with sustained release after 6 hours.

Whilst the addition of PEs slowed down the initial release and modified the release profile from biphasic to triphasic, the total amount of drug released after 24 hours increased for all 8 formulations **(Table 5.4).** For example, F7 NFs released 86.71% after 1440 minutes; 18.47% more than PE-free NFs. Due to this increase in TM release from the atomised coatings with *in vitro* testing, it can be hypothesised drug bioavailability may be enhanced, a theory which will be scrutinised with subsequent *ex vivo* testing.

Table 5.4 The percentage difference of timolol maleate release between permeation enhancer-free coatings and permeation enhancer loaded coatings

Formulation	*Percentage Difference (%)*
F1	16.38
F2	15.67
F3	13.23
F4	12.03
F5	16.58
F6	13.69
F7	18.47
F8	9.08

Whilst F1-F8 released similar percentage of TM after 24 hours, the release profiles for formulations containing different PE were contrastingly different; highlighting the fact that fiber composition has evidently influenced the release of TM. F1 and F5 released 72% and 75%, respectively, after 6 hours as opposed to F2 and F6, which only released 56% and 57% of loaded TM, respectively. This drastic difference (~20 %) in release could also be as a result of the morphology of BAC-loaded NFs. The beaded fibers can cause uneven distribution of drug molecules throughout the polymeric fibers; resulting in burst release from the beads upon dissolution hence releasing drug much faster than those with smooth fibers. NFs containing high TM concentration and borneol as PE released the most drug after 24 hours (86.72%±3.09%) whilst F8 NFs released the least amount after 24 hours (77.33%±8.1%). A noticeable difference is the slow initial release of F6 compared to burst release of other formulations. After 10 minutes, 4.9% of the loaded drug had been released from F6 NFs whilst F5 fibers had released 31.1% TM. This may be attributed to the fiber size: F6 NFs had an average size of 117 nm, with a majority of NFs being above 100 nm. As a result of this decreased surface area, dissolution rate of the NFs is slower than that of thinner fibers as with F5, hence, the drug is released much slower. There was a statistical significance ($p<0.05$) difference in the release of TM from polymeric matrix containing different PEs as demonstrated by one way ANOVA; p=0.0345 and p=0.0358 for 5 %w/w TM-loaded NFs and 15 %w/w TM-loaded NFs respectively.

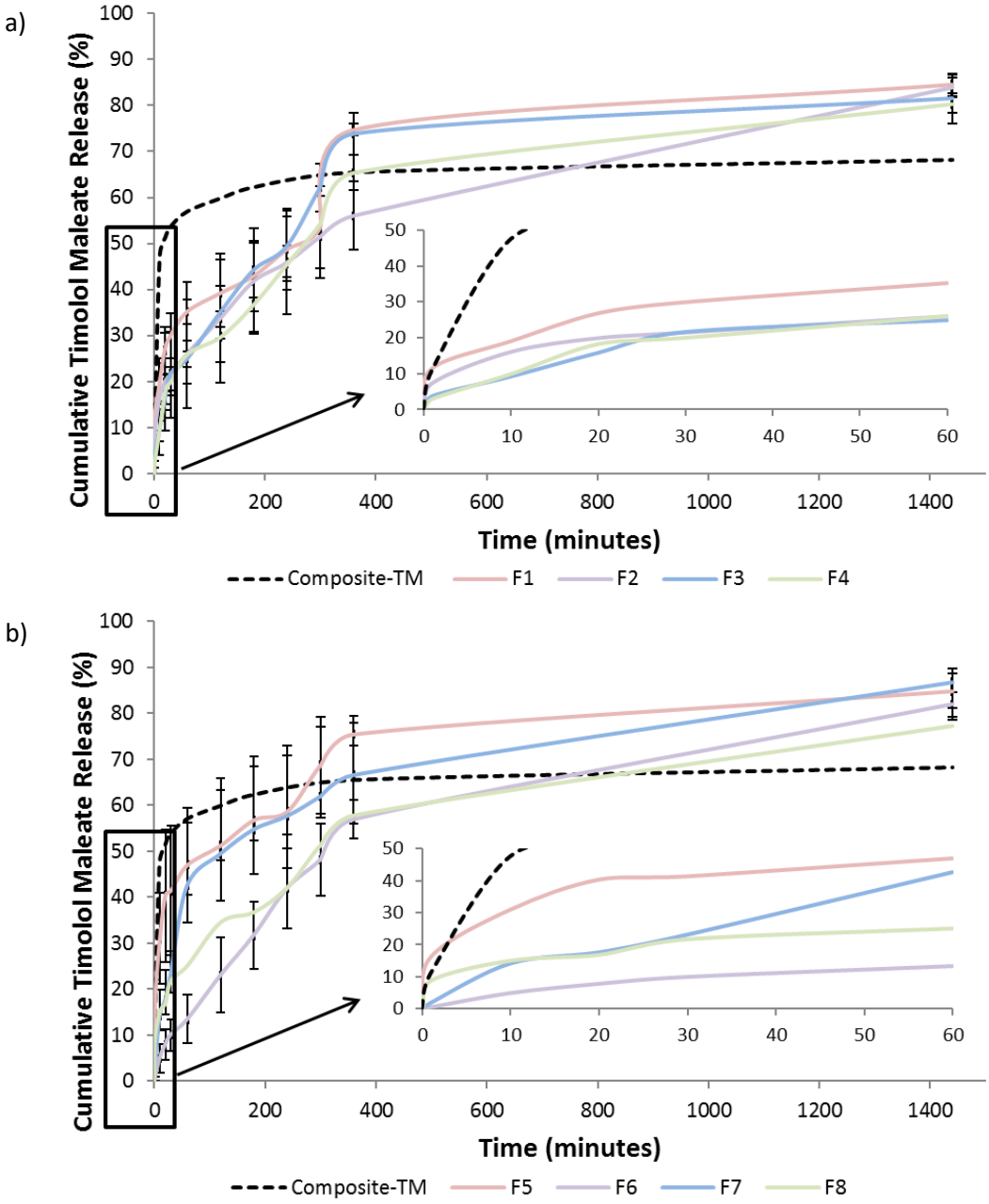

Figure 5.9 In Vitro cumulative timolol maleate release from electrospun fibers containing a) 5 %w/w timolol maleate and b) 15 %w/w timolol maleate

Figure 5.10 shows *in vitro* release between the 2 drug loadings; 5 %w/w and 15 %w/w. It is clear to see that the initial drug concentrations had no effect on the cumulative release of TM after 24 hours with ANOVA statistical analysis showing there was no significant difference between these results (p=0.08).

It was extremely challenging to compare these results to existing research as the materials and fiber compositions used here as well as the method and application have not yet been explored. However, Gangandeep et al developed electrospun PCL nanofibers and PVA nanofibers loaded with TM both of which were found to exhibit a 2 phase release profile, releasing 74% and 86% of timolol, respectively after 24 hours (Gagandeep et al., 2014). This is similar to what was found here with PVP and PNIPAM nanofibers.

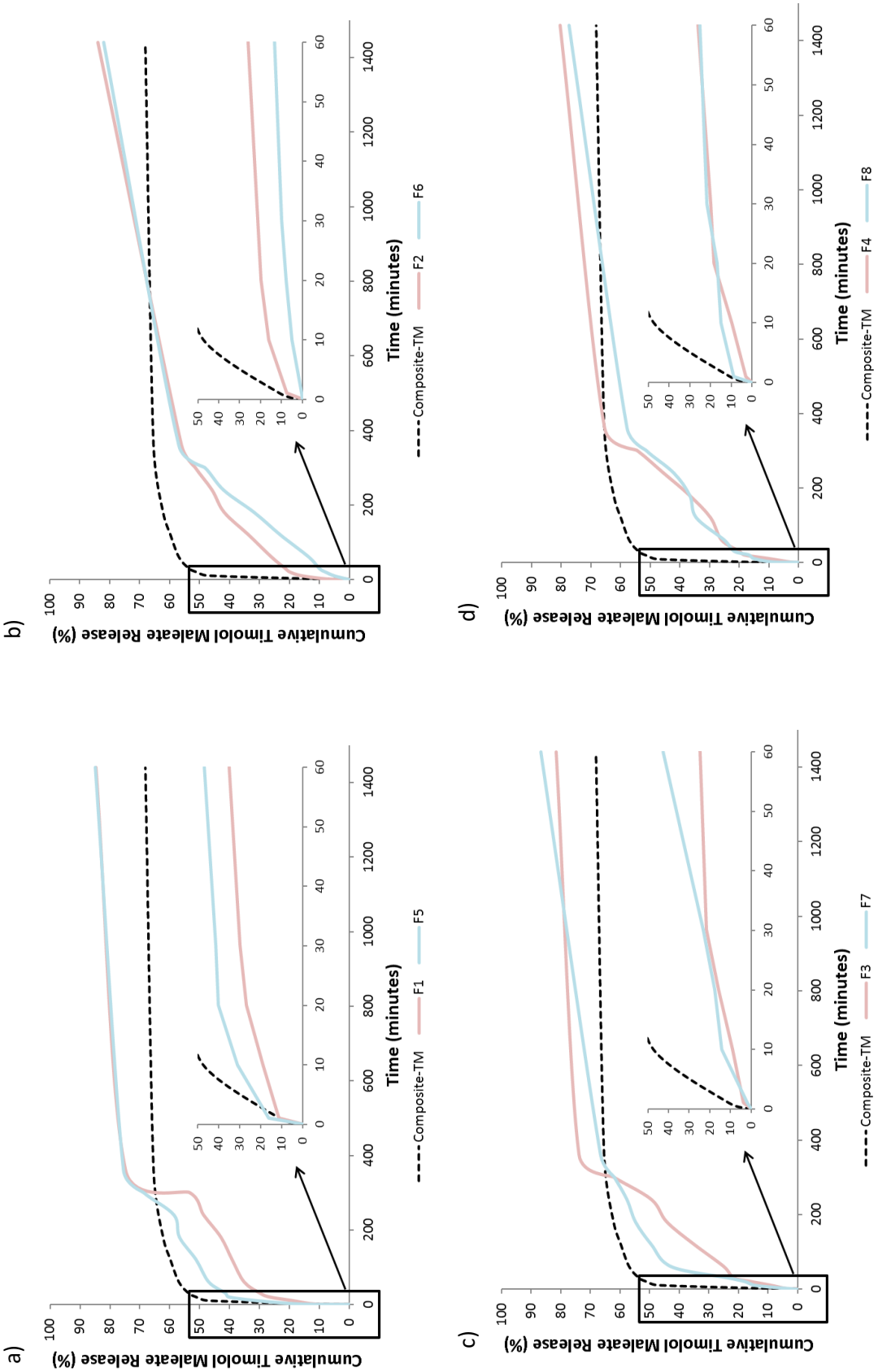

Figure 5.10 Comparing in Vitro cumulative timolol maleate release from electrospun fibers between two drug loadings. In Vitro drug release data with formulations containing a) BAC, b) EDTA, c) Borneol and d) Brij® 78

5.4.3.6.2 In Vitro Probe Release

Figure 5.11 exhibits the probe release data both from the electrospun coatings on contact lenses and into release medium (PBS, pH 7.4, 37 °C) in order to show the affinity of the coatings to the dehydrated contact lenses whilst mimicking drug release, respectively. Probe-encapsulated NFs were produced with the same composition as in **Table 5.1**, with rhodamine B replacing TM as the active. The release of dye was depicted as DI on the lens (using fluorescence microscopic images) and DI of PBS (UV-Spectroscopy; absorbance as a function of time).

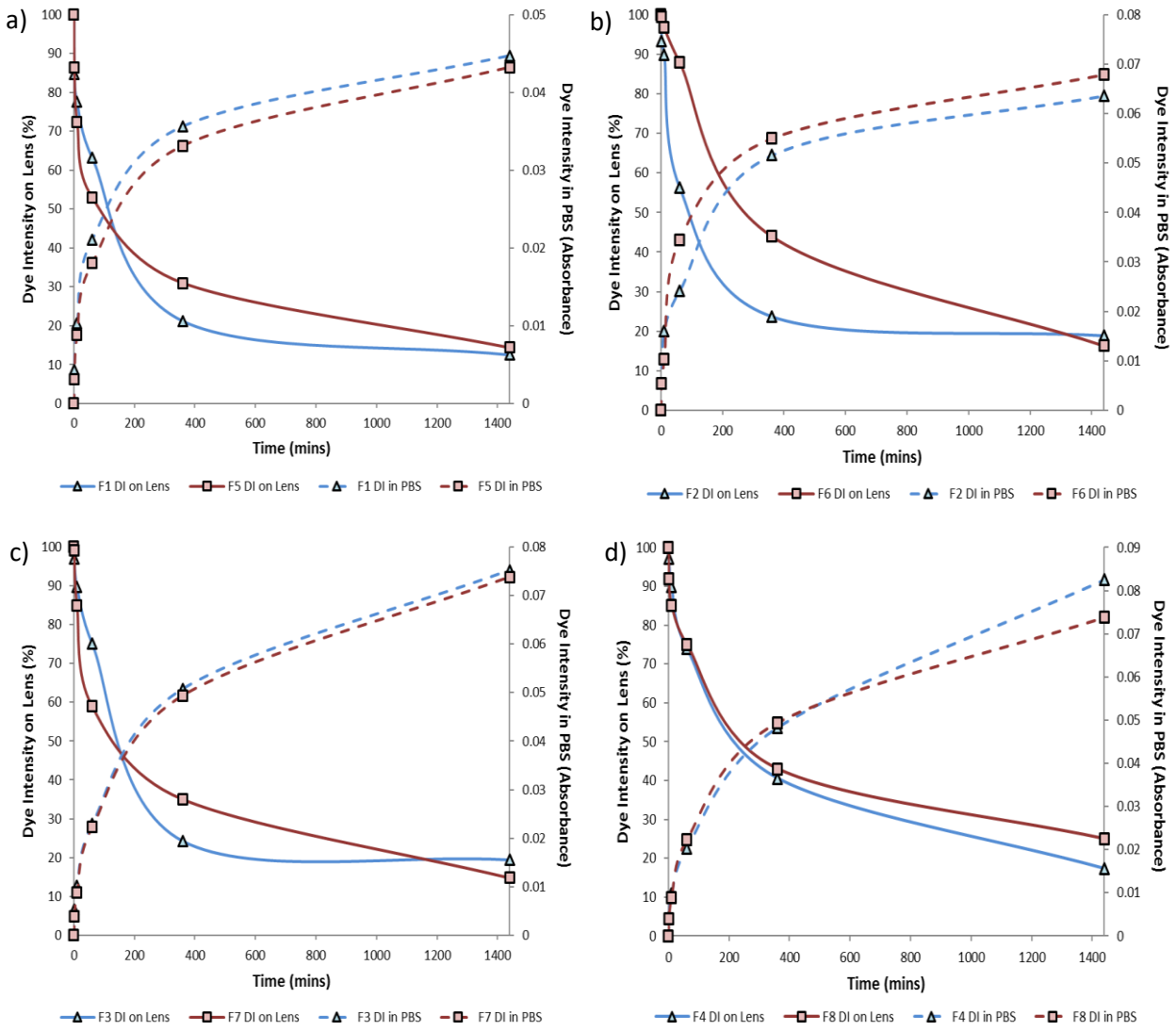

Figure 5.11 In vitro cumulative probe release from electrospun coatings containing a) BAC b) EDTA c) Borneol d) Brij® 78 at two different drug loadings; 5 %w/w and 15%w/w

The fact the two profiles (DI on lens and DI of PBS) mirror each other for all 8 formulations show the atomised coatings do not detach from the contact lens upon exposure to the release medium, ensuring sustained release of the therapeutic active (in this case model probe) over time.

5.4.3.6.3 Release Kinetics

The data from *in vitro* TM release was applied to various release kinetic models to ascertain the prominent release mechanism of TM from the electrospun fibers.

The data was fitted to zero-order (**Figure 5.12**), first-order (**Figure 5.13**), Higuchi (**Figure 5.14**) and Korsmeyer-Peppas (**Figure 5.15**) models; with the derived regression values and relevant component values being recorded in **Table 5.5.**

Table 5.5 Regression Coefficients and release components derived from four different kinetic models

Formulation	Zero Order	First Order	Higuchi	Korsmeyer-Peppas	
				R^2	n
F1	0.6257	0.8135	0.88	0.9858	0.329
F2	0.7352	0.6394	0.9614	0.9948	0.339
F3	0.5858	0.7428	0.8696	0.9896	0.502
F4	0.6727	0.7592	0.9207	0.9802	0.509
F5	0.4816	0.7301	0.8357	0.9739	0.2367
F6	0.7526	0.7274	0.9537	0.9318	0.4445
F7	0.5537	0.8308	0.9561	0.9550	0.5
F8	0.6962	0.8724	0.9457	0.9756	0.319

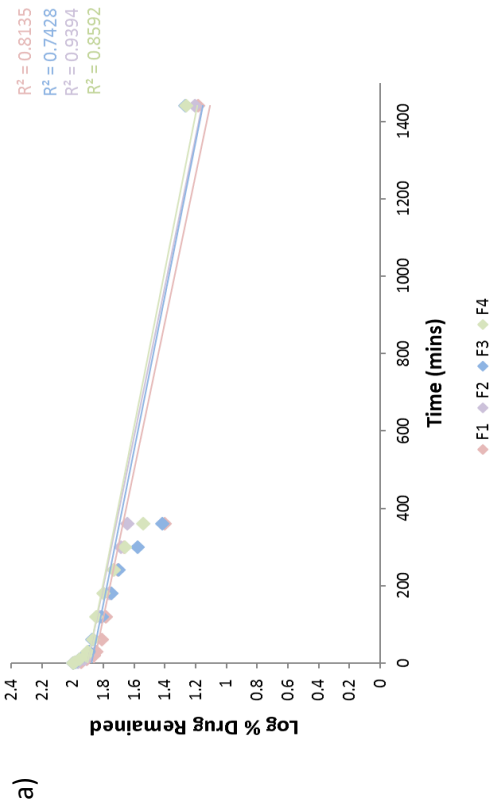

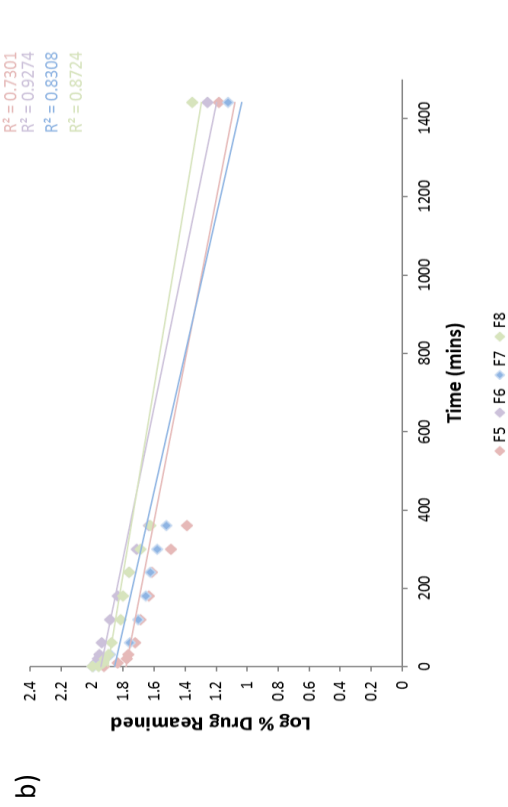

Figure 5.13 Timolol Maleate Release from electrospun polymeric fibers according to the First Order model for a) 5%w/w TM and b) 15%w/w TM

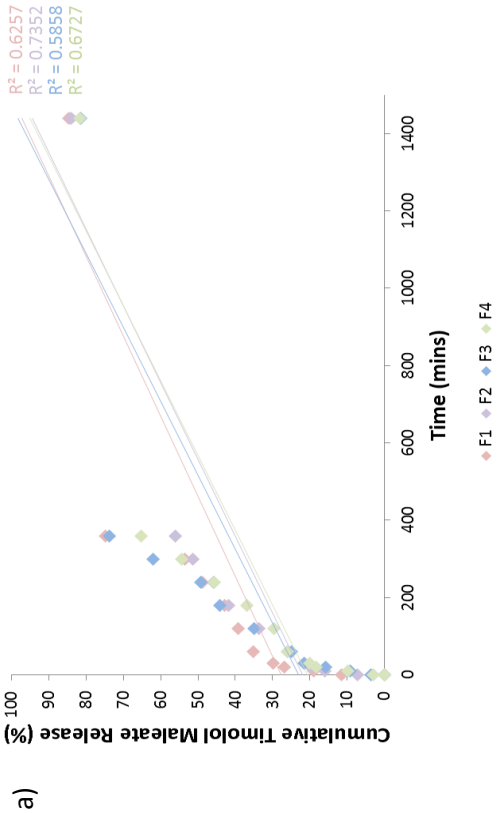

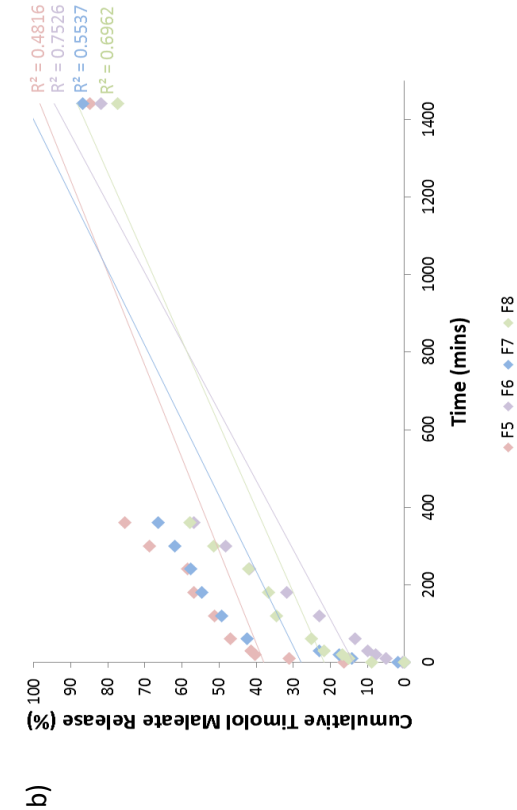

Figure 5.12 Timolol Maleate Release from electrospun polymeric fibers according to Zero Order model for a) 5%w/w TM and b) 15%w/w TM

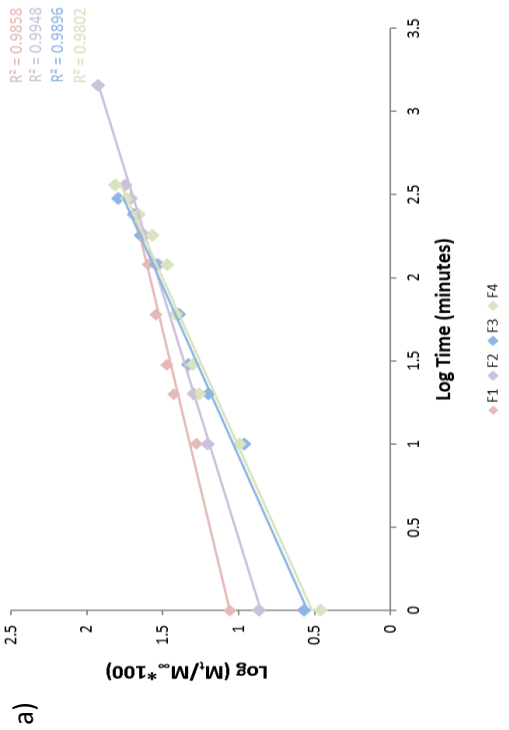

Figure 5.15 Timolol Maleate Release from electrospun polymeric fibers according to the Korsmeyer-Peppas model for a) 5%w/w TM and b) 15%w/w TM

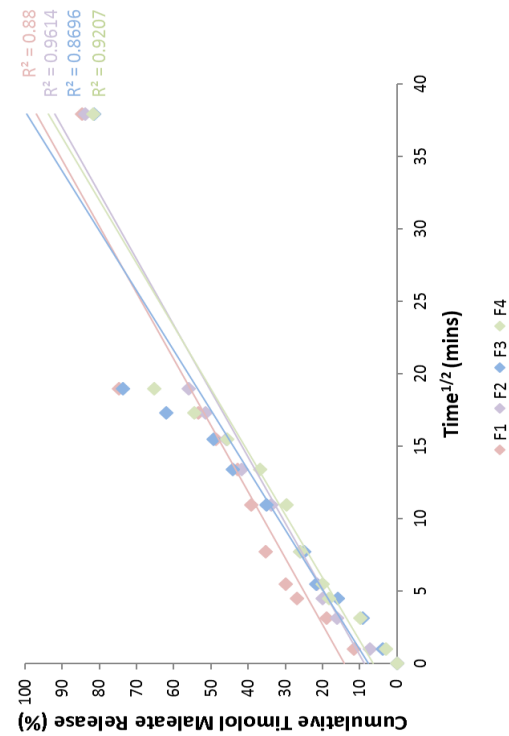

Figure 5.14 Timolol Maleate Release from electrospun polymeric fibers according to the Higuchi Zero Order model for a) 5%w/w TM and b) 15%w/w TM

The low R^2 values derived from zero-order and first order models indicated poor linearity and therefore a poor fit for this type of release kinetics. Relatively high (>0.9300) R^2 values for all 8 formulations from Higuchi model analysis suggests TM was released via quasi-Fickian diffusion; a mechanism which involves partial diffusion through swollen matrix whilst water fills pores in the matrix. This derivation was further confirmed by the results from applying release data (first 60%) to Korsmeyer-Peppas model. F1, F2, F5 and F8 showed characteristics for quasi-Fickian release with n values less than 0.45, whilst the remaining formulations released TM via Fickian diffusion.

Applying the *in vitro* release data to these 4 kinetic models signify the release of TM from these atomised coatings was primarily diffusion-based. However, the lack of linearity of the plots achieved indicates these models may not represent the release mechanisms accurately with respect to this drug delivery system developed here.

5.4.3.7 Biological Evaluation of Electrospun Fibrous Coatings

The main purpose of the cornea is to protect the eye and therefore it must remain impenetrable to any foreign bodies or materials that may compromise the structure and/or function of the cornea, (Abdelkader et al., 2015; Wilson, Ahearne and Hopkinson, 2015). Any damage that affects the corneal structure (and subsequently cornea permeability) can be detected with fluorescent dyes under a filtered fluorescent light source. Whilst in chapter 4 it was found the combination of PVP and PNIPAM with TM did not inflict any damage to the cornea, it is vital to repeat this study with these new formulated coatings as the PEs have been incorporated at their maximum safety concentration. Whilst the mode of action of these PEs involves interaction with tight junctions between corneal epithelial cells, the structure of the cells themselves should not be compromised. Hence it is crucial to eliminate the possibility of ocular intolerability with respect to this of these formulation-modified atomised coatings.

Figure 5.16 depicts the reaction of bovine corneal opacity to formulations F5-F8. **Figure 5.16a-c** demonstrates the effects of saline (negative control), acetone (mild positive control) and NaOH (positive control). Visual examination of the cornea treated with saline showed no damage (absence of cloudy region) whilst those treated with acetone showed a light, clouded region at the site of sample application **(Figures 5.16b and e).** As mentioned earlier in chapter 4, acetone

interacts with the lipids in the layers of the cornea; causing damage to the corneal epithelial cells. This in turn can aggravate the ocular mucosal membrane; irritating the eye. With respect to NaOH, severe opacification and strong fluorescence can be observed **(Figure 5.16c, 5.16f).** Upon application of NaOH to the cornea surface, saponification of the fatty acids present in corneal cell membranes is triggered. Subsequently, not only are intracellular tight junctions comprised, but the entire corneal epithelial layer is. As a result of this deterioration, the penetration of the dye through the cornea increases.

BAC has previously found to be harmful to various cultured cells and animal corneas when used at clinical concentrations (Okahara et al., 2013) with EDTA also showing ocular intolerability in a study characterising ketorolac tromethamine eye drops (Ahuja et al., 2008). With respect to Brij® 78, the ocular tolerability is a direct effect of the interaction between the hydrophobic regions of the non-ionic surfactant structure (the stearyl and ceyl chains) and the lipid bilayer of the cells (Kapoor, Howell and Chauhan, 2009). As a result of these incompatibilities, the loading of these PEs into ocular formulations needs to be assessed acutely to ensure there are no safety concerns.

Despite all the PEs being used at their maximum safety concentrations, the BCOP analysis in the present study revealed no damage to the cornea when exposed to formulations F5 to F8; as portrayed in **Figure 5.16g-n,** with lack of fluorescence of sodium fluorescein dye under cobalt blue light. The formulations with highest drug loading were tested here with the impression if these formulations indicated some biological interaction with the corneal issue, the lower drug loading formulations would be further tested. Due to no visual damage being detected and the lack of dye penetration indicates these TM-loaded-NFs are biocompatible formulations for contact lens coatings.

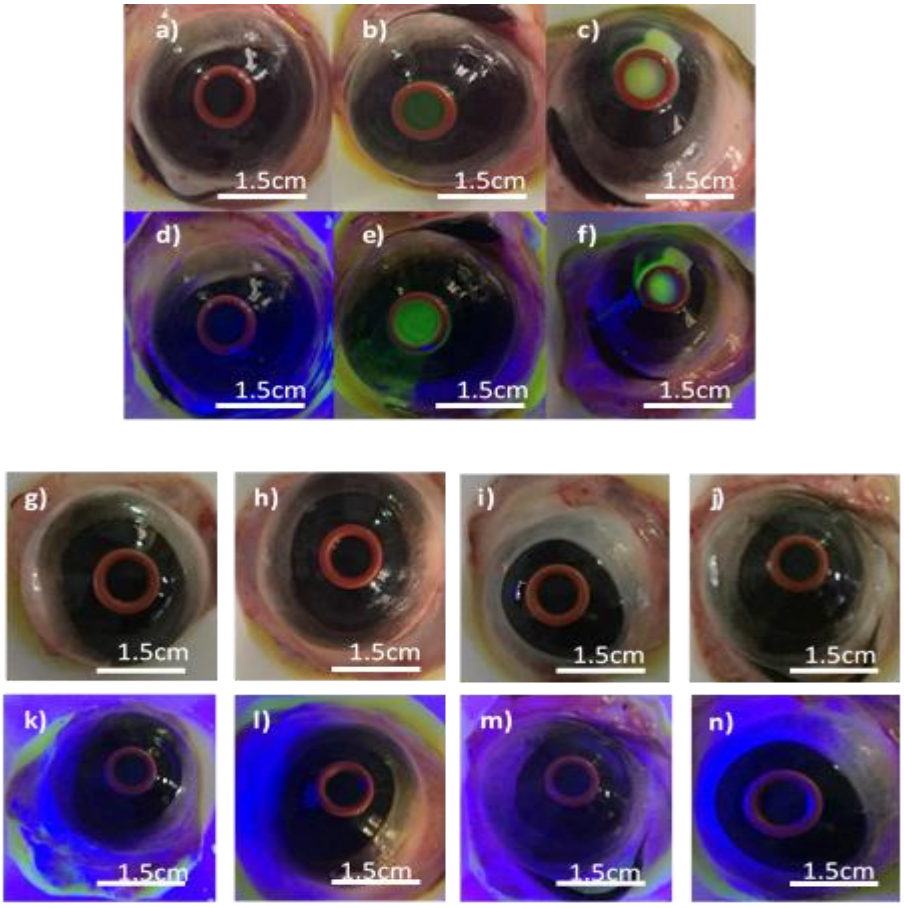

Figure 5.16 BCOP test digital images with corresponding fluorescence images of freshly excised bovine cornea treated with (a,d) Negative control, (b,e) Mild positive Control, (c,f) positive control (g,k) F5, (h,l) F6, (I,m) F7, (j,n) F8

5.4.3.8 Ex Vivo Permeability Testing

Figure 5.17 shows the permeation of TM through freshly excised bovine cornea following release from the electrospun PE-loaded coatings with **Table 5.6** summarising the parameters derived from these *ex vivo* studies. A lag time of 30 minutes was deciphered for all 8 formulations, highlighted in **Table 5.6.** This temporal measurement is quantified here as the time taken for the TM to diffuse/move through the electrospun polymeric matrix of the coating and through the cornea before being released into the release medium in the receptor compartment. This was a six fold decrease from the lag time calculated for PE-free coatings, highlighting the fact that the proposed reasoning for using PEs in this application was successful.

The lag time of TM permeation was reduced; giving a more controlled and faster drug permeation.

Table 5.6 Summary of parameters derived from ex-vivo studies

Formulation	Steady State Flux (µg/cm^2/min)	Apparent Permeability Coefficient (cm^2/min)	Lag Time (mins)
Composite-TM	0.057±0.017	0.012±0.0038	180
F1	0.07612±0.017	0.017±0.0039	30
F2	0.098±0.010	0.037±0.0038	30
F3	0.104±0.010	0.038±0.0087	30
F4	0.101±0.0058	0.049±0.0027	30
F5	0.057±0.0042	0.0084±0.0027	30
F6	0.074±0.0044	0.00613±0.00037	30
F7	0.098±0.0088	0.011±0.00095	30
F8	0.059±0.0099	0.0048±0.00081	30

The cumulative amount of TM permeated achieved with composite-TM was approximately 53.39±3.95 µg/cm^2 after 24 hours, the lowest of all 9 formulations. Regardless of specificity of PE, the incorporation of the additives increased the total amount of TM permeated through the cornea after 24 hours. Formulations containing EDTA (F2 and F6) showed to have the lowest amount of drug permeated per area after 24 hours. This could be attributed to these formulations existing as suspensions before EHD processing. EDTA is not soluble in ethanol and hence stayed particulate in F2 and F6. These EDTA particles may act as additional diffusional barriers; hindering the movement of TM through the polymeric matrix and the corneal membrane.

A study carried out by Burgalassi et al found that BAC, EDTA and Brij® 78 all found to enhance the permeation of timolol by 3.06, 1.63 and 1.16 fold, respectively, with BAC being the most active enhancer (Burgalassi et al., 2001). Similar results were found in the present study; with

formulations containing BAC achieving highest amount of TM permeated through the cornea per area (5 %w/w drug loading: 97.6 µg/cm^2 and 15 %w/w: 146.8 µg/cm^2.

The influence of borneol has been previously assessed on *in vitro* release and permeation of hydrophilic quinolone antibiotic ofloxacin. It was found the incorporation of the naturally occurring compound resulted in a 2.15 fold increase in the release of the antibiotic (Yang et al., 2009). Borneol has also found to enhance the permeability of the blood-ocular barrier to dye Evan's Blue (Yang et al., 2008); suggesting its use as a useful penetration enhancer in ophthalmic drug delivery. Its use in these electrically atomised coatings also mirror these results: the amount of TM permeating through the cornea is greatly increased compared to PE-free coatings.

A permeability coefficient higher than 20x10^{-6} cm^2/hr (as seen here with all 9 formulations) is indicative of high/good permeability. The evidence collated from *in vitro* probe release showing the atomised coatings does not detach from the lens shows there is increased contact time with the corneal surface in the pre-corneal region. This along with the hydrophilicity of timolol maleate and the excipients used (i.e. the permeation enhancers) aided the release and permeation of TM through the cornea at a much more sustained rate than without PE **(Figure 5.17).** These values are considerably lower than that of commercial eye drops (20.458 µg/cm^2/hr) (Shafie and Rady, 2012), showing these electrospun coatings on contact lenses delayed TM transport through the corneal membrane. This permits for less frequent dosing and hence reduces the risks of systemic absorption and ocular toxicity associated with high drug loading.

As expected, the amount of TM released and permeated from F5-F8 was a lot higher than their lower drug loading counterparts. This, however, contradicts the results found with *in vitro* drug release studies. The drug loading did not affect the cumulative percentage release of TM, however there is an evident difference with *ex vivo* permeation studies. This could be a direct result of the fact that the cellophane dialysis membrane may not be an adequate membrane to mimic biological membrane. It is because of this *in vitro* drug release, probe release and *ex vivo* studies are vital to conduct in conjunction to get a more accurate conclusion.

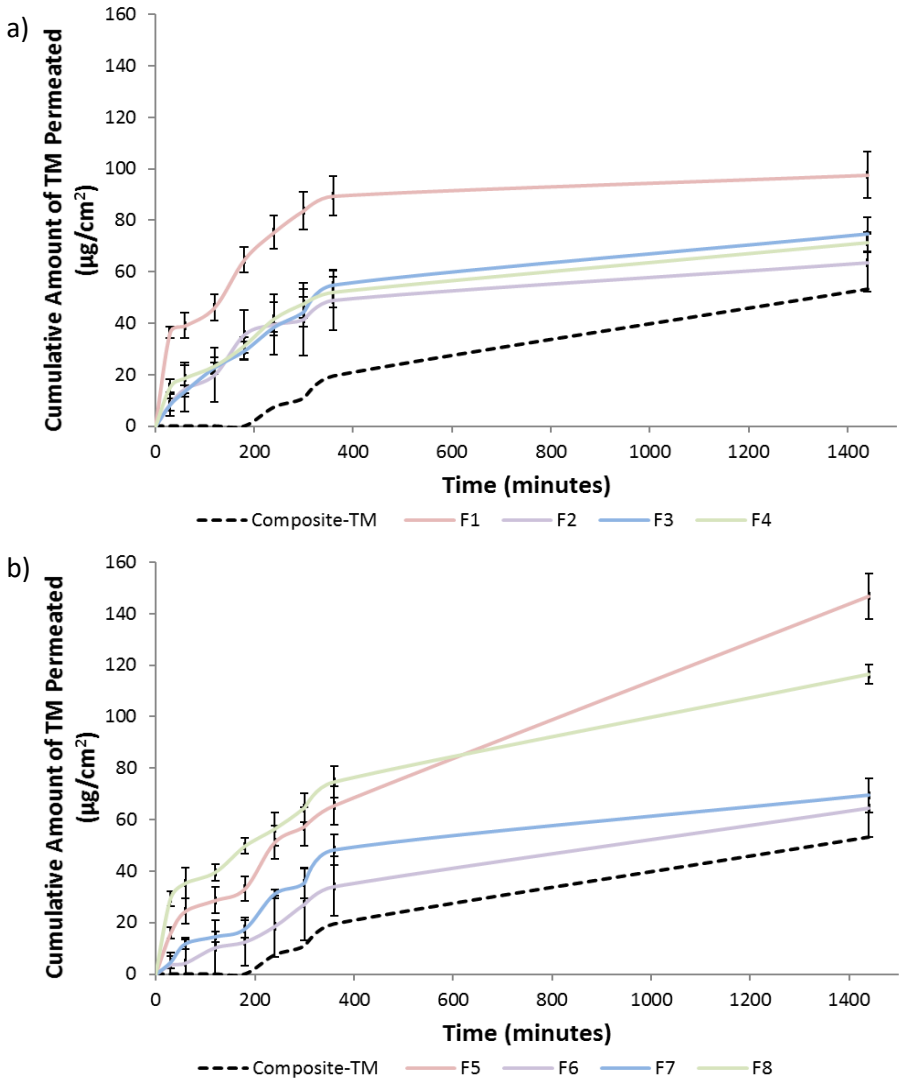

Figure 5.17 Ex Vivo cumulative amount of timolol maleate permeated across freshly excised bovine cornea for initial drug loading of a) 5%w/w and b) 15%w/w

5.5 Conclusion

This chapter was focussed on enhancing TM release from atomised contact lens coatings and TM permeation through the cornea. Morphological studies exhibited smooth nanofibers for the large majority with some formulations producing beaded-nanofibers. Thermal analysis confirmed the stability of nanofibers with DSC also showing the drug was molecularly distributed in an amorphous state throughout the polymeric matrix with all 8 formulations. There were significant differences (p<0.05) in the TM-release profiles depending on the permeation enhancer used, with borneol presenting the most promising data for sustained release (20% more drug was released compared to permeation-enhancer-free fibers). TM release was based on quasi-Fickian or Fickian diffusion as shown by application of Higuchi and Korsmeyer-Peppas models whilst biological evaluation (using freshly excised bovine cornea) confirmed the biocompatibility of the formulations. *Ex vivo* permeation studies showed some improvement in the amount of TM through the cornea with F1-F8, showing the potential of modifying the polymeric solution from a formulation view point.

As a result of these findings and thorough research in new developments with respect to PEs, F7 was taken forward to be further modified to achieve the ultimate aim of efficacious drug release and permeation from electrically atomised coatings for contact lenses. The high encapsulation efficiency of TM and stability of the engineered coatings using F7 is promising however *ex vivo* studies suggest further modification can fully optimise the formulation and achieve a safe and effective drug delivery device for the eye.

5.6 References

ABDELKADER, H., PIERSCIONEK, B., CAREW, M., WU, Z. and ALANY, R.G., 2015. Critical appraisal of alternative irritation models: three decades of testing ophthalmic pharmaceuticals. *British Medical Bulletin,* 113(1) pp. 1-13.

ABDELKADER, H., ALANI, A.W.G. and ALANY, R.G., 2014. Recent advances in non-ionic surfactant vesicles (niosomes): self-assembly, fabrication, characterization, drug delivery applications and limitations. *Drug delivery,* 21(2), pp. 87-100.

AHUJA, M., DHAKE, A.S., SHARMA, S.K. and MAJUMDAR, D.K., 2008. Topical ocular delivery of NSAIDs. *AAPS Journal,* 10(2), pp. 229-241.

BARRERO, A., GANAN-CALVO, A., DAVILA, J., PALACIOS, A. and GOMEZ-GONZALEZ, E., 1999. The role of the electrical conductivity and viscosity on the motions inside Taylor cones. *Journal of Electrostatics,* 47(1-2), pp. 13-26.

BOCK, N., DARGAVILLE, T.R. and WOODRUFF, M.A., 2012. Electrospraying of polymers with therapeutic molecules: State of the art. *Progress in Polymer Science,* 37(11), pp. 1510-1551.

BRAGHIROLLI, D.I., STEFFENS, D. and PRANKE, P., 2014. Electrospinning for regenerative medicine: a review of the main topics. *Drug Discovery Today,* 19(6), pp. 743-753

BURGALASSI, S., CHETONI, P., MONTI, D. and SAETTONE, M.F., 2001. Cytotoxicity of potential ocular permeation enhancers evaluated on rabbit and human corneal epithelial cell lines. *Toxicology Letters,* 112(1), pp.1-8.

DE LOS ANGELES RAMOS-CADENA, M. and SPAETH, G.L., 2016. Ocular surface disease and glaucoma. *Expert Review of Ophthalmology,* 11(3), pp. 215-226.

FUKUDA, M. and SASAKI, H., 2015. The Transcorneal Penetration of Commercial Ophthalmic Formulations Containing Timolol Maleate in Rabbit Eyes. *Journal of Ocular Pharmacology and Therapeutics,* 31(1), pp. 57-60.

GAGANDEEP, GARG, T., MALIK, B., RATH, G. and GOYAL, A.K., 2014. Development and characterization of nano-fiber patch for the treatment of glaucoma. *European Journal of Pharmaceutical Sciences,* 53, pp. 10-16

GUPTA, S., SAMANTA, M.K. and RAICHUR, A.M., 2010. Dual-Drug Delivery System Based on In Situ Gel-Forming Nanosuspension of Forskolin to Enhance Antiglaucoma Efficacy. *Aaps Pharmscitech,* 11(1), pp. 322-335.

HAIDER, A., HAIDER, S. and KANG, I., 2015. A comprehensive review summarizing the effect of electrospinning parameters and potential applications of nanofibers in biomedical and biotechnology. *Arabian Journal of Chemistry.*

HUANG, S., ZHOU, L., LI, M., WU, Q., KOJIMA, Y. and ZHOU, D., 2016. Preparation and Properties of Electrospun Poly (Vinyl Pyrrolidone)/Cellulose Nanocrystal/Silver Nanoparticle Composite Fibers. *Materials,* 9(7), pp. 523.

HUANG, Z., ZHANG, Y., KOTAKI, M. and RAMAKRISHNA, S., 2003. A review on polymer nanofibers by electrospinning and their applications in nanocomposites. *Composite Science and Technology,* 63(15), pp. 2223-2253

JOSHI, G.V., KEVADIYA, B.D., PATEL, H.A., BAJAJ, H.C. and JASRA, R.V., 2009. Montmorillonite as a drug delivery system: Intercalation and in vitro release of timolol maleate. *International Journal of Pharmaceutics,* 374(1-2), pp. 53-57.

KAPOOR, Y., HOWELL, B.A. and CHAUHAN, A., 2009. Liposome Assay for Evaluating Ocular Toxicity of Surfactants. *Investigative Ophthalmology & Visual Science,* 50(6), pp. 2727-2735.

KAUR, I.P. and SMITHA, R., 2002. Penetration Enhancers and Ocular Bioadhesives: Two New Avenues for Ophthalmic Drug Delivery. *Drug Development and Industrial Pharmacy,* 28(4), pp. 353-369.

KHAN, H., MEHTA, P., MSALLAM, H., ARMITAGE, D. and AHMAD, Z., 2014. Smart Microneedle coatings for controlled delivery and biomedical analysis. *Journal of Drug Targeting,* 22, pp. 790-795.

KHAN, W.S., ASMATULU, R. and ELTABEY, M.M., 2013. Electrical and Thermal Characterization of Electrospun PVP Nanocomposite Fibers. *Journal of Nanomaterials*, pp. 160931.

KIM, N.J., HARRIS, A., ELGHOUCHE, A., GAMA, W. and SIEKY, B., 2016. Ocular Permeation Enhancers. In: Y. PATHAK, V. SUTARIYA and A.A. HIRANI, eds, *Nano-Biomaterials For Ophthalmic Drug Delivery.* 1st edn. Cham: Springer, pp. 177-209.

KONG, B. and MI, S., 2016a. Electrospun Scaffolds for Corneal Tissue Engineering: A Review. *Materials,* 9(8), pp. 614.

LI, X., WANG, X., YU, D.G., YE, S., KUANG, Q., YI, Q. and YAO, X., 2012. Electrospun Borneol-PVP Nanocomposite. *J. Nanomaterias,* 2012, pp. 1-8.

MALHOTRA, M. and MAJUMDAR, D.K., 2001. Permeation through cornea. *Indian Journal of Experimental Biology,* 39, pp. 11-24.

MEHTA, P., JUSTO, L., WALSH, S., ARSHAD, M.S., WILSON, C.G., O'SULLIVAN, C.K., MOGHIMI, S.M., VIZIRIANAKIS, I.S., AVGOUSTAKIS, K., FATOUROS, D.G. and AHMAD, Z., 2015. New platforms for multi-functional ocular lenses: engineering double-sided functionalized nano-coatings. *Journal of Drug Targeting,* 23(4), pp. 305-310.

MONTENEGRO, L., BUCOLO, C. and PUGLISI, G., 2003. Enhancer effects on in vitro corneal permeation of timolol and acyclovir. *Pharmazie,* 58(7), pp. 497-501.

MORRISON, P.W.J. and KHUTORYANSKIY, V.V., 2014. Enhancement in corneal permeability of riboflavin using calcium sequestering compounds. *International Journal of Pharmaceutics,* 472(1-2), pp. 56-64.

MUN, E.A., MORRISON, P.W.J., WILLIAMS, A.C. and KHUTORYANSKIY, V.V., 2014. On the Barrier Properties of the Cornea: A Microscopy Study of the Penetration of Fluorescently Labelled Nanoparticles, Polymers, and Sodium Fluorescein. *Molecular Pharmaceutics,* 11(10), pp. 3556-3564.

NAZARI, K., KONTOGIANNIDOU, E., AHMAD, R.H., GRATSANI, A., RASEKH, M., ARSHAD, M.S., SUNAR, B.S., ARMITAGE, D., BOUROPOULOS, N., CHANG, M., LI, X., FATOUROS, D.G. and AHMAD, Z., 2017. Development and characterisation of cellulose based electrospun mats for buccal delivery of non-steroidal anti-inflammatory drug (NSAID). *European Journal of Pharmaceutical Sciences,* 102, pp. 147-155.

OKAHARA, A., TANIOKA, H., TAKADA, K. and KAWAZU, K., 2013. Ocular Toxicity of Benzalkonium Chloride Homo logs Compared with Their Mixtures. *Journal of Toxicologic Pathology,* 26(4), pp. 343-349.

PAWAR, M.D., RATHNA, G.V.N., AGRAWAL, S. and KUCHEKAR, B.S., 2015. Bioactive thermoresponsive polyblend nanofiber formulations for wound healing. *Materials Science & Engineering C-Materials for Biological Applications,* 48, pp. 126-137.

REDDY, J.S. and AHMED, M.G., 2013. Sustained Ocular Delivery of Sparfloxacin from pH Triggered *In Situ* Gelling System. *Journal of Pharmaceutical Sciences,* 40(3), pp. 16-25.

SAETTONE, M., CHETONI, P., CERBAI, R., MAZZANTI, G. and BRAGHIROLI, L., 1996. Evaluation of ocular permeation enhancers: In vitro effects on corneal transport of four beta-blockers, and in vitro in vivo toxic activity. *International Journal of Pharmaceutics,* 142(1), pp. 103-113.

SAHOO, R.K., BISWAS, N. and GUHA, A., 2014. Nonionic Surfactant Vesicles in Ocular Delivery : Innovative Approaches and Perspectives. *Biomedical Research International,* 2014, pp. 263-304.

SHAFIE, M.A.A. and RADY, M,A,H, 2012. In vitro and In vivo Evaluation of Timolol Maleate Ocular Inserts Using Different Polymers. *Journal of Clinical & Experimental Ophthalmology,* 3, pp. 1-9.

STEPHANSEN, K., GARCIA-DIAZ, M., JESSEN, F., CHRONAKIS, I.S. and NIELSEN, H.M., 2016. Interactions between Surfactants in Solution and Electrospun Protein Fibers: Effects on Release Behavior and Fiber Properties. *Molecular Pharmaceutics,* 13(3), pp. 748-755.

SUNDARAY, B., BABU, V.J., SUBRAMANIAN, V. and NATARAJAN, T.S., 2008. Preparation and Characterization of Electrospun Fibers of Poly(methyl methacrylate) - Single Walled Carbon Nanotube Nanocomposites. *Journal of Engineered Fibers and Fabrics,* 3(4), pp. 39-45.

SURESH, C. and ABHISHEK, S., 2016. pH Sensitive in Situ Ocular Gel : A Review. *Journal of Pharmaceutical Science and Bioscientific Research,* 6(5), pp. 684-694.

TASKAR, P., TATKE, A. and MAJUMDAR, S., 2017. Advances in the use of prodrugs for drug delivery to the eye. *Expert Opinion on Drug Delivery,* 14(1), pp. 49-63.

TU, E.Y., 2014. Balancing antimicrobial efficacy and toxicity of currently available topical ophthalmic preservatives. *Saudi Journal of Ophthalmology,* 28(3), pp. 182-187

WILSON, S.L., AHEARNE, M. and HOPKINSON, A., 2015. An overview of current techniques for ocular toxicity testing. *Toxicology,* 2(327), pp.32-46

WU CHUN-JIE, HUANG QIN-WAN, QI HONG-YI, PING, G. and HOU SHI-XIANG, 2006. Promoting effect of borneol on the permeability of puerarin eye drops and timolol maleate eye drops through the cornea in vitro. *Pharmazie,* 61(9), pp. 783-788.

YANG, H.B., LI, Z.J., YU, N.N. and CUI, H., 2008. Effect of borneol in improving permeability of blood-ocular barrier. *International Journal of Ophthalmology,* 8(8), pp. 15761578.

YANG, H., XUN, Y., LI, Z., HANG, T., ZHANG, X. and CUI, H., 2009. Influence of Borneol on In Vitro Corneal Permeability and on In Vivo and In Vitro Corneal Toxicity. *Journal of International Medical Research,* 37(3), pp. 791-802.

Chapter 6 Observing the effect of chitosan on *in vitro* timolol maleate release

6.1 Introduction

Whilst most of the formulations in Chapter 5 could be further modified to achieve efficacious local release of TM, F7 was selected as the formulation with the most potential for the EHD processing of contact lens coatings. F7 achieved over 99% encapsulation efficiency and released over 85% of the encapsulated TM via Fickian Diffusion during *in vitro* studies, the most out of all 8 formulations studied. However, with *ex vivo* studies, F7 only attained a cumulative release of 69 µg/cm^2 after 24 hours. Hence, F7 was taken forward to be further optimised to match the total amount of drug that is usually achieved with commercial eye drops for treatment of glaucoma.

6.2 Background

Commercial TM eye drops (e.g. Timoptol®) are typically administered twice a day, one drop in each affected eye (MHRA., 2015). This frequent dosing is needed due to an array of biological and physiological reasons. Firstly, the introduction of the eye drop to the eye instigates tear production, consequently leading to drug dilution. This production of tears also increases the volume of fluid in the precorneal region. Excess fluid (combination of eye drops and tears) will overflow and leak out of the eye. Some of this excess liquid may also drain into the nasolacrimal duct and then be taken away into the systemic blood flow (Agrahari et al., 2016; Djebli et al., 2017; Forrester et al., 2015). As a result of these obstacles, drug BA is greatly reduced and hence frequent administration is required.

The anatomical barrier of the eye (predominantly the cornea) also poses challenges with respect to obtaining sufficient drug BA in ODD. The varying degrees of hydrophilicity of the cornea (made up of 5 layers) can hinder the movement of drug molecules through this tissue, reducing the total dose permeating through the cornea, and consequently reaching the targeted tissue (Djebli

et al., 2017; Forrester et al., 2015; Kearns and Williams, 2009). As mentioned before, there have been various attempts to overcome this through the use of PEs as seen in chapter 5.

More recently, because of material development and the exponential increase in research in this remit, certain polymers have found to possess permeation enhancing capabilities. Chitosan is a primary example of these "modern PEs" (Kumar, Vimal and Kumar, 2016). This cationic polysaccharide has gained particular interest in pharmaceutics due to its mucoadhesiveness and non-toxicity (Mahaling and Katti, 2016; Muxika et al., 2017). Consequently, chitosan does not disrupt or compromise the corneal epithelium. It is thought the cationic nature of chitosan interacts with the cell membranes, disrupting tight junction proteins and enhancing paracellular drug transport (Kumar et al., 2016).

Chitosan has previously been utilised as a PE for an array of biological membranes including buccal tissue (Duttagupta, Jadhav and Kadam, 2015; Kontogiannidou et al., 2017), intestinal tissue (Chougule et al., 2014; Maher, Mrsny and Brayden, 2016; Ates, Kaynak and Sahin, 2016), and the nasal cavity (Krauland, Guggi and Bernkop-Schnurch, 2006; Benediktsdottir, Baldursson and Masson, 2014; Giuliani et al., 2018). Chitosan has also been scrutinised in ocular drug delivery and has been found to act as a penetration enhancer, with drugs such as ofloxacin (Di Colo et al., 2004), triamcinolone acetonide (Raval, Khunt and Misra, 2018) and timolol maleate (Rodriguez et al., 2017). Most studies demonstrated enhanced *ex vivo* permeation of drug upon incorporation of chitosan or chitosan derivatives.

Based on these findings, examining the potential chitosan may have to further improve the release and permeation of TM across the cornea when incorporated into electrically atomised coatings for contact lenses seemed the natural progression for this research. EHDA was still used as the method of coating engineering, with PVP and PNIPAM being used as the base composite polymeric matrix.

6.3 Materials and Methods

6.3.1 Materials

PVP ($4.4x10^4$ g/mol) was obtained from Ashland, Worcestershire, UK. PNIPAM ($2\text{-}4x10^4$ g/mol), low molecular weight chitosan ($5.0x10^4 – 1.9x10^5$ g/mol), ethanol, TM (>98%), acetone, sodium hydroxide, rhodamine B, and borneol were all purchased from Sigma Aldrich (Dorset, UK). PureVision® Balafilcon A silicone hydrogel contact lenses were supplied by Bausch and Lomb (New York, USA). All reagents used were of analytical grade.

6.3.2 Methods

6.3.2.1 Formulation Preparation

A 5 %w/v polymeric solution was prepared by dissolving 2.5 %w/v PVP and 2.5 %w/v PNIPAM in ethanol. This mixture was the base solution used to prepare a series of formulations (each 20 ml) containing various concentrations of chitosan. **Table 6.1** shows the composition of formulations. Each formulation also contained 15 %w/w TM (with respect to the 5 %w/v polymer concentration). All solid excipients were weighed using an analytical balance and were mixed using a magnetic stirrer for 30 minutes to ensure homogeneity. One thing to note here is chitosan is insoluble in ethanol, and therefore homogenous suspensions were formed.

6.3.2.2 Formulation Characterisation

Each formulation was characterised based on three physical liquid properties; viscosity, surface tension and electro-conductivity. The measurements were carried out as stated in **Section 3.2.1**, in triplicate, with an average reading taken.

6.3.2.3 EHDA Set-Up and Optimisation

The system set-up was similar to that specified in **Section 4.3.2.4.** Briefly, polymeric formulations were drawn into 5 mL syringes which were attached to a syringe infusion pump. This pump enabled the flow of the formulation to be controlled throughout the atomization process. The liquid was infused through silicone tubing to a single stainless steel conductive coaxial needle device (where only the outer needle was used) at various flow rates. This set-up

was connected to a high power voltage supply. All atomization processes were carried out in ambient conditions (23 °C).

As with the formulations in chapter 5, jetting mode maps need to be created to ensure the most optimum process parameters are being used for the newly formulated suspensions. Each formulation was processed at flow rates in increasing increments of 1 µl/min from 0 µl/min up to 20 µl/min. At each flow rate, the voltage that was required to produce various spraying modes (stable, unstable, dripping) were logged; providing data to generate jetting mode maps.

Table 6.1 Formulation composition of each formulation. Each formulation contained 2.5 %w/v PVP, 2.5 %w/v PNIPAM and 15 %w/w TM

Formulation	Borneol Concentration (%w/v)	Chitosan Concentration (%w/v)
Composite-TM	0	0
F0	0.1	0
F1	0.1	1
F2	0.1	2
F3	0.1	5
F4	0	1
F5	0	2
F6	0	5

6.3.2.4 Coating Engineering

As mentioned previously in chapter 4 and 5, microscope slides were used as a preliminary collection device for initial pilot characterisation studies. Hereafter, *in vitro* and *ex vivo* characterisation were conducted on coated commercial contact lenses. To ensure the contact lens shape was maintained, the lenses were dried in a desiccator on a novel lens holder for 30 minutes. The lenses were weighed before and after the coating process to ascertain the weight of the coating sample. Controlled deposition was again achieved using a modified lens holder and a mask arm; producing peripherally coated lenses.

6.3.2.5 Characterisation of TM-Loaded Coatings

6.3.2.5.1 Imaging

Morphological and structure size analysis was carried out as stated in **Section 4.3.2.7.1**. Coatings on both microscope slides and dehydrated contacted lenses were analysed using SEM at magnification of x5k and x50k.

6.3.2.5.2 Drug Encapsulation Efficiency and Coating Composition

To determine TM encapsulation efficiency; weighed coating samples were dissolved in ethanol for 1 week. UV spectroscopy (λ=295 nm) was used to determine the amount of drug loaded into the weighed sample. **Equation 4.1** was used to calculate encapsulation efficiency.

6.3.2.5.3 Thermal Behaviour

The stability and thermal behaviour (i.e. melting point) were assessed using TGA and DSC, respectively. Both studies were carried out as stated in **Section 4.3.2.7.3** (DSC) and **4.3.2.7.4** (TGA). Both raw materials and atomised coatings were analysed under the flow of nitrogen gas at a heating rate of 10 °C/min.

6.3.2.5.4 Goniometry

Contact angle hysteresis was determined using contacts lenses with the atomised coatings, as specified in **section 4.3.2.7.5**. 10 µl of distilled water was introduced to the samples and each sample was measured in sessile mode at pre-determined time points. Readings were taken in triplicate and an average was derived.

6.3.2.5.5 FTIR

Any potential interactions between the raw excipients during and following electrohydrodynamic processing was assessed using FTIR. Both raw materials and atomised coatings were analysed over the range 400-4000 cm^{-1} using FTIR Platinum-ATR fitted with Bruker Alpha Opus 27 FT-IT at an average of 10 scans at a resolution of 4 cm^{-1}.

6.3.2.5.6 In vitro Release and Kinetics

Drug release and probe release was evaluated as stated in **Section 4.3.2.7.7.** Briefly, weighed coated contact lenses were introduced to the donor compartment; which had been specially designed to maximise surface contact between the lens and the synthetic dialysis membrane (which separated the donor compartment and the receptor compartment). Upon fixing the lenses in the holder, the entire device was submerged into the "receptor compartment"; a vial containing 10 ml PBS at pH 7.4. At predetermined time points, 1 ml of release medium was retracted and replaced with fresh 1 ml PBS. Probe release from the coatings into the release medium was as described in **Section 4.3.2.7.7.2**. Both drug release and probe release studies were conducted in triplicate at 37 °C. *In vitro* drug release data was collated and plotted in various kinetic models to assess the release kinetic models to ascertain the mechanism of TM release from the various polymeric coatings.

6.3.2.5.7 Biological Evaluation of Atomised Coatings

To ensure the formulations and ultimately the engineered coatings are biocompatible and do not compromise epithelial membrane integrity, a BCOP test was performed as stated in **Section 4.3.7.8.**

6.3.2.5.8 Statistical Analysis

ANOVA test was carried to compare the release of TM from the atomised coatings. Derived *p* values less than 0.5 were considered statistically significant.

6.4 Results and Discussion

6.4.1 Solution Characterisation

Whilst EHDA is a simple process to operate, there is some complexity to the process which is reflected in the various physical liquid properties which affect both size and morphology of the resulting atomised structures. **Table 6.2** shows the average readings of viscosity, surface tension and electrical conductivity for all 8 formulations.

Table 6.2 Summary of physical liquid properties of all formulations. Data is shown as mean ± S.D.

Formulation	Viscosity (mPa.s)	Surface Tension (mNm^{-1})	Electrical conductivity (μScm^{-1})
Composite-TM	4.29±0.03	20.88±0.46	199.20±0.02
F0	4.08±0.06	22.38±0.47	221.30±0.56
F1	4.10±0.01	22.34±0.02	114.34±0.03
F2	4.57±0.02	25.00±0.04	154.48±0.02
F3	5.18±0.06	25.33±0.03	170.83±0.04
F4	4.72±0.01	22.8±0.02	104.05±0.02
F5	4.61±0.02	25.25±0.05	136.89±0.55
F6	5.21±0.02	20.21±0.01	170.72±0.04

Previous literature has reported the incorporation of chitosan in solution form yielded liquids with higher viscosities than the pure solvent (Sun and Li, 2011). However, these formulations have been produced by dissolving chitosan to yield homogenous solutions. In this thesis, chitosan was used as solid particles, formulating homogenously dispersed suspensions, therefore the effect on viscosity was negligible, as seen in **Table 6.2**.

In order for a stable cone jet to form, the electrical field applied must be able to overcome the ST of the formulation being processed. The ST is the function of the solvent as it makes up the largest proportion of the solution/suspension. As with viscosity, the incorporation of chitosan did not have a considerable impact on the ST of the formulations. All values measured here are below 50 mNm^{-1} hence the electrical field would not be exceeded upon application of voltage (Smith, 1986; Tang and Gomez, 1995).

The electrical conductivity of the polymeric liquids are as a result of combination of solvent, polymer, additives or excipients which are present in their ionised form. Previously in this thesis, it was found incorporating borneol barely had an effect on electro-conductivity (due to being present in such small quantities) showing an average reading of 221.35 μScm^{-1} with PE-free solution showing a reading of 119.26 μScm^{-1}. Incorporating chitosan in these formulations reduced the EC slightly. Despite the cationic nature of chitosan in solution, here the chitosan exists as solid particles and not in solution therefore not drastically altering the EC. All EC values here are within the ideal range for EHD processing (Kelly, 1990; Ganan-Calvo et al., 2016).

6.4.2 EHD Process Optimisation

The jetting maps produced in **Figure 6.1** demonstrate the range of flow rates and corresponding applied voltages required to achieve various EHD modes. When the flow rate is too slow/fast and the voltage is not high/low enough (depending on the formulation in question) there are 2 possible scenarios. Dripping mode can occur when the voltage applied is not strong enough to overcome the ST of the liquid to break up and form a stable cone jet, demonstrated in **Figure 6.1** as peach coloured regions. Unstable jetting occurs when the ST is competing with the electrical field, resulting in the liquid partially breaking up; yielding non-uniform structures with large size distributions (emphasised in blue in **Figure 6.1**). The lilac regions highlight the optimum window of operation where a stable jet is formed. All 6 formulations showed a wide range within which a stable jet could be formed. At 10 µl/min at 17.8 kV all 6 formulations formed a stable cone jet; so these process parameters were selected as the optimum EHD conditions. As with chapter 4 and 5, the synapse between the stainless steel needle exit and the collection plate was kept constant at 12 cm; ensuring no bias towards the working distance.

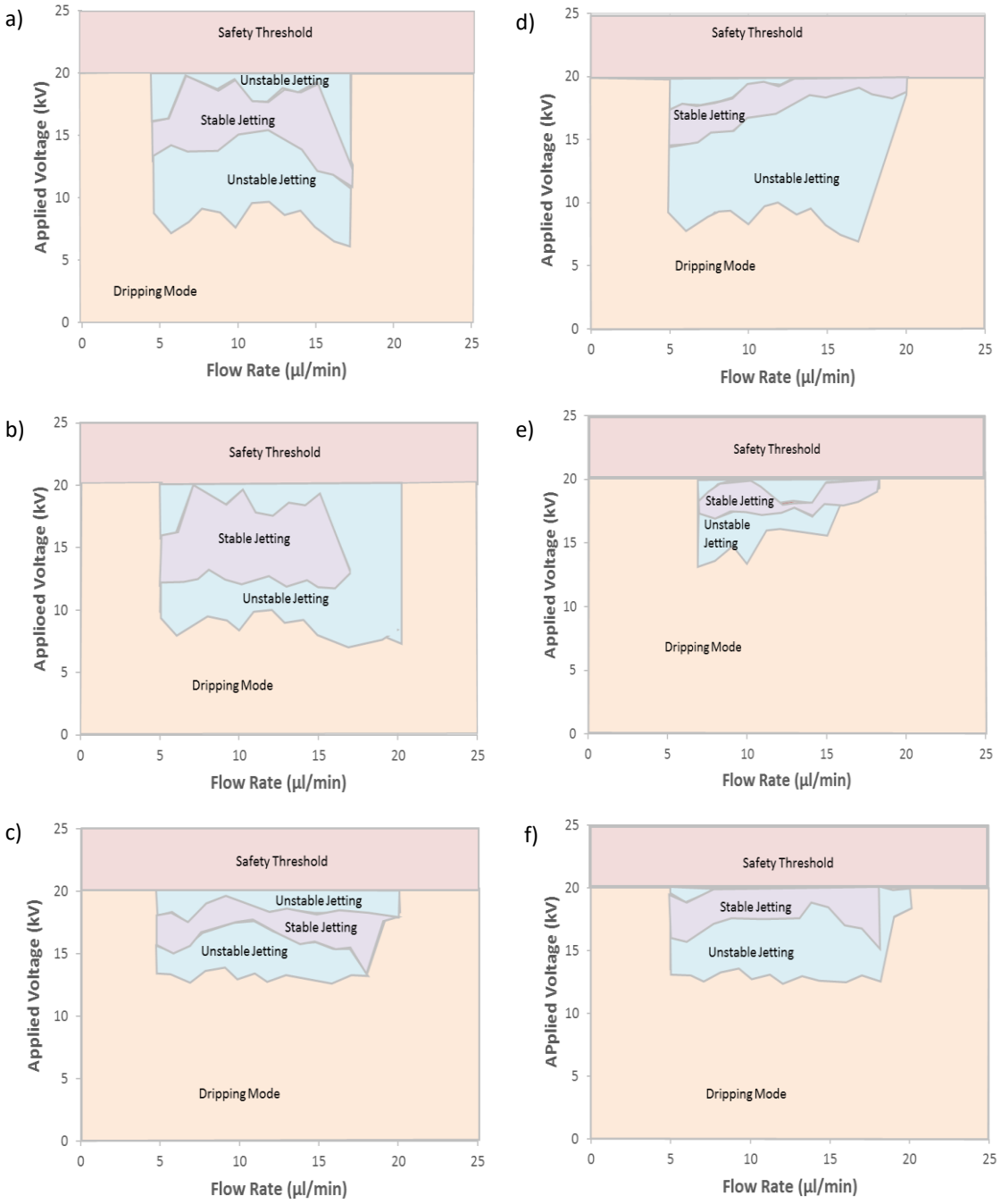

Figure 6.1 Jetting Maps to determine the relationship between flow rate and applied voltage a) F1, b) F2, c) F3, d) F4, e) F5, f) F6

6.4.3 Coating Characterisation

6.4.3.1 Imaging and Size Distribution

The morphological effect of utilising chitosan in this study can be observed in **Figure 6.2**. Atomising Composite-TM formulations presented beaded fibers as a result of an inadequate gap between the needle exit and the collection plate. This is could also be due to the combination of PVP and PNIPAM, polymers that usually yield particle and fibers when electrohydrodynamically processed separately (**Figure 4.1**). Addition of PE borneol yielded smooth-surfaced NFs with bell-shaped size distribution, an average of 74 nm in width; thinner than previously found when electrospinning borneol and PVP (Li et al., 2012). With respect to chitosan-loaded coatings it is clear to see there is a drastic morphological difference. Upon incorporating chitosan, the resulting atomised structures have now formed particles held together by scarce fibers. **Figures 6.2c-e** show the effect of chitosan concentration on the morphology of atomised coatings containing borneol with **Figure 6.2f-h** showing the effect of chitosan without borneol. It is clear to see the use of chitosan as solid particles has increased the over particle size and hence the particle size distribution. The chitosan particles may be trapped inside the composite matrix, hence increasing the overall size of the particles being produced. In the presence of borneol, there seems to be less particle/fiber aggregation; presumably due to the surface active agent properties of the PE.

Increasing chitosan concentration also had an impact on the morphology of the structures that made up the coatings. As concentration increased, the proportion of the final composition that is made up of PE decreases, reducing the fibrous network of the coatings. The smallest average diameter size was 114 nm achieved by electrospraying F1 with the highest being yielded by F6 (919 nm). Whilst there is such a large difference in the size distributions between these formulations, all formulations yielded coatings consisting of structures less than 10 µm in diameter, the threshold for foreign body detection in the eye (Agrahari et al., 2016). F1, F4 and F5 all demonstrated right skewed distribution (**Figure 6.3**), with more than 44% of all particles produced being under 100 nm. F2 and F6 showed negatively skewed data, highlighting at least 45% of the structures were more than 200 nm in diameter for both formulations. F3 showed a multimodal distribution, with 75% of the structures being over 200 nm, 15% under 100 nm and 9% between the range 100 nm and 200 nm.

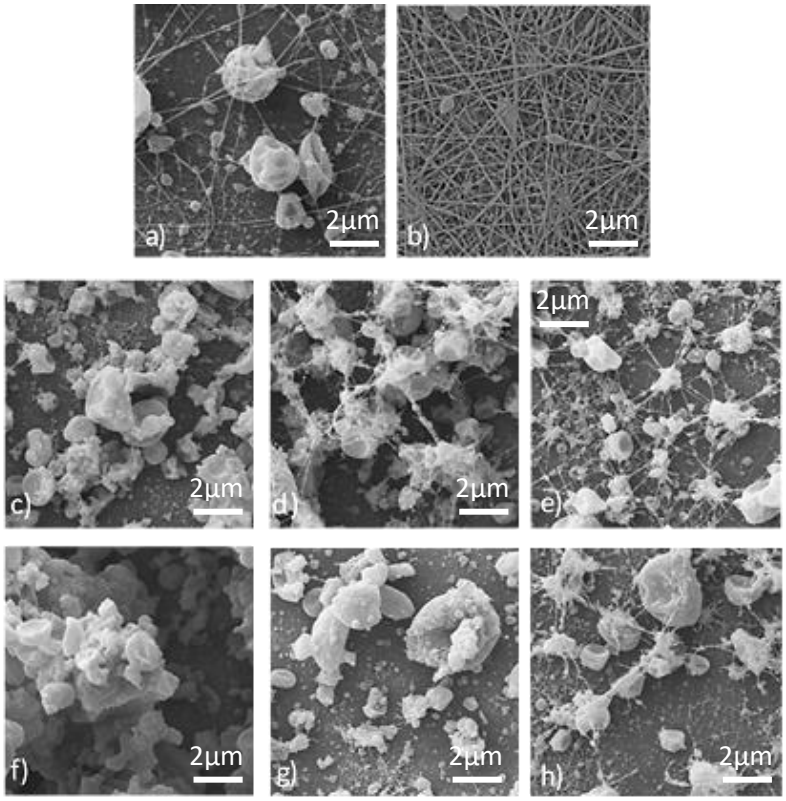

Figure 6.2 SEM Images of EHD atomised a) Composite-TM, b) F0, c) F3, d) F2, e) F1, f) F6, g) F5 and h) F4

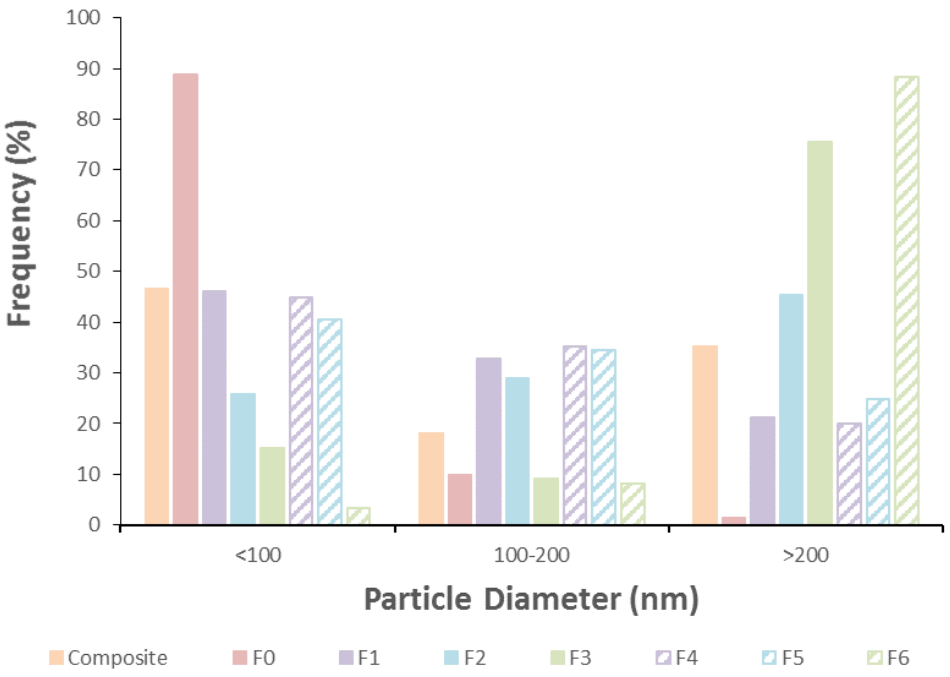

Figure 6.3 Size Distribution for all 8 atomised coating samples

6.4.3.2 Drug Encapsulation Efficiency and Coating Composition

The EE for each formulation is displayed in **Table 6.3.** The highest encapsulation was exhibited by F1 (97.93%) with F6 showing the lowest EE at 88.38%. As the concentration of chitosan increases in the formulations containing borneol, the EE seems to reduce to 93.92% (2 %w/v chitosan) and 90.69% (5 %w/v chitosan). This pattern was also observed with borneol-free samples. Saroha et al found similar results with low concentrations of chitosan giving the maximum TM EE (75.34%) when using ionic gelation to develop NPs for improved ocular drug delivery (Saroha, Pandey and Kaushik., 2017). Regardless of these reductions in EE, all formulations are considered to have very high encapsulation.

Table 6.3 Coating Composition and drug encapsulation efficiencies for each atomised coating

Formulation	Polymer Matrix (%w/w)	Timolol Maleate (%w/w)	Borneol (%w/w)	Chitosan (%w/w)	Encapsulation Efficiency (%)
Composite-TM	89.96	13.04	--	--	99.7
F0	85.47	12.82	1.71	--	99.7
F1	72.99	10.95	1.46	14.60	97.93
F2	63.70	9.55	1.27	25.48	93.92
F3	46.08	6.91	0.93	46.08	90.69
F4	74	11.2	--	14.82	90.45
F5	64.52	9.69	--	25.80	88.80
F6	46.51	6.98	--	46.51	88.38

6.4.3.3 DSC

Figure 6.4 displays the DSC thermograms for F0-F6, with raw TM, raw chitosan and composite-TM atomised coatings. Pure drug showed a defined melting point of 218 °C and the lack of this prominent peak in the thermograms for all EHD processed coatings shows TM was now encapsulated in amorphous form in the polymeric matrix as opposed to in its original crystalline form, just as seen in chapter 4 and 5. The similar melting points for the broad endotherms of F1-F6 labelled in **Figure 6.4** (125 °C – 129 °C) are lower than the raw composite (131 °C); highlighting

TM was evenly distributed throughout the coatings. Thermal glass transitions (T_g) can be detected in these thermograms between 59 °C and 77 °C as a result of the base polymer materials. Due to PVP and PNIPAM being amorphous materials, there is a temperature threshold at which they will transform from amorphous state to a part rubber part glass state (Khan, Asmatulu and Eltabey, 2013; Pawar et al., 2015). Here, it was difficult to ascertain the exact T_g when incorporating chitosan.

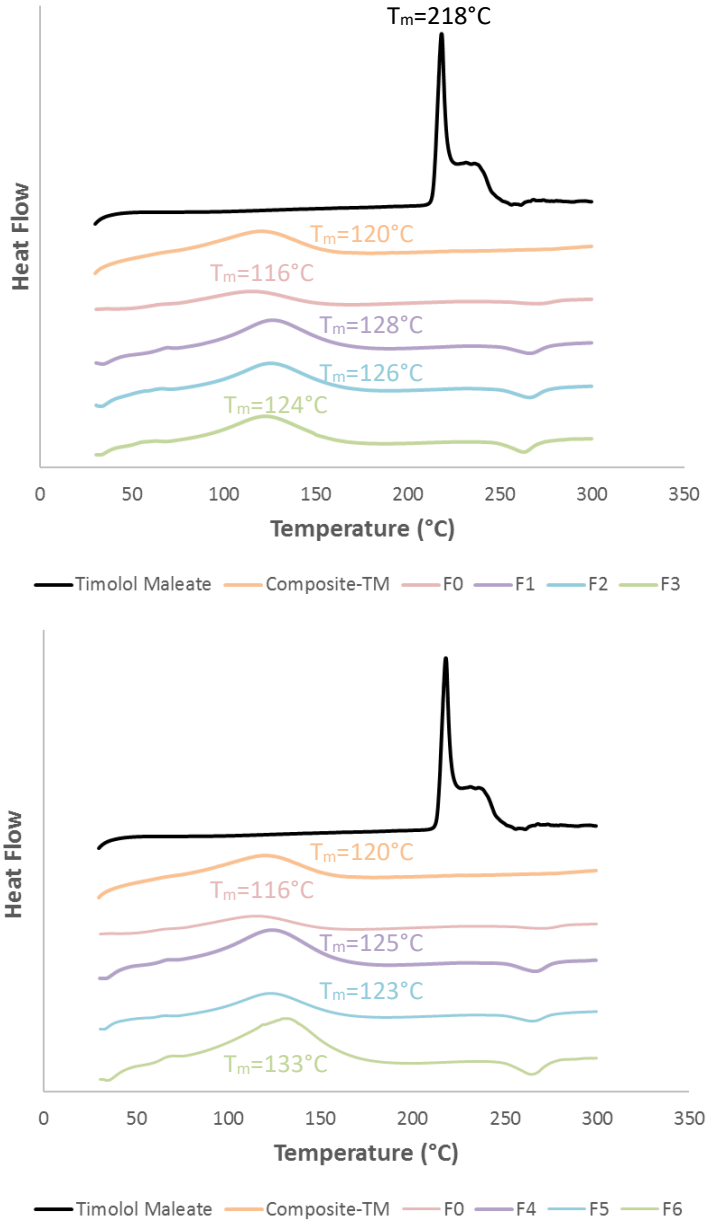

Figure 6.4 DSC Analysis of electrically atomised coatings with a) Formulations containing borneol and b) Formulations free of borneol

Chitosan is semi-crystalline as a result of strong inter- and intra-molecular bonds and its amorphicity is due to the heterocyclic units (**Figure 3.3**).

When heated to temperatures lower than its degradation temperature, changes in heat capacity/flow are too small to be distinguished (Wan et al., 2009). Additionally, this could also be due to water or moisture forming intermolecular hydrogen bonds and acting as a plasticizer in chitosan (Sarwar et al., 2015). The weak T_g also suggests the initial atomised coatings were predominantly amorphous to begin with which is as predicted with PVP and PNIPAM making up a large proportion of these coatings.

The inclusion of chitosan in the formulations also resulted in an extra exothermic event in each thermograms (F1-F6). Chitosan possesses few crystalline regions due to high degree of acetylation and therefore goes through thermal degradation without melting, highlighted by the absence of melting endotherm in **Figure 6.4**. The exothermic peaks between 263 °C and 267 °C (depending on chitosan concentration) are most likely due to the thermal decomposition of chitosan (Corazzari et al., 2015; Bizarria, d'Avila and Mei, 2014; Fei et al., 2016). The formation of two peaks here also further confirms chitosan being present as solid particles. As mentioned in previous discussions about DSC thermograms, single endotherms confirm the physical structures of raw materials were not compromised and were acting as one system. Here, the presence of the exotherm responsible for the crystallisation of chitosan indicates chitosan was acting independent to the EHD processed coating.

6.4.3.4 TGA

Figure 6.5 shows the resulting thermograms following TGA of raw TM, raw chitosan and atomised coatings. Pure TM again showed a sharp weight loss event between 20 °C and 370 °C; highlighting the temperature at which the drug thermally degraded (Abou-Sekkina et al., 2002; Joshi et al., 2009). Raw chitosan showed a total weight loss of 76%. The first weight loss event (starting at 57°C) is due to water desorption (Hong et al., 2007). The initiation of water loss here occurred at a low temperature; indicative of the water lost at this step was loosely bound moisture (Hong et al., 2007). 2nd weight loss event began at 254 °C, which has been previously found to be due to pyrolytic degradation (Corazzari et al., 2015).

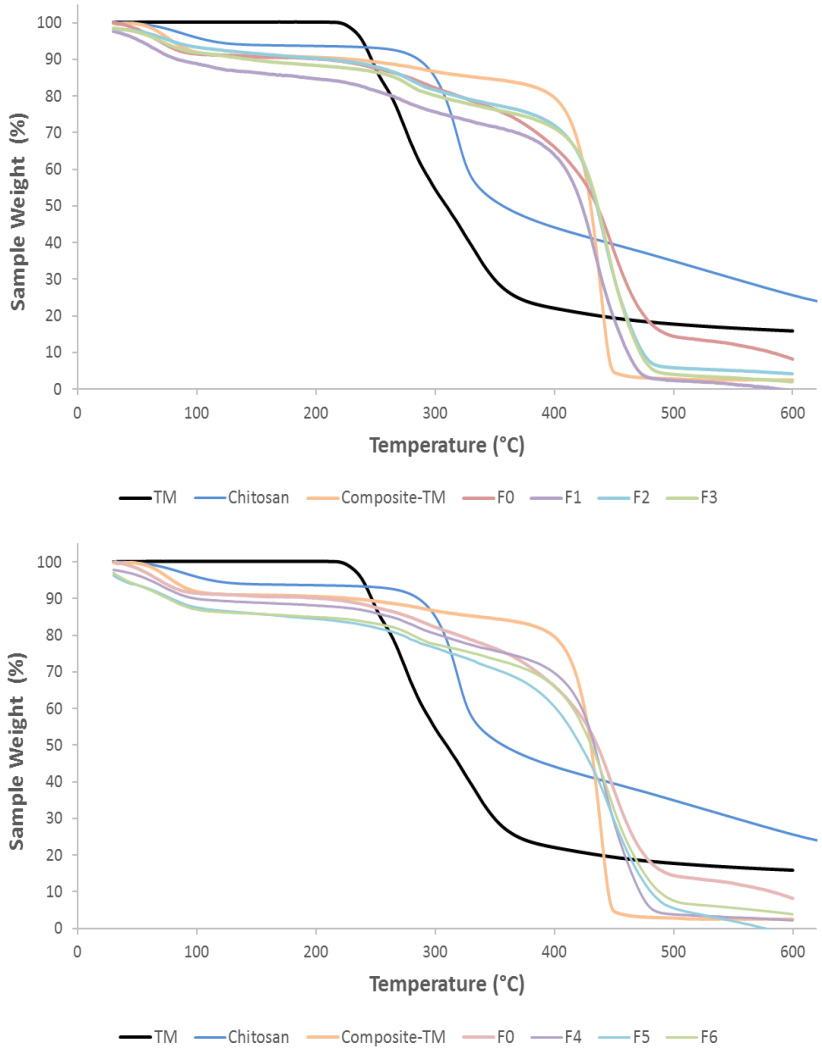

Figure 6.5 TGA Analysis of raw timolol maleate, raw chitosan and electrically atomised coatings

All 8 atomised coatings demonstrated two weight loss events: initial water loss and subsequent thermal degradation. The temperature at which decomposition was initiated dropped slightly for formulations containing chitosan with degradation occurring over a wider temperature range (230 °C-520 °C) compared to chitosan-free formulation (300 °C -540 °C). This confirms TM and borneol have been encapsulated and the formulations are more thermally stable, showing both PE and chitosan slowed the degradation of the polymeric matrix (PVP and PNIPAM) (Sundaray et al., 2008; Nazari et al., 2017; Abou-Sekkina et al., 2002).

Just as found in chapter 4 and 5, within the range of biological interest (35 °C -38 °C) there were no distinctive physical or chemical changes when heating the atomised coatings for TG analysis.

6.4.3.5 Contact Angle Analysis

Due to further modifying the solutions from a formulation point of view, the hydrophilicity of the resulting atomised coatings could be affected. **Figure 6.6** shows digital images of the liquid droplet on the sample and how it dissipated over time. **Figure 6.7** shows the CA analysis on the atomised coatings on the contact lenses. PE-free and chitosan-free coatings (Composite-TM) showed a high initial CA at 126.27°. Upon inclusion of borneol, the initial contact angle was found to be 71.5°, almost 2-fold reduction compared to the composite-TM samples. Here, the introduction of an excipient used primarily as a PE, was also found to double as a surface active agent; lowering the surface tension between the liquid droplet and fibrous coatings. Regardless of chitosan's hydrophilic nature, the initial CA of the formulations containing both borneol and chitosan had increased to 96.70°, 91.21° and 91.36° for F1, F2 and F3, respectively. This increase in CA could be attributed to the incorporation of solid particles of chitosan; the particles may act as an additional barrier, which may fill voids and pores between the particles. Therefore, the water droplet has to penetrate through both the chitosan as well as the polymeric matrix of PVP and PNIPAM.

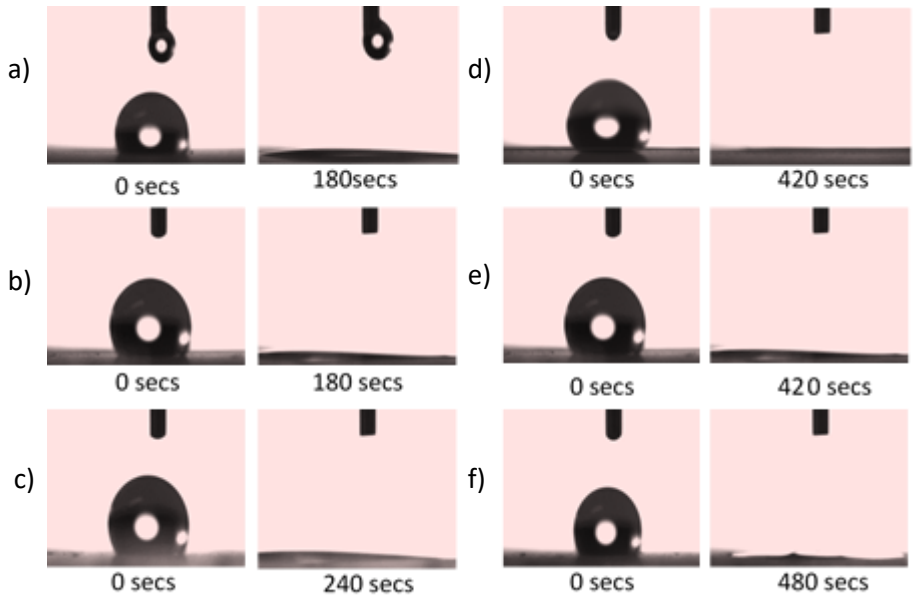

Figure 6.6 Digital images taken during contact angle analysis over time for a) F1, b) F2, c) F3, d) F4, e) F5, f) F6

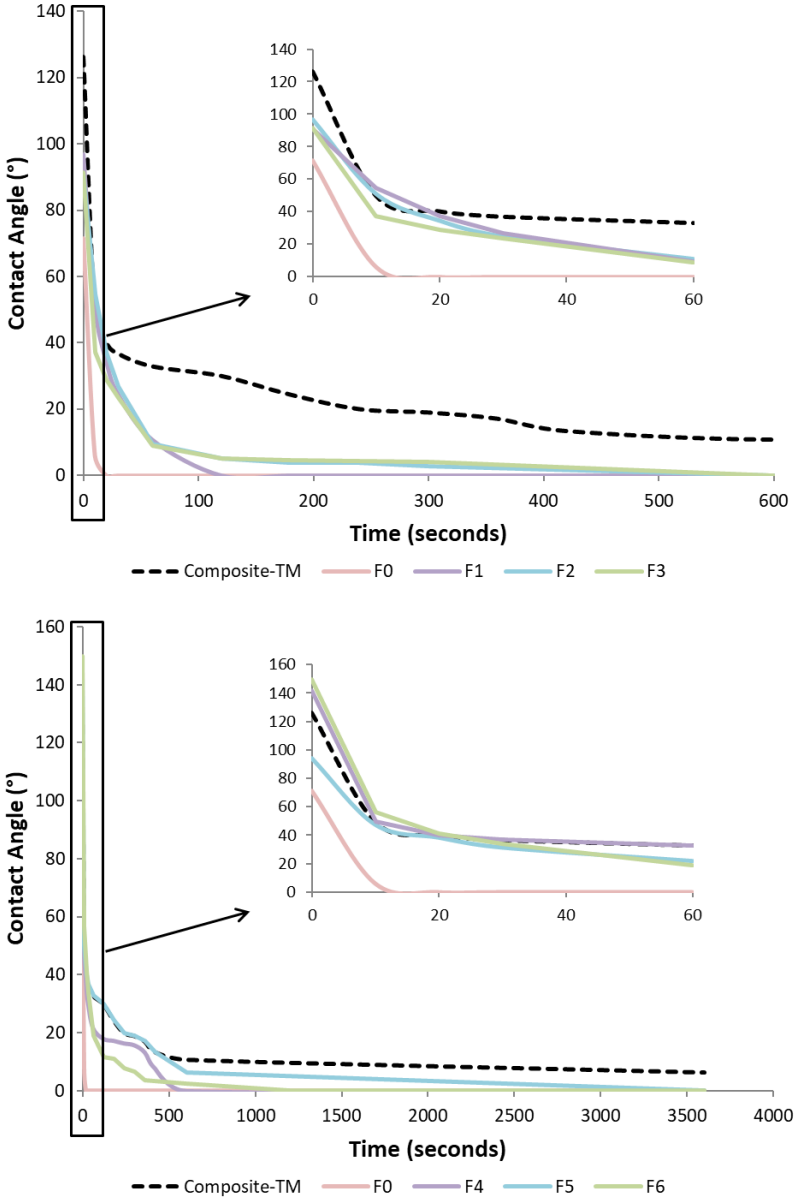

Figure 6.7 Contact angle analysis over time for F1-F6 compared to composite-TM coatings and F0 coatings

The water droplet introduced to the composite-TM atomised coatings completely dissipated within 30 mins while the droplet placed on F0 samples completely spread within 20 seconds; highlighting the role of borneol as a surface active agent and helping to increase the hydrophilicity of the coatings. Incorporating chitosan into formulations containing borneol increased the time required for the water droplet to penetrate/dissolve through the coatings. The concentration of chitosan apparently affected CA over time; the higher the concentration, the longer it took for the water droplet to completely spread. This increased period of time could also be due to the increased density of the sample (as a result of the increased concentration). This increase in density can cause particle agglomeration and due to this air can become trapped between the particles; hindering water penetration and spreading.

Formulations containing no PE but various concentrations of chitosan showed some interesting results. The absence of borneol showed an increase in the initial CA of F4, F5 and F6 to higher than that found with composite-TM samples. The higher the concentration of chitosan, the higher the initial CA. F4 and F5 took 7 minutes for the water droplet to spread whilst F6 took 8 minutes on average. These timings are twice as longer than those with borneol and chitosan (3/4 minutes). This prolongation of water spreading may possibly aid the affinity of the coatings to the hydrophilic contact lenses, aiding the attachment of the coatings to the lens.

6.4.3.6 FTIR Analysis

It is vital to ensure the compatibility of the excipients used during EHDA. It is especially important here, as chitosan has not been used in solution. The use of chitosan in the form of solid particles may interfere with the resulting atomised coatings therefore FTIR analysis was used to ensure this was not the case. The characteristic peaks of TM, PVP and PNIPAM studied in chapter 4 and 5 have also been found here; **(Figure 6.8)** in the fingerprints of the raw materials. Pure TM shows characteristic peaks at 2968 cm^{-1} (aliphatic C-H stretching), 3063 cm^{-1} (aromatic C-H stretching), 1718 cm^{-1} (C=O), 1229 cm^{-1} (O-H bending), 954 cm^{-1} (C-O stretching vibrations). The characteristic peak at 1651 cm^{-1} in all spectra for 6 formulations corresponds to C=O stretching vibrations in PVP whilst absorption peaks that are indicative of PNIPAM spectra included amide II bond at 1550 cm^{-1}, C=O stretching and CH_3 asymmetric stretching vibrations at 1650 cm^{-1} and 2970 cm^{-1}, respectively. With respect to chitosan, the peak at 1636 cm^{-1} is due to N-H bending of NH_2 group of the chitosan structure; whilst the peaks at 2890 cm^{-1} and 1028 cm^{-1} are as a

result of C=O amide group and C=O stretching vibrations. The stretching vibrations of the amino group gave rise to a peak at 1420 cm^{-1} and O-H stretching and amine N-H symmetric vibrations produced a peak at 3329 cm^{-1}.

These prominent peaks that are found with pure chitosan are also present in the fingerprints for all six formulations. No extreme shifts in the peaks can be detected showing the dissolved components had not interacted with the chitosan during the EHD process; i.e. no bonds seemed to form between the oligo saccharide and the polymers or drug.

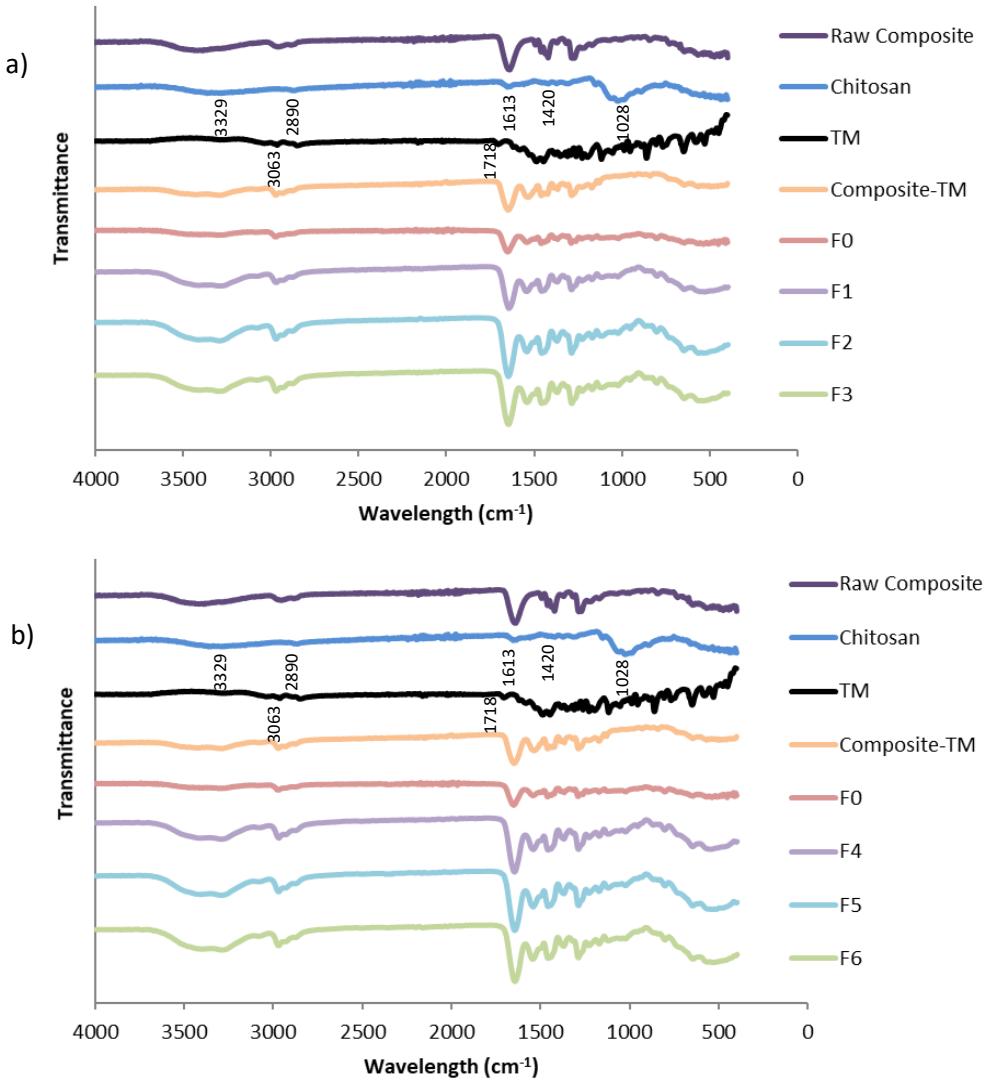

Figure 6.8 FTIR analysis of raw timolol maleate, chitosan and electrohydrodynamically processed coatings

One thing to note here is the increase in peak intensity that can be seen at 1710 cm^{-1}, 2964 cm^{-1}, 1286 cm^{-1} and 3274 cm^{-1}. This increase is indicative of mass increase as frequency of vibration is inversely proportional to mass. This could also be due to chitosan being present outside the atomised structures as opposed to being encapsulated (Merlini et al., 2014).

6.4.3.7 *In Vitro* Release and Kinetics

6.4.3.7.1 In Vitro Drug Release

Figure 6.9 shows the *in vitro* release of TM from all six atomised coatings alongside PE free atomised coatings and chitosan-free coatings.

The release from PE-free coatings demonstrated a biphasic profile as previously seen in chapter 4, with 67% of encapsulated TM being released after 24 hours. Similar to what was concluded in chapter 5, F1-F6 demonstrated triphasic release profiles. However, in this case the initial release phase was a slow gradual release as opposed to an initial burst release. The maximum amount released after 10 minutes was only 9.8% by F1 and F5; contradicting what was found with PE free (47.5%) and chitosan free (14.15%). This delay in drug release could be due to drug diffusion being hindered by the barrier of solid chitosan particles. As discussed with contact angle analysis, these particles fill the pores and voids in the coatings matrix, reducing the spatial environment available for the drug molecules to diffuse out.

Another reason for this delay in drug release could be attributed to the very high EE achieved for all six formulations. Almost all of the drug was trapped within the polymeric matrix (with hardly any surface associated drug), therefore this matrix must swell or dissolve before drug release can occur. Furthermore, chitosan also prevents the release medium (PBS) from entering the polymeric matrix at a rate that would otherwise by faster; causing the dissolution and/or swelling of the polymeric matrix to occur at a much slower rate.

The two subsequent release phases are due to the polymer base of PVP and PNIPAM. The 2nd release phase is due to the eventual dissolution of PVP and breaking of PNIPAM chains whilst the 3rd phase is release due to polymer erosion. As seen in chapter 5 and now here, the DSC thermograms indicated a thermal transition of polymer from rubbery state to glassy state. This could provide an explanation for the sustained release of TM observed in phase 2 and phase 3.

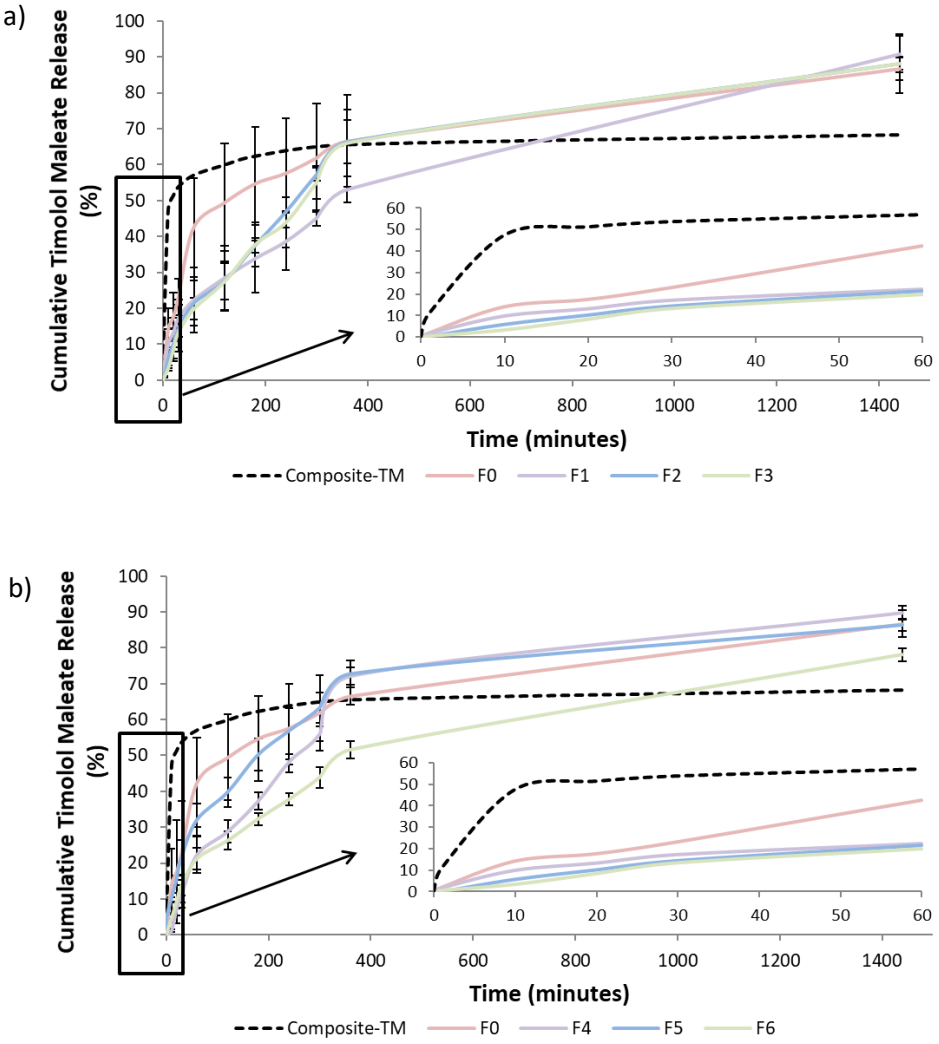

Figure 6.9 *In Vitro* Cumulative TM release from electrically atomised coatings

Some of the drug may be trapped within the crystalline regions of the polymer, hence is isolated from the release medium in the donor compartment. Only upon polymer degradation can the trapped drug be released, resulting in gradual sustained release (forming the 3rd release phase) (Natu, de Souza and Gil, 2011).

Fulĝencio et al developed mucoadhesive chitosan films loaded with TM and achieved 85% drug release over two weeks (Fulgencio et al., 2012). Whilst this release was successfully prolonged, the practicality of such a device is questionable. Whilst the research presented here is mainly a proof of concept, the use of contact lenses has already been proven successful in vision correction and cosmetics. Furthermore, over 89% of drug was delivered with 24 hours, a more

convenient dosing period for the patient. Agarwal et al used chitosan and nanocarrier niosomes to assess their combined ability to enhance TM release (Aggarwal and Kaur, 2005). Their study found that by coating the niosomes with chitosan, drug release was significantly prolonged from 91% in 2 hours to 40.43% within 10 hours.

The concentration of chitosan did significantly affect the total cumulative percentage released (p=0.0276), albeit only slightly. Formulations containing 1% chitosan (F1 and F4) released 89.7% and 90.78% TM with this decreasing to 88.16% and 78.05% for F3 and F6, respectively. Increasing the concentration of chitosan means there is a greater proportion of solid particles dispersed throughout the atomised matrix further delaying drug diffusion.

6.4.3.7.2 In Vitro Probe Release

Figure 6.10 shows the release of rhodamine B from the atomised coatings on the contact lenses and into PBS (pH 7.4; 37 °C). The atomised coatings were composed of the same materials as stated in table 6.1; however, rhodamine B replaced TM. The fluorescing of the contact lens at the sampled time points indicates the coatings did not detach from the lens upon introduction to the release medium whilst the probe release into PBS found to mirror the results found with *in vitro* drug release in **Section 6.4.3.7.1**

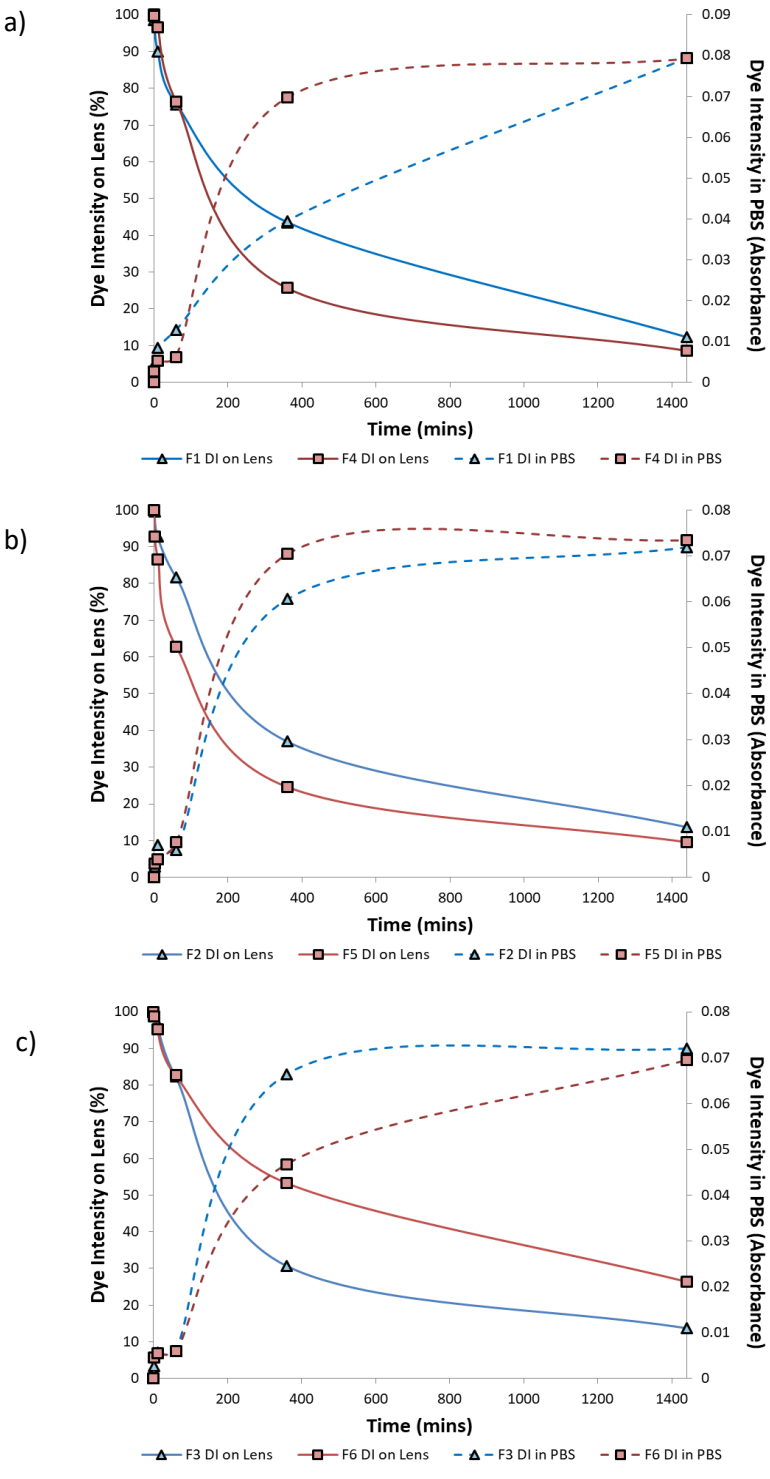

Figure 6.10 *In Vitro* Probe Release from atomised coatings into PBS from a) F1 and F4, b) F2 and F5, c) F3 and F6

6.4.3.7.3 Drug Release Kinetics

The *in vitro* data collated in section 6.4.3.7.1 was fitted to various kinetic models: zero order **(figure 6.11),** first order (**Figure 6.12),** Hixson-Cromwell **(Figure 6.13**), Higuchi (**Figure 6.14)** and Korsmeyer-Peppas **(Figure 6.15).** Analysing the resulting plots, the mechanism of TM release can be found. **Table 6.4** collates the regression coefficients for the first 4 models; with **Table 6.5** summarising the important parameters derived from the Korsmeyer-Peppas model.

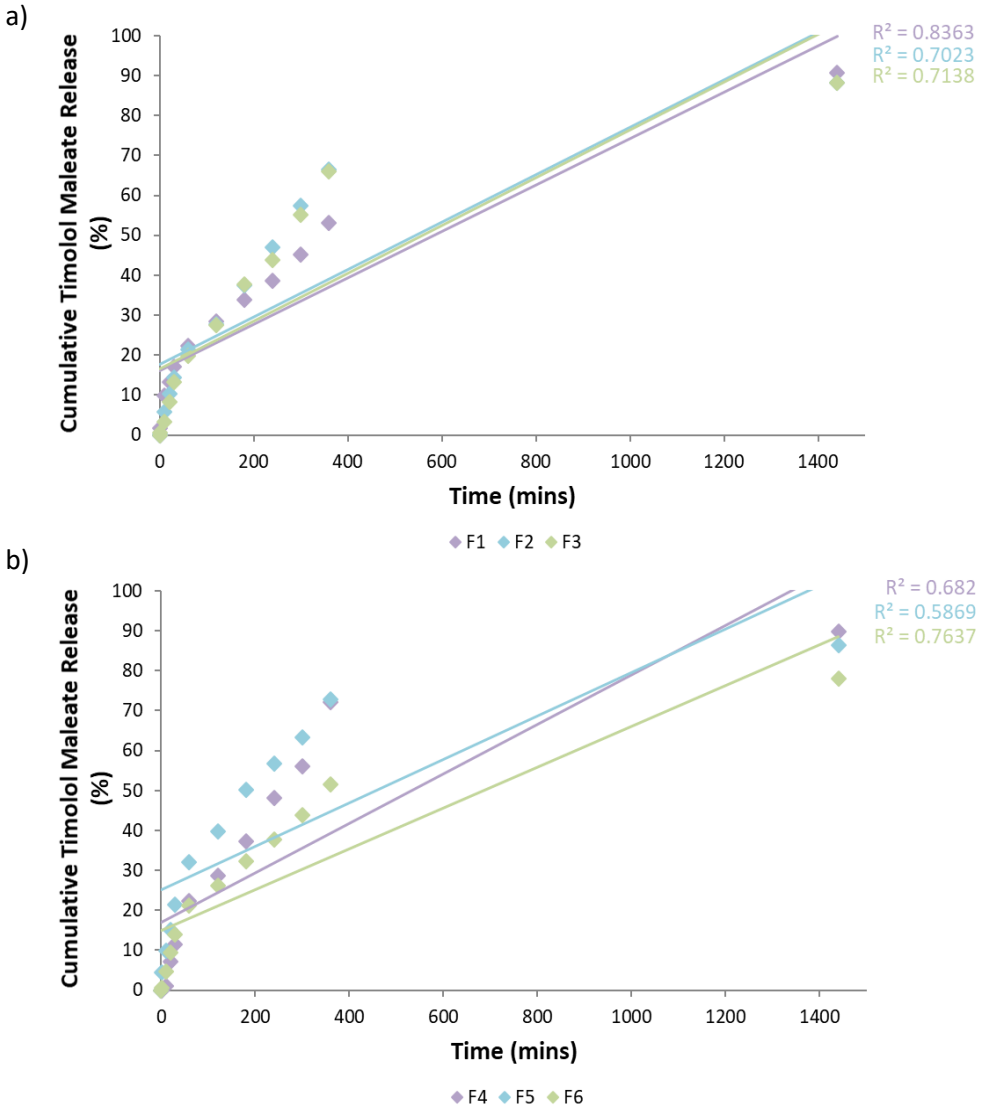

Figure 6.11 Release of Timolol Maleate from atomised coatings according to the zero order model for formulations a) containing borneol and b) free of borneol

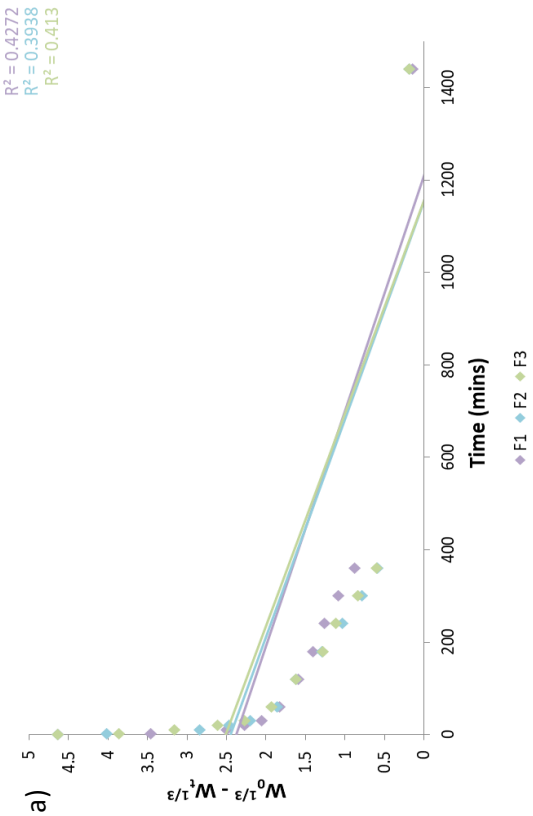

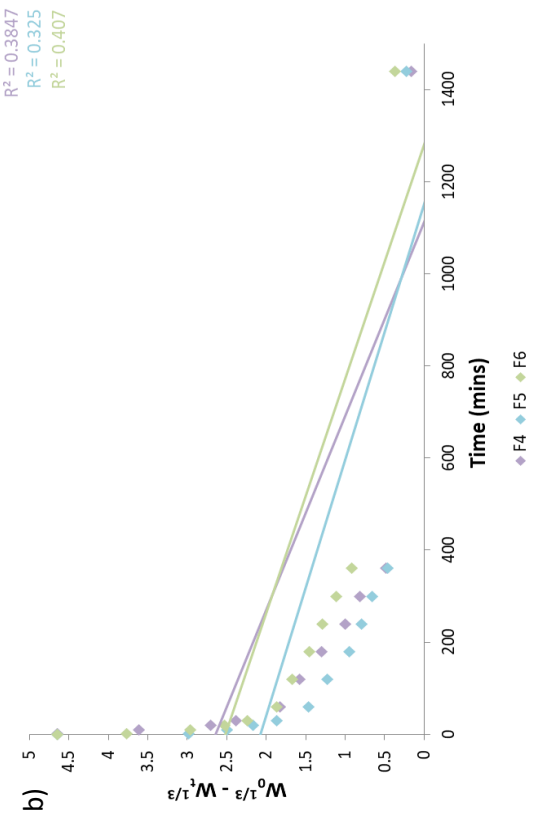

Figure 6.13 Release of Timolol Maleate from atomised coatings according to the Hixson-Cromwell model for formulations a) containing borneol and b) free of borneol

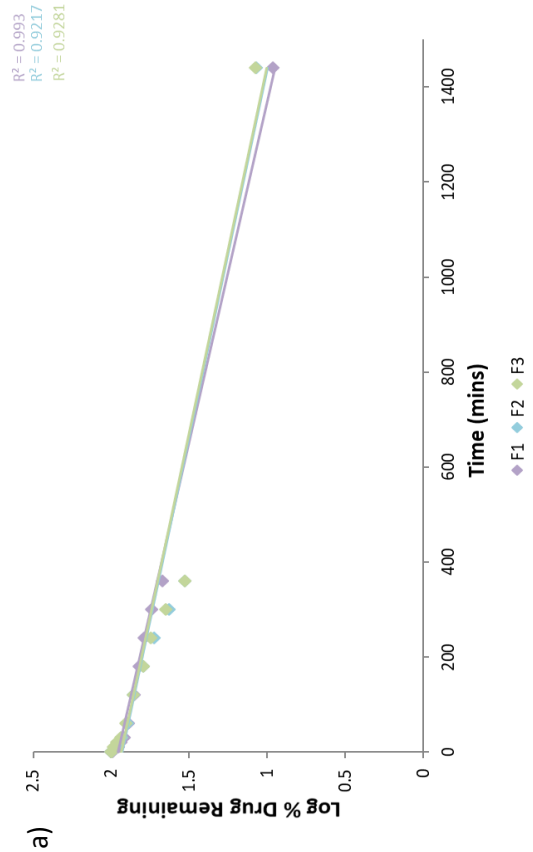

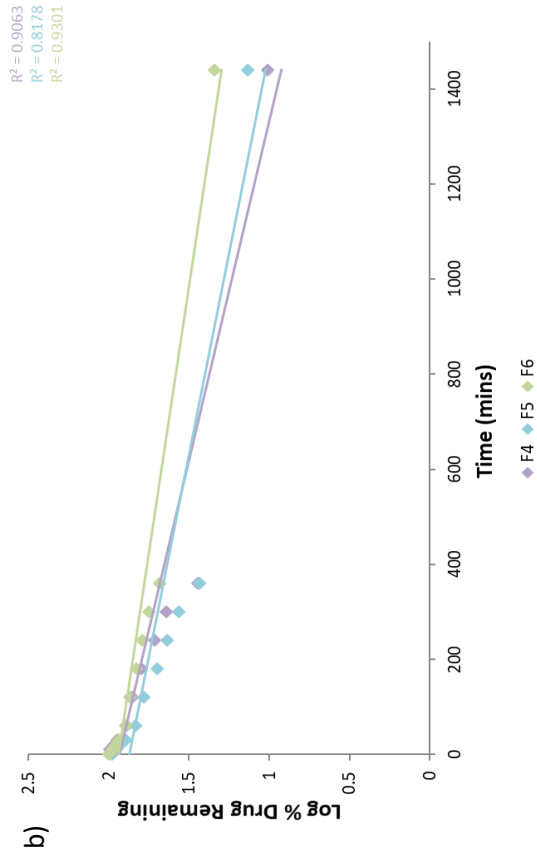

Figure 6.12 Release of Timolol Maleate from atomised coatings according to the first order model for formulations a) containing borneol and b) free of borneol

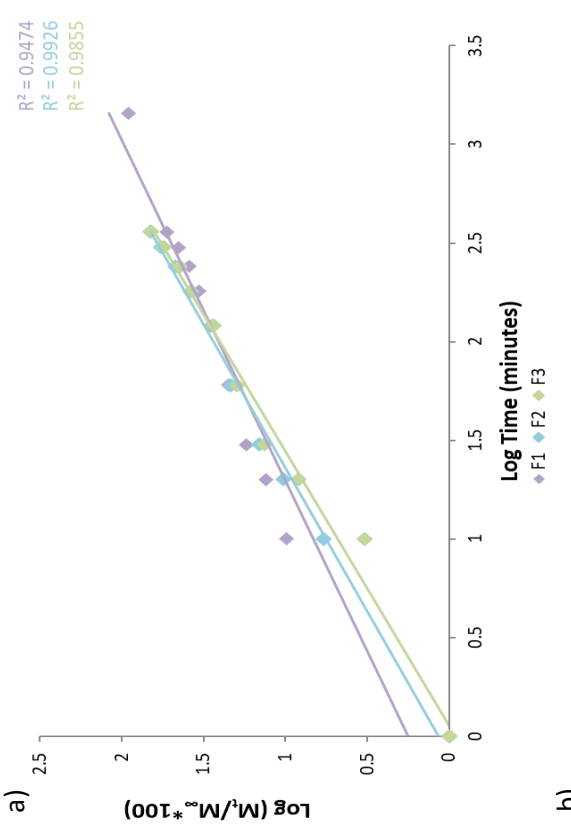

Figure 6.15 Release of Timolol Maleate from atomised coatings according to the Korsmeyer-Peppas model for formulations a) containing borneol and b) free of borneol

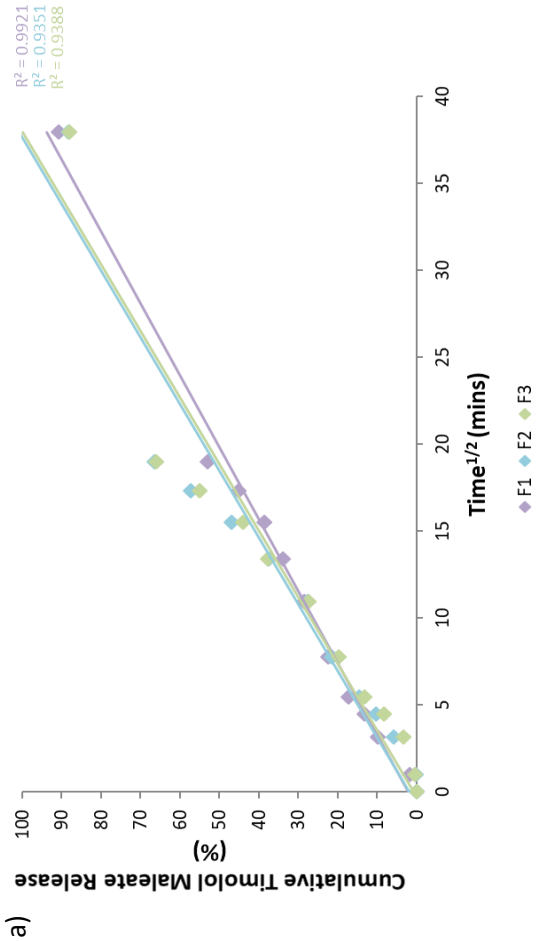

Figure 6.14 Release of Timolol Maleate from atomised coatings according to the Higuchi model for formulations a) containing borneol and b) free of borneol

Table 6.4 Kinetic Models for timolol maleate release expressed by regression coefficient, R^2

Formulation	*Zero Order*	*First Order*	*Hixson-Cromwell*	*Higuchi*
F1	0.8363	0.993	0.4272	0.9921
F2	0.7023	0.9217	0.3938	0.9351
F3	0.7138	0.9281	0.4130	0.9388
F4	0.6820	0.9063	0.3847	0.9178
F5	0.5869	0.8178	0.3250	0.8807
F6	0.7637	0.9301	0.4070	0.9707

All 6 formulations demonstrated poor fit to the zero-order model with R^2 values ranging from 0.5869 to 0.8363. When fitted to first order release kinetic model, high R^2 values (0.8178-0.9930) were calculated, indicating the rate of TM release was dependent on the initial drug concentration. Fitting the *in vitro* data to the Hixson-Cromwell model showed TM was not being released via dissolution (low R^2 values). This, however, does not confirm drug release was via diffusion. Due to this, Higuchi and Korsmeyer-Peppas models were also utilised. If R^2 values above 0.95 were derived from the Higuchi kinetic model, the drug release is considered to be diffusion based. High R^2 values were obtained from F1 and F6 (0.9921 and 0.9707, respectively) suggesting TM was released from the atomised coatings via Fickian Diffusion; based on Fick's Law of release being square root time dependent. Formulations F2-F5 had R^2 values ranging between 0.8807 and 0.9388; suggesting a non-Fickian diffusion mechanism. This is mirrored by the n values calculated from the Korsmeyer-Peppas model. F1 and F6 had n values of 0.5399 and 0.5609, which again indicate Fickian diffusion. F2-F5 had values that suggested TM release with these coatings was because of both diffusion and swelling and the release was time dependent, which mirrored the results collated from the first order kinetic model.

One thing to note here is as the concentration of chitosan increased, the more the release was based on swelling, as the release mechanism changed from Fickian Diffusion when using 1 %w/v chitosan (F1) to non-Fickian diffusion using 5 %w/v (F3).

Table 6.5 Summary of Korsmeyer-Peppas model parameters for TImolol Maleate Release

Formulation	R^2	n	Mechanism of Release
F1	0.9474	0.5399	Fickian Diffusion
F2	0.9926	0.6873	Non-Fickian Diffusion
F3	0.9855	0.7274	Non-Fickian Diffusion
F4	0.9248	0.7799	Non-Fickian Diffusion
F5	0.9862	0.48	Non-Fickian Diffusion
F6	0.9741	0.5609	Fickian Diffusion

6.4.3.8 Biological Evaluation of Atomised Coatings

Any formulation that is to be in contact with the eye must be biocompatible and not interfere with the integral epithelial cells of the cornea. If the cell membrane is compromised, the cornea can no longer work to protect the eye; allowing foreign bodies to enter the eye (Abdelkader et al., 2015; Wilson, Ahearne and Hopkinson, 2015). BCOP testing allows samples to be tested to ensure the materials used do not interfere with corneal membrane proteins and cause any toxicity. **Figure 6.16** shows how the cornea of freshly excised bovine cornea reacted when treated with F3, F8 and a range of controls.

Saline posed as the negative control, showing no signs of toxicity (which can be visually observed with no change in opacity of the cornea) (**Figure 6.16a, f**). Contrasting this is the application of either acetone (mildly positive control) or NaOH (positive control). Treating the cornea with acetone showed a slight cloudy region which is more prominent under the blue cobalt

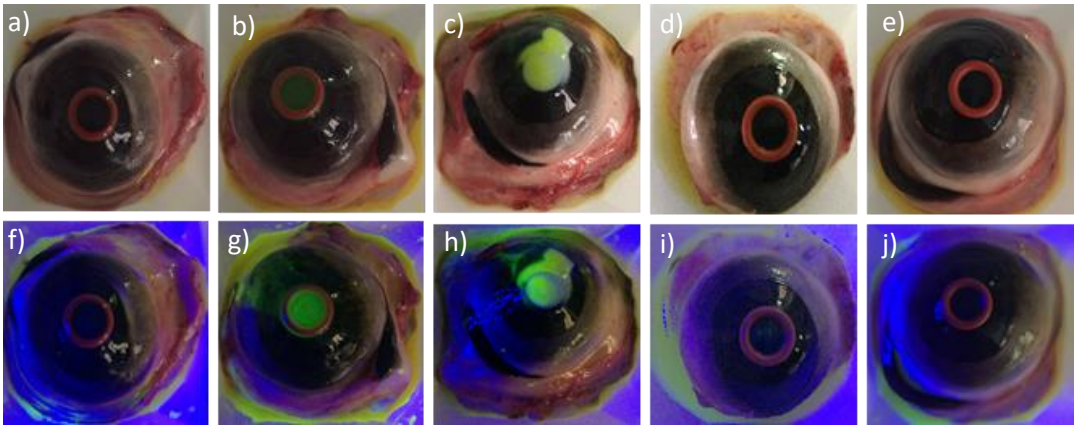

Figure 6.16 BCOP results of freshly excised bovine cornea. Digital Images of cornea treated with a) Saline, b) Acetone, c) NaOH, d) F3 and e) F8. Fluorescence images of cornea under cobalt blue filter treated with f) saline, g) acetone, h) NaOH, i) F4, j) F8

fluorescent light (**Figure 6.16g and h**)**.** This permeation of fluorescein dye through the cornea indicated there was some ocular irritancy as a result of interaction with lipids in the epithelial membrane (Maurer et al., 2001). NaOH was utilised here to demonstrate the effect non-compatible materials with the cornea. NaOH has the ability to initiate saponification of fatty acids present in corneal cells; disrupting the entirety of the epithelial layer (Reim, Schrage and Becker, 2001). This in turn increases the permeability of the cornea to foreign bodies. **Figure 6.16c and h** shows the severe, evident damage done to the cornea which is visible even without the use of the blue cobalt filtered light.

With respect to testing the formulations used in this study, the only changing variables was the presence of borneol and the concentrations of chitosan used. Therefore, only F3 (borneol and 5 %w/v chitosan) and F8 (5 %w/v chitosan) were tested. If these formulations showed any ocular toxicity, all other formulations would be tested to identify if lower concentrations of chitosan displayed any signs of incompatibility. The staining of F3 and F6 treated bovine cornea showed no any visual opacification under natural light (**Figure 6.16d and e**) and no indication of fluorescence under a fluorescent light (**Figure 6.16i and j**), highlighting these formulations were biocompatible and suitable for use in ocular drug delivery.

6.5 Conclusion

This chapter looked at the effect of chitosan on the release of TM from electrically atomised coatings. The incorporation of chitosan into polymeric formulations loaded with TM and borneol changed the morphological characteristics of the structures that made up the atomised coatings to particles (as opposed to the fibers produced with formulations without chitosan). Subject to chitosan concentration, a wide range of particle size distributions were derived for each formulation. Thermal analysis confirmed TM was continually being encapsulated in amorphous form and that chitosan was present as solid particles, as confirmed by the occurrence of an exotherm at ~ 260 °C. The critical assessment of the effectiveness of chitosan (*in vitro/ex vivo*) found the oligo polysaccharide found to be successful as a PE, increasing TM release up to 23% more than composite-TM coatings and up to 11% from borneol-loaded coatings (F0). In conclusion, the incorporation of chitosan as a PE showed promising results. The results indicate the engineered coatings have the ability to achieve sustained release over 24 hours, overcoming

the need for frequent administration and prolonging drug retention; drawbacks usually met using conventional dosage forms like eye drops.

The novelty of combining an on-demand engineering process like EHDA for drug delivery and an already established ocular drug delivery device has not yet been explored and the results found in this study show great potential in this field.

6.6 References

ABDELKADER, H., PIERSCIONEK, B., CAREW, M., WU, Z. and ALANY, R.G., 2015. Critical appraisal of alternative irritation models: three decades of testing ophthalmic pharmaceuticals. *British Medical Bulletin,* 113(1), pp. 1-13.

ABOU-SEKKINA, M.M., EL-RIES, M.A., MOLOKHIA, A.M., RABIE, N. and WASSEL, A.A., 2002. γ-Induced Thermal Stability And Thermal Studies On Timolol β-Blocker. *Journal of Thermal Analysis and Calorimetry,* 68(3), pp. 1017-1023.

AGGARWAL, D. and KAUR, I., 2005. Improved pharmacodynamics of timolol maleate from a mucoadhesive niosomal ophthalmic drug delivery system. *International journal of pharmaceutics,* 290(1-2), pp. 155-159.

AGRAHARI, V., MANDAL, A., AGRAHARI, V., TRINH, H.M., JOSEPH, M., RAY, A., HADJI, H., MITRA, R., PAL, D. and MITRA, A.K., 2016. A comprehensive insight on ocular pharmacokinetics. *Drug Delivery and Translational Research,* 6(6), pp. 735-754.

ATES, M., KAYNAK, M.S. and SAHIN, S., 2016. Effect of permeability enhancers on paracellular permeability of acyclovir. *Journal of Pharmacy and Pharmacology,* 68(6), pp. 781-790.

BENEDIKTSDOTTIR, B.E., BALDURSSON, O. and MASSON, M., 2014. Challenges in evaluation of chitosan and trimethylated chitosan (TMC) as mucosal permeation enhancers: From synthesis to in vitro application. *Journal of Controlled Release,* 173, pp. 18-31.

BIZARRIA, M.T.M., D'AVILA, M.A. and MEI, L.H.I., 2014. Non-Woven Nanofiber Chitosan/peo Membranes obtained by Electrospinning. *Brazilian Journal of Chemical Engineering,* 31(1), pp. 57-68.

CHOUGULE, M.B., PATEL, A.R., PATLOLLA, R., JACKSON, T. and SINGH, M., 2014. Epithelial transport of Noscapine across cell monolayer and influence of absorption enhancers on in vitro permeation and bioavailability: implications for intestinal absorption. *Journal of Drug Targeting,* 22(6), pp. 498-508.

CORAZZARI, I., NISTICÒ, R., TURCI, F., FAGA, M.G., FRANZOSO, F., TABASSO, S. and MAGNACCA, G., 2015. Advanced physico-chemical characterization of chitosan by means of TGA coupled on-line with FTIR and GCMS: Thermal degradation and water adsorption capacity. *Polymer Degradation and Stability,* 112, pp.1-9

DI COLO, G., BURGALASSI, S., ZAMBITO, Y., MONTI, D. and CHETONI, P., 2004. Effects of different N-trimethyl chitosans on in vitro/in vivo ofloxacin transcorneal permeation. *Journal of Pharmaceutical Sciences,* 93(11), pp. 2851-2862.

DJEBLI, N., KHIER, S., GRIGUER, F., COUTANT, A., TAVERNIER, A., FABRE, G., LERICHE, C. and FABRE, D., 2017. Ocular Drug Distribution After Topical Administration: Population

Pharmacokinetic Model in Rabbits. *European Journal of Drug Metabolism and Pharmacokinetics,* 42(1), pp. 59-68.

DUTTAGUPTA, D.S., JADHAV, V.M. and KADAM, V.J., 2015. Chitosan: A Propitious Biopolymer for Drug Delivery. *Current Drug Delivery,* 12(4), pp. 369-381.

FEI, X., YU, M., ZHANG, B., CAO, L., YU, L., JIA, G. and ZHOU, J., 2016. The fluorescent interactions between amphiphilic chitosan derivatives and water-soluble quantum dots. *Spectrochimca Acta part A: Molecular and Biomolecular Spectroscopy,* 5(152), pp.343-351

FULGENCIO, G.D.O., BRETAS VIANA, F.A., RIBEIRO, R.R., YOSHIDA, M.I., FARACO, A.G. and CUNHA-JUNIOR, A.D.S., 2012. New Mucoadhesive Chitosan Film for Ophthalmic Drug Delivery of Timolol Maleate: In Vivo Evaluation. *Journal of Ocular Pharmacology and Therapeutics,* 28(4), pp. 350-358.

GANAN-CALVO, A.M., LOPEZ-HERRERA, J.M., REBOLLO-MUNOZ, N. and MONTANERO, J.M., 2016. The onset of electrospray: the universal scaling laws of the first ejection. *Scientific Reports,* 6, pp. 32357.

GIULIANI, A., BALDUCCI, A.G., ZIRONI, E., COLOMBO, G., BORTOLOTTI, F., LORENZINI, L., GALLIGIONI, V., PAGLIUCA, G., SCAGLIARINI, A., CALZA, L. and SONVICO, F., 2018. In vivo nose-to-brain delivery of the hydrophilic antiviral ribavirin by microparticle agglomerates. *Drug Delivery,* 25(1), pp. 376-387.

HONG, P.Z., LI, S.D., OU, C.Y., LI, C.P., YANG, L. and ZHANG, C.H., 2007. Thermogravimetric Analysis of Chitosan. *Journal of Applied Polymer Science,* 105(2), pp. 547-551.

JOSHI, G.V., KEVADIYA, B.D., PATEL, H.A., BAJAJ, H.C. and JASRA, R.V., 2009. Montmorillonite as a drug delivery system: Intercalation and in vitro release of timolol maleate. *International .Journal of Pharmaceutics,* 374(1-2), pp. 53-57.

KEARNS, V.R. and WILLIAMS, R.L., 2009. Drug Delivery Systems for the eye. *Expert Reviews of Medical Devices,* 6(3), pp. 277-290.

KELLY, A.J., 1990. Charge Injection electrostatic atomization modeling. *Aerosol Science and Technology,* 12(3), pp. 526.

KHAN, W.S., ASMATULU, R. and ELTABEY, M.M., 2013. Electrical and Thermal Characterization of Electrospun PVP Nanocomposite Fibers. *Journal of Nanomaterials,* pp. 160931.

KONTOGIANNIDOU, E., ANDREADIS, D.A., ZOGRAFOS, A.L., NAZAR, H., KLEPETSANIS, P., VAN DER MERWE, S.M. and FATOUROS, D.G., 2017. Ex vivo buccal drug delivery of ropinirole hydrochloride in the presence of permeation enhancers: the effect of charge. *Pharmaceutical development and technology,* 22(8), pp. 1017-1021.

KRAULAND, A., GUGGI, D. and BERNKOP-SCHNURCH, A., 2006. Thiolated chitosan microparticles: A vehicle for nasal peptide drug delivery. *International Journal of Pharmaceutics,* 307(2), pp. 270-277.

KUMAR, A., VIMAL, A. and KUMAR, A., 2016. Why Chitosan? From properties to perspective of mucosal drug delivery. *International Journal of Biological Macromolecules,* 91, pp. 615-622.

LI, X., WANG, X., YU, D.G., YE, S., KUANG, Q., YI, Q. and YAO, X., 2012. Electrospun Borneol-PVP Nanocomposite. *Journal of Nanomaterials,* 2012, pp. 1-8.

MAHALING, B. and KATTI, D.S., 2016. *Understanding the influence of surface properties of nanoparticles and penetration enhancers for improving bioavailability in eye tissues in vivo.*

MAHER, S., MRSNY, R.J. and BRAYDEN, D.J., 2016. Intestinal permeation enhancers for oral peptide delivery. *Advanced Drug Delivery Reviews,* 106, pp. 277-319.

MAURER, J., MOLAI, A., PARKER, R., LI, L., CARR, G., PETROLL, W., CAVANAGH, H. and JESTER, J., 2001. Pathology of ocular irritation with acetone, cyclohexanol, parafluoroaniline, and formaldehyde in the rabbit low-volume eye test. *Toxicologic Pathology,* 29(2), pp. 187-199.

MERLINI, C., BARRA, G.M.O., ARAUJO, T.M. and PEGORETTI, A., 2014. Electrically pressure sensitive poly(vinylidene fluoride)/polypyrrole electrospun mats. *RSC Advances,* 4(30), pp. 15749-15758.

MHRA., 2015-last update, PACKAGE LEAFLET: INFORMATION FOR THE USER Timoptol® Eye Drops 0.25% / Timolol Eye Drops 0.25% (timolol maleate),. Available: http://www.mhra.gov.uk/spc-pil/?prodName=TIMOPTOL%20EYE%20DROPS%200.25//&subsName=TIMOLOL%20MALEATE&pageID=SecondLevel.

MUXIKA, A., ETXABIDE, A., URANGA, J., GUERRERO, P. and DE LA CABA, K., 2017. Chitosan as a bioactive polymer: Processing, properties and applications. *International Journal of Biological Macromolecules,* 105(pt2), pp 1358-1368

NATU, M.V., DE SOUZA, H.C. and GIL, H., 2011. Electrospun Drug-Eluting Fibers for Biomedical Applications. *Active Implants and Scaffolds for Tissue Regeneration,* 8, pp. 57-85.

NAZARI, K., KONTOGIANNIDOU, E., AHMAD, R.H., GRATSANI, A., RASEKH, M., ARSHAD, M.S., SUNAR, B.S., ARMITAGE, D., BOUROPOULOS, N., CHANG, M., LI, X., FATOUROS, D.G. and AHMAD, Z., 2017. Development and characterisation of cellulose based electrospun mats for buccal delivery of non-steroidal anti-inflammatory drug (NSAID). *European Journal of Pharmaceutical Sciences,* 102, pp. 147-155.

RAVAL, N., KHUNT, D. and MISRA, M., 2018. Microemulsion-based delivery of triamcinolone acetonide to posterior segment of eye using chitosan and butter oil as permeation enhancer: an in vitro and in vivo investigation. *Journal of Microencapsulation,* 35(1), pp. 62-77.

REIM, M., SCHRAGE, N.F. and BECKER, J., 2001. Interactions between ocular surface fluid and cornea related to contact lenses. *European Journal of Ophthalmology,* 11(2), pp. 105-115.

RODRIGUEZ, I., ANTONIO VAZQUEZ, J., PASTRANA, L. and KHUTORYANSKIY, V.V., 2017. Enhancement and inhibition effects on the corneal permeability of timolol maleate: Polymers, cyclodextrins and chelating agents. *International Journal of Pharmaceutics,* 529(1-2), pp. 168-177.

SAROHA, A., PANDEY, P. and KAUSHIK, D., 2017. Development of Timolol Maleate Loaded Chitosan Nanopartices for Improved Ocular Delivery. *Pharmaceutical Nanotechnology,* 5(4), pp. 310-316.

SARWAR, A., KATAS, H., SAMSUDIN, S.N. and ZIN, N.M., 2015. Regioselective Sequential Modification of Chitosan via Azide-Alkyne Click Reaction: Synthesis, Characterization, and Antimicrobial Activity of Chitosan Derivatives and Nanoparticles. *Plos One,* 10(4), pp. UNSP e0123084.

SMITH, D., 1986. The Electrohydrodynamic Atomization of liquids. *IEEE Translations on Industrial Applications,* 1A-22, pp. 527-535.

SUN, K. and LI, Z.H., 2011. Preparations, properties and applications of chitosan based nanofibers fabricated by electrospinning. *Express Polymer Letters,* 5(4), pp. 342-361.

SUNDARAY, B., BABU, V.J., SUBRAMANIAN, V. and NATARAJAN, T.S., 2008. Preparation and Characterization of Electrospun Fibers of Poly(methyl methacrylate) - Single Walled Carbon Nanotube Nanocomposites. *Journal of Engineered Fibers and Fabrics,* 3(4), pp. 39-45.

TANG, K.Q. and GOMEZ, A., 1995. Generation of Monodisperse Water Droplets from Electrosprays in a Corona-Assisted Cone-Jet Mode. *Journal of Colloid and Interface Science,* 175(2), pp. 326-332.

WAN, Y., LU, X., DALAI, S. and ZHANG, J., 2009. Thermophysical properties of polycaprolactone/chitosan blend membranes. *Thermochimica Acta,* 487(1-2), pp. 33-38

WILSON, S.L., AHEARNE, M. and HOPKINSON, A., 2015. An overview of current techniques for ocular toxicity testing. *Toxicology,* 2(327), pp.32-46

Chapter 7 Conclusions and Future Perspectives

7.1 General Conclusion

The aim of this research was to demonstrate the applicability of using EHDA to engineer coatings for ocular contact lenses. The thesis is split into three sections: the first was finding a suitable polymeric matrix to function as a biodegradable, stable drug carrier (Chapter 4). The following two chapters focussed on optimising the base formulation selected in chapter 4 to improve TM release and enhance TM permeation through the cornea.

Explicit details on specific aims and objectives are stated in **section 1.2** and **1.3**.

Chapter 4 looks at the effects of using two different polymers on the encapsulation, release and permeation of TM within and from EHD processed coatings respectively. PVP, a rapidly dissolving polymer, and PNIPAM (thermo-responsive polymer) were separately analysed and also in conjunction; creating a composite formulation. Firstly, the EHDA process was optimised to deduce the specific optimum processing window for each formulation that was developed. Once the process parameters were selected the resulting coatings were characterised using various techniques. The atomised coatings were found to be made up of particles (PVP) or beaded fibers (PNIPAM, composite); both within the nanometre range. Particles as small as 50 nm were observed using PVP-TM solutions, yielding an average diameter of 183 nm. Formulations containing PNIPAM yielded beaded fibers as a result of increased formulation viscosity. All 3 formulations assessed here demonstrated adequate EE (>64%) and higher stability with no material incompatibility. Thermal behaviour analysis showed TM was encapsulated and homogenously dispersed within the polymeric matrix in amorphous formulation. *In vitro* release studies showed TM release to follow a biphasic release profile with an initial burst release followed by subsequent sustained release. *Ex vivo* studies using bovine cornea indicated significant differences ($p<0.05$) between the 3 different polymeric matrices used with respect to TM penetration.

From these results, it was found using PVP and PNIPAM in conjunction provided excellent EE (99.7%) with great potential to be further modified to achieve controlled drug delivery.

Chapter 5 focussed on using this composite polymeric matrix as a base formulation to try and improve TM permeation due to the weak *ex vivo* results found in chapter 4. Here, four different PEs were incorporated. The EHDA process was optimised again due to the inclusion of new additives. As in chapter 4, the coatings were subjected to various characterisation with all coatings demonstrating similar results. The inclusion of PEs still yielded structures within the nanometre range, however smooth-surfaced fibers were found with a majority of formulations with some exhibiting beaded NFs. Thermal analysis confirmed TM was still in amorphous form and FTIR analysis established the structure of all excipients used were not compromised and hence functioned as they should. Significant differences were found with *in vitro* release and *ex vivo* studies depending on the PE used. The use of different PEs found to improve cumulative TM release by at least 9.08%. Release kinetics hinted at release of TM was via quasi-Fickian or Fickian diffusion from the atomised coatings. *Ex vivo* permeation studies showed some improvement in TM permeation through bovine cornea, with lag times reducing from 180 minutes with PE-free coatings to 30 minutes with PE-loaded coatings.

The work in chapter 6 detailed using chitosan as a modern PE to further increase TM permeation; with an aim for 100% permeation through the cornea. Using various concentrations of chitosan significantly affected the size of the atomised structures. Chitosan was introduced to the base formulations in the form of solid particles, increasing the diameter of the resulting atomised structures. Incorporation of chitosan also enhanced *in vitro* drug release up to 23% more than composite TM coatings.

7.2 Future Perspective

Using EHDA and contact lenses in conjunction in this research proposes a novel formulation and ODD device to enhance TM release for the treatment of glaucoma. This evidence of proof-of-concept highlights the potential of EHDA. There is great potential in using this approach in clinical practise However, extensive further work is required to compliment this data and to further highlight the potential of these coated lenses as viable DD devices.

7.2.1 Material

- Only two polymers were assessed in this research; PVP and PNIPAM. There are an array of polymers that have previously been utilised in ODD. Characterising a more diverse range of polymers such as pHEMA, PLGA, PAA and PLA may demonstrate more positive results compared to PVP and PNIPAM. pHEMA is a conventional contact lens material whilst PLGA has previously been used in HGs and as NPs for ocular application. PLGA has also been processed using EHDA with extremely promising results. PAA is capable of forming hydrogen bonds between its carboxyl groups and sialic-carboxylic group of mucin glycoproteins. This in turn increases formulation viscosity *in situ*, increasing residence time.
- It is also possible to load multiple drugs into these atomised structures, providing multi-functional DD devices. For example, to prevent any infections alongside treating glaucoma, antibiotics can be incorporated with the anti-glaucoma active; providing a bi-functional application
- In this research, only four PEs were chosen in Chapter 5 and a modern PE in Chapter 6. There are an array of PEs which may show more promising results than those assessed here. The PEs were also used at their maximum safety concentrations, different concentrations may alter drug release and permeation.

7.2.2 Process

- For all atomization experiments across all three chapters in this thesis, the working distance was kept constant at 12 cm. There is some evidence to suggest this distance between the collection plate and then needle exit can affect the morphology and size of the atomised structures. This is another aspect which can be studied.
- The evolution of EHDA as evaluated in Chapter 2 has led to the development of various atomization/experimental set-ups, yielding various structures. Coaxial EHDA using multiple concentrically arranged needles can produce multi-layered structures to provide sustained and/or controlled drug release. These layers can also house multiple actives, developing multi-functional DD devices.

- EHD jet printing or 3D printing can also provide another avenue in this application. The method can be utilised to print bespoke lenses with respect to not only therapy but size and comfort for the patient.

7.2.3 Characterisation

- The atomised coatings here were characterised by *in vitro* techniques and *ex vivo* methods. Studying *in vivo* behaviour of these coatings would be advantageous. Introducing these TM-loaded coatings to *in vivo* IOP models such as glaucomatous beagle dogs or New Zealand white rabbits with glaucoma can confirm the effectiveness of the coatings with respect to drug release, permeation and IOP reduction.
- With respect to the kinetic models used in this study, there are evident limitations. The models used here are weak and are suggestive as opposed to being definitive. The linearity of the kinetic plots derived throughout this work is questionable. They require refining/optimisation to correctly reflect the release mechanisms in this drug delivery system; something that relates to the mathematical approach to the model itself.

7.3 Final Comments

To the best of my knowledge, this work is the first of its kind; utilising an already successful device and combining it with an engineering process that has shown great potential in the drug delivery remit. The work presented here has potentially opened avenues to be further investigated in a field that I have become very passionate about which I hope to continue to work in in the future.

Appendix A Characteristic Infrared Absorption Wavenumbers of some Functional Groups

Group	Type of Compound	Wavenumber (cm^{-1})	Intensity
-O-H	Alcohols , phenols	3650-3590	Variable, sharp
-O-H	Hydrogen bonded alcohols & phenols	3400-3200	Strong, Broad
$-NH_2$ & =NH	Hydrogen bonded amines	3400-3100	Medium
$-NH_2$	Amines (primary)	3500-3300 double peak	Medium
=NH	Amines (secondary)	3500-3300 single peak	Medium
-O-H	Hydrogen bonded acid	3200-2500	Variable, broad
≡C-H	Alkynes	3250	Strong, sharp
=C-H	Alkenes & arenas	3100-3010	Medium
-C-H	Alkanes	2960-2850	Strong
O=C-H	Aldehydes	2900-2700	Weak
-C≡N	Nitriles	2300-2200	Strong
-C≡C	Alkynes	2260-2150	Variable
-C=O	Acid Chlorides	1815-1790	Strong
-C=O	Aldehydes	1740-1720	Strong
-C=O	Ketones	1740-1705	Strong
-C=O	Acids & Esters	1750-1700	Strong
-C=O	Amides	1650	Strong
-C=C	Alkenes	1660-1610	Weak
$-NH_2$	Amines (primary)	1620-1600	Medium
-NH	Amines (secondary)	1600-1560	Weak
-C=C	Arenas	1600 & 1500	Medium
$-NO_2$	Nitro-compounds	1550 &1350	Strong
$-CH_2$ &$-CH_3$	Alkanes	1460-1430	Strong
$-CH_3$	Alkanes	1390-1370	Medium
-C-O	Alcohols, ethers, acids & esters	1300-1000	Variable
-O-H	Acids	1000-940	Medium, broad